FINAL REPORT

Multi-Scale Experiments to Evaluate Mobility Control Methods for Enhancing the Sweep Efficiency of Injected Subsurface Remediation Amendments

SERDP Project ER-1486

AUGUST 2010

John E. McCray
Junko Munakata-Marr
Jeffrey A.K. Silva
Sean Davenport
Megan M. Smith
Colorado School of Mines

SERDP
DOD ▪ EPA ▪ DOE

Report Documentation Page

Form Approved
OMB No. 0704-0188

1. REPORT DATE	2. REPORT TYPE	3. DATES COVERED
AUG 2010	**N/A**	**-**

4. TITLE AND SUBTITLE
Multi-Scale Experiments to Evaluate Mobility Control Methods for Enhancing the Sweep Efficiency of Injected Subsurface Remediation Amendments

5a. CONTRACT NUMBER
5b. GRANT NUMBER
5c. PROGRAM ELEMENT NUMBER

6. AUTHOR(S)

5d. PROJECT NUMBER
5e. TASK NUMBER
5f. WORK UNIT NUMBER

7. PERFORMING ORGANIZATION NAME(S) AND ADDRESS(ES)
Colorado School of Mines

8. PERFORMING ORGANIZATION REPORT NUMBER

9. SPONSORING/MONITORING AGENCY NAME(S) AND ADDRESS(ES)

10. SPONSOR/MONITOR'S ACRONYM(S)
11. SPONSOR/MONITOR'S REPORT NUMBER(S)

12. DISTRIBUTION/AVAILABILITY STATEMENT
Approved for public release, distribution unlimited

13. SUPPLEMENTARY NOTES
The original document contains color images.

14. ABSTRACT

This research investigates enhanced delivery of remediation agents to hydraulically inaccessible zones using water-soluble polymers, with a focus on chemical oxidation and bioremediation of chlorinated solvents. Our investigations revealed that the xanthan polymer may be compatible with both permanganate and persulfate oxidants, but the xanthanpermanganate pair is most promising for future use. Both polymers are compatible with bioaugmentation remediation, but neither polymer was demonstrated to be an effective electron donor to achieve complete dechlorination. The confirmation of the presence of simple reducing sugar compounds resulting from xanthan biodegradation leads us to infer that the use of xanthan polymers in the subsurface should not results in long-term deleterious effects on groundwater quality. Polymer injections will result in some clogging near the injection zone, but this is not expected to significantly influence field application. Batch and column tests were helpful in constructing numerical models in up-scaled systems (2-D tanks). The UTCHEM model was able to successfully simulate 2-D experimental data for layered heterogeneous systems. Experimental data from intermediate-scale 2-D systems, and from hundreds of numerical simulations, suggest that polymer floods are very effective at improving sweep efficiency in layered systems, and that performance is improved in systems with more layers. Additional 2-D experiments confirmed that a polymer-oxidant flood enhanced mass removal and reduced postremediation mass flux, whereas the effectiveness of treatment depends on the delivery method. Overall, polymer flooding shows considerable promise for improving delivery of remediation agents in heterogeneous media where contaminants reside in hydraulically inaccessible zones. Relevant conclusions from the research conducted under SERDP Project ER-1486, Multi-Scale Experiments to Evaluate Mobility Control Methods for Enhancing the Sweep Efficiency of Injected Subsurface Remediation Agents are presented in accompanying tables on the following pages.

15. SUBJECT TERMS

16. SECURITY CLASSIFICATION OF:			17. LIMITATION OF ABSTRACT	18. NUMBER OF PAGES	19a. NAME OF RESPONSIBLE PERSON
a. REPORT **unclassified**	b. ABSTRACT **unclassified**	c. THIS PAGE **unclassified**	**SAR**	**166**	

Standard Form 298 (Rev. 8-98)
Prescribed by ANSI Std Z39-18

LIST OF FIGURES

LIST OF TABLES

LIST OF ACRONYMS

cP	centipoise
DCE	dichloroethene
DNSA	dinitrosalicyclic acid
GC	gas chromatograph
HPAM	hydrolyzed polyacrylamide
HPLC	high-performance liquid chromatography
KB-1	commercial name; microbial consortium capable of complete dechlorination
NAPL	non-aqueous phase liquid
NOD	natural oxidant demand
NOM	natural organic matter
PCE	tetrachloroethene
PTFE	polytetrafluoroethylene
TCE	trichloroethene
VC	vinyl chloride

KEYWORDS

Biodegradation
Chemical oxidation
DNAPLs
Enhanced delivery
Groundwater remediation
Heterogeneity
Hydrolyzed polyacrylamide
Permanganate
Persulfate
Polymer
Source-zone treatment
Sweep efficiency
Tetrachloroethene (PCE)

ACKNOWLEDGMENTS

The research described in this report was supported by the U.S. Department of Defense, through the Strategic Environmental Research and Development Program (SERDP). Dr. Andrea Leeson and other SERDP staff are gratefully acknowledged for their assistance and support. We appreciate the laboratory management and budget accounting provided by Ms. Kathryn Lowe at Colorado School of Mines (CSM). Professor Matthew Liberatore at CSM provided important technical guidance, and access to analytical instruments, related to polymer viscosity measurements.

ABSTRACT

This research investigates enhanced delivery of remediation agents to hydraulically inaccessible zones using water-soluble polymers, with a focus on chemical oxidation and bioremediation of chlorinated solvents. Our investigations revealed that the xanthan polymer may be compatible with both permanganate and persulfate oxidants, but the xanthan-permanganate pair is most promising for future use. Both polymers are compatible with bioaugmentation remediation, but neither polymer was demonstrated to be an effective electron donor to achieve complete dechlorination. The confirmation of the presence of simple reducing sugar compounds resulting from xanthan biodegradation leads us to infer that the use of xanthan polymers in the subsurface should not results in long-term deleterious effects on groundwater quality. Polymer injections will result in some clogging near the injection zone, but this is not expected to significantly influence field application. Batch and column tests were helpful in constructing numerical models in up-scaled systems (2-D tanks). The UTCHEM model was able to successfully simulate 2-D experimental data for layered heterogeneous systems. Experimental data from intermediate-scale 2-D systems, and from hundreds of numerical simulations, suggest that polymer floods are very effective at improving sweep efficiency in layered systems, and that performance is improved in systems with more layers. Additional 2-D experiments confirmed that a polymer-oxidant flood enhanced mass removal and reduced post-remediation mass flux, whereas the effectiveness of treatment depends on the delivery method. Overall, polymer flooding shows considerable promise for improving delivery of remediation agents in heterogeneous media where contaminants reside in hydraulically inaccessible zones.

Relevant conclusions from the research conducted under SERDP Project ER-1486, “Multi-Scale Experiments to Evaluate Mobility Control Methods for Enhancing the Sweep Efficiency of Injected Subsurface Remediation Agents” are presented in accompanying tables on the following pages.

POLYMER FLOW & TRANSPORT

- Dominant polymer transport and/or retention processes (e.g., sorption, mechanical plugging, etc.) can be quantified using polymer transport column experiments and well-characterized porous media; these processes can be modeled using UTCHEM.
- The parameters obtained from these bench-scale experiments, which involved only minor modifications to permeability, were sufficient to simulate the larger 2-D tank experiments. UTCHEM modeling performed very well in reproducing the shapes of injection tracer and polymer solutions over time, the calculated sweep efficiencies, and the pressure drops over the flow domain.
- Polymers can significantly improve the sweep efficiencies within layered systems; two-dimensional (2-D) tank experiments demonstrated up to a four-fold increase in overall sweep efficiency using less than two pore volumes of injected fluid, and a strong improvement in the ability of the fluid to sweep low permeability layers.
- Polymer-enhanced sweep efficiency is not only dependent on the permeability contrast between layers, but also on the relative positioning of layers with respect to the most conductive layer in the system.
- The results of the tank experiments and associated modeling show that UTCHEM parameters derived from column experiments are sufficient to simulate the 2-D experiments, and suggest that bench-derived parameters may be sufficient to parameterize a larger-scale field system, provided the larger system is appropriately characterized.
- By enabling sweep of lower-permeability zones by remediation fluid that is typically not possible, use of polymers should minimize the impact of contaminant rebound caused by diffusion of contaminants from low-permeability zones into more permeable media that was initially cleaned by the remediation effort.

NUMERICAL SIMULATIONS

- Increasing polymer strength decreases the number of injected pore volumes needed to achieve 100% sweep of the sand tank, for all cases.
- For two-layer systems, polymer-enhanced solutions can achieve a 100% sweep in one pore volume, if the permeability contrast is less than four.
- Sweep efficiency improvement diminishes as polymer concentrations exceed 500 mg/L.
- For a given permeability contrast between layers, reducing the thickness of the lower-permeability layer results in a decrease in the number of pore volumes necessary to achieve 100% sweep. The opposite holds true for a polymer-free tracer; the flushed pore volumes needed to achieve 100% sweep increases as the thickness of the lower-permeability layer decreases.
- The effect of increasing the number of layers in a system, while maintaining constant media proportions, reduces the number of pore volumes needed to achieve 100% sweep efficiency. This effect is most pronounced for permeability contrasts greater than 10. This result suggests that most aquifer (which can have many layers not discernible even from well borings) may achieve sweep efficiencies more favorable than predicted in these 2-D experiments and simulations.

POLYMER/OXIDANT COMPATIBILITY & TRANSPORT

- Xanthan polymers retain a high percentage of solution viscosity, with low to moderate nonproductive oxidant consumption levels, after 72 hours of exposure to permanganate ($KMnO_4$) oxidant, and do not inhibit the oxidation of chlorinated contaminant by the oxidant. Thus, this combination is most compatible for further polymer-enhanced chemical oxidation research.
- HPAM polymer is incompatible for use with either persulfate ($Na_2S_2O_8$) or permanganate ($KMnO_4$) oxidants, as a result of significant solution viscosity losses. Xanthan polymer retains slightly more of its original solution viscosity in contact with persulfate oxidant, but further experimentation or modeling will be necessary to determine if the resulting viscosity and shear-thinning behavior would permit enhanced aquifer sweep efficiencies.
- Viscous mixtures of xanthan polymer and permanganate oxidant flow more evenly through an experimental dual-permeability system, and this mixture can penetrate more of the fine-grained regions than does a low viscosity, aqueous (polymer-free) oxidant solution. As a result of this increased sweep, more contaminant mass (~2-3 times more) is destroyed per mass of applied oxidant in an experimental setting. Separate injections of oxidant followed by polymer are less effective at penetrating finer-grained regions, and experience more initial flow bypassing, than a pre-mixed polymer/oxidant solution.

POLYMER/BIOAMENDMENT COMPATIBILITY & TRANSPORT

- Neither xanthan nor HPAM polymer impedes the dechlorinating capability of the KB-1 microbial consortium, as long as methanol is supplied to the system as an electron donor. In microcosms where sufficient methanol is supplied, microbial dechlorination in polymer solutions often outperforms the corresponding polymer-free medium control experiments.
- No complete PCE-ethene biotransformation is observed in polymer-containing microcosms which lack methanol; instead partial degradation often results in undesirable accumulations of daughter products (DCE, vinyl chloride). Thus, xanthan and HPAM do not serve as adequate electron donors in and of themselves in the experimental matrices monitored here.
- Only small viscosity decreases were noted for xanthan and HPAM experiments supplied with PCE and methanol electron donor, and over the timespan of these experiments, such relatively stable solution viscosities would be unlikely to affect polymer-related sweep efficiency. However, these results are obtained in idealized batch microcosms involving intentionally limited microbial communities, and are thus not thought to be indicative of the timescales over which solution viscosity might be maintained in a more microbially diverse, natural field site.
- In both batch and column experiments conducted with natural soils and groundwaters, unknown microorganisms degraded xanthan polymer and induced viscosity losses. Although xanthan degradation was noted under both aerobic and anaerobic batch conditions, degradation proceeded more rapidly under anaerobic conditions.
- Simple reducing sugars were detected concurrently with xanthan degradation noted from viscosity losses in batch and column experiments; the detection of such break-down products leads us to infer that the use of xanthan polymers in the subsurface should not result in long-term negative effects on groundwater quality. Some bio-clogging was noted during polymer application in column experiments, but is not expected to significantly influence polymer delivery in field applications.

1. OBJECTIVES

The primary objective of this research is to provide information that will advance the state of the science in enhanced delivery of remedial agents to heterogeneous contaminated zones. This project directly addresses the SERDP Statement of Need (SON) to improve delivery of remedial agents to contaminated zones.

The aim of this research is to improve the subsurface sweep efficiency of injected remediation agents (e.g., chemical oxidants and bioamendments) using viscous solutions of water-soluble polymers. Remediation of organic contaminants in the subsurface is often inefficient in heterogeneous systems due to bypassing around low-permeability strata and because of the associated mass-transfer limitations. Polymer solutions can mitigate these problems by improving the subsurface sweep efficiency of fluids, thereby enhancing the contact between remediation amendments and the target contaminant. Improved sweep efficiency has been demonstrated for enhanced oil recovery, but at much larger scales, at different heterogeneity structures, and for different distributions of organic chemicals, than are typical for ground-water remediation efforts. Thus, understanding the interplay between the site-specific heterogeneity and injected polymer solutions is crucial to optimizing the distribution of remediation amendments in the subsurface. This study endeavors to understand fundamental processes governing polymer transport and polymer-enhanced remediation-amendment distribution by integrating multidimensional laboratory experiments and mathematical modeling.

In theory, polymer solutions can improve delivery of injected remediation fluids to heterogeneous porous media. However, some questions arise about the compatibility of polymers with common remediation agents. The focus of this research is on chemical oxidants and bioremediation agents. An obvious potential problem for polymer-oxidant applications is that oxidation may destroy the polymer, thus diminishing the viscosifying effect. In addition, oxidation of polymer may deplete the oxidant concentrations, reducing the efficiency of contaminant destruction. With respect to bioremediation, microbes that degrade contaminants may also degrade the polymer, destroying the enhanced-viscosity effect. On the other hand, some degradation of the polymer could be advantageous if the polymers could also be used as an electron donor.

The goals of this research are twofold: to conduct screening studies to ensure that polymers are compatible with chemical oxidation and bioremediation, and to gain a fundamental understanding of the processes governing polymer transport and polymer-enhanced sweep efficiency for conditions relevant to ground-water remediation. With respect to compatibility, evaluating all likely combinations of polymer-enhanced chemical oxidation or bioremediation would be an immense task, and is beyond the scope of this project. Rather, we endeavor to determine if polymer-enhanced flushing can be used with at least one chemical oxidant, and with at least one bioremediation application, and what practical limitations exist to these applications. With respect to polymer transport, we endeavor to identify a polymer that is compatible with the selected remediation agents, and conduct transport studies at the batch, column, and 2-D tank scale to understand the processes governing improved sweep efficiency. Mathematical models are used to analyze the data. These mathematical models can also be used to assess the viability of the technology using hypothetical site data and scenarios and would also be useful in the

ultimate field-scale application of this technology. This research should allow us to move closer to field implementation of the technology, ideally resulting in design rules that can be used by engineers for practical implementation or to design further research.

To achieve the goals previously discussed, the following project tasks have been delineated:

Task 1 - Batch Studies: Batch experiments will be performed to: a) Investigate polymer and amendment interaction with aquifer materials (i.e., sorption), b) Assess the compatibility of polymers with chemical oxidants and develop polymer/oxidant formulations appropriate for ISCO applications, and c) Assess the compatibility of polymers and various bioremediation amendments used to enhance in situ biodegradation.

Task 2 - Column Studies: Column experiments will be performed to: a) Isolate and assay the retention contribution of mechanical and hydrodynamic entrapment (i.e., filtering) on polymer transport, b) Measure effective and relative permeabilities for various soil types during polymer delivery, c) Examine the relative transport of polymer and model amendment, and d) Examine non-Newtonian effects of polymer-assisted transport.

Task 3 – 2-D Experiments and Model Simulations: 2-D tank experiments will focus on assessing the deliverability of polymer-amended fluids within heterogeneous aquifer systems. Chemical oxidants and/or bioamendments will not be used in these experiments. Rather, conservative surrogate amendments (e.g., chemical dyes and/or salt solutions) will be utilized. Areal sweep efficiency (ASE), defined as the integrated area contacted by the amendment versus the total area of the 2-D tank, will be the metric used to assess amendment deliverability. Areal sweep efficiencies will be correlated with various heterogeneity metrics in order to develop a database from which the benefits and limitations of polymer-assisted delivery of remediation agents can be assessed. UTCHEM will be used to conduct numerical simulations for experimental design, and will also be used to analyze the experimental data. A number of experimental heterogeneous aquifer systems will be tested. Sweep efficiencies will be measured within the tanks and also from numerical simulations.

Task 4 – 2-D Tank Experiments with Oxidant: 2-D tank experiments will focus on comparing different oxidant and polymer-enhanced delivery strategies in a dual-permeability system. Specifically, an aqueous oxidant (polymer-free) application will be compared to two different methods of polymer-enhanced injection delivery: a co-injection (which would require above-ground mixing of polymer and oxidant before introduction to the subsurface), and an unmixed sequential bank injection (where aqueous oxidant slugs are injected first, followed by separate polymer "push" floods; this strategy would not require above-ground mixing). These experiments should provide guidance for optimization of polymer-enhanced oxidant distribution, as well as an improved understanding of the interplay between polymers, oxidants, and NAPL.

<u>Task 5 – Upscaled Numerical Simulation</u>: Information gained from the 2-D studies will be used to conduct simulations of amendment delivery using the UTCHEM simulator. The focus of this work will be to further investigate the deliverability of remediation amendments in heterogeneous layered geologic media, in the absence and presence of polymer addition.

2. BACKGROUND

This research addresses the difficult problem of remediation in heterogeneous media, with a goal to enhance delivery of remediation agents to the contaminant zone. Past remediation efforts have been successful at removing contamination from highly permeable and hydraulically accessible zones. However, the inability to clean up the less accessible zones has resulted in long term "rebound" of contaminant concentrations to above acceptable limits, and in many cases has prevented site closure. Remediation agents are effective when delivered, but the delivery of the remedial agents to heterogeneous contaminated zones has been largely ineffective. The SERDP program stated a need to improve delivery of remedial agents to areas that are hydraulically inaccessible to traditional aqueous amendments. This project directly addresses that need.

The efficiency and efficacy of engineered remediation strategies that involve the introduction of chemical amendments (e.g., chemical oxidants and reducing agents, biochemical nutrients and stimulants) into the subsurface are dependent on achieving an efficient subsurface sweep applied amendment within the contaminated zone. This is true of forced-injection strategies that rely on direct contact between the amendment and the target contaminant, as well as for strategies that rely on uniform placement of amendments and subsequent dissolution of the amendment. Many of the injected remediation amendments in current use are introduced to the subsurface as viscous liquids: aqueous solutions, emulsified liquids, or liquid suspensions. Examples include surfactant solutions, aqueous solutions of chemical oxidants, diluted or emulsified edible oils, diluted molasses or acetate solutions, and emulsion formulations containing zero-valent nanoscale iron. The magnitude of amendment fluid viscosities varies between technologies with a general trend towards the use of a viscosity near that of water (i.e., 1 centipoise, or cp) to facilitate rapid injection.

However, when injected under an applied pressure gradient the resulting subsurface distribution is impacted greatly by the architecture of the subsurface permeability field because the amendments will seek preferential flow paths through more permeable media, resulting in a less efficient sweep of the target zone by the injected amendments. The extent to which this occurs in a given heterogeneous system largely depends on the physicochemical properties of the injected fluid, the mode of introduction (e.g., injection rates, orientation and placement of well screens), the permeability distribution, the location of the contaminant zone (in high-permeability zones, within clay zones, etc), and the interaction of the fluid with the solid media at the pore-scale. Therefore, understanding the interplay between the site-specific heterogeneity of the subsurface and the injected remediation fluids is crucial to optimizing the distribution of applied amendments in the subsurface, thereby enhancing the contact between the amendment and the target contaminant.

Mobility control defines a class of strategies involving the modification of in-situ fluid viscosities. This strategy was developed by the petroleum industry for enhanced oil recovery to overcome preferential flow and other bypassing effects produced by geological heterogeneities. Mobility control mechanisms have been used by the petroleum industry since the 1960's to improve chemical flood efficiency and maximize oil production from lower permeability strata. Traditional mobility control techniques in petroleum reservoir engineering have involved the use of polymers, which increase the viscosity of the injected solutions. The increased viscosity of

the injected fluid minimizes the effects of the aquifer heterogeneities by promoting strong transverse fluid movement, or cross-flow, across heterogeneous reservoir units (Lake, 1989: Sorbie, 1991), providing an enhanced sweep efficiency. The occurrence and benefits of cross-flow during polymer flooding for oil recovery is well documented (see Seright and Martin, 1991, Sorbie, 1991 and references therein) and a summary of recent applications in environmental restoration may be found in Jackson et al. (2003).

A simplified illustration of the cross-flow mechanism is provided below for linear flow of a viscous Newtonian fluid in a two-layered aquifer system (permeability $k_1 > k_2$).

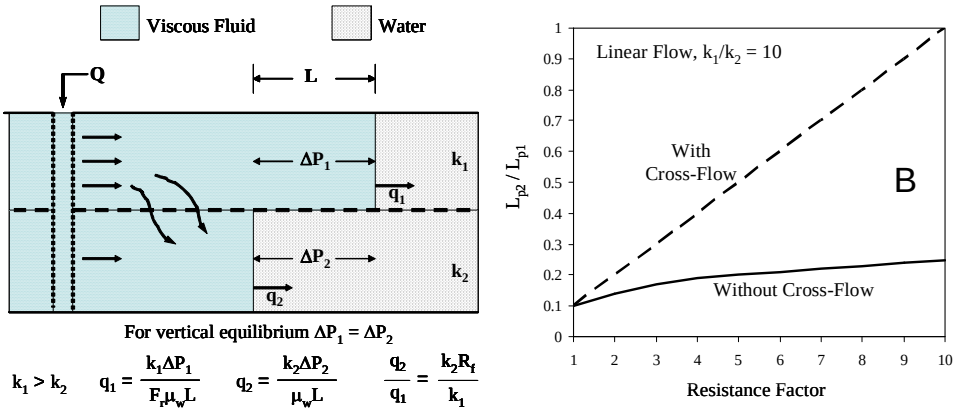

Figure 2-1. *Simplified illustration of the cross-flow mechanism (from Seright and Martin, 1991). $k_1 > k_2$. The cross-flow condition occurs more readily with injected polymer.*

When a viscous fluid is injected into the subsurface, a transverse pressure gradient is induced between higher and lower permeability strata causing fluid to flow from the more permeable strata into less permeable strata in an attempt to attain vertical equilibrium (i.e., $\Delta P_1 = \Delta P_2$). The result is a smoothing of the viscous liquid frontal advance within heterogeneous porous media and diminished viscous fingering (i.e., enhanced sweep efficiency) as the fluid propagates away from the point of injection. The effects of the cross-flow mechanism are better shown in Figure 2-1b, where the calculated ratio of the positions of the viscous fronts in both layers (L_2/L_1, see Figure 1) are plotted for the case of no cross-flow versus that with unrestrained cross-flow for an increasing resistance factor (R_f). R_f is the ratio of the fluid injectivity (Q divided by the difference in pressure between the point of injection and a defined distant point of reference) of water to that of the viscous fluid and can be thought of as a fluid-specific measure of resistance to flow. As shown, an increase in the amendment resistance to flow decreases the relative positions of the viscous fronts between layers when cross-flow occurs (i.e., L_2/L_1 approaches unity). The effect of cross-flow in real geologic systems would fall between these two curves because the resistance to transverse flow is not negligible. The net result is that preferential flow and bypassing of low permeability media is reduced, improving amendment sweep efficiency.

Technically, the term “mobility control” relates to defining an optimum mobility ratio (i.e., mobility of injected fluid greater than that of the displaced fluid) to displace a viscous pore

fluid (oil or viscous NAPLs) from porous media. When a viscous fluid is used to displace pore water and promote lateral dispersion of the injected fluid within variable permeability media (as is the case in this research), the term "heterogeneity control" is more appropriate. Viscosity modification of engineered remediation amendments, whether by the addition of polymers or other modifications to amendment formulations, should promote similarly favorable heterogeneity control results for amendment emplacement in environmental systems as those observed in the petroleum industry. Moreover, heterogeneity control strategies can be applied to improve the efficiency of a variety of *in situ* remediation technologies, including: *in situ* chemical oxidation/reduction and delivery of enhanced bioremediation amendments, which are used in this research.

However, a need exists for fundamental study of the applicability of heterogeneity control within near-surface geologic systems before these strategies can be used to their optimum potential benefit. Typical polymer applications in oil reservoirs exhibit temperature, pressure, salinity and permeability conditions that differ significantly from those found in environmental systems. Therefore many of the design criteria used by the petroleum industry for predicting the applicability and efficiency of polymer mobility and heterogeneity control methods in petroleum reservoirs may not be directly applicable to ground water aquifers. Screening rules for site-appropriateness must be developed for environmental application. Also, protocols for site-specific application of heterogeneity control must be established to optimize remediation amendment delivery and subsurface distribution. However, prior to practical application of such technologies, much fundamental research is needed. In addition, some obvious questions arise about the compatibility of polymers with common remediation agents. An obvious potential problem is that the oxidants may destroy the polymer, and diminish the viscosifying effect. In addition, there is a concern that oxidation of polymer may deplete the oxidant concentrations, reducing the effectiveness of contaminant destruction. Both topics are addressed in this research.

3. TASK 1: BATCH STUDIES

Polymers used in this study include xanthan biopolymers and partially hydrolyzed polyacrylamides (HPAM). These polymer classes were selected for use in enhancing the *in situ* delivery of remediation agents because of their history of use in the petroleum industry and the availability of literature data with which to supplement our investigation. Xanthan biopolymers (or xanthan gums) are bacterially produced polysaccharides, consisting of a cellulosic backbone with repeating trisaccharide chains of glucose, mannose, and glucuronic acid. Xanthan polymer is safe for human consumption and is a common thickening agent used in many food products (CP Kelco, 2004). HPAMs are synthetically produced polymers of acrylamide monomers wherein OH^- is substituted for NH_2 on a controlled portion of the acrylamide monomer, giving the polymer a net negative charge (See Figure A-1). Both polymers possess average molecular weights in excess of 10^6 g/mol and provide viscous solutions at low polymer concentrations.

The viscosifying properties of these polymers, coupled with their non-toxic nature and economics of use, make them excellent candidates for use in environmental restoration to enhance the distribution of injected environmental remediation amendments. First, however, the physicochemical characteristics of these polymer solutions must be investigated to ensure suitability for subsurface injection and compatibility with co-injected remediation amendments. Thus, we are conducting batch studies to characterize adsorptive properties (with selected soils that are representative of aquifer material), chemical compatibility with chemical oxidants (i.e., potassium permanganate and sodium persulfate), and biological compatibility with our selected microbial culture (KB-1 reductive dechlorinators).

3.1 Sub-task A: Polymer Batch Tests, Sorption

The polymers used in enhanced oil recovery and in this work carry a net negative (anionic) charge. Polymers used for *in situ* mobility and/or heterogeneity control are anionic to mitigate polymer adsorption, which can adversely impact polymer subsurface transport. Adsorption of anionic polymers likely occurs to some degree due to mechanisms described below. Thus, characterizing adsorption amounts (i.e., mg/kg_{soil} or $mg/m^2_{surfaces}$) for a given porous media system and polymer solution formulation is an important factor in the design of polymer-enhanced flushing.

Mineral adsorption of anionic xanthan and HPAM is generally considered to occur as a result of a coupling of van der Waals interactions and hydrogen bonding facilitated by a bridging cation (Nadler and Letey, 1989; Malik and Letey, 1991; Letey, 1994; Lu et al., 2002; Dontsova and Bigham, 2005). Provided that sufficient sorbent surface area is available, anionic polymer adsorption has been shown to increase under the following conditions: increasing solution cationic strength (particularly with divalent cationic strength); increasing anionic charge on the polymer molecule, and increasing clay content. As an electrostatic process, polymer adsorption is also expected to be dependent on solution pH. These adsorption dependencies, along with the specific molecular weight of the polymer in use, can impact the nature of the polymer sorption isotherm. For example, Nadler and Letey (1989) found Langmuir adsorption characteristics for HPAM possessing an anionic charge density of 2%, whereas HPAM of similar molecular weight possessing 21% charge density exhibited linear isotherm behavior and significantly higher adsorbed concentrations on field soils. Also, anionic polymer sorption has been shown to

increase with decreasing organic matter content (Nadler and Letey, 1989; Lu et al., 2002). Given the complexities of anionic polymer adsorption, it is important to characterize adsorption amounts and isotherm character for a given test, field site, or implementation condition so as to understand its contribution to polymer transport in porous media.

Batch sorption experiments were designed and conducted to provide an independent measure of xanthan and HPAM adsorption to the porous media used throughout this investigation. Despite consulting the literature and following standard batch sorption techniques, it was difficult to obtain meaningful measures of adsorption for these polymers using these methods. However, we found that meaningful adsorption concentrations could be obtained as a result of our column testing work described in Section 4.1. Thus, it was deemed unnecessary to conduct numerous batch tests for sorption. Batch adsorption methods and discussion of results are provided below.

Materials and Methods

Four commercial silica sands with significantly different permeabilities were selected for use in characterizing polymer transport (to be completed during Task 3). Providing an independent measure of polymer adsorption for these sands became the initial focus of these batch experiments. The sands consisted of two UNIMIN sands (#30 and #70 mesh), one Ottawa foundry sand (110 mesh) and a ground silica medium sieved to contain particles retained on a 250 mesh (SIL-CO-SIL 250). The sands were used as provided without washing or other pre-treatment.

Xanthan biopolymer solutions (Keltrol-T®, CP Kelco, Atlanta, GA) were prepared at three concentrations (100, 500, and 1000 mg/L) using a 25% dilution of an artificial groundwater described in Table 3-1. These solutions were prepared following the manufacturers recommendations and were added to each test sand at solution:soil mass ratios of 50:1, 20:1, 10:1, and 5:1. These batches were prepared in 50 mL centrifuge tubes and allowed to equilibrate for 24 hours on an end-over-end tumbler. Following equilibration the batches were centrifuged at approximately 3,000 revolutions per minute for twenty minutes prior to analysis of the supernatant.

Xanthan solution concentrations following equilibration and centrifugation were determined using a total carbohydrate colorimetric assay method described by Dubois et al. (1956). Briefly, this method involves the addition of one milliliter of 5% phenol solution and five milliliters of concentrated sulfuric acid to one or two milliliters of supernatant, depending on the expected xanthan concentration. After reagents were added, the samples were allowed to react for ten minutes and subsequently cooled to room temperature in a 25°C water bath. A Hach DV/4000 UV/Vis spectrophotometer was used to measure xanthan concentrations at wavelength of 486 nm.

Results and Discussion

The results of the batch tests are inconclusive. The majority of these batch tests provide solution concentrations after sorption in excess of the parent solution controls, which suggests issues associated with the quantification limits of the analytical method, or unknown interference. This effect appears to increase with increasing polymer concentration. Furthermore, batches that do show solution concentrations less than the controls provide adsorbed

concentrations well above (e.g., 500 to 2000 mg/kg) those expected for xanthan sorption onto silica (e.g., 10 to 40 mg/kg). Earlier attempts to quantify batch solution concentrations using a TOC (total organic carbon) analyzer were also problematic. We have also observed, when using lower solution:soil ratios, that these polymers appear to flocculate fines in our batch tests. These flocculated fines are then removed from solution during centrifugation, producing elevated sorbed mass values (i.e., polymer not in solution is assumed to be sorbed to the soil phase as a result of mass balance). We have been successful at quantifying sorption using the column tests (described in Section 4-1), so batch tests for polymer sorption are not necessary.

Polymer Sorption Test Conclusions

- Batch test results were inconclusive.
- The necessary parameters for UTCHEM model input can be alternatively derived from polymer transport column studies (see Section 4-1).

3.2. Sub-task B: Chemical Oxidant Batch Tests

Batch tests were performed to assess the compatibility of xanthan biopolymers and HPAM with the chemical oxidants potassium permanganate ($KMnO_4$) and sodium persulfate ($Na_2S_2O_8$). Experiments were performed to understand the influence of the cations naturally present in the oxidant solution on viscosity, as well as to separately assess the influence of oxidation on polymer-solution viscosity. Our primary criteria for chemical compatibility included the stability of polymer/oxidant solution viscosity through time and the level of non-productive oxidant demand posed by the polymer. A significant loss of viscosity would negate the mixtures' ability to enhance the sweep efficiency of the oxidant, while a high non-productive chemical oxidant demand would decrease the efficiency of treatment (i.e., more oxidant needed than required for contaminant degradation alone). Any polymer/oxidant mixture found to adequately satisfy these two initial criteria was then subjected to a secondary criterion involving the determination of competitive effects (if any) that the polymer might pose during the contaminant oxidation reaction.

The available literature makes few direct references to oxidation of either xanthan or hydrolyzed polyacrylamide by permanganate or persulfate. Observations from published studies involving permanganate or persulfate oxidation of structurally similar molecules may provide some insight as to these compounds' reactivity, as discussed below, but experiments were still deemed necessary to quantitatively evaluate potential polymer oxidation.

Permanganate reaction with polysaccharides similar to xanthan, including pectin, chitosan, carrageenan, alginate, and methyl cellulose, indicates that free radicals were not involved in the oxidation of these compounds (Hassan, 1993; El-Khatib, 2002; Abdel-Hamid et al, 2003; Ahmed et al., 2003; Ahmed et al., 2007). In these reactions, consumed permanganate/polysaccharide ratios range between 0.8 for pectin, to one to two for all other compounds. Although acrylamide (the monomer unit polymerized to form polyacrylamide) has been shown to be vulnerable to permanganate oxidation in water treatment systems (Ma et al., 1994), the extent to which HPAM will react with permanganate is currently unknown. Polyvinylamine and paraffin wax (two compounds similar to hydrolyzed polyacrylamide in having multiple single C-C bonds with small functional groups) are both resistant to

permanganate and are used to deliver the oxidant without substantial degradation of the compound (Prabhakaran et al., 1999; Ross et al., 2005). Organic chemistry theory states that hemiacetal structures (present in polysaccharides such as xanthan) may provide some degree of resistance to attack by permanganate (Stewart, 1964); thus, the lack of such structures in HPAM may indicate a comparatively decreased resistance to permanganate exposure.

Specific experiments involving activated persulfate and the polymers of interest in this work are scarce, although numerous references are made to the use of persulfate as a free radical initiator and powerful non-specific oxidant during some polymerization reactions. The "persulfate method" (Sharp, 1973) is commonly used to oxidize organic carbon compounds before total carbon analysis, although Sharp (1973) and Spiteller and Saiz-Jimenez (1990) both note that persulfate oxidation may not degrade the entire suite of compounds present in a natural sample of organic matter or even all of the functional groups present in a single compound.

Research involving the reaction of hydroxyl and other oxygen-active radicals (produced and involved in persulfate oxidation) with sugar molecules indicates that saccharides may exhibit some small degree of resistance to free radical activity. Over a timespan of minutes, Morelli et al. (2003) noted that disaccharides were resistant to hydroxyl radical activity. Conversely, other authors have observed a lack of any antioxidative properties over five days in solutions of simple sugars (e.g., glucose, fructose and ribose) (Wehmeier and Mooradian, 1994). Oil emulsion experiments, designed to evaluate polysaccharide stabilizers for use in salad dressing, identified xanthan as displaying antioxidant behavior over periods of days to several months (Kishk and Al-Sayed, 2007; Paraskevopoulou et al., 2007). Recent work by Chursin (2007), however, indicates that cellulosic polysaccharides are quickly degraded by both hydrogen peroxide and persulfate. Thus the literature supports the necessity of this experimental task.

Materials and Methods

Polymers formulations used were xanthan (Keltrol T®, CP Kelco, Inc., Houston TX) and hydrolyzed polyacrylamide, HPAM (Superfloc®, Cytec, Inc., Woodland Park, NJ). All polymer solutions were prepared in deionized water. Preparation of solutions involves the slow addition of powdered polymer to a vortex created in solvent water by an overhead stirrer. Solutions are stirred for 2-3 hours, then allowed to rest for at least 12 hours before use. Polymer concentrations are given in weight percent, as opposed to molar units, as the molecular weights of these polymers are characterized as a range of values (polydisperse) instead of a single weight. The rheology of both types of polymers was determined at varying concentrations from 10-8,000 mg/L, and with various salt (KCl, NaCl, $CaCl_2$) concentrations over a shear rate range of 0.1-100 sec^{-1} (representative of ambient groundwater conditions) in order to characterize the solutions before combination with oxidants or microbes. Solution viscosity was measured using either a manually operated benchtop DX-LX viscometer (Brookfield, Middleboro, MA) or with an automated AR-G2 rheometer (TA Instruments, New Castle, DE).

Chemical oxidants used were potassium permanganate, $KMnO_4$, USP grade 99% purity (Cairox Corp., Peru, IL) and sodium persulfate, $Na_2S_2O_8$, 99% purity (Sigma-Aldrich, St. Louis, MO). All oxidant solutions were prepared in deionized water. These oxidants were selected due to their high aqueous solubilities, their relative ease of application, and the literature available to document their usage. Permanganate does not require an activation catalyst; thermal activation

was chosen for persulfate to avoid issues of free radical scavenging and dosing requirements required by iron catalysis (Liang et al., 2004).

A calibrated pH meter was used to monitor pH levels in batch experiments. Filtered batch samples (0.2 μm) were analyzed for permanganate (MnO_4^-) concentration using a Hach Model DV4000U spectrophotometer after the method of Crimi & Siegrist (2004) at a wavelength of 525nm ($MnO_{2(s)}$ concentrations were also qualitatively monitored at 418nm). Persulfate ($S_2O_8^{2-}$) samples were reacted and measured spectrophotometrically using absorbance at 450 nm according to the method of Huang et al. (2002). Before testing, full-wavelength scans of each of the polymer solutions were conducted to determine possible interference at the wavelengths of interest for oxidant determination. Polymer solutions exhibited absorbances at wavelengths <150nm and thus do not interfere with these measurements.

Before batch investigation, the viscosity profiles (shear rate versus viscosity) of pure polymer solutions were determined by rheometry, as well as decreases to the solution viscosity effected by ionic salt solutions (caused by the interaction of aqueous ions with charged functional groups along the polymers' molecular backbone; see Sorbie (1991) for a full discussion of the "salt effect"). This characterization allows polymer solution viscosity losses due to the presence of salts to be distinguished from losses associated with oxidation of the polymer.

Batch experiments were then designed to test both the oxidant demand of each polymer and the change in viscosity as a result of polymer/oxidant interactions. Test conditions are provided in Table 2-1. Batches were assembled in clean amber 40-mL borosilicate glass vials with Teflon®-lined caps. Polymer and oxidant solutions were prepared at higher concentrations and mixed immediately prior to testing to achieve the concentrations in Table 3-1. The initial polymer concentrations provide a range of initial viscosities encompassing more than three orders of magnitude (see Figure A-2 for full viscosity data). The chosen oxidant concentration is well within range of published laboratory studies, although lower than many field applications (Tunnicliffe and Thomson, 2004; Zhai et al, 2006; Waldemer and Tratnyek, 2006; Krembs, 2008). These concentrations provide molar oxidant concentrations many orders of magnitude greater than molar polymer concentrations (as a result of the polymers' high formula weights) and thus potentially negative effects of the oxidants should be observed at this mixing ratio.

Table 3-1: *Polymer/Oxidant Batch Compatibility Test Conditions*

Sample Descriptions	**Polymer (Xanthan, HPAM)**	**Oxidant ($KMnO_4$, $Na_2S_2O_8$)**	**Added Cations* (K^+ or Na^+)**
	(mg/L)	**(mg/L)**	**(mM)**
Polymer Control	160; 800; 1600	0	0
Polymer/Salt Control	160; 800; 1600	0	12.6; 8.4
Polymer/Oxidant Test	160; 800; 1600	2000	0
Oxidant Control	0	2000	0

** The first number refers to added potassium ions; the second number refers to added sodium ions. These concentrations provide cations in concentrations equal to that produced in a solution of 2000 mg/L oxidant (12.6 mM $KMnO_4$ or 8.4 mM $Na_2S_2O_8$).*

Batch tests were conducted in duplicate over a 72-hour time period, realistic for an actual application using either a "push" of oxidant solution into a DNAPL source zone, or for a line-drive sweep of a source zone. All batches were shaken intermittently during the test period. Permanganate batches were stored in the dark at constant temperature (22 ±1°C). Persulfate batches were stored in a dark 40±2 °C water bath for thermal activation (Liang et al., 2004), and were removed only for sampling. Duplicates of both heated and unheated test experiments were utilized in persulfate trials. Two to three individual samples were taken from each batch experiment every 4, 24, 48, and 72 hours to monitor oxidant concentrations. Solution viscosity was monitored using the AR-G2 Rheometer over a shear rate range of 1 to 100 sec^{-1}. Persulfate experiments were allowed to cool to room temperature before viscosity measurement.

The oxidation rate of PCE in both aqueous and polymer-containing solutions was determined by equilibrating solutions with pure-phase PCE for several days. A later version of this experiment was also conducted using phosphate-buffered polymer and oxidant solutions. After determining the initial dissolved-phase PCE concentrations, the solutions were combined in duplicates with oxidant at varying polymer concentrations and a slightly lower oxidant concentration of 1000 mg/L. This oxidant concentration was selected to provide a practical time period over which to measure contaminant destruction, and to avoid excessive manganese oxides generation. Initial permanganate molar concentrations were kept in one order of magnitude excess of both PCE and polymer molar concentrations. Aqueous PCE-permanganate rate control experiments were run concurrently with each polymer-containing batch as an experimental methods check, and the derived rate constants were compared against previously published aqueous oxidation rates. Sacrificial vials were used to avoid the possibility of PCE loss during continued sampling events. Samples were extracted in hexane and immediately analyzed on a Shimadzu GC-17A gas chromatograph equipped with a flame ionization detector.

Results and Discussion

The results and conclusions presented here were summarized previously in Smith et al. (2008). Figure 3-1 illustrates the different responses of these polymers to added salts. Briefly, HPAM solution viscosity decreases as more salt is introduced into solution, while xanthan solutions experience a fixed decrease that is not dependent on the salt concentration.

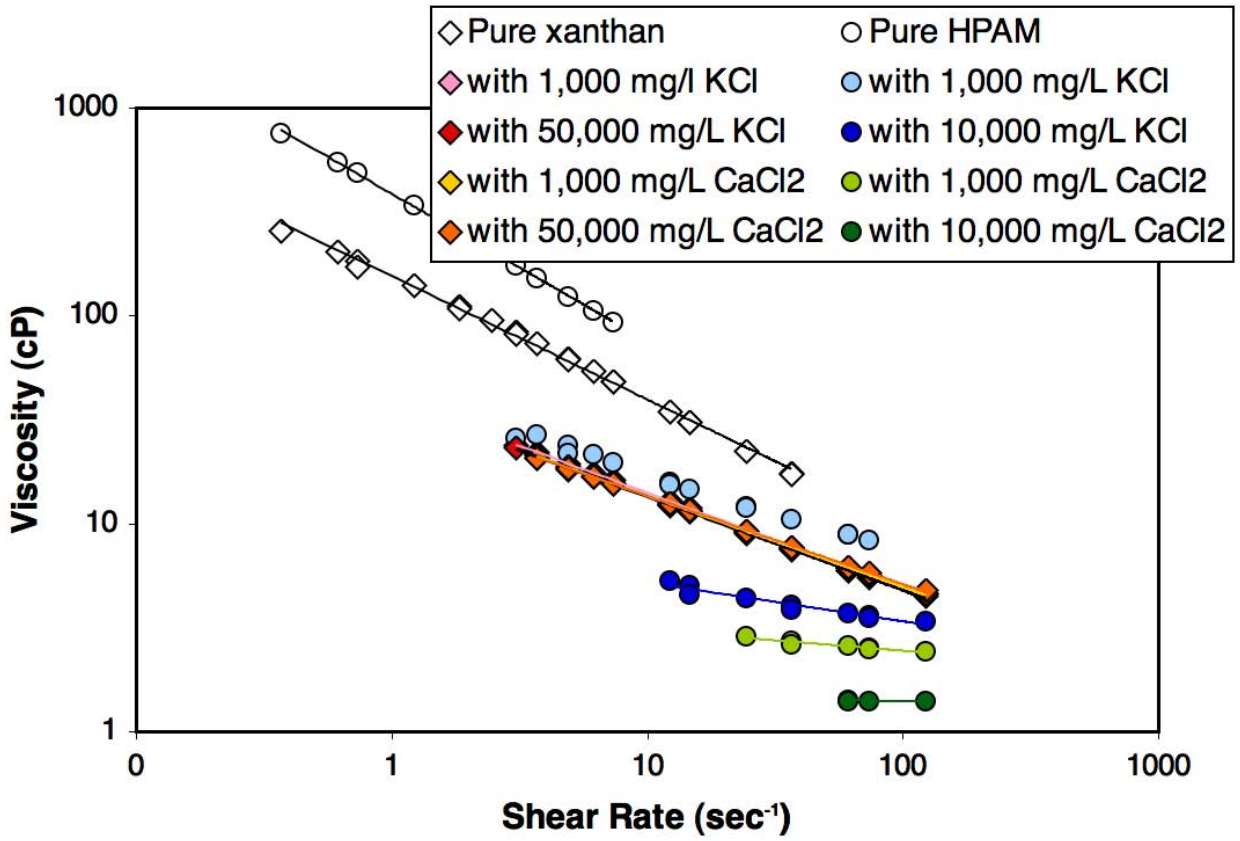

Figure 3-1: *Viscosity versus shear rate for pure 500 mg/L solutions of xanthan and HPAM polymer, with increasing additions of KCl and CaCl2 salts.*

Viscosity Retention

After 72 hours of exposure to permanganate oxidant, we can compare the retention of viscosity in both 1600 mg/L xanthan and HPAM solutions in Figure 3-2. For the mid-range shear rate value of 10 sec^{-1}, xanthan solutions retain approximately 80% of their initial viscosity, corresponding to an actual viscosity of ~70 cP, while HPAM solutions retain less than 5%. Similar trends of high viscosity retention for xanthan solutions (see Table A-1 for 800 and 160 mg/L data) and low retention for HPAM solutions were also noted. Xanthan/permanganate mixtures still display a shear-thinning rheology, while the HPAM viscosity profile is drastically decreased and flat over a range of shear rates. Figure 3-2 also demonstrates that for a given concentration of potassium ions, xanthan/salt controls possess a much higher viscosity than do HPAM/salt controls. However, the difference between the retained viscosity profile of the xanthan/permanganate mixture and the xanthan/salt control is much less than that between the HPAM/permanganate and HPAM/salt control, which may indicate that permanganate chemistry played a relatively smaller role in xanthan solution viscosity decrease.

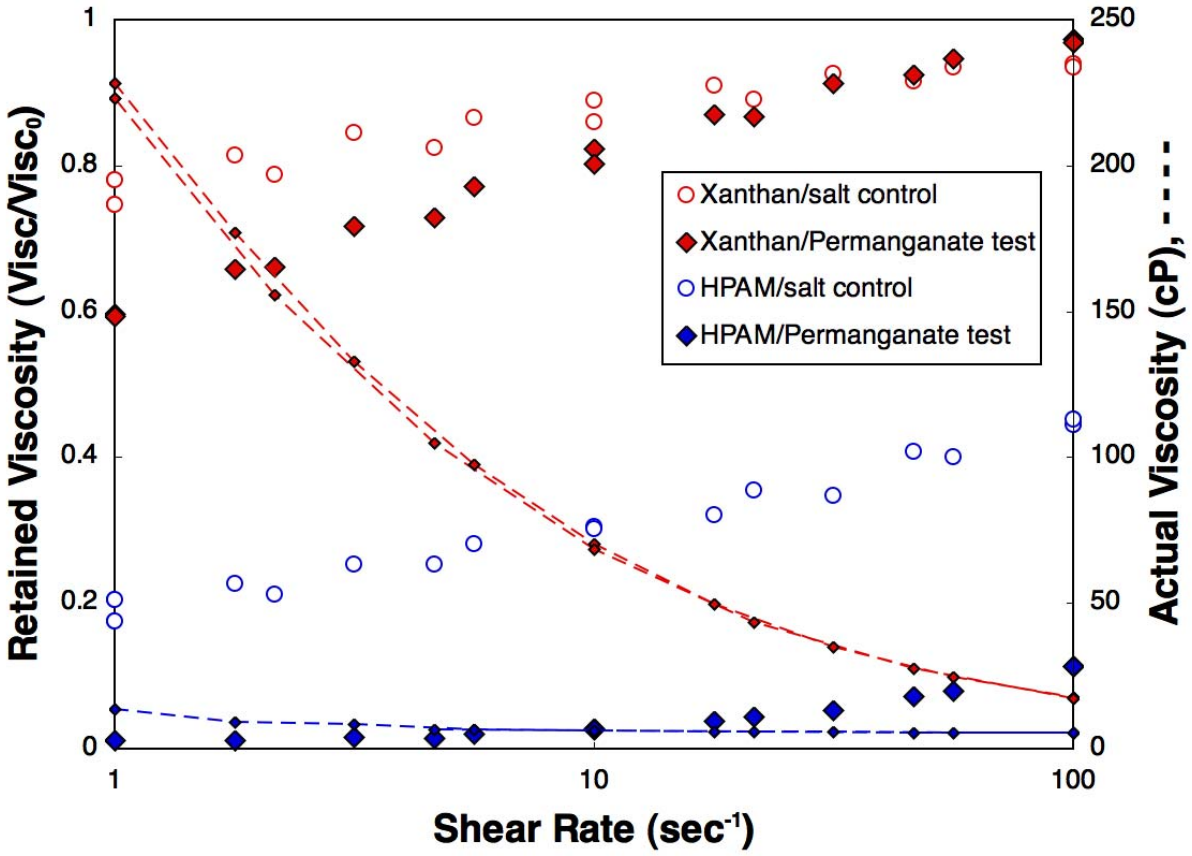

Figure 3-2: *Normalized viscosity (expressed as the ratio of 72-hour to initial viscosity) on the left-hand y-axis and actual viscosity (represented by connected smaller symbols) on the right-hand y-axis versus shear rate for 1600 mg/L polymer/$KMnO_4$ experiments; all data taken after 72 hours. Xanthan experiments are shown in red; HPAM experiments are shown in blue. Note the log scale of the x-axis. Figure modified from Smith et al., 2008.*

Figure 3-3 shows the viscosity response of 1600 mg/L xanthan and HPAM solutions to 72 hours of exposure to persulfate oxidant. While xanthan solutions still display some shear-thinning character, actual viscosity values are reduced below 8 cP at all shear rates, in contrast to the high viscosities retained by xanthan solutions in the presence of permanganate. HPAM solutions show little evidence of shear-thinning behavior and are essentially reduced to water-like viscosity, as also occurs after permanganate exposure. Interestingly, unheated polymer/persulfate mixtures also show drastically reduced viscosity in comparison to polymer/salt control solutions. This result suggests both that exposure to activated persulfate and the resulting host of free radical reactants has a negative effect on polymer viscosity, and that unactivated persulfate can also significantly degrade the polymer molecules or otherwise reduce viscosity.

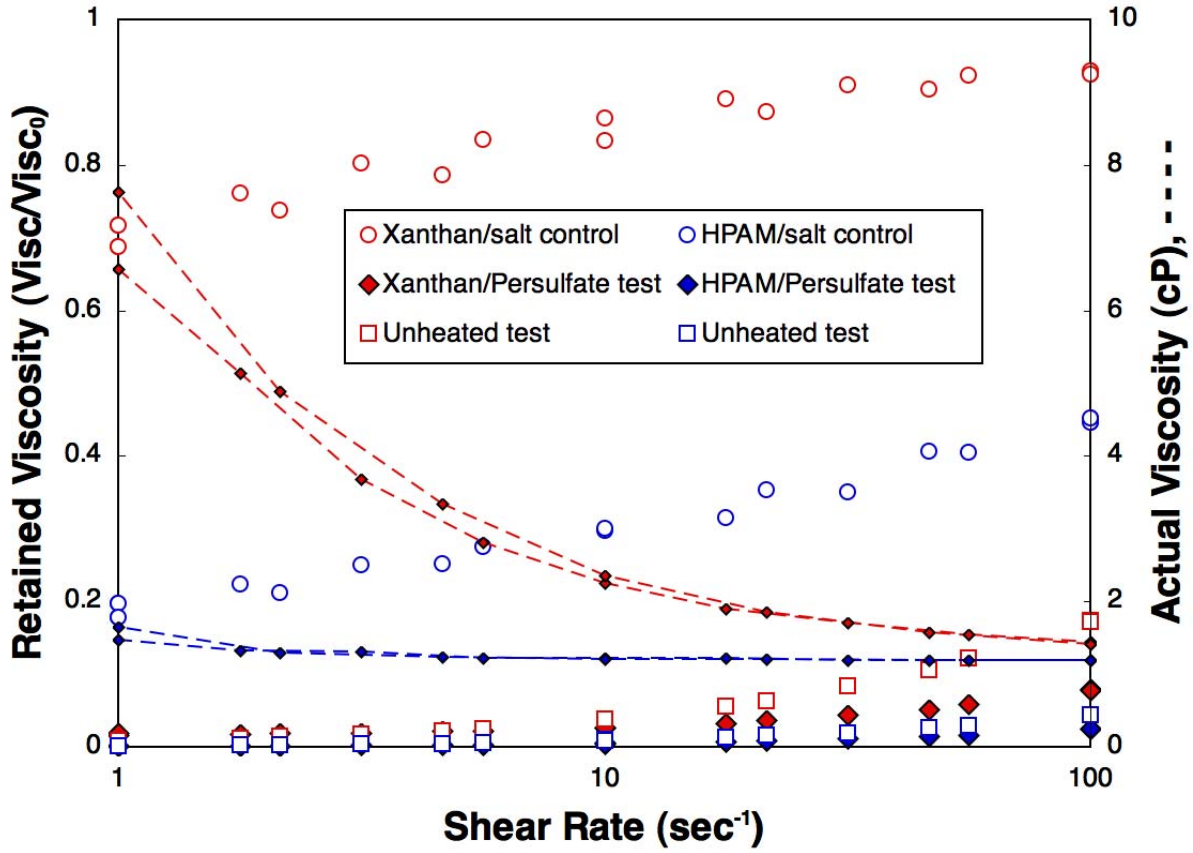

Figure 3-3: *Normalized viscosity (expressed as the ratio of 72-hour to initial viscosity) on the left-hand y-axis and actual viscosity (represented by connected smaller symbols) on the right-hand y-axis versus shear rate for 1600 mg/L polymer/$Na_2S_2O_8$ experiments; all data taken after 72 hours. Xanthan experiments are shown in red; HPAM experiments are shown in blue. Note the log scale of the x-axis. Figure modified from Smith et al., 2008.*

Although persulfate is an attractive oxidant choice due to its reactivity toward a wider class of contaminants and lack of solid reaction byproducts, neither xanthan nor HPAM polymer appears to be able to withstand exposure to this oxidant without losing most or all of the polymers' original solution viscosity. Thus, only the combination of xanthan polymer and permanganate oxidant can be recommended for further polymer/oxidant experimentation, based on that mixture's excellent viscosity retention properties. If particular molecular structures are identified to be resistant to activated persulfate oxidation, perhaps polymers possessing similar structures may then be more chemically compatible with persulfate oxidant.

Oxidant Demand

HPAM polymer, which experienced near-complete loss of viscosity after exposure to both permanganate and persulfate oxidants, demonstrated less than 10% overall oxidant consumption in both cases, as shown in Figure 3-4. For the case of both oxidants, nonproductive consumption was higher for xanthan than for HPAM. More oxidant was retained in

xanthan/permanganate mixtures than in xanthan/persulfate mixtures, in keeping with the higher viscosity retention also observed for xanthan/permanganate solutions. For the two formulations of xanthan, permanganate oxidant consumption ranged between 5 and 25% of the available mass, and appeared to be loosely related to initial xanthan concentration. Unfortunately, polymer concentrations could not be concurrently monitored, as the strong color of the permanganate interfered with the reaction and color changes used for colorimetric quantitation of xanthan content (Dubois et al., 1956), and thus the reaction stoichiometry cannot be determined. However, many permanganate/contaminant reactions proceed on scales of minutes to hours; because the oxidant demand posed by xanthan appears to react on a slower timescale, we hypothesize that xanthan demand for polymer does not interfere with destruction of our test contaminant.

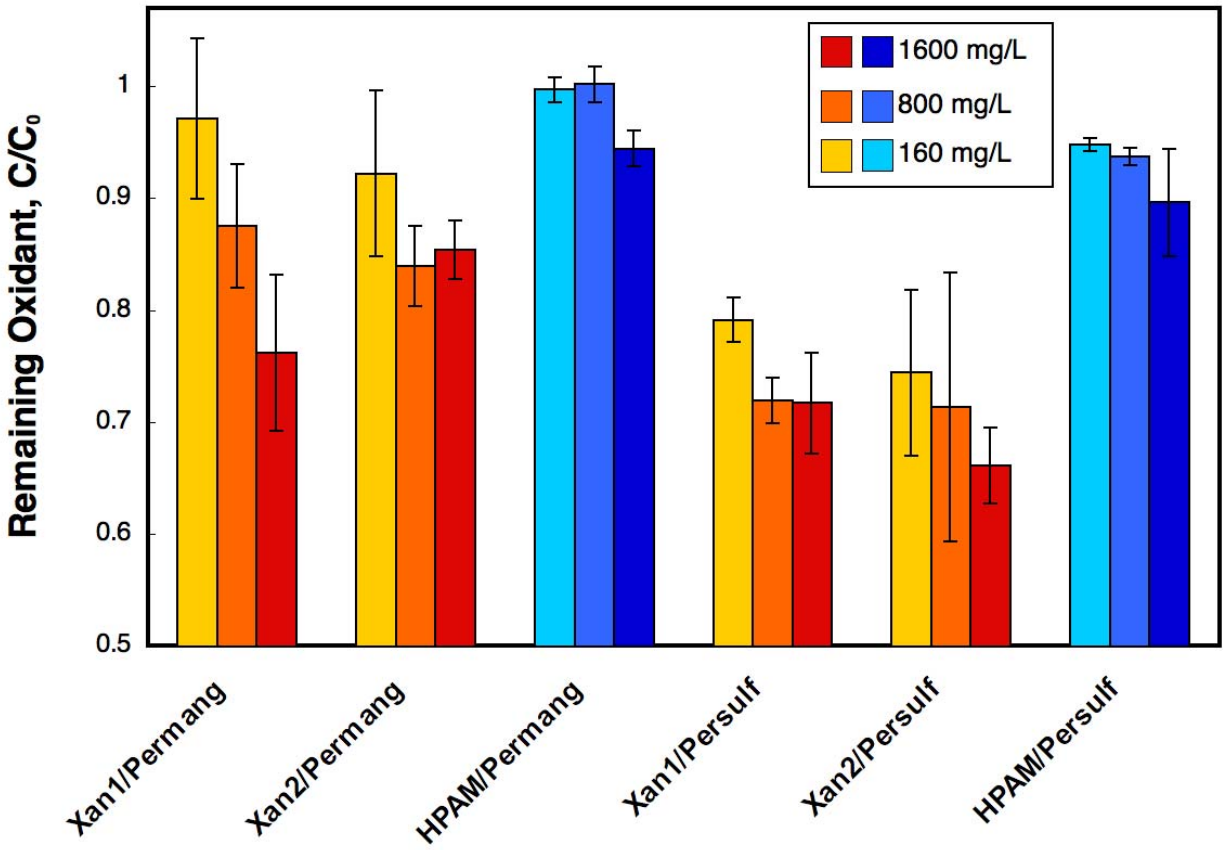

Figure 3-4: *Normalized oxidant concentration remaining after 72 hours of polymer/oxidant exposure. Error bars represent propagated standard errors. "Xan1" and "Xan2" represent Keltrol T® and Xanvis® xanthan formulations (CP Kelco), respectively, while "HPAM" represent Superfloc A-130 high molecular weight formulation (Cytec, Inc.). Figure modified from Smith et al., 2008.*

PCE/$KMnO_4$ Oxidation Rate

Only xanthan/permanganate mixtures were subjected to contaminant oxidation rate experiments. Three initial xanthan concentrations (1600, 800, and 160 mg/L, as in previous batch experiments) were equilibrated with dissolved-phase PCE and monitored for contaminant

destruction. The results of these experiments, as well as the three aqueous-phase PCE/permanganate control experiments, are shown in Figure 3-5. These datasets were statistically indistinguishable from each other.

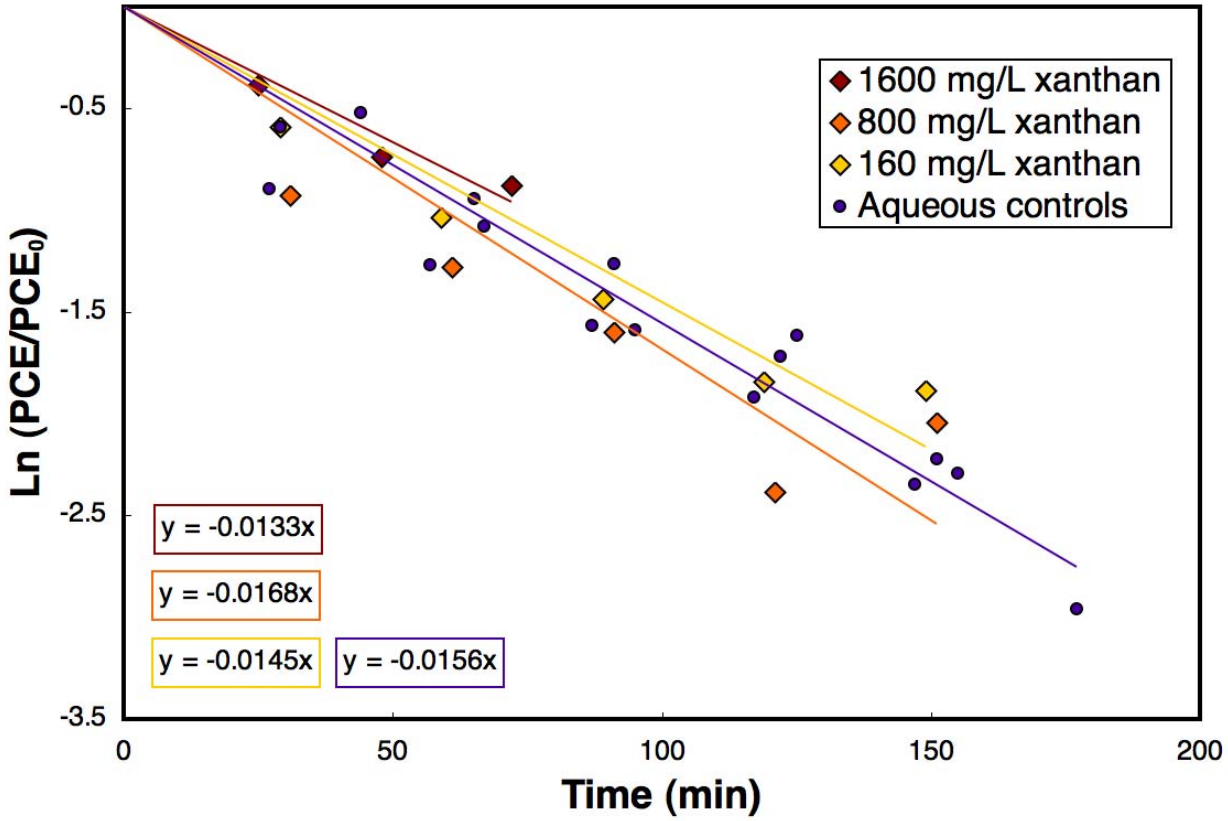

Figure 3-5: *Natural log of remaining PCE (C/C_0) versus time. PCE/$KMnO_4$/xanthan experimental data shown in reds and yellow; data from baseline control aqueous polymer-free experiments shown in purple. Linear regressions (forced through zero) are shown in lower left. Note log scale of y-axis. Figure modified from Smith et al., 2008.*

In order to compare these data to published values of PCE/permanganate reaction rates, the linear regression coefficients (effectively k_{obs} values) were converted into second-order reaction rate coefficients. Because the PCE-permanganate oxidation reaction has been shown to have first-order dependence on both oxidant and contaminant concentrations, the initial oxidation concentration is used to convert k_{obs} into a k_2 value (see Hood et al., 2000). In order to apply this operation to our derived values, we must assume that the PCE oxidation reaction does not depend on polymer concentrations. According to Figure 3-6, the rates derived from these experiments fall well within the range of published values, indicating that PCE oxidation (and not xanthan degradation) should dominate in a three-component system of similar concentrations.

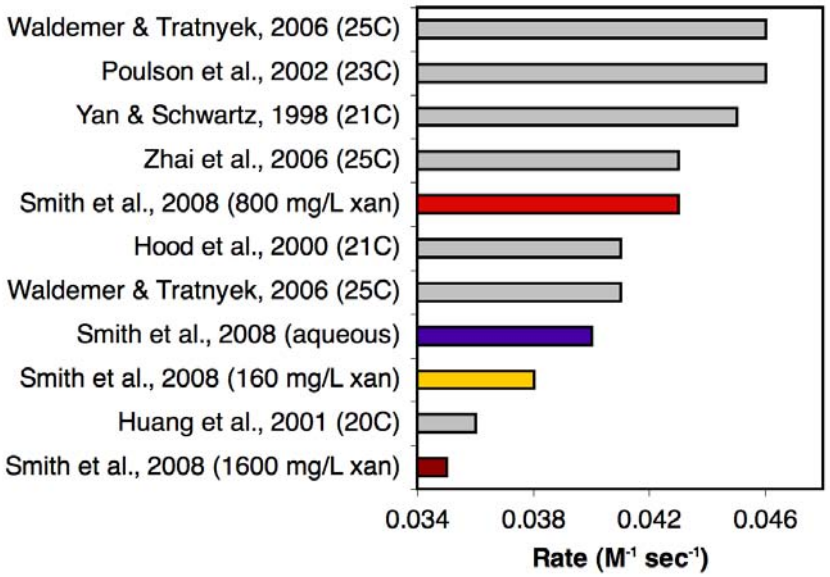

Figure 3-6: *Second-order reaction rate constants for oxidation of PCE by permanganate. Literature values shown in gray; values from this study (conducted at 22±1°C) shown in colors corresponding to Figure 3-5. Figure modified from Smith et al., 2008.*

Although xanthan did not interfere with PCE oxidation, the oxidation reaction appears to have affected the xanthan solution. Over the course of the PCE oxidation experiments (three to four hours), a complete loss of solution viscosity was observed (Figure 3-7), in contrast to the much slower and smaller loss of viscosity observed when PCE was absent from the system. Xanthan/PCE/$KMnO_4$ test batches experienced a more severe pH drop than non-PCE-containing control solutions (Figure 3-7, purple versus orange and yellow symbols), and thus these experiments were repeated at a later date in buffered solutions to determine if pH change affects the magnitude of viscosity loss. Dontsova and Bigham (2005) report pK_a values for xanthan solutions between 3.5 and 5.5, and so xanthan and permanganate stocks were buffered at a considerably higher value (pH ~7) using phosphate solutions. As Figure 3-8 shows, pH-buffered solutions experience very little viscosity loss compared to unbuffered experiments, which decrease to ~1 cP viscosity like that of water after several hours (Figure 3-7). As in the previous experiments, these batches were sampled to confirm complete PCE destruction. The xanthan product literature (CP Kelco, 2004) states that xanthan viscosity should be unaffected by pH changes within a range of 3 to 12; thus these results imply that the xanthan molecule becomes more vulnerable to oxidative reaction under low pH-conditions.

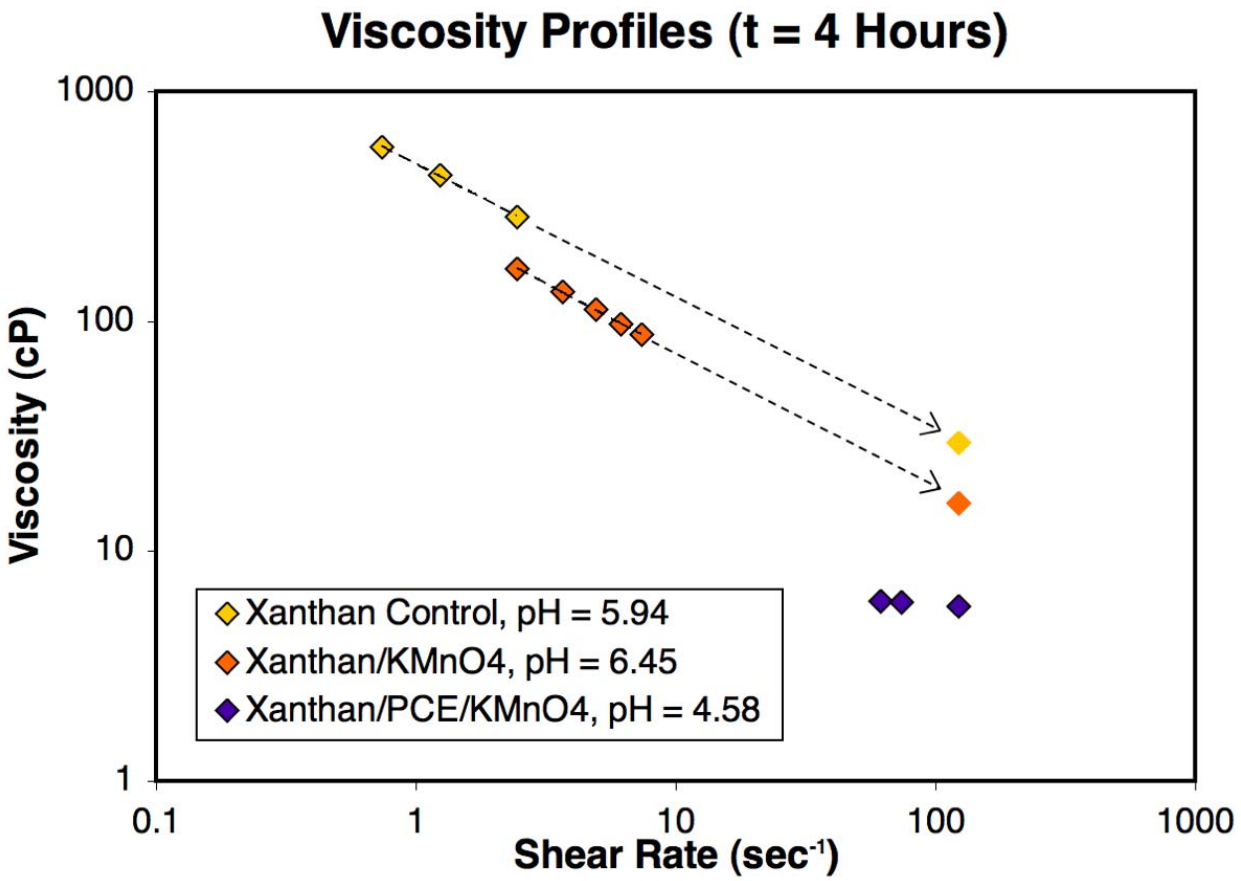

Figure 3-7: *Solution viscosity versus shear rate for $KMnO_4$/PCE oxidation experiments in xanthan solution at 4 hours. "Xanthan Control" data represent xanthan-only control solutions, and "Xanthan KMnO4" data represent xanthan/permanganate solutions. Due to limitations of the Brookfield viscometer, solutions could not be tested at all shear rates, thus regressions were used to extrapolate xanthan control (permanganate-, PCE-free) and xanthan/permanganate control (PCE-free) datasets to a comparable shear rate value for comparison for PCE-containing batches. Regressions are valid here as viscosity profiles have been shown to be log-log linear over this shear rate range. Note log scale of axes.*

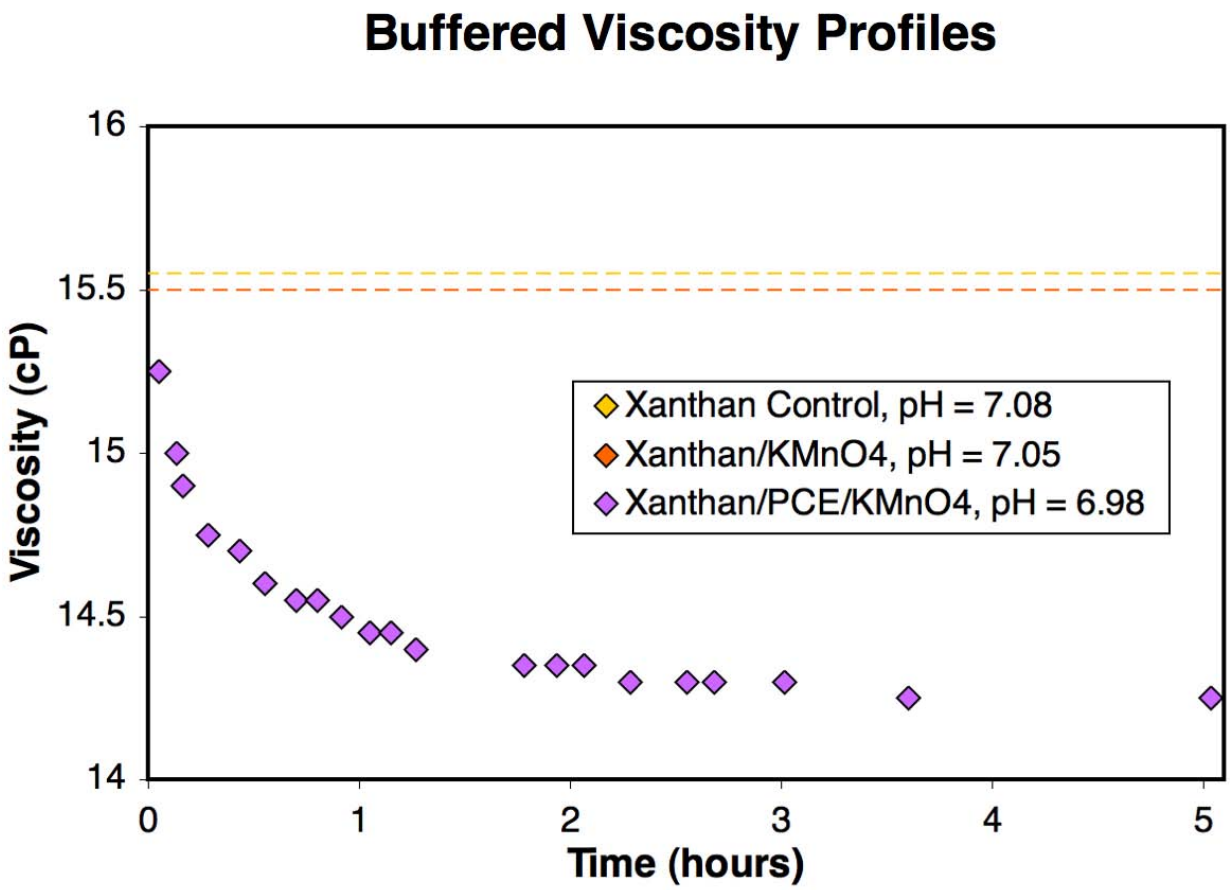

Figure 3-8: *Solution viscosity at fixed shear rate of 14.7 sec^{-1} versus time for buffered $KMnO_4$/PCE oxidation experiments in xanthan solution.*

Mixtures of xanthan and permanganate oxidant must possess a viscosity greater than water in order to better sweep a heterogeneous aquifer region. If a viscous xanthan solution can bring permanganate oxidant into contact with contaminant, then the ensuing complete viscosity loss may be a beneficial consequence of successful contaminant destruction, as the permeability field of the aquifer will then be restored to its original state. The xanthan/permanganate mixture must, however, retain viscosity *en route* to contaminants if it is to achieve this increased sweep. Therefore, if the oxidation of other naturally occurring compounds (collectively termed "natural organic matter," or NOM) also results in complete loss of viscosity, this polymer/oxidant mixture would not enhance oxidant delivery any more than an aqueous injection would. Therefore, column experiments involving natural soils (see Section 4-2) will be needed to determine if the presence of NOM will initiate the same viscosity drop seen when during contaminant oxidation.

Given the outcomes of initial batch viscosity testing, mixtures of xanthan and permanganate were re-tested using a broader range of concentrations. Xanthan polymers of up to 5,000 mg/L strength were tested in combination with permanganate solutions of up to 20,000 mg/L (results shown in Figure 3-9).

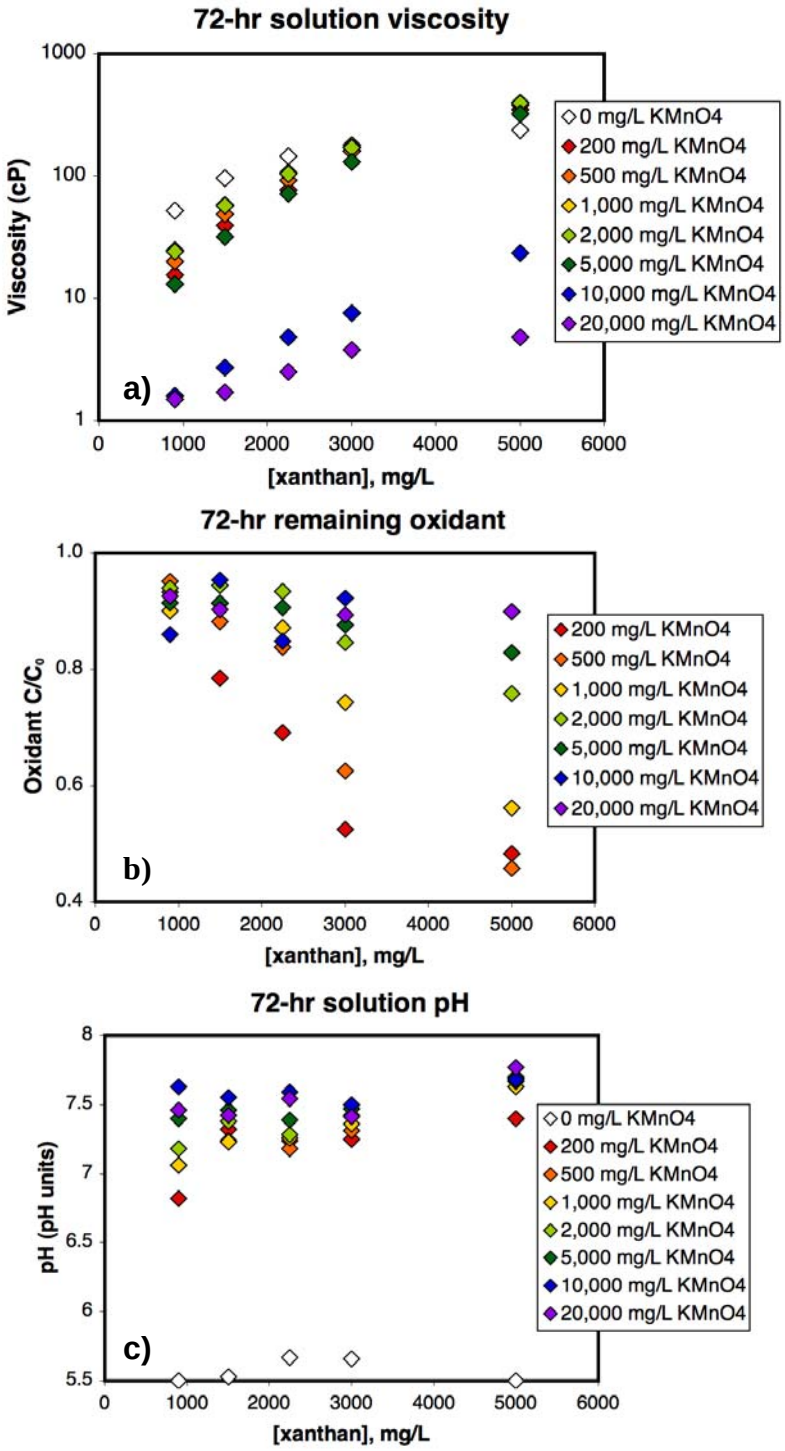

Figure 3-9: *Results of broader xanthan/$KMnO_4$ batch testing: a) solution viscosity (measured at sec^{-1}), b) remaining $KMnO_4$ (expressed as C/C_0), and c) solution pH for various batch combination after 72 hours of xanthan/$KMnO_4$ exposure.*

Figure 3-9a demonstrates that retained solution viscosity is maximized for mixtures of 200 – 2,000 mg/L KMnO4 and ~3,000 mg/L xanthan. At higher xanthan concentrations, solution viscosity actually increases (signifying the formation of a gel), and higher permanganate strengths results in drastic viscosity loss. Oxidant demand/consumption, however, is minimized by using lower concentrations of xanthan polymer (in the 1,000 to 2,000 range, see Figure 3-9b). Data such as these could be of use during the remediation design process.

Polymer/Oxidant Compatibility Test Conclusions

- HPAM polymer does not retain any significant portion of its initial viscosity during 72-hour exposure tests with either permanganate or persulfate oxidant, and is thus chemically incompatible with these oxidants and unsuitable for further polymer-enhanced experimentation.
- Xanthan polymer at "high" concentrations (1600 mg/L) retains a very small (<10%) percentage of its initial viscosity after 72 hours of exposure to activated persulfate oxidant, corresponding to a viscosity of 2-3 cP at an average shear rate of 10 sec^{-1}. This viscosity is only a few times greater than that of water (1 cP) but may be great enough to permit increased crossflow in formations with a low degree of heterogeneity. Further investigation would be required to determine if this viscosity level and degree of remaining shear-thinning behavior would permit enhanced aquifer sweep, or if other polymers may prove more resistant to and more compatible with persulfate exposure.
- Xanthan polymer retains a large percentage of its initial viscosity after 72 hours of exposure to permanganate oxidant, with accompanying low to moderate levels of non-productive oxidant demand. Thus, this polymer/oxidant combination is deemed chemically compatible and is selected for further larger-scale experimentation for polymer-enhanced chemical oxidation.
- Unbuffered xanthan solutions experience near-complete loss of viscosity during oxidation of PCE contaminant by $KMnO_4$ in batch experiments. Buffering of the solutions to prevent pH decrease during contaminant oxidation can minimize this viscosity loss.

3.3 Bioamendment Batch Tests

Batch tests were performed to assess the compatibility of xanthan and HPAM polymers with an anaerobic microbial consortium proven for use in bioremediation settings. The KB-1 microbial consortium used in these experiments contains dehalogenating bacteria capable of the overall dechlorination reaction (Bradley, 2003):

$$PCE\ (+\ 2e^-) \rightarrow TCE\ (+\ 2e^-) \rightarrow DCE\ (+\ 2e^-) \rightarrow VC\ (+\ 2e^-) \rightarrow ethene,$$

in which chlorinated solvents are biotransformed under highly reducing conditions through the daughter products trichloroethene, dichloroethene, and vinyl chloride, into a mineralized and nontoxic end-product. Depending on the type of bioremediation treatment, nutrients and/or electron donors may be injected into an aquifer to drive the subsurface to the reducing conditions necessary to encourage growth of native dechlorinating bacteria, or enriched cultures of bacteria may be injected to spur desired biodegradation. In either scenario, a more thorough distribution of injected biostimulants or microbes should lead to increased effectiveness and efficiency of

treatment. As a first step towards demonstrating such increased effectiveness, polymer/bioamendment batch tests are required.

Specific batch experiments were performed to understand the effects of the polymers (if any) on microbial survival and continued ability to degrade chlorinated contaminants. Primary criteria for polymer/microbe compatibility included comparisons of PCE biotransformation rates in polymer solution as compared to those in polymer-free medium, and the stability of polymer solution viscosity through time. Polymer/microbe experiments that successfully meet these criteria and demonstrate viable biodegradation of the test contaminant (PCE) are deemed chemically stable combinations. Such a polymer would be recommended for further polymer-enhanced bioremediation studies, involving the polymer either as a donor/nutrient delivery enhancement agent (for biostimulation applications) or as a microbial delivery agent (for bioaugmentation applications).

Additional microcosm experiments were also initiated to test whether these microbes can utilize polymers as a source of electrons (a necessary component for the dehalogenation reaction shown above). In nature, hydrogen is assumed to be the most frequently used electron donor, but mixed cultures have been shown to rely on a variety of compounds such as methanol, lactate, benzoate and propionate (Maymo-Gatell et al., 1995; Yang and McCarty, 1998; Bradley, 2003). Experimental studies by and personal communication with Dr. Elizabeth Edwards (University of Toronto, 2009) do not support the hypothesis that dehalogenating bacteria are capable of degrading or fermenting a larger and more complex molecule (such as the polymers involved in this work), but it is unknown if other microbes naturally present in the subsurface may transform these molecules into a form more bioavailable to the dehalogenating species.

Materials and Methods

In early rounds of testing, polymer solutions were prepared in artificial groundwater and then inoculated with microbes. Biodegradation reactions proceeded very slowly under such conditions, and eventually polymer solutions prepared in anaerobic nutrient medium (see Table A-2) identical to that in which the KB-1 microbial stock had been grown were substituted. These polymer solutions were prepared by directly adding powdered polymers to a vortex of anaerobic medium created with an overhead stirrer, within an anaerobic chamber. As in previous batch tests, the polymer solutions were stirred for 2-3 hours and then allowed to rest for at least 12 hours before microcosm assembly. Xanthan stock solutions were prepared at a concentration of 1,250 mg/L, such that when combined with microbial inoculum in 4:1 ratios, an effective xanthan concentration of 1,000 mg/L is achieved. This relatively high polymer strength was utilized so that decreases in viscosity due to polymer-microbe interactions, polymer-feed interactions, or polymer-medium interactions would still yield a measurable solution viscosity. The response of HPAM solutions to added salts (data presented in Figure 3-1) was used to predict an effective polymer concentration (955 mg/L) that would yield a solution of similar viscosity to xanthan, when prepared in anaerobic medium.

Aliquots of Colorado School of Mines' KB-1 consortium (originally obtained from Dr. Elizabeth Edwards, University of Toronto, 2004) were used in all microcosm experiments. The KB-1 consortium consists of methanogens, sulfate reducers, and reductive dechlorinators capable of complete PCE mineralization (Duhamel et al., 2002). These anaerobic cultures have been maintained in an anaerobic nutrient medium (see Table A-2) and fed regularly with either PCE

or TCE, and methanol as an electron donor. For polymer compatibility testing purposes, monitored PCE and byproduct (TCE, DCE, VC) concentrations serve as a proxy for the continued activity of the culture. A decrease in the PCE concentration coupled with increases in the daughter compounds shows that the culture is still active.

Anaerobic microbes collected by Colorado School of Mines student Jackson Lee in 2009 from a sludge holding tank at a beer brewery were also utilized in select microcosm experiments. These microbes (referred to as the "NBB" consortium) are known to metabolize large organic carbon molecules present in brewery waste, and were therefore selected to serve as a gross analogue for the wide variety of possible anaerobes that may be capable of degrading polymer molecules such as xanthan or HPAM in a reduced aquifer setting. The addition of these supplementary microbes provides a measure of expected polymer "lifespan" under more diverse microcosm conditions. In addition, polymer degradation by NBB microbes may produce additional hydrogen or other electron donor species. The NBB microbes were grown for several months in nutrient medium initially amended with 500 mg/L xanthan polymer before use in batch experiments.

Batch test matrices were assembled in an anaerobic chamber according to the conditions outlined in Table 3-2. The first six experimental conditions were conducted with four replicate microcosms; the remaining conditions utilized two to three replicates. These first six experimental conditions were designed to evaluate PCE dechlorination rate and/or polymer stability in the following environments:

1. KB-1 microbes supplied with the traditional electron donor (methanol), in polymer solution as compared to polymer-free conditions.
2. KB-1 microbes denied the traditional electron donor (methanol), in polymer solution as compared to polymer-free conditions.
3. KB-1 denied the traditional electron donor (methanol) but supplied with additional NBB anaerobes capable of metabolism of a wider range of carbon sources.

The purpose of Environment 1 was to simply determine if the polymer had any effect, positive or negative, on the rate of contaminant biotransformation as compared to the rate measured in control medium. This condition comprised the most basic and most important test of polymer/microbe compatibility in terms of polymer suitability for larger-scale polymer/bioamendment experimentation. Environment 2 served to elucidate whether "raw" polymer molecules could be directly utilized by the KB-1 consortium as a source of electrons to fuel the PCE dechlorination reaction. Continued PCE degradation in the absence of methanol would have constituted proof that another electron donor was being utilized; the polymer-free condition served to prove that polymer, and not another constituent of the nutrient medium, was the source of such electrons. In addition, viscosity loss in the polymer-containing experiments would also have indicated utilization or modification of the polymer molecules. Environment 3 tested another derivative of the Environment 2 scenario, wherein the NBB anaerobes (capable of fermentation of large organic molecules) could provide the dechlorinating bacteria with more bioavailable electron donor sources as a result of polymer degradation.

Table 3-2: *Experimental conditions for polymer/bioamendment batch experiments.*

Description	Polymer[a]	PCE	Methanol	KB-1 Microbes	NBB Microbes
Base (test)	x	x	x	x	------
Base (control[b])	------	x	x	x	------
e- donor (test)	x	x	------	x	------
e- donor (control[b])	------	x	------	x	------
e- donor/NBB (test)	x	x	------	x	x
e- donor/NBB (control[b])	------	x	------	x	x
Viscosity/No Feed(controls[c])	------	x	------	x	± x
Feed (controls[c])	± x	x	± x	------	------
Poly/Medium (controls[c])	± x	------	------	------	------

[a]*All polymer solutions were prepared in the same nutrient medium in which KB-1 microbes were grown.*
[b]*All polymer-free control solutions contained nutrient medium in lieu of polymer.*
[c]*All other polymer-containing controls were diluted with nutrient medium to achieve equal polymer strength as in equivalent test conditions.*

Autoclaved 120- or 160-mL serum bottles, PTFE-lined rubber stoppers, aluminum crimp tops, polymer solutions, and ethanol-rinsed tools were kept in the anaerobic chamber for at least one day before microcosm assembly. Depending on serum bottle size, total liquid contents were fixed at 60 or 80 mLs (approximately half the serum bottle volume) so that sufficient headspace would remain for sampling purposes. Polymer solutions (or medium in the case of some controls) were always added to the serum bottles first. The microcosms were inoculated with bacteria in random order from the same well-shaken inoculum bottle, and then hand shaken and stoppered (but not crimped). The anaerobic nutrient medium contained an oxygen-sensitive indicator compound (resazurin) that remains pink in the presence of oxygen, but turns clear under anaerobic conditions. If the microcosms showed traces of pink color after several hours, a few drops of 10 mM sodium dithionite (an oxygen-scavenging) solution were added to ensure truly anaerobic conditions before the tops were crimped and the batch experiments were removed from the chamber. This step was usually necessary.

After removal from the anaerobic chamber, microcosm headspaces were analyzed to obtain a baseline level for all analytes, and sparged with ultra-high purity nitrogen gas if high levels of chlorinated compounds were detected as carryover from KB-1 inoculum. PCE or PCE/methanol feed was then gravimetrically added and recorded. Concentrations of PCE were kept below at or below solubility (~120 mg/L; 7.6 µL in 120-mL serum bottles and 10 µL in 160-mL serum bottles) and methanol (44 µL for 120-mL serum bottles and 59 µL for 160-mL serum bottles) was added to ensure 10 meq per every 1 PCE meq. Microcosms were then continuously shaken on a shaker table, shielded from light, for the first week or until initial PCE concentrations stabilized (determined by daily headspace analysis). After this period, the microcosms were stored in a horizontal position (such that the underside of the bottle stopper was in contact with liquid, not headspace), hand shaken once per day and analyzed for chlorinated compounds on a weekly basis.

Quantitative monitoring of PCE, TCE, DCE, vinyl chloride, ethene, and methane, as well as qualitative monitoring of methanol concentration, was conducted by gas chromatographic (GC) analysis. A Shimadzu GC-17A equipped with a flame ionization detector was used to analyze a manually injected 200 µL headspace sample. Headspace analysis was selected over aqueous sampling to avoid issues of column contamination from large polymer molecules. The inlet was set to a split ratio of 8:1 with helium as the carrier gas and air as the makeup gas. The injector temperature was set at 250°C and the detector at 280°C. The oven was set to 60°C and held for three minutes, then ramped to 125°C at a rate of 10.5°C/min and held for 0.5 minutes. An oven equilibration time of one minute was used between samples. A Zebron® column (Phenomenex, Torrance, CA) was used, which allowed for excellent separation among PCE, TCE, DCE, and vinyl chloride peaks but slight overlap between ethene and methane peaks if methane concentrations were high.

Gas calibration standards were made for PCE, TCE, and cis-DCE using a gravimetically prepared stock solution of all three compounds dissolved in pentane. A calculated volume of stock solution was injected into stoppered serum bottles and allowed to completely vaporize. 200-µL gas samples were then used to create a four-point calibration curve. Gas standards were similarly created for ethene (Air Liquide, Houston, TX), methane, and vinyl chloride (Matheson Tri-gas, Santa Fe, NM). Check standards were run after approximately every 30 samples, and calibrations were re-run if check standards varied by more than 15% of their calculated value. Equilibrium Partitioning in Closed Systems EPICS-style experiments were conducted according to the method of Gossett (1987) to determine if the Henry's Law constants determined by the same author for PCE, TCE, DCE, and VC in water were appropriate for use in xanthan-containing experiments, and our experimental values agreed well (data not shown) with the water-based values, provided that microcosms were given ~48 hours of equilibration time. HPAM-containing experiments were then allowed 48 hours of equilibration after feeding, and as good mass balances resulted, no further Henry's Law experiments were performed. Laboratory temperatures were monitored during GC analysis and temperature-dependent dimensionless Henry's Law coefficients (in Table 3-3) were used to convert measured gas concentrations to aqueous concentrations.

Table 3-3: *Dimensionless Henry's Law constants, from Gossett (1987)*

	20°C	**21°C**	**22°C**
PCE	0.550	0.580	0.612
TCE	0.299	0.315	0.332
DCE	0.123	0.129	0.135
VC	0.909	0.941	0.974

Early progress reports noted our efforts to analyze microcosms for short-chain fatty acids produced as a possible result of polymer degradation, using high-performance liquid chromatography (HPLC). Unfortunately, no reliable methods of polymer precipitation or removal were found that could prevent irreparable clogging of HPLC columns and thus this type of analysis had to be abandoned.

At the end of each round of experiments, the batch microcosms were sacrificed in order to analyze solution viscosity and pH. Polymer control batches were monitored first to provide a baseline value for solution viscosity, using the Brookfield bench-top viscometer. Due to wide variations in final solution viscosity and the inherent limitations of the Brookfield instrument, not every microcosm could be measured at every available shear rate, but every possible viscosity/shear rate datum was collected.

Results and Discussion

Two rounds of xanthan-containing experiments and one round of HPAM-containing experiments were successfully completed.

Xanthan/Microbe Batch Experiments, Round One

These results date from the earliest round of successful experiments, inoculated with a KB-1 culture initiated in September of 2004. Because these experiments were conducted before the inclusion of NBB microorganisms was considered, these experimental results do not include variations with NBB microbes. For the sake of clarity, certain analytes (TCE and ethene) are omitted from the following plots. Ethene peaks were often masked by large methane peaks, while TCE was always quickly converted to DCE.

Comparative Dechlorination Rates

The results of batch experiments containing only KB-1 microorganisms, fed with both PCE and methanol electron donor, are shown in Figure 3-10. For both the xanthan-containing test case and the corresponding polymer-free control, the first dose of PCE/MeOH feed was completely dechlorinated to ethene in approximately four weeks. However, only the KB-1 microbes in the xanthan base test experiments (Figure 3-10a) were able to completely dechlorinate a second dose of PCE/methanol feed. The polymer-free base control experiments appeared to stall mid-way through the dechlorination process, as indicated by the level DCE data. Addition of extra methanol (see pink arrow in Figure 3-10b) may have spurred some conversion of DCE to VC, but these control microcosms were unable to achieve complete conversion of VC to ethene even after an additional two weeks. These results demonstrate that xanthan polymer does not play any inhibitory role in the microbially mediated biotransformation of PCE to ethene, and may actually support this process in some way. The final pH of the xanthan base test experiments was lower than that of the polymer-free control batches and most of the xanthan control batches (Table 3-4); this low pH would indicate an abundance of hydrogen (the preferred electron donor), but it is unknown if any of this hydrogen was derived from polymer breakdown.

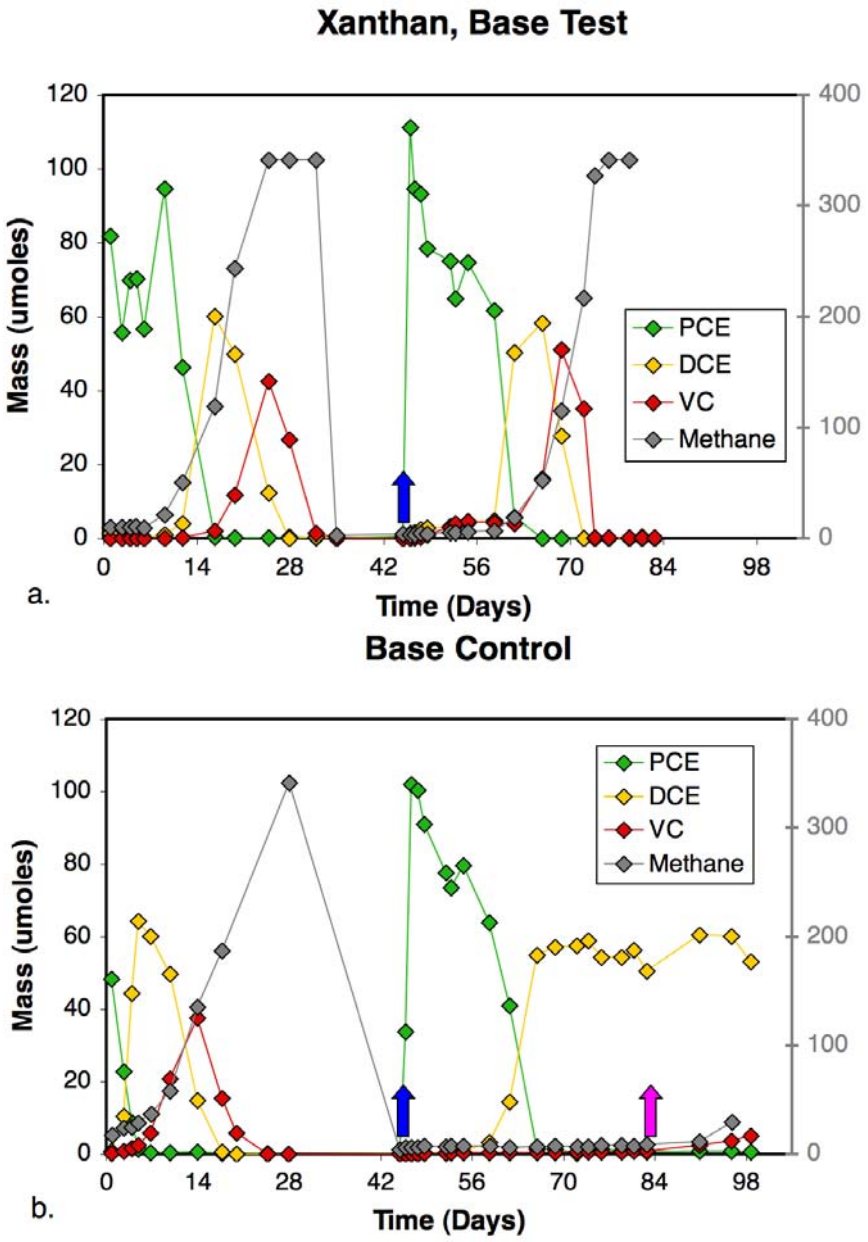

Figure 3-10: *Total (liquid- + gas-phase) analyte mass versus time for xanthan base experiments (a) and nutrient medium base control experiments (b), from round one. Note that methane concentrations (shown in gray) refer to the right-hand y-axis. Blue arrows indicate second round of PCE/methanol feed addition; pink arrow indicates addition of methanol only. Data points shown are averages of four replicates.*

Table 3-4: *Final pH values for xanthan/microbes batch, round one*

Sample Description	Replicates	Final pH
Xanthan, Base Test	4	6.71
Base Control	*4*	*7.26*
Xanthan, e- Donor Test	4	6.74
e- Donor Control	*4*	*7.26*
Xanthan Polymer Control	2	7.16
Xanthan Feed Control	2	6.97
Xanthan Viscosity Control	3	7.06
bulk xanthan stock	2	7.62
Medium Control	*1*	*7.71*
Medium Feed Control	*2*	*7.69*
Medium Viscosity Control	*3*	*7.36*
bulk medium stock	*2*	*7.82*

The results of xanthan/microbe experiments in which methanol was omitted are shown in Figure 3-11. These test conditions were intended to explicitly determine whether KB-1 microbes would derive some benefit (potentially in the form of additional electron donor material) from the presence of xanthan, as opposed to polymer-free nutrient medium. The data do not show a conclusive benefit of xanthan polymer in the absence of methanol, as complete dechlorination of one PCE feed dose was not observed over a period of more than 3.5 months, as opposed to a period of one month for methanol-containing batches. However, DCE was completely converted to VC in xanthan-containing batches (Figure 3-11a), while polymer-free control experiments achieved only small amounts of DCE-to-VC conversion (Figure 3-11b). The addition of methanol (indicated by pink arrows in Figure 3-11) appeared to reinvigorate the dechlorination process for the xanthan batch, but did not have as striking an effect in the following two weeks for the polymer-free condition. This reactivation of dechlorination in Figure 3-11a would seem to indicate that the microcosms were electron donor-limited, and that xanthan polymer is not a complete substitute for smaller and more bioavailable methanol molecules. As was the case for methanol-containing base experiments, however, the pH of the xanthan-containing condition was significantly lower than that of the polymer-free control at the time of microcosm sacrifice.

Concentrations of methane (an undesirable byproduct) in these experiments show increasing trends with progression of PCE conversion (see the latter weeks of Figure 3-10a versus 3-10b), and with polymer presence as opposed to medium-only batch tests (Figure 3-10a versus 3-11b). Interestingly, KB-1 microbes produce larger quantities of methane when in contact with xanthan polymer as compared to nutrient medium solutions. The final methane concentrations of feed-free "Viscosity controls," containing only microbes in either xanthan or nutrient medium matrix, are plotted alongside "electron donor" results in Figure 3-11 and show an order of magnitude or greater increase in methane production in xanthan solution. This average of ~300 μmoles methane is on the order of that produced by actively dechlorinating microbes supplied with methanol as shown in Figure 3-10.

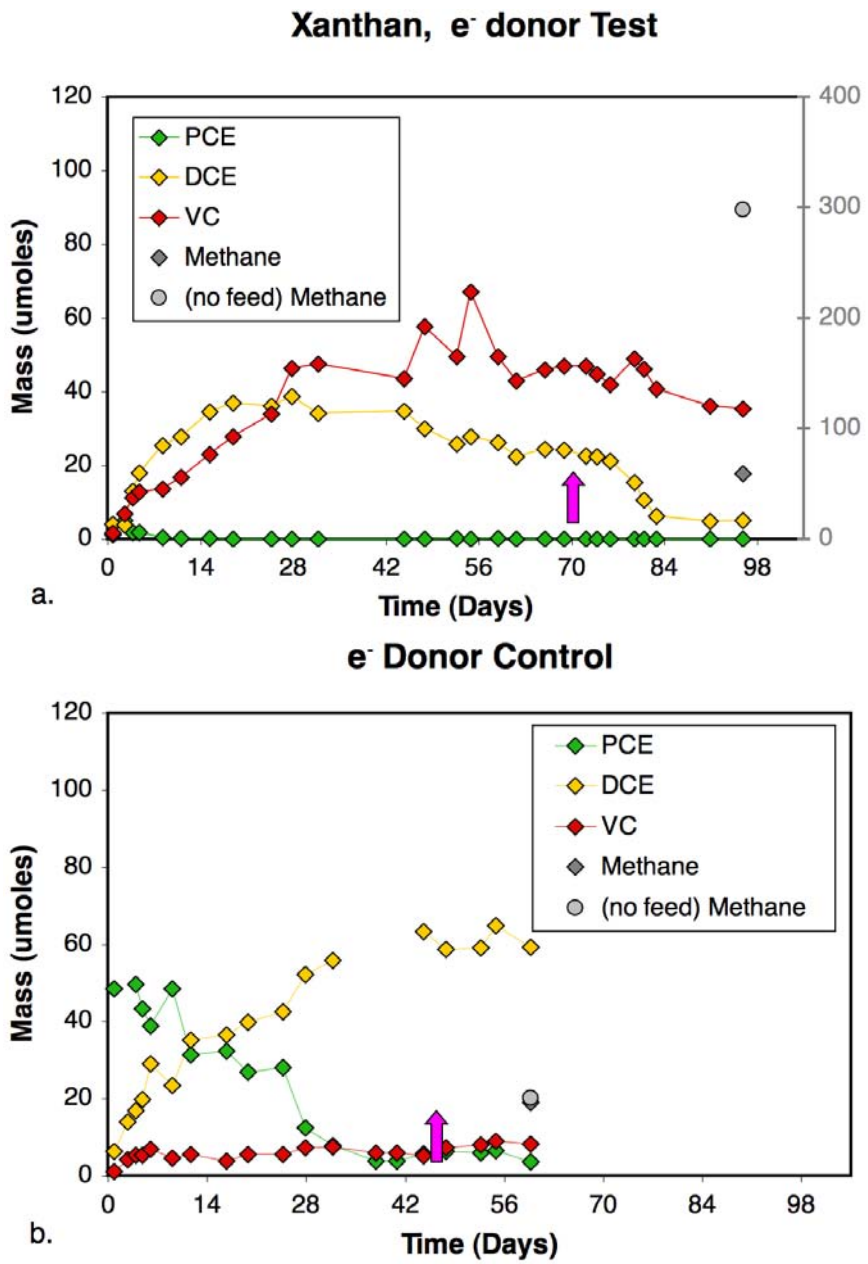

Figure 3-11: *Total (liquid- + gas-phase) analyte mass versus time for xanthan e-donor experiments (a) and nutrient medium e- donor control experiments (b), from round one. Note that methane concentrations (shown in gray) refer to the right-hand y-axis for Figure 3.X.a only. Pink arrows indicate addition of methanol only. Data points referred to as "no feed Methane" are final methane measurements taken from "Viscosity control" (i.e., control experiments of either xanthan or nutrient medium containing microbes with no PCE feed). Data points shown are averages of three to four replicates (see Table 3-4).*

Viscosity Retention

The results of viscosity measurements taken on the Brookfield viscometer after sacrificing the xanthan/microbe experiments are shown in Figure 3-12. No significant differences

in final solution viscosity among xanthan-containing experiments are noted, even if the scale of the y-axis is expanded. The xanthan base test condition appears to possess a higher viscosity profile, but the other xanthan-containing batches fall well within the reach of standard deviations for these averages values (standard deviations not plotted to preserve clarity of the figure). Small, naturally occurring variations in polymer solution viscosity are likely responsible for the individual variations in viscosity profiles noted among replicates of the same experimental condition. It should be emphasized that the KB-1 microbes present in the xanthan base test condition completely biodegraded two doses of PCE feed (with methanol) without causing any viscosity loss of the polymer solution. Additionally, the partial dechlorination observed in the xanthan e- donor tests had no effect on the batch viscosity. Although it is unlikely that xanthan solution viscosity would remain so stable in a naturally more diverse subsurface setting, this complete lack of effect on xanthan solution viscosity indicates that KB-1 microbes are likely incapable of degrading xanthan molecules over timescales of several months.

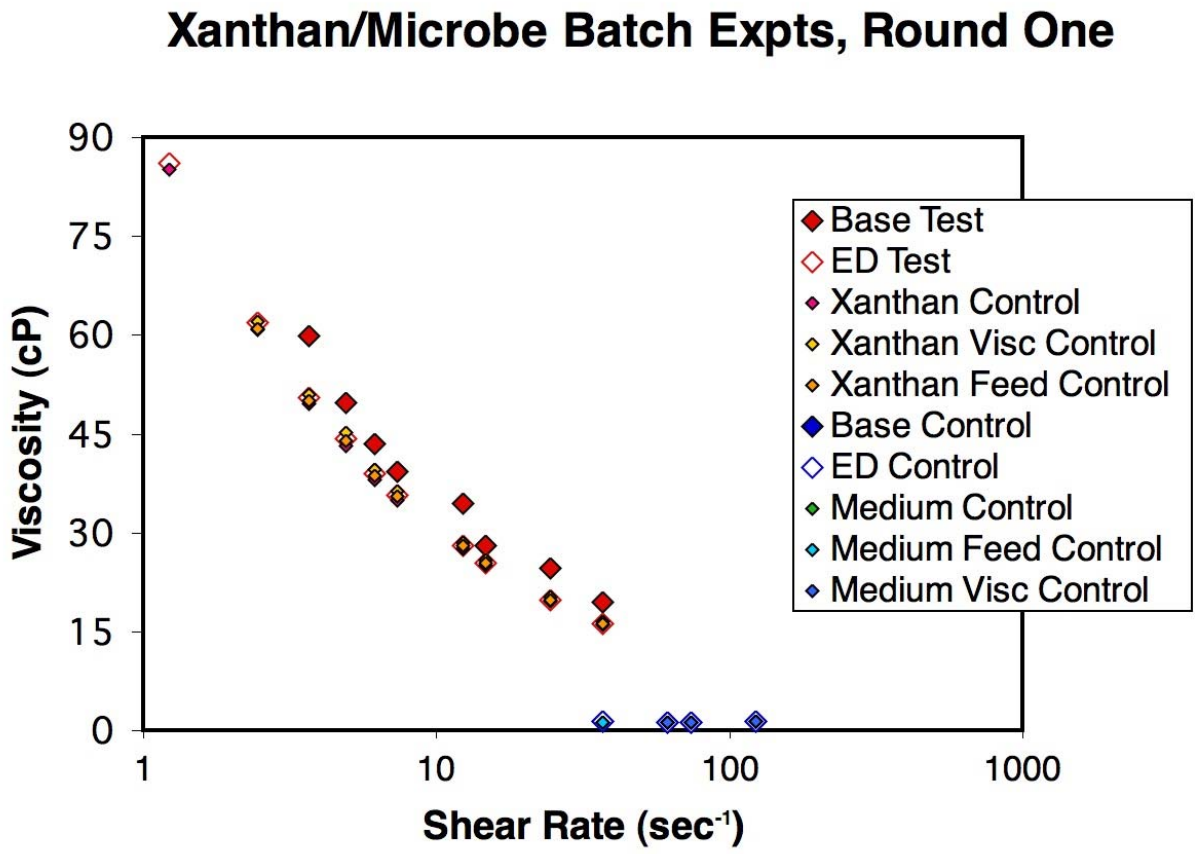

Figure 3-12: *Viscosity versus shear rate for sacrificed xanthan/microbe batch experiments (round one). Experiments containing xanthan polymer are represented in red and orange; experiments containing medium only are represented in blue and green. Data shown are averages of all replicates. Note the log scale of the x-axis.*

Xanthan/Microbe Batch Experiments, Round Two

This round of experiments was conducted six months after the previous xanthan/microbe round, and its microcosms were inoculated with a later KB-1 culture (one initiated in March of 2005). This round of testing was intended to build on the results of the previous round and broaden the dataset by including systems with added NBB anaerobes, and thus the xanthan base test condition was omitted from this round.

Comparative Dechlorination Rates

The results of xanthan/microbe batch experiments containing KB-1 and NBB microorganisms and fed only PCE are shown in Figure 3-13. Neither the xanthan-containing experiments nor the polymer-free controls experienced complete dechlorination of one PCE dose, and after 6.5 months, both conditions had accumulated ~60 μmoles of DCE. PCE is, however, more persistent in the xanthan-containing batch experiments (Figure 3-13a) than in the polymer-free versions (Figure 3-13b). These dechlorination extent is much lower than that observed during round one of xanthan testing. The base control experiments also show stalled behavior with accumulated VC as opposed to DCE (Figure 3-14), and this common lag time may indicate that this particular KB-1 inoculum is simply slower to dechlorinate than the previous September, 2004 culture. In fact, no experiment (xanthan- or nutrient medium-based) in this series of experiments displayed complete PCE biotransformation to ethene, and those experiments inoculated with KB-1 only (and not additional NBB, Figure 3.14) show increased levels of VC. These results overall indicate an unsatisfactory starting KB-1 inoculum, as both xanthan-containing and polymer-free experimental conditions displayed unsatisfactory dechlorination progress.

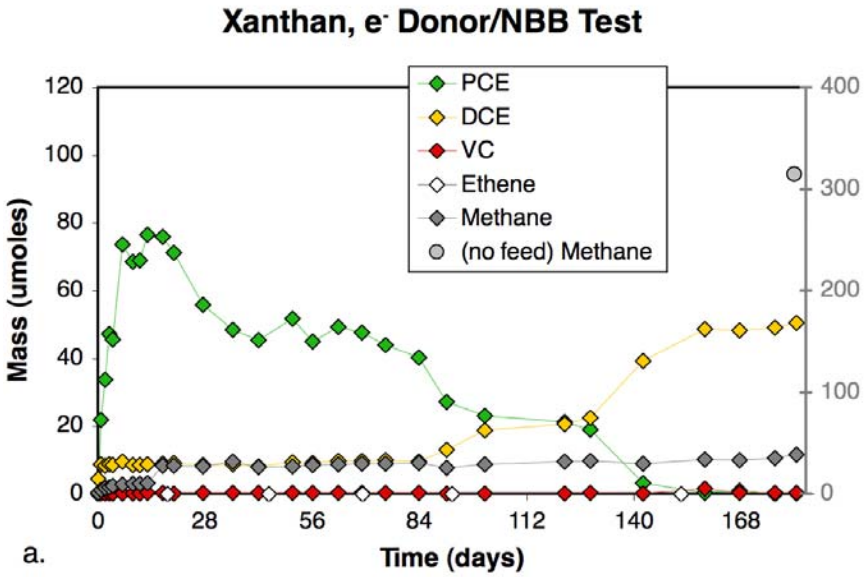

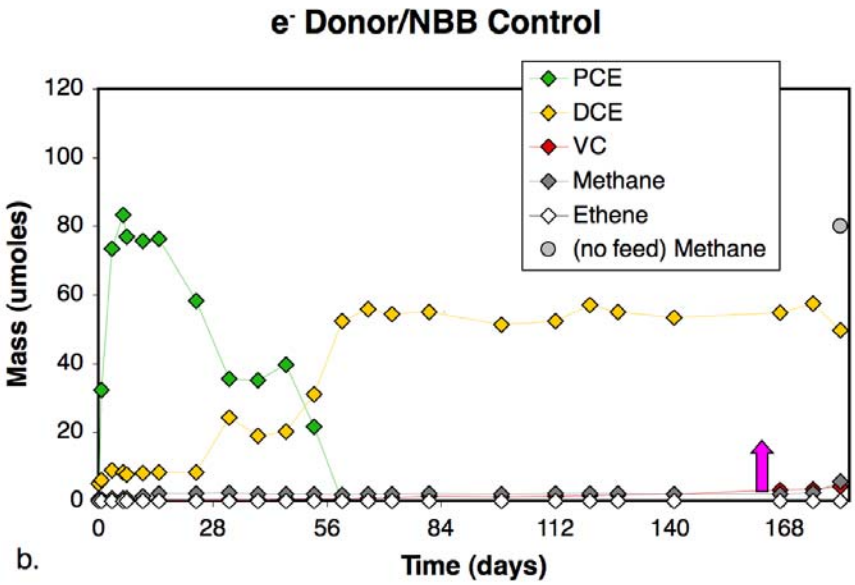

Figure 3-13: *Total (liquid- + gas-phase) analyte mass versus time for xanthan e- donor/NBB experiments (a) and nutrient medium e- donor/NBB control experiments (b), from round two. Note that methane concentrations (shown in gray) refer to the right-hand y-axis for Figure 3.A.a only. Pink arrow indicates addition of methanol only. Data points referred to as "no feed Methane" are final methane measurements taken from "NBB/Viscosity control" (i.e., control experiments of either xanthan or nutrient medium containing both KB-1 and NBB microbes with no PCE feed). Data points shown are averages of three to four replicates (see Table 3-5).*

Methane concentrations in these experiments were all lower than those determined in the earlier round of xanthan testing. Increased methane concentrations were noted for those experiments with added methanol, and in the "Viscosity/NBB control" conditions, plotted as a single value in Figures 3-13a and Figure 3-13b. In comparison to those values (260 total μmoles for Xanthan/KB-1/NBB viscosity controls and 80 total μmoles for Medium/KB-1/NBB viscosity controls) only 56 total μmoles of methane were produced in xanthan microcosms without added NBB microbes. Even at these relatively lower methane concentrations, ethene peaks were often overshadowed on the GC, resulting in reported ethene values of zero. Final solution pH values (Table 3-5) were lower in xanthan-containing microcosms than in polymer-free ones, although this may be attributed to the higher initial pH of the nutrient medium solutions.

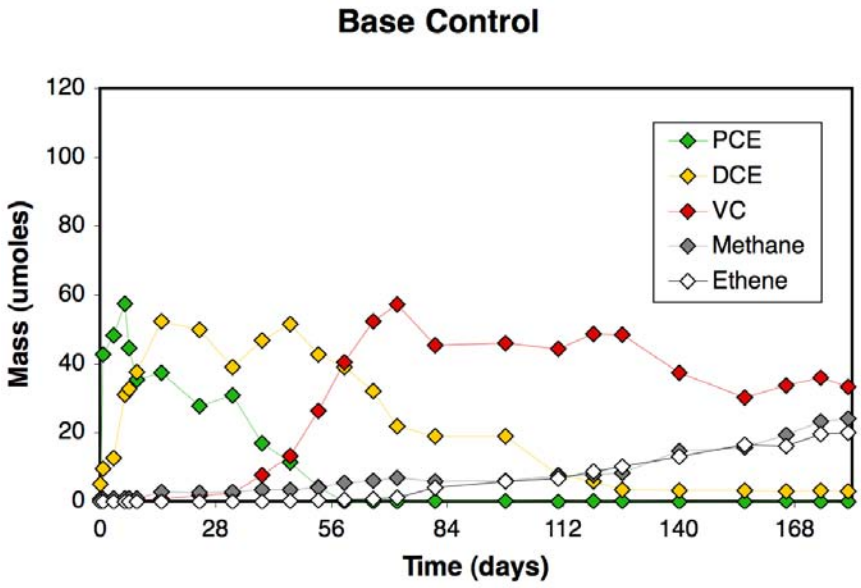

Figure 3-14: *Total (liquid- + gas-phase) analytes mass versus time for nutrient medium base control experiments, from round two. Data points shown are averages of four replicates.*

Table 3-5: *Final pH values for xanthan/microbes batch, round two*

Sample Description	Replicates	Final pH
Xanthan, Base Test	4	6.97
Base Control	*4*	*7.22*
Xanthan, e- Donor Test	N/A	N/A
e- Donor Control	*4*	*7.39*
Xanthan, e- Donor/NBB Test	4	6.80
e- Donor/NBB Control	*4*	*7.47*
Xanthan Polymer Control	2	6.96
Xanthan Feed Control	3	6.91
Xanthan Viscosity Control	3	6.82
Medium Control	*1*	*8.39*
Medium Feed Control	*3*	*8.25*
Medium Viscosity Control	*3*	*7.87*

Viscosity Retention

The final viscosity measurements for this group of experiments were difficult to interpret. This particular series of testing lasted for 6.5 months, almost twice as long as the previous xanthan experiments. When the polymer control and polymer/feed control microcosms were sacrificed, the solution viscosity in those experiments was observed to have dropped to that of water. It is unknown if this observation represents the extent of time over which xanthan solutions can be considered stable, or if microbial degradation contributed to this viscosity loss. Based on personal observations and experience with storage of other xanthan solutions, we are

inclined to attribute this loss to microbial activity, especially because the polymer/viscosity microcosms (containing KB-1 and NBB microbes) as well as the xanthan ED/NBB test microcosms (none of which experienced complete dechlorination) exhibited the same viscosity drop. Indeed, the only experimental condition to retain any significant solution viscosity was the xanthan ED test condition.

HPAM/Microbe Batch Experiments

HPAM, as a polymer molecule composed of less complex functional groups (see Figure A-1b) may be more likely to already exist in or easily transform into a more bioavailable compound for use by either KB-1 or NBB microbes during the PCE dechlorination process. Given the better dechlorination performances noted in the first set of xanthan experiments as compared to the second, HPAM/bioamendment batch tests were inoculated with the same September 2004 KB-1 culture used in the initial xanthan experiments. To reduce the number of microcosms for analysis, the electron donor control condition was omitted.

Comparative Dechlorination Rates

The results from this subset of experiments illustrate the importance of evaluating dechlorination data only between test conditions and equivalent appropriate control conditions from similar rounds of experiments. Although microbes in the round one xanthan experiments dechlorinated a dose of PCE within one month and these HPAM experiments required at least 3.5 months, we cannot definitively attribute this delay to the HPAM polymer. The microbial inoculum itself may have been exposed to oxygen, or allowed to become too acidic (or too alkaline), or have undergone a shift in microbial distribution favoring one biotransformation step over another. Alternatively, errors in microcosm assembly could have contributed to the apparently slower rates of PCE conversion.

Comparing the HPAM base test results (Figure 3-15a) to the polymer-free base control experiments (Figure 3-15b), it is apparent that biodegradation actually occurred at a much faster rate in the HPAM-containing batches than in the control experiments. At the end of 3.5 months, when microbes have almost completely transformed the remaining vinyl chloride in the polymer batch tests, DCE concentrations are still rising in the corresponding control experiments. As noted for other rounds of polymer/bioamendment testing, final pH values are lower for polymer-containing batch experiments than for controls (Table 3-6). The difference in resulting methane concentrations between these experimental conditions is striking: 5 μmoles of methane produced by KB-1 microbes in methanol-amended nutrient medium versus more than 500 μmoles of methane produced by similar microbes in a solution of methanol-amended HPAM.

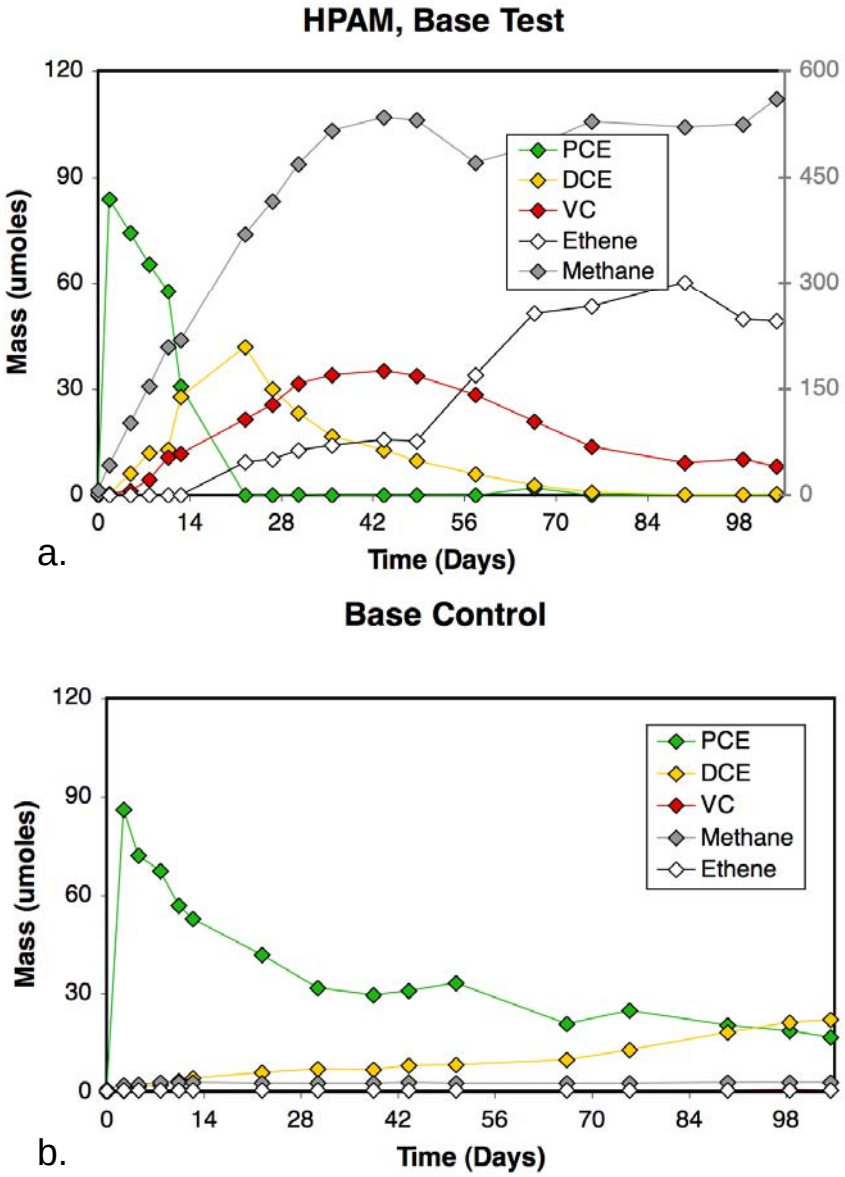

Figure 3-15: *Total (liquid- + gas-phase) analyte mass versus time for HPAM base experiments (a) and nutrient medium base control experiments (b). Note that methane concentrations (shown in gray) refer to the right-hand y-axis for Figure 3-14.a only. Data points shown are averages of three to four replicates (see Table 3-6).*

For both methanol-free HPAM experimental conditions, dechlorination appeared to stall at the DCE-to-VC step even weeks after an addition of methanol, while PCE concentrations in the methanol-free nutrient medium control mimicked those observed in the base control (figures 3-16a-c). Methane concentrations for these experiments were generally low (< 50 μmoles) but the HPAM/KB-1/NBB viscosity control generated ~250 μmoles in the absence of PCE/methanol feed. Although the HPAM ED and EDNBB test conditions had significantly lower pH values

than their polymer-free counterparts, the HPAM viscosity control generated the lowest pH measured in these polymer/microbe batch tests.

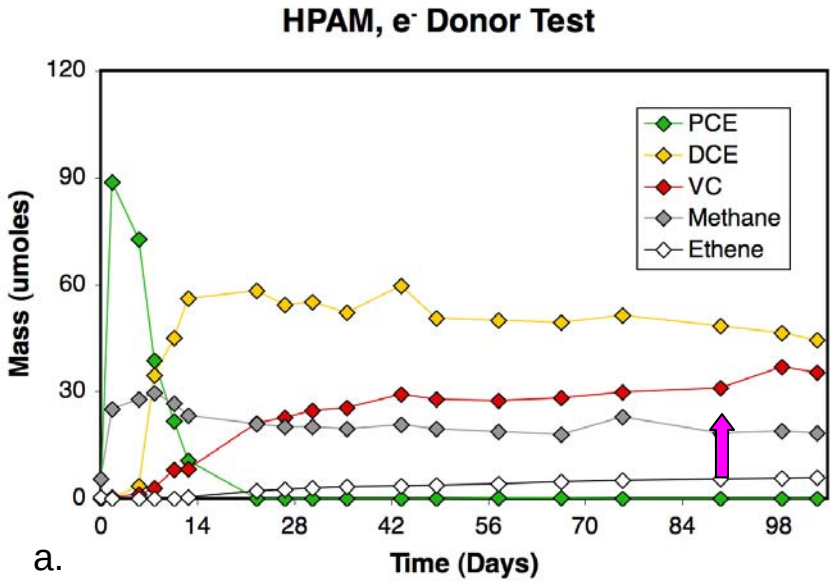

a.

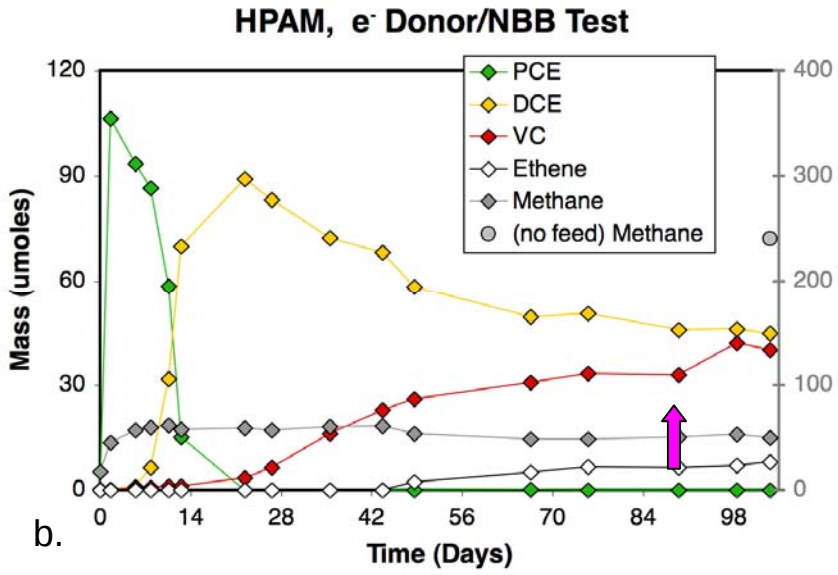

b.

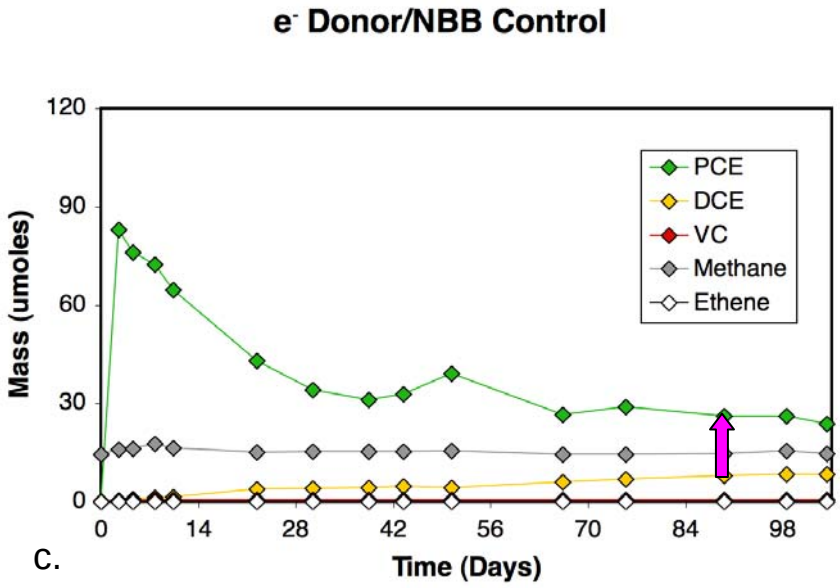

Figure 3-16: *Total (liquid- + gas-phase) analyte mass versus time for HPAM e- donor experiments (a), HPAM e- donor/NBB experiments (b) and nutrient medium e- donor/NBB control experiments. Pink arrows indicate addition of methanol only. Note that methane concentrations (shown in gray) refer to the right-hand y-axis for Figure 3-15b only. Data point referred to as "no feed Methane" is final methane measurements taken from "HPAM/KB-1/NBB/Viscosity control" (i.e., control experiments of HPAM containing both KB-1 and NBB microbes with no PCE feed). Data points shown are averages of three to four replicates (see Table 3-6).*

Table 3-6: *Final pH values for HPAM/microbes batch*

Sample Description	Replicates	Final pH
HPAM, Base Test	4	6.55
Base Control	*4*	*7.27*
HPAM, e- Donor Test	4	6.73
e- Donor Control	*N/A*	*N/A*
HPAM, e- Donor/NBB Test	4	6.69
e- Donor/NBB Control	*4*	*7.37*
HPAM Polymer Control	4	7.46
HPAM Feed Control	5	7.13
HPAM Viscosity Control	3	5.31
Medium Control	*1*	*7.64*
Medium Feed Control	*3*	*7.80*
Medium Viscosity Control	*N/A*	*N/A*

Viscosity Retention

Although calculation of a concentration of HPAM that would remain highly viscous when mixed with nutrient medium was attempted, resulting solutions, including the polymer control samples, were far less viscous than xanthan solutions prepared at a similar strength (compare Figure 3-17 to Figure 3-12). Unlike the results of the xanthan/microbe batch tests,

where all polymer-containing samples possessed high, shear-thinning viscosity profiles at the end of the test duration, here one HPAM-containing condition experienced a complete loss of viscosity. The data for HPAM/KB-1/NBB/Visc control exhibited low viscosity values close to 1 cP, similar to all of the polymer-free batches, and so cannot be distinctly displayed in Figure 3-17. This complete loss of viscosity in this experimental set was accompanied by the lowest measured pH value and moderate production of methane (Table 3-6, Figure 3-16c).

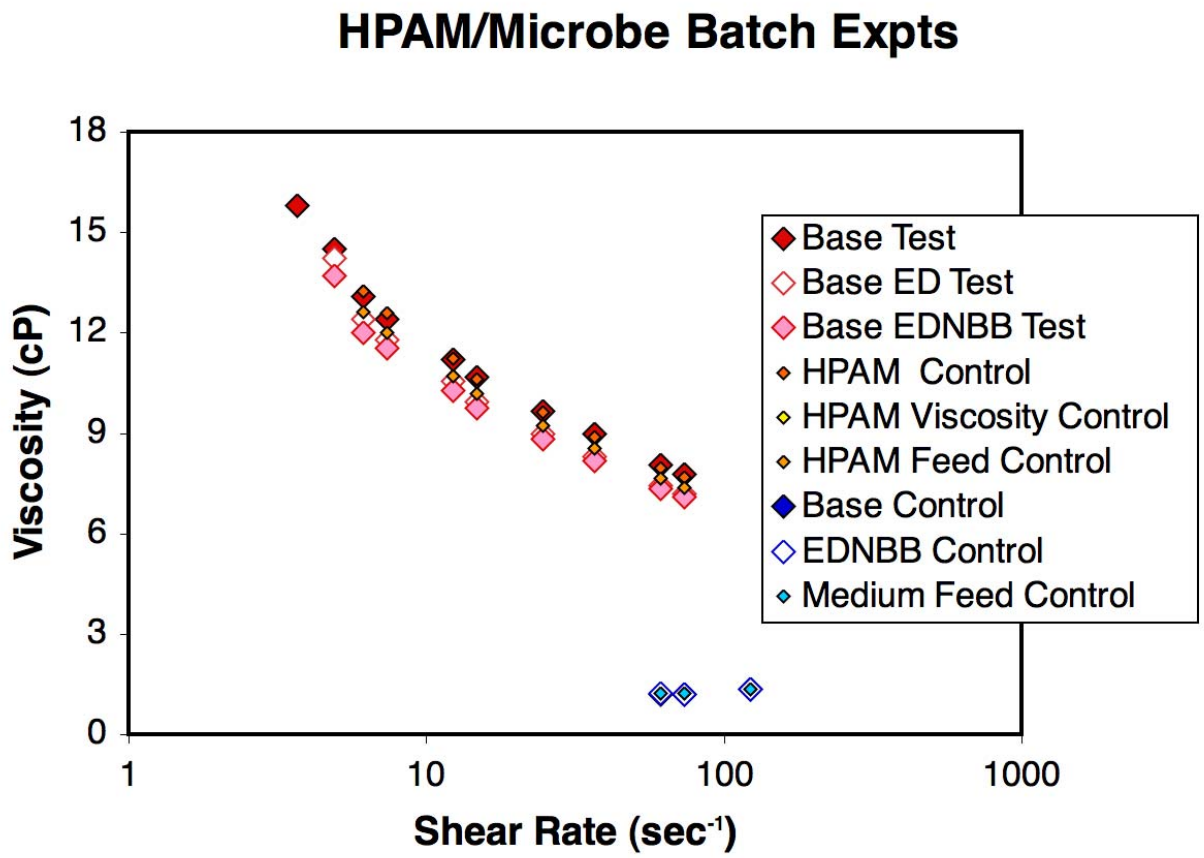

Figure 3-17: *Viscosity versus shear rate for sacrificed HPAM/microbe batch experiments. Experiments containing HPAM polymer are represented in red and orange; experiments containing medium only are represented in blue. HPAM Viscosity control values cannot be distinguished from the other samples with viscosities of approximately ~1 cp. Data shown are averages of all replicates. Note the log scale of the x-axis.*

Polymer/Bioamendment Compatibility Test Conclusions

- Xanthan and HPAM polymer do not impede and may actually enhance the dechlorinating ability of KB-1 consortia to convert PCE into ethene, as long as methanol is supplied to the system as an electron donor.
- No complete PCE-to-ethene biotransformation is observed in polymer-containing experiments lacking methanol; instead, partial degradation often results in undesirable accumulations

of more toxic daughter-products (DCE or VC). Thus, xanthan and HPAM do not serve as adequate electron donors in the experimental matrices monitored here.

- In two experiments out of three complete sets, polymer solution viscosity decreases were not observed to accompany either complete or partial PCE dechlorination; this observation supports the inference that neither KB-1 nor NBB microbes can break down xanthan or HPAM polymer molecules into smaller utilizable compounds for use as electron donors. The near-complete loss of viscosity in all xanthan-containing experiments during the second testing round is attributed to contamination by additional unknown microbes during microcosm assembly stage.
- Moderate (one-half pH unit or more) decreases in solution pH were observed for all polymer solutions in contact with microbes over the duration of these experiments (multiple months).
- The viscosity decreases noted in xanthan and HPAM base tests (polymer, KB-1, PCE/methanol feed) were of such small magnitude, and were produced over such a relatively long timescale compared to the duration of a typical bioamendment injection, that they are unlikely to impact polymer-related flow effects or sweep efficiencies. These results, though, were obtained from idealized batch experiments involving intentionally controlled and limited microbial communities, and are thus not indicative of the timescales over which injected polymer viscosities would be retained at a more microbially diverse, natural subsurface site.

4. TASK 2: COLUMN STUDIES

In this work, 1-D column experimental methods were employed to investigate the mechanisms of polymer retention and transport in porous, homogeneous media. Specifically, the results of polymer flooding column tests were used to compare the effective permeability of polymer and water, and to derive input parameters for UTCHEM model simulations of polymer transport. The relative transport of polymers and selected remediation amendments were also observed. We have limited our column investigations to the use of xanthan because this polymer is less sensitive to changes in solution salinity, and generally appears to be a more robust choice in terms of ease of design and application with chemical oxidants (i.e., permanganate).

4.1 Sub-task A: Polymer Transport Parameters, Column Testing

The principal objectives of this task are to:

1. Examine the effects and dynamics of polymer retention in porous media as a function o media chemical characteristics and permeability,
2. Develop an appropriate correlation between viscometer-measured viscosity/shear rate functions and observed *in situ* viscosity/shear rate function,
3. Develop methods to quantify polymer retention and acceleration contributions to polymer transport, and
4. Provide input parameters for simulating polymer transport and the effects of polymer flooding using the UTCHEM simulator.

The importance of this task is to obtain a fundamental understanding of the mechanisms affecting polymer transport and the potential of these mechanisms to aid or limit heterogeneity control for the purpose of enhancing the subsurface distribution of co-injected remediation agents. Excessive polymer retention could significantly limit heterogeneity control and reduce the effectiveness of the process to better deliver remediation amendments to lower permeability strata. Furthermore, excessive polymer retention can result in elevated pressure requirements at the injection well, possibly resulting in surfacing of the injected solution around the injection well during implementation.

Polymer Rheology

Xanthan and hydrolyzed polyacrylamide (HPAM) solutions used in this research are shear thinning; that is, the solution viscosity decreases as the rate of shear applied to the solution increases. This effect occurs as a result of the polymer molecules aligning in the direction of the applied shear. During injection into porous media, this behavior causes the polymer solutions to be less viscous at the injection well (high shear conditions), potentially enhancing the injectivity of the solution. As the velocity of the injected solution decreases with radial distance from the injection well, so does the *in situ* shear rate and thus polymer solution viscosities increase. As the velocity of the injected solution decreases with radial distance from the injection well, *in situ* shear rates will also decrease, increasing polymer solution viscosities with radial distance.

Estimating shear rates within porous media generally involves the description of the media as a bundle of capillaries. One of the simplest forms of the capillary bundle model use to estimate *in situ* shear rates is (Zaitoun and Kohler, 1987):

$$\gamma_{pm} = \alpha \frac{4u}{\sqrt{8k\phi}}$$

where u is the average linear velocity and is an empirical shape parameter associated with pore structure (α=1 when all capillaries within the bundle are of uniform diameter). The denominator in the equation above is the calculated value of the average pore/capillary radius. Darcy's law can then be used to estimate the apparent viscosity of the polymer solution within porous media (μ_{app}) as:

$$\mu_{app} = \frac{k\rho_w g}{v}\frac{\Delta H}{L}$$

where k is the porous media permeability, ρ_w and g are the density of water and the gravititational constant, v, is the Darcy velocity, ΔH is the head loss (or pressure drop) over a distance L. This equation is commonly used in characterizing *in situ* polymer rheology because often the objective is to provide bulk estimates of transport parameters (Sorbie, 1991).

Polymer Retention

The mechanisms contributing to polymer retention during transport within porous media include:

- Polymer adsorption,
- Mechanical entrapment, and
- Hydrodynamic entrapment.

These mechanisms are portrayed schematically in Figure 4-1.

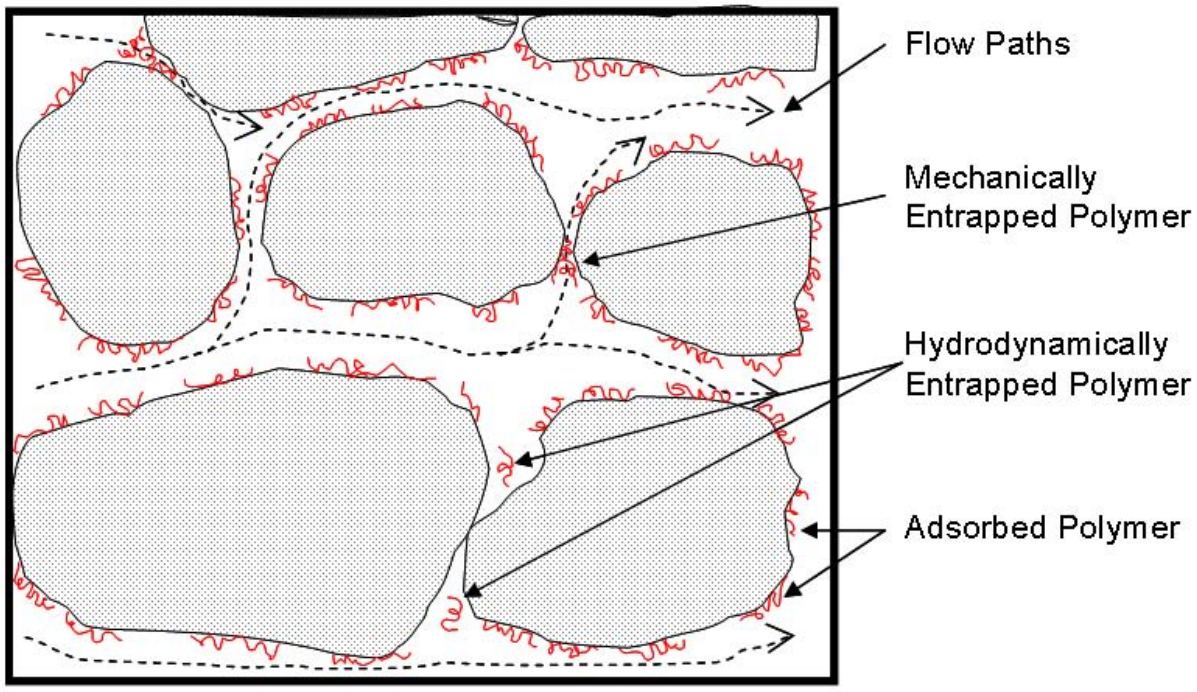

Figure 4-1: *Schematic representation of polymer retention mechanisms in porous media (modified from Sorbie, 1991).*

The adsorption of polymers used for mobility and heterogeneity control has been shown to exhibit Langmuir isotherm character (Sorbie, 1991; Lu et al., 2002), suggesting a self-sharpening polymer breakthrough front during transport. Mineral adsorption of these anionic polymers is generally considered to occur as a physical adsorption process (Nadler and Letey, 1989; Dontsova and Bigham, 2005). Polymer adsorption is largely considered to be irreversible (Sorbie, 1991). However, evidence exists to indicate that some fraction of adsorbed polymer may in fact be reversible (Chauveteau and Lecourtier, 1986), as a result of competitive adsorption processes resulting from the inherent polydispersivity of polymer molecular weights (i.e., larger polymer molecules displacing smaller sorbed polymer molecules from mineral surfaces).

Polymer retention by mechanical entrapment (or mechanical filtration) can be viewed as the trapping of polymer molecules as they flow through the narrowest of pore pathways (Sorbie, 1991). This trapping leads to blocking of pores and a reduction of the effective permeability to polymer, and in severe cases to water as well. Consistent with this conceptual model, mechanical entrapment should then predominate in finer grained media where mean pore diameters approach the effective hydrodynamic diameter of the polymer molecule (which is generally considered to be about 1 micron, (Dominguez and Willhite, 1977)). A practical effect regarding polymer solutions is that polymer solutions will increase the fraction of flow through fine-grained media in a heterogeneous system.

Hydrodynamic retention is thought to occur in regions of the porous medium that are adjacent to but not contributing to flow. These regions temporarily trap polymer molecules during transport within zones of stagnation, and polymer molecules are only removed from these zones by diffusion. Hydrodynamic retention is the least well defined of polymer retention mechanisms (Sorbie, 1991). The concept was first introduced to explain observations of increased polymer retention with decreasing flow rate (Dominguez and Willhite, 1997). The contribution of hydrodynamic retention may be quantified by stopping flow to the column for a time necessary to allow for polymer diffusion back into the main flow pathways, and then restoring flow and monitoring effluent polymer concentrations. Integrating the resulting peak provides a measure of the polymer mass associated with hydrodynamic retention.

These retention mechanisms affect polymer transport by first removing polymer mass from the transporting fluid and reducing the viscosity of the solution at the injection front. This process in turn can reduce the effectiveness of the cross-flow mechanism for improving sweep-efficiencies. Secondly, the adsorption of these large polymer molecules can enhance mechanical entrapment beyond its intrinsic contribution by reducing the effective diameter of pores, thereby reducing the effective media permeability for polymer and reducing the overall injectivity of the solution. As a coupled process, isolating and quantifying the individual contributions of these retention mechanisms is challenging. However, modeling retention as a coupled process and relating permeability reduction potentials to bulk measures of polymer retention has been successful in this research.

Polymer Acceleration

The mechanisms that can promote the acceleration (i.e., early polymer arrival relative to a conservative tracer) of polymer molecules during transport within porous media include inaccessible pore volume and surface-exclusion chromatography effects (Chauveteau and

Lecourtier, 1986; Sorbie and Huang, 1991). Inaccessible pore volume (IPV) is the fraction of the media pack pore volume that is inaccessible to polymer molecules as a result of physical exclusion of large polymer molecules within the smallest of pores and pore throats. Polymer solution acceleration then occurs as a result of the lower effective pore volume for polymer than for water. Surface exclusion chromatography (SEC) effects relate to the preferential longitudinal orientation of polymer molecular chains nearest pore walls. This exclusion is envisioned to result in a depleted layer of polymer molecules adjacent to pore walls, reducing the effective pore volume for polymer over that of water (Sorbie and Huang, 1991).

Both acceleration mechanisms, if they occur, enhance the apparent velocity of the polymer solution by reducing the effective pore volume for polymer compared to that of water or a conservative tracer. The importance of these acceleration mechanisms for a given porous medium depends on the concentration of polymer, polymer molecular conformation in solution (e.g., coiled vs. linear conformation), media permeability and tortuosity, and media surface chemistry characteristics. As such, much of the existing experimental results relating to these processes are of limited predictive value. Additionally, the few predictive relationships that exist in the published literature are largely specific to the media and experimental conditions used.

Complicating the picture further is the likelihood that these polymer acceleration mechanisms are *not* operating independently of the aforementioned retention mechanisms. Rather, they are most likely operating simultaneously and in some cases cooperatively. For example, and as mentioned previously, polymer adsorption can contribute to mechanical entrapment as a result of large adsorbed polymer molecules reducing the effective diameter of pores. Therefore, as adsorption contributes to polymer retention and the blocking of pores to polymer, it is logical to assume a concurrent enhancement in polymer acceleration resulting from an increased IPV.

Modeling Polymer Transport in Porous Media

Based on the previous discussions, modeling and/or simulating polymer transport in porous media requires:

1) a relationship describing polymer solution viscosity as a function of shear rate;
2) a relationship describing polymer solution viscosity as a function of polymer concentration;
3) a relationship describing polymer solution viscosity as a function of salinity;
4) a relationship between viscometer measured viscosity/shear rate function and apparent (i.e., *in situ*) viscosity/shear rate function;
5) a relationship between polymer adsorption (or total uptake) as a function of polymer concentration (i.e., sorption isotherms);
6) a relationship between measured permeability reduction as a function of media intrinsic permeability; and
7) a measure of the reduction in effective porosity for polymer (i.e., the degree of polymer acceleration).

Currently, a numerical simulator exists that accounts for these relationships: the UTCHEM simulator. UTCHEM is a three-dimensional, multi-component, multi-phase (water, NAPL, microemulsion, air) compositional simulator that was developed at the University of

Texas at Austin's Center for Petroleum Engineering to support polymer and other chemical flooding operations for enhanced oil recovery modeling. Details of UTCHEM theory and application can be found in the technical documents supporting the simulator (CPGE, 2000a,b). The technical documentation for this simulator does not, however, provide explicit guidance on how to derive the various input parameters required to simulate polymer flooding. Therefore, as a part of this research, specific experimental methods will be developed to meet the input data requirements for this simulator. Of course, many of the processes above are likely coupled, as described above, and therefore it is likely not possible to determine a unique set of model input parameters from any experimental data set. Thus, the dominant processes are the ones most important to quantify, and other parameters can be fixed at reasonable values or lumped into other parameters.

Materials and Methods

Xanthan, the polymer used throughout this work, was a clarified food-grade product (Keltrol T®, CP Kelco, Houston, TX) in dry powder form. The xanthan powder was first hydrated in deionized water (in 1.5 L batches) using an overhead laboratory mixer set at 1,000 – 1,500 revolutions per minute to create a vortex with sufficient mixing energy to properly hydrate the powder as per the manufacturer's recommendation (CP Kelco, 2004). The powder was slowly and intermittently added to the edge of the vortex to avoid clustering of the polymer and the formation of multi-molecular aggregates. After 203 hours of continuous mixing, $CaCl_2$ salt was added to provide solution salinity and the solution was mixed until the salt dissolved. The solution was then allowed to rest overnight to complete polymer hydration.

Characterizing the fluid dynamics of these non-Newtonian solutions required measuring viscosity as a function of shear rate. Throughout this work, polymer solution viscosities were measured as a function of shear rate using an AR-G2 cone-and-plate rheometer (TA Instruments, New Castle, DE) at 25°C. During methods development, it was found that a 2-inch stainless steel cone with a 2-degree slope was optimal to properly characterize the shear-thinning character of these fluids.

Columns were dry-packed using a tap-and-fill procedure. Once packed with sand and sealed, CO_2 gas was introduced at a low flow rate (~0.1 cm^3/min) for several hours to replace the air within the media porosity. The purpose of this is to prevent entrapped air within the columns during saturation. The columns were then positioned vertically and a 400 mg/L $CaCl_2$ aqueous solutions was introduced at a rate of 0.1 cm^3/min to saturate the columns. Porous media bulk densities (ρ_b), porosity (ϕ), and the column pore volume (PV) were estimated using standard soil-physics methods. Once the columns were packed and saturated, hydraulic conductivities for each media category were determined by measuring the pressure drop across the column for a fixed flow rate and applying Darcy's Law.

Four commercial-grade silica sands were selected for use in these experiments. The relevant characteristics of these sands are provided in Table 4-1. These sands were selected to cover a 4-order of magnitude range of permeability. The SILCOSIL media (representing a silt-sized media) was sieved to achieve two particle size fractions as shown. The sands were used as purchased without further treatment. These same sands are also used in the oxidant column experiments also in Task 2, in the 2-D tank experiments in Task 3, and in the 2-D tank experiments with oxidant in Task 4.

Table 4-1: *Porous Media Properties*

Media	Hydraulic Conductivity (cm/sec)	Permeability (darcy)	Bulk Density (g/cm3)	Porosity	Average Pore Diameter (μm)
UNIMIN 30	8.25E-02	82.5	1.67	0.38	82
UNINIM 70	1.37-02	13.7	1.6	0.38	34
F110 Ottawa	4.00E-03	4.00	1.62	0.35	20
SILCOSIL_CF	5.60E-04	0.56	1.54	0.33	7
SILCOSIL_FF	1.50E-05	0.02	1.52	0.32	1.2

A schematic of the test system used in these experiments is presented as Figure 4-2. An HPLC pump was be used to deliver fluids to a pre-column and test column. The purpose of the pre-column was to provide a polymer solution that is free of multi-molecular aggregates (or "microgels") that can result during hydration of the polymer powder. Effluent leaving the pre-column entered the test column. The pressure drop across the test column and effluent concentrations of a conservative tracer (i.e., chloride ion) and xanthan were monitored on-line using a flow-through chloride ion probe and TOC analyzer, respectively. The TOC analyzer was plumbed to facilitate on-line analysis and programmed to measure polymer concentration in the column effluent as total carbon. The experimental variable in these experiments was media permeability.

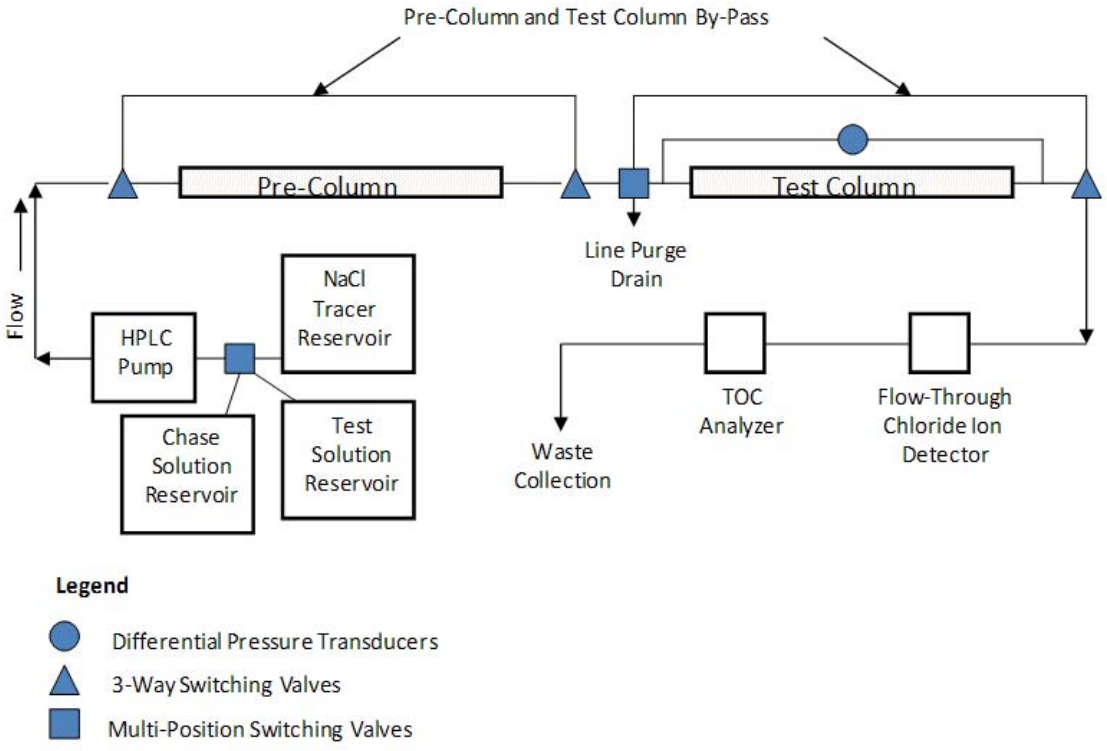

Figure 4-2: *Experimental setup used to obtain polymer transport parameters.*

Each experiment was initiated by first performing a conservative tracer test on the test column. This tracer provided a baseline transport condition from which to compare with later polymer-flooding tests. The tracer solution in this case was an 800 mg/L solution of NaCl. Hydraulic conductivities of the test media were also determined from the recorded column pressure drop and the application of Darcy's law. The tracer solution was then purged from the test column by flushing the column with a 400 mg/L $CaNO_3$ chase solution to remove all chloride ions from the column and to precondition the test column by the addition of calcium cations at the same cationic strength as that in the test polymer/$CaCl_2$ solution.

Thus, subsequent experimental procedures consisted of sequentially loading the test column with polymer/tracer test solution (at a fixed concentration, salinity, and flow rate) until effluent chloride and polymer concentrations equaled those measured for the influent; waiting for the pressure drop across the column to stabilize; and completely un-loading the column by flooding with the $CaNO_3$ chase solution. Using this procedure, repeated experiments provided a sequence of conservative tracer (i.e., chloride ion) and polymer breakthrough profile pairs that were used to extract the contributions of polymer retention and acceleration mechanisms. A schematic example of this concept is provided as Figure 4-3.

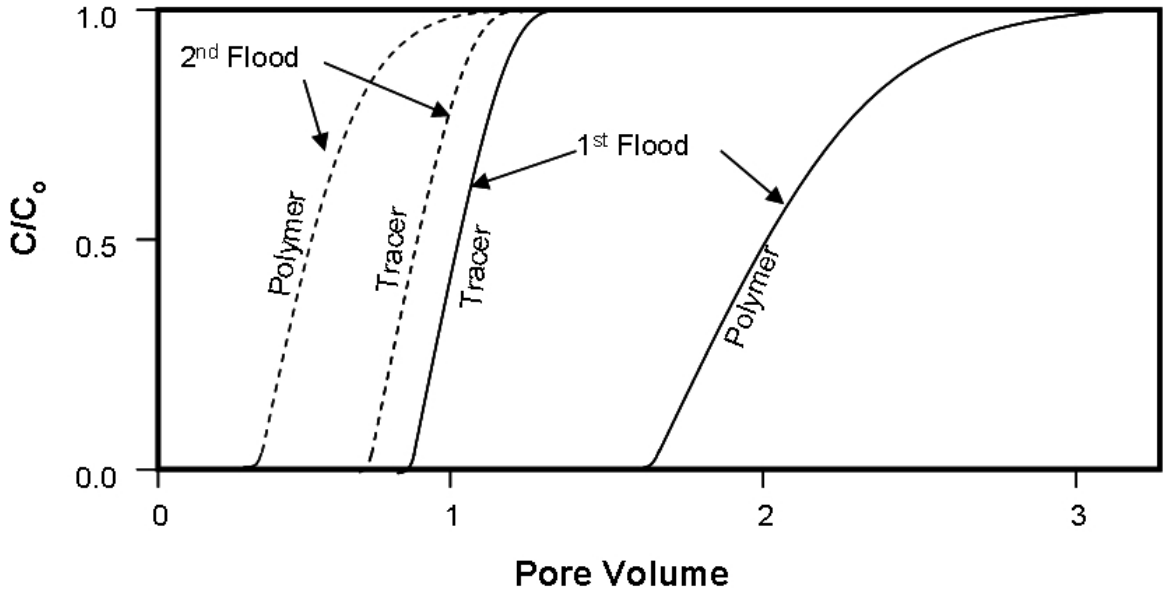

Figure 4-3: *Schematic example of chloride and polymer breakthrough profiles.*

Conservative tracers were used to define the pore volume of the test column during initial polymer floods. Polymer breakthrough was retained, relative to the conservative tracer, if polymer adsorption and mechanical entrapment were important mechanisms within the test sand. During the second flood, tracer breakthrough occurs at less than one pore volume if the polymer retention mechanisms during the initial polymer flood reduced the pore volume accessible to water. Similarly, polymer breakthrough occurs at less than one pore volume if the retention

mechanisms during the first flood reduced the pore volume accessible to polymer. The integrated area between the first tracer breakthrough profile and the first polymer profile represents the sum of the contributions of all retention and acceleration mechanisms on polymer transport. The area between the second tracer profile and the second polymer profile represents the sum of the contributions of all acceleration mechanisms (i.e., IPV and SEC). Subtracting these areas provided a measure of the sum of the contributions of all retention mechanisms at work in this system. Calculations such as these were used to extract retention and acceleration contributions for all test media used in this research.

The reduction in fluid mobility and permeability reduction during transport within all test media were determined using the methods of Zaitoun and Kohler (1987):

$$R_M = \Delta P_{polymer} / \Delta P_{pre\text{-}polymer} \cong (k_{polymer}/\mu_{polymer}) / (k_{int}/\mu_{water})$$
$$R_K = \Delta P_{post\text{-}polymer} / \Delta P_{pre\text{-}polymer} = k_{post\text{-}polymer} / k_{int}$$

where R_M and R_K are the mobility and permeability reduction factors, k_{int} is the intrinsic media permeability, and $\Delta P_{pre\text{-}polymer}$ is the pressure drop across the test column before introducing polymer, $\Delta P_{polymer}$ the pressure drop during polymer flooding, and $\Delta P_{post\text{-}polymer}$ the pressure drop after water-flooding to remove polymer.

Data describing the apparent viscosity as a function of shear-rate was collected during polymer flooding by stepwise increasing and decreasing the flow velocity and monitoring ΔP. Apparent viscosities (μ_{app}) are those that occur within a porous media pack under polymer solution flow and were determined at each flow condition using the equation:

$$\mu_{app} = (k\rho g / v_{darcy}) * (\Delta P / L) * 100$$

where k is the media permeability (cm_2), ρ is the fluid density (g/cm_3), g is the gravitational constant (cm/sec_2), ΔP is the measured pressure drop across the column (cm) during polymer flooding, and L is the column length. The factor 100 is used to convert viscosity units from $g \bullet cm^{-1}sec^{-1}$ to mPa•sec or centipoise (cP). In applying the above equation it is important that the permeability used is not the intrinsic value but that value measured after the polymer has been swept out of the column with chase solution.

Corresponding *in situ* or porous-media equivalent shear rates (γ_{eq}) were determined for each flow condition using the following Blake-Kozeny capillary bundle model modified for multi-phase flow (Hirisaki and Pope, 1974):

$$\gamma_{eq} = \gamma_C * u * (kSk_r\phi)^{-0.5}$$

where u is the average linear velocity, k is the average permeability and k_r and S are the relative permeability and fluid saturation of the advecting fluid, respectively. For a single aqueous phase, $S = 1$ and $k_r = 1$, and the rooted term in the denominator of the equation reduces to the product of k and ϕ. The term γ_C is used to describe the degree of shear thinning and the potential degree of departure between calculated μ_{app} values and corresponding bulk viscosities that can result from non-ideal effects such as slip along pore walls. The UTCHEM technical

documentation (CPGE, 2000b) defines γ_C as being equal to 3.97C, where C is the shear rate coefficient and is an input parameter for UTCHEM.

Results and Discussion

Xanthan Solution Viscosity as a Function of Shear Rate

The results of viscosity/shear rate measurements made for solutions of Keltrol® xanthan are presented in Figure 4-4. Xanthan concentrations range between 250 and 1000 mg/L. $CaCl_2$ concentration in these solutions was fixed at 400 mg/L.

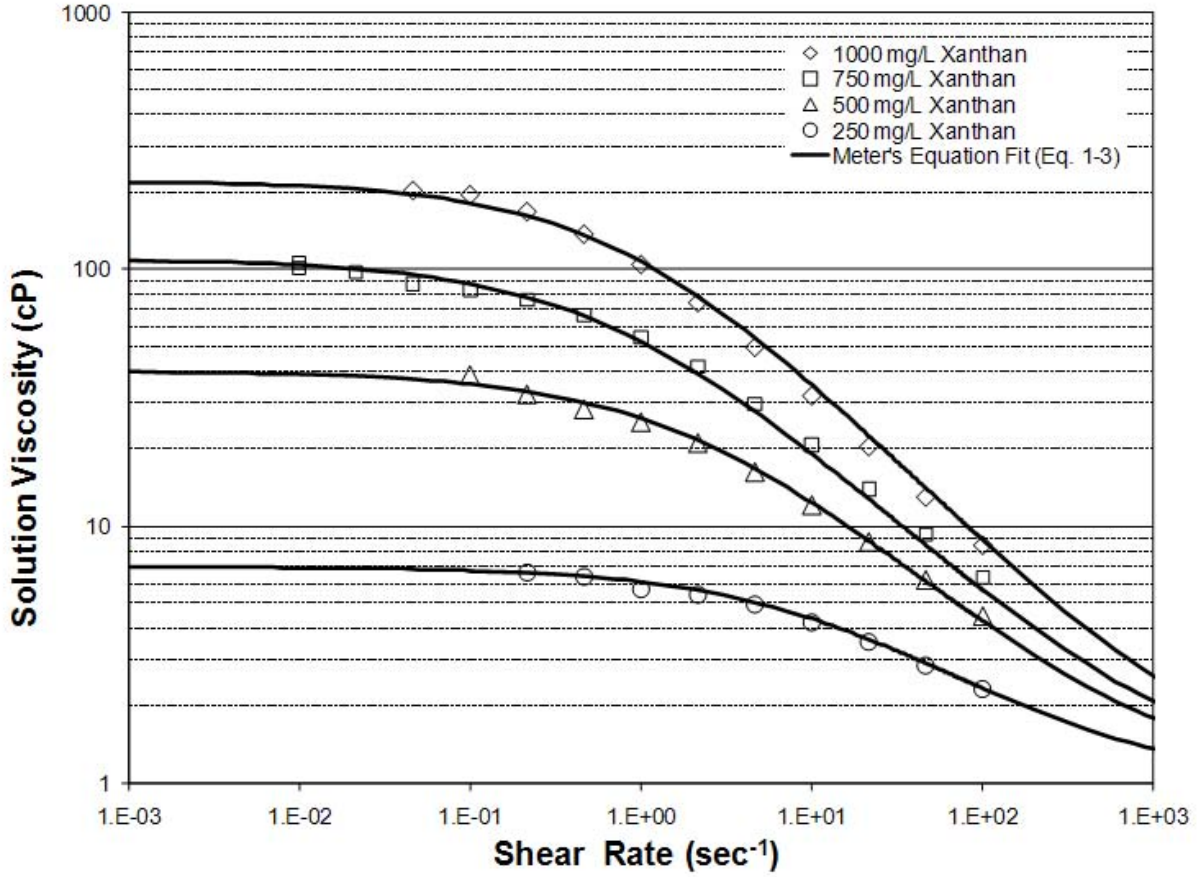

Figure 4-4: *Viscosity/shear rate profiles for xanthan solutions in 400 mg/L $CaCl_2$.*

The data present in Figure 4-4 was modeled as a function of shear rate using Meter's equation (Meter and Bird, 1964):

$$\mu_p = \mu_w + \frac{\mu_p^0 - \mu_w}{1 + \left(\frac{\gamma}{\gamma_{1/2}}\right)^{P_\alpha - 1}}$$

where μ^0_p is the polymer solutions viscosity at zero shear rate (read from the Newtonian plateau region of lowest measurable shear rate change), μ_w is the water viscosity (here assumed to be 1 cP), $\gamma_{½}$ is the shear rate at which the polymer solution viscosity is half that of the zero shear rate viscosity, and P_α is an empirical coefficient which governs the abruptness of the change of viscosity with shear. This equation was used to fit the experimental shear rate/viscosity data using P_α and $\gamma_{½}$ as fitting parameters. Whenever the Newtonian plateau was not readily discernable from the measured data, μ^0_p was employed as an additional fitting parameter. As shown in Figure 2-4, these xanthan solutions exhibited shear-thinning character across three to five decades of shear rate change. The results of Meter's equation fits to the data presented in Figure 4-4 are presented in Table 4-2 below.

Table 4-2: *Meter's equation fits to viscosity/shear rate profiles as a function of xanthan concentration.*

Concentration (mg/L)	**Zero-shear Viscosity (μ^0_p, cP)**	**P_α**	**($\gamma_{½}$, sec^{-1})**
1000	220	1.68	0.83
750	110	1.65	0.83
500	40	1.65	2.5
250	7	1.65	15

The purpose of fitting this data was to provide input parameters for the UTCHEM simulator. The primary input parameters here are P_α and $\gamma_{½}$. P_α, which describes the curvature of the viscosity/shear rate profile, is here found to be essentially independent of solution xanthan concentration.

Polymer Solution Viscosity as a Function of Salinity

To model the dependence of polymer solution viscosity on salinity, UTCHEM uses an effective salinity term (C_{SEP}, meq/mL) that is based on the anion and divalent cation concentrations in the aqueous phase. The use of divalent cation concentrations, as opposed to monovalent cations, is based on the consideration that divalent cations can have a much stronger impact on polymer viscosity. C_{SEP} is defined as:

$$C_{SEP} = \frac{C_{51} + (\beta_p - 1) \cdot C_{61}}{C_{w1}}$$

where C_{51}, C_{61} and C_{w1} are the anion, divalent cation and water concentrations in the aqueous phase. β_P is used to magnify the strength of the divalent cation concentration and is an input parameter for the UTCHEM simulator. β_p was assigned a value of 1.2.

Xanthan solutions were additionally prepared at 250, 500, and 1000 mg/L to determine the SSLOPE (or S_p) parameter used by UTCHEM to calculate polymer solution viscosity as a function of effective salinity. For each xanthan concentration, the concentration of $CaCl_2$ was fixed at 1000, 500 and 250 mg/L within individual solution batches. Solution viscosities were then measured as a function of shear rate using the AR-G2 rheometer as described previously. The results of these measurements are presented in Figures 4-5 through 4-7.

For each initial xanthan concentration, the addition of $CaCl_2$ (adding salinity) is shown to reduce solution viscosity relative to the case for zero salinity (i.e., DI water - no $CaCl_2$ addition). However, solution viscosity/shear rate profiles in all cases appear to essentially stabilize for solutions containing $CaCl_2$ in excess of 100 mg/L. This is the result of exceeding salinity (as $CaCl_2$) thresholds for xanthan in each case, below which viscosity is more dependent on salinity. For each case, the effective salinity was calculated according to the equation above for C_{SEP}. Using the zero shear rate viscosities, apparent viscosities were calculated as:

$$\text{Apparent Viscosity} = \left(\frac{\mu_p^0 - \mu_w}{\mu_w} \right).$$

A plot of apparent viscosity versus C_{SEP} on a log-log plot is shown as Figure 4-8 for each xanthan concentration. S_p is then determined from the slope of a power-law fit to the data. Here, S_p is found to vary between -0.057 and -0.08 for the three different polymer concentrations, reflecting the general lack of solution viscosity reduction with increasing $CaCl_2$ salinity between 100 and 1000 mg/L $CaCl_2$ that was observed from the rheometer dataset. An average S_p value of -0.07 was used in the simulator.

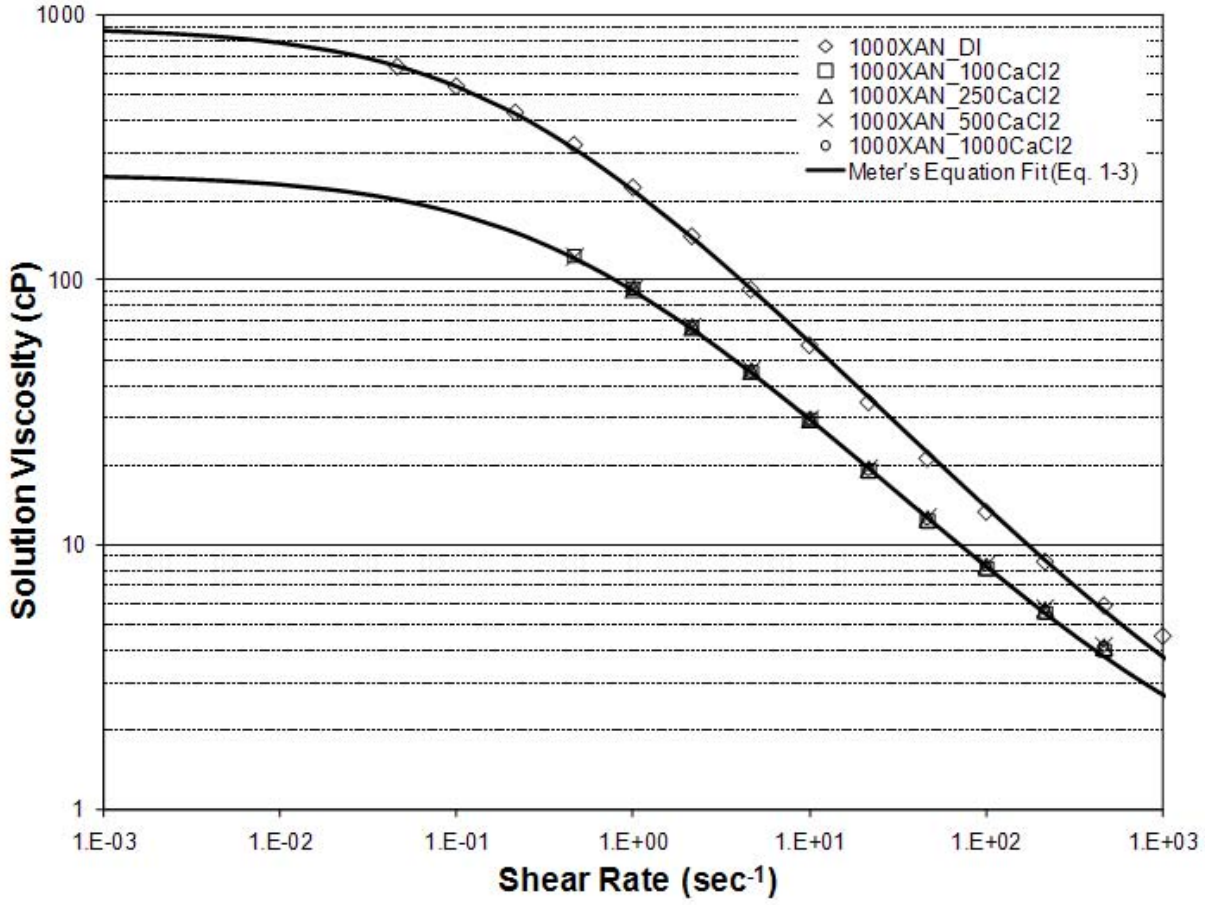

Figure 4-5: *Viscosity/shear rate for 1000 mg/L xanthan solutions as a function of $CaCl_2$ concentration.*

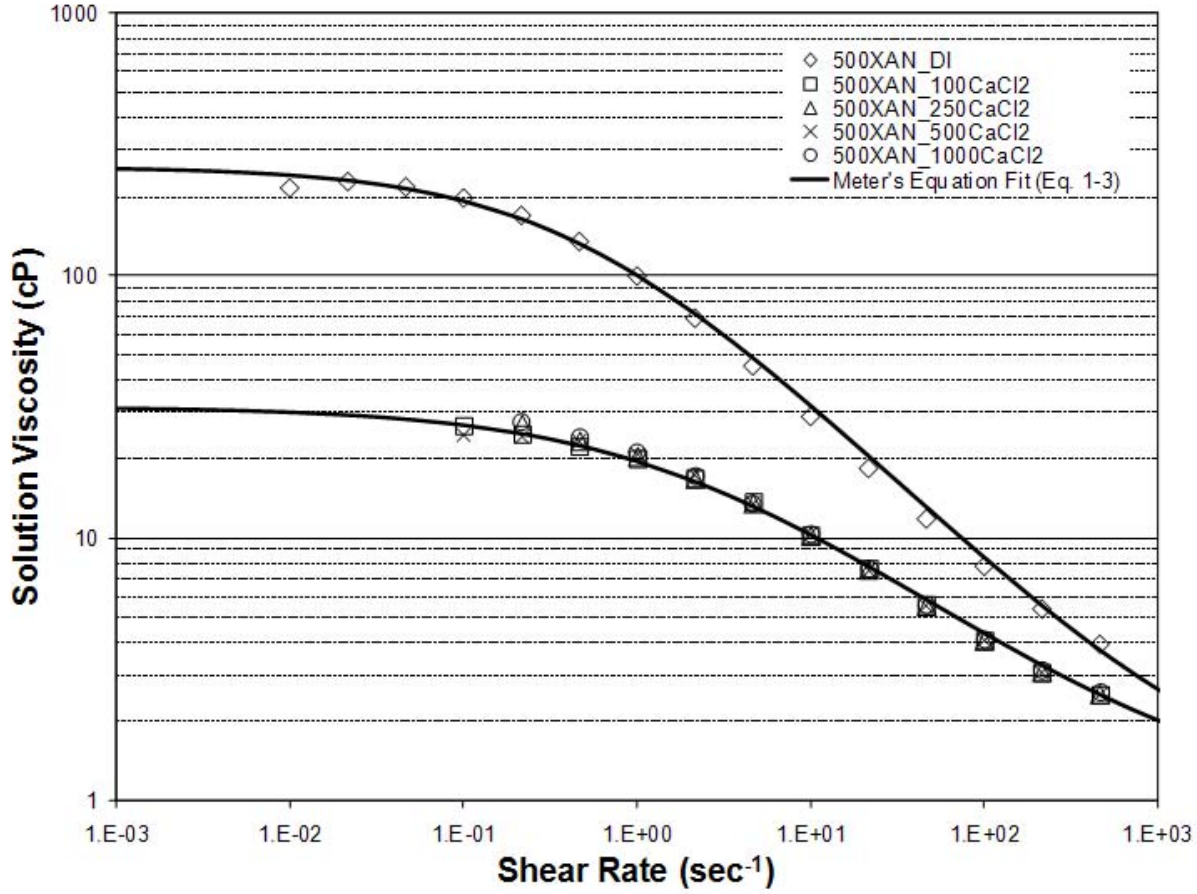

Figure 4-6: *Viscosity/shear rate for 500 mg/L xanthan solutions as a function of $CaCl_2$ concentration.*

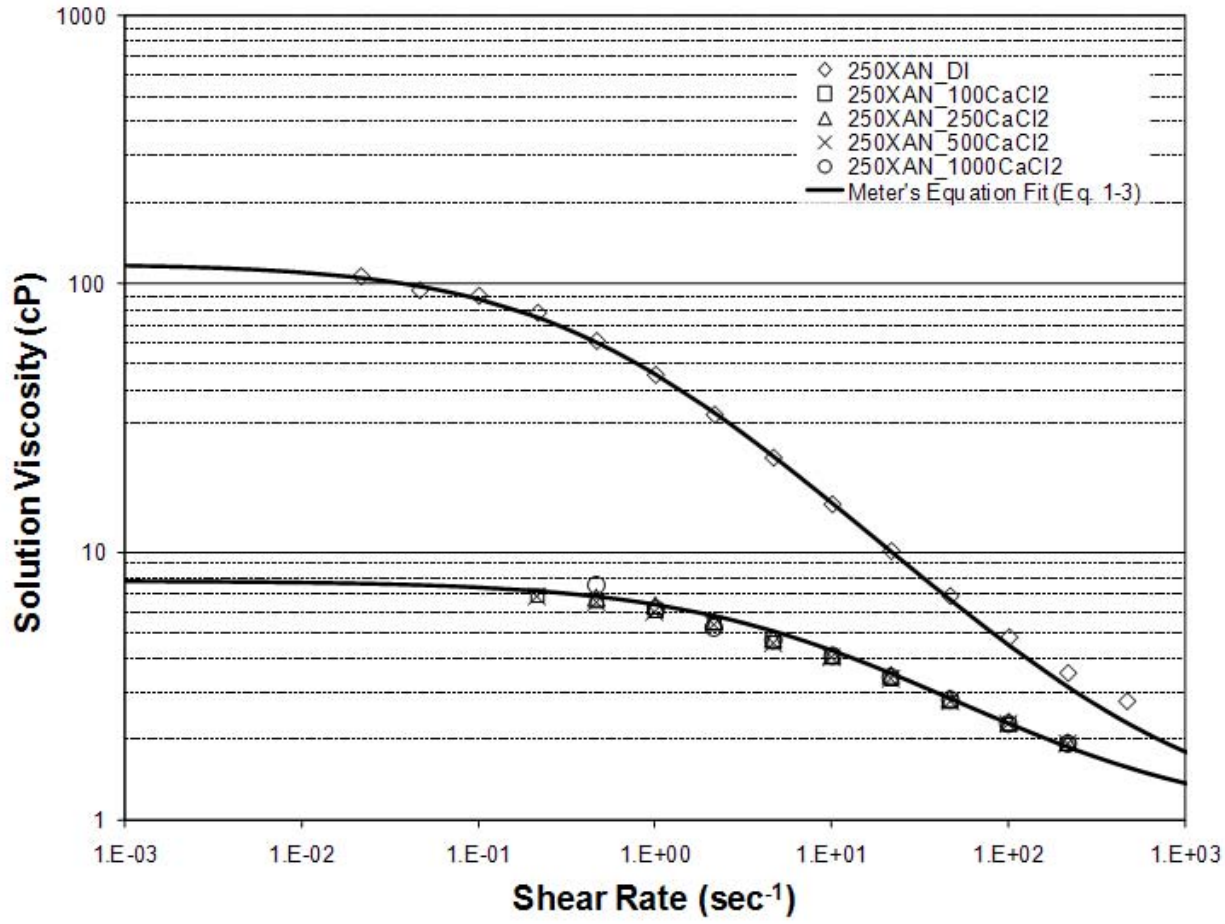

Figure 4-7: *Viscosity/shear rate for 200 mg/L xanthan solutions as a function of $CaCl_2$ concentration.*

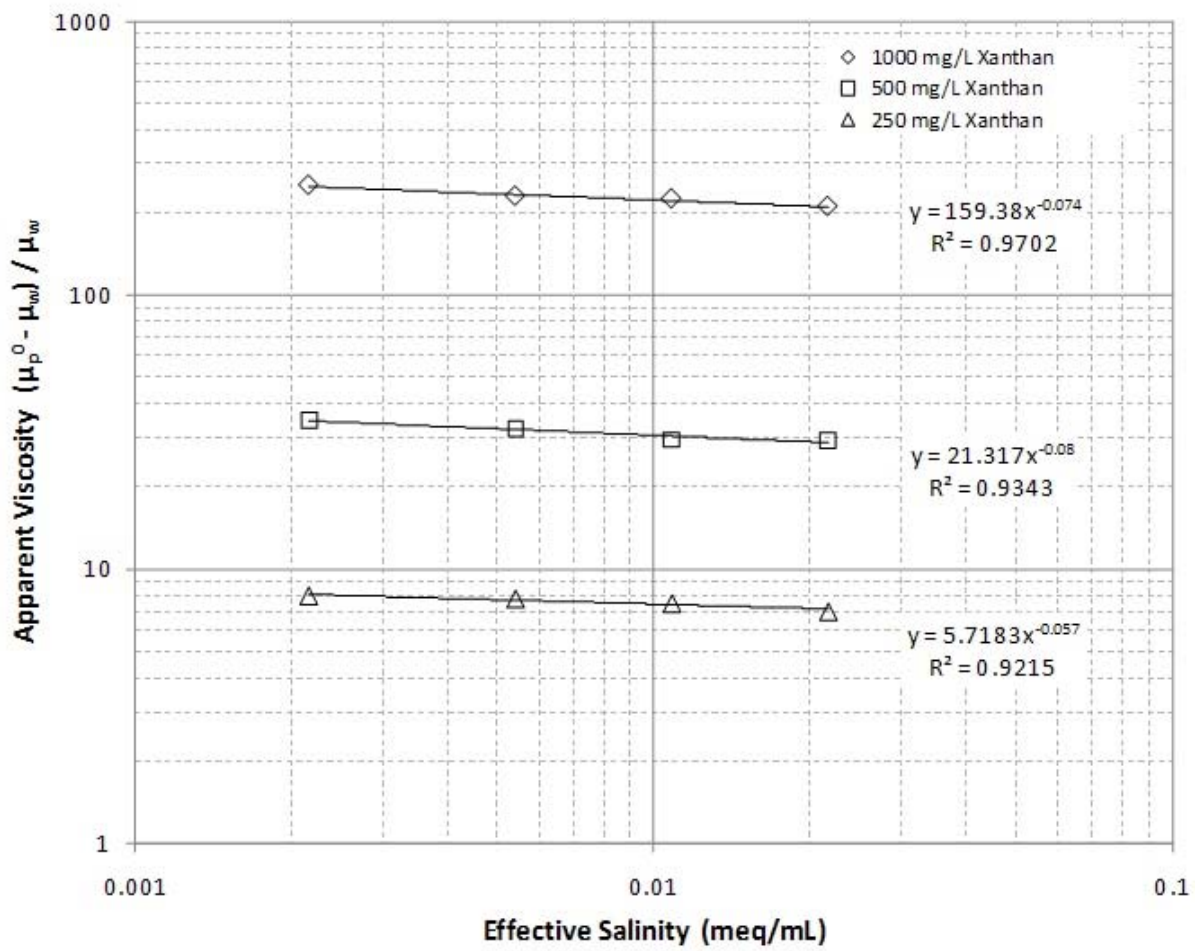

Figure 4-8: *Curve fit for estimating polymer solution viscosity as a function of salinity.*

Polymer Solution Viscosity as a Function of Polymer Concentration

After the zero-shear viscosities and salinity parameters were determined, the next step was to determine the UTCHEM parameters needed to describe polymer solution behavior as a function of polymer concentration. UTCHEM uses the following modified form of the Flory-Huggins equation (Flory, 1953) to model polymer viscosity as a function of both polymer concentration and salinity:

$$\mu_p^0 = \mu_w \left[1 + \left(A_{p1} \cdot C_{41} + A_{p2} \cdot C_{41}^2 + A_{p3} \cdot C_{41}^3\right) \cdot C_{SEP}^{S_p}\right]$$

The known parameters in this equation are water viscosity, effective salinity, and S_p. The dependent variable (C_{41}) is the aqueous polymer concentration in wt% units. The constants A_{p1}, A_{p2} and A_{p3} are input parameters in UTCHEM.

The zero shear viscosities presented in Table 4-2 were plotted against xanthan solution concentration (converted to weight % polymer). The above equation was then used to fit this data using A_{p1}, A_{p2} and A_{p3} as fitting parameters. The result of this process is presented in Figure 4-9. Strictly, these fitted results are valid for a fixed solution $CaCl_2$ concentration of 400 mg/L (C_{SEP} = 0.008 meq/mL). However, given that measured zero-shear viscosities were found to be

largely insensitive to increasing salinity between a $CaCl_2$ concentration of 100 and 1000 mg/L, these A_p-parameters should be additionally applicable for effective salinities within this range.

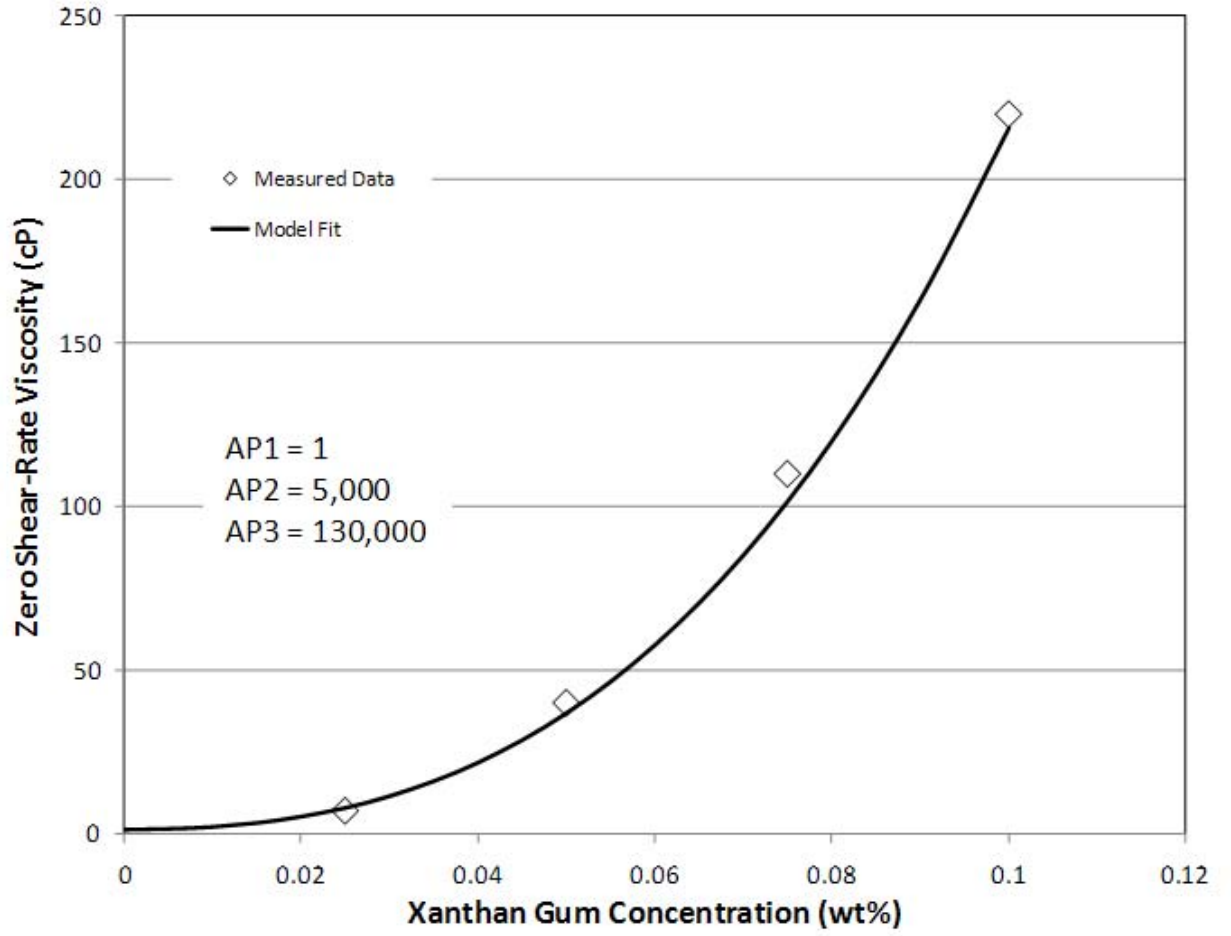

Figure 4-9: *Zero-shear viscosity/concentration data fit for use in UTCHEM simulator.*

Column Experiments

Effluent elution profiles for the first two tracer-containing polymer slugs are presented for four of the five test sands (i.e., UNIMIN 30, UNIMIN 70, F110 Ottawa, SILCOSIL_CF) as Figure 4-10. Column experiments performed using the SILCOSIL_FF sand were unsuccessful in that the polymer plugging within this low-permeability media resulted in column inlet pressures that were in excess of that maintainable by the experimental apparatus. Polymer and tracer elution profiles for subsequent repeat experiments (total of 4 repeat experiments per media category) were found to be coincident with those of the second profiles (as presented in Figure 4-11), indicating a steady-state condition was attained. Additionally, pressure drops, in all successful experimental cases, stabilized after 3 pore volumes and remained stable throughout the flood (i.e., 4 pore volume flood for each experiment), indicating a steady-state flow condition was achieved.

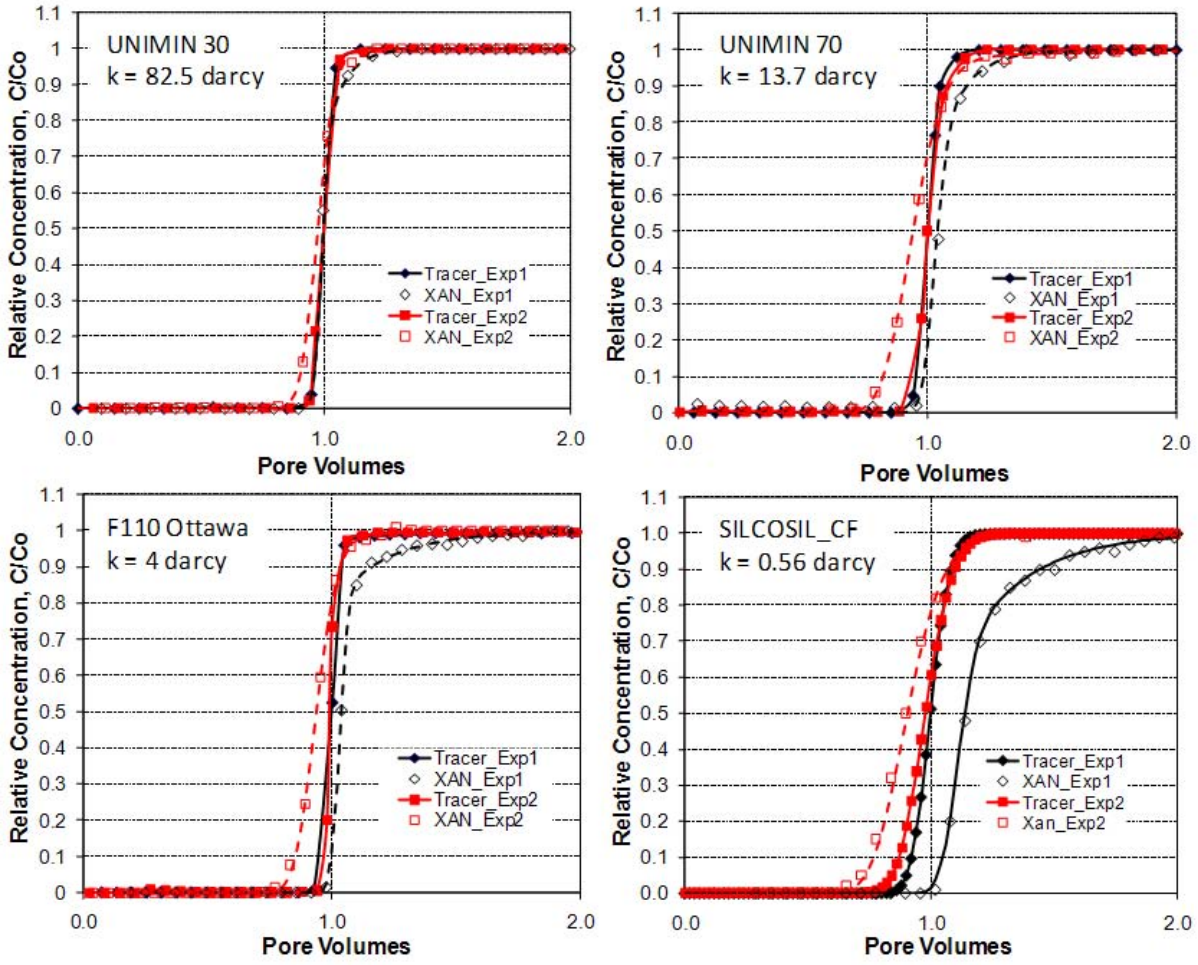

Figure 4-10: *Effluent breakthrough profiles for co-injected tracer/polymer experiments.*

For all test sands, the first tracer effluent profile is shown to breakthrough ($C/C_0 = 0.5$) at exactly 1 pore volume, indicating that the presence of xanthan in the co-injected solution did not impact the transport of the conservative tracer during initial flooding. With the exception of the coarsest sand (UNIMIN 30), the frontal positions of the first polymer slugs are observed to be delayed relative to that of the co-injected tracer, demonstrating the dominance of polymer retention processes (e.g., as a combined effect of adsorption, mechanical entrapment, and hydrodynamic retention) over that of polymer acceleration processes (i.e., IPV and surface exclusion chromatography effects) as the initial polymer solution front propagates through these porous media. One explanation for the tailing (i.e., slow approach to $C/C_0 = 1$) observed in the polymer elution profiles for the F110 Ottawa and SILCOSIL_CF media is the polydispersity of polymer molecular size (i.e., chain lengths) common to polysaccharide polymers such as xanthan that result from manufacturing processes (CP Kelco, 2004). Polymer size polydispersity results in the preferential removal of the largest polymer molecules during transport either by mechanical filtration or preferential adsorption processes. These preferential removal processes results in chromatographic separation of polymer molecular weight fractions and favors the

initial elution of the smaller polymer size fraction. This process is akin to size exclusion chromatography. As preferential removal "sites" within the sand pack are filled and the system achieves either mechanical or adsorptive thermodynamic equilibrium, larger and larger polymer size fractions are allowed to elute. For these low adsorbing test sands, this process is shown to increase with decreasing media permeability.

With the exception of the UNIMIN30 results, breakthrough of the second polymer slug for all remaining media is observed to occur earlier than the first polymer slug, indicating a reduction in the pore volume to polymer. This pore volume reduction is observed to increase with decreasing media permeability. Additionally, the second xanthan breakthrough profile is observed to be less disperse (i.e., faster approach to $C/C_0 = 1$), suggesting the presence of entrapped polymer within the sand packs act to promote more efficient polymer transport.

For the UNIMIN 30, UNIMIN 70, and F110 Ottawa sands, breakthrough of the conservative tracer during the second polymer/tracer flood is observed to be coincident with that of the first flood. This indicates that polymer entrapment and polymer pore volume reduction did not affect the pore volume available to the tracer for media permeabilities greater than 4 darcy. However, as the media permeability approaches 0.56 darcy (that for the SILCOSIL_CF sand), it is clear that effects of polymer entrapment are beginning to reduce the pore volume available to the tracer, resulting in early tracer arrival.

The contributions of the polymer retention and acceleration mechanisms can be estimated by comparing the integrated areas above the polymer and tracer elution profiles shown in Figure 4-11. For example, the area between the first tracer profile and the first polymer profile represents the sum of the contributions of all retention and acceleration mechanisms on polymer transport ($\Sigma_{ret+accel}$). The second polymer elution profile arrives earlier than the first, indicating that the capacities for adsorption and entrapment (mechanical and hydrodynamic) have been met at this flow condition. Therefore, the area between the second tracer profile and the second polymer profile represents the sum of the contributions of all polymer acceleration mechanisms (Σ_{accel}). Subtracting these areas provides a measure of the sum of the contributions of all retention mechanisms at work in this system (Σ_{ret}). The results of this analysis for the media categories used in this work are presented in Table 4-3. These results are also presented graphically in Figure 4-11.

Table 4-3: *Calculated Results for Polymer Retention/Acceleration Contributions.*

	Integrated Areas				**Retention and Acceleration Contributions (Fraction of PV)**		
Media	**Tracer BTC1**	**Polymer BTC1**	**Tracer BTC2**	**Polymer BTC2**	$\Sigma_{Ret + Accel}$	Σ_{Accel}	Σ_{Ret}
UNIMIN 30	1	1	1	1	0	0	0
UNIMIN 70	1	1.06	1	0.95	0.06	0.05	0.01
F110 Ottawa	1	1.08	1	0.95	0.08	0.05	0.03
SILCOSIL_CF	1	1.2	0.98	0.92	0.2	0.06	0.14

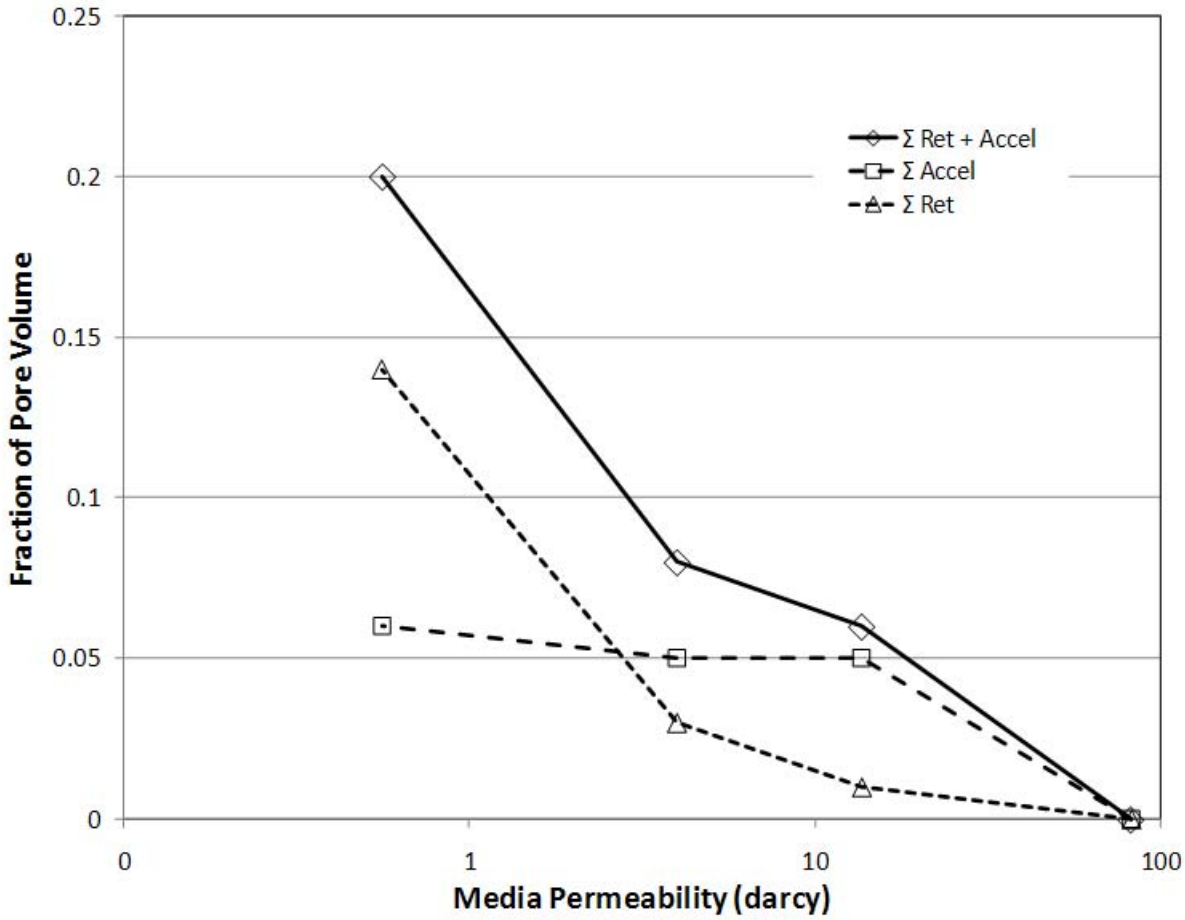

Figure 4-11: *Plot of polymer retention/acceleration contributions.*

UTCHEM treats Σ_{accel} as a measure of the polymer IPV (i.e., the pore volume rendered inaccessible to polymer during polymer flooding due to the accumulation and blocking of pores) and reduces the intrinsic media porosity in the conservation equation for polymer by a factor representing the reduction in porosity due to polymer plugging. This factor is an input parameter for UTCHEM (i.e., EHPI4). Here, an average value of 0.055 PV is chosen to represent the Σ_{accel} for media permeabilities ranging between 13.7 and 0.56 darcy. EHPI4 would then be 1PV-0.055PV = 0.945PV. Even though UTCHEM calls acceleration processes IPV, mathematically the model treats the value of EHPI4 as a general reduction in pore volume regardless of the mechanism (i.e., IPV or surface exclusion processes).

Polymer Transport Parameter Column Test Conclusions

- Many processes related to polymer retention (e.g., sorption, mechanical plugging, etc.) are interrelated and not easily mechanistically separated. We were able to identify and quantify the dominant processes regarding polymer retention and relate these processes to UTCHEM model input parameters. The parameters associated with these processes for the different soils (used in our later experiments) are also utilized as input parameters for the

2-D simulations of tank experiments in Task 3. We continue to analyze the data for journal manuscript preparation.

4.2 Sub-task B: Chemical Oxidant Column Testing

Column tests utilizing polymers and chemical oxidants are necessary to observe and quantify the relative transport of each constituent throughout a homogeneous porous media. While clean sand column tests were used to demonstrate the physical transport characteristics of a xanthan/permanganate mixture, experiments involving natural soil were used to investigate the effects of chemical reactions involving naturally occurring organic matter (NOM) on transport of the mixture. The results of this natural soil experiment are crucial to determining if oxidation of NOM will result in the same complete viscosity loss observed during oxidation of PCE.

Materials and Methods

A 30 cm long, 4.8 cm inner diameter borosilicate glass column (Chromaflex, Kimble/Kontes, Vineland, NJ) was used for polymer/oxidant 1-D transport experiments. The column was outfitted with Teflon endpieces and frits, as well as a fine stainless steel mesh at either column end to prevent shifting of packed media. The columns were dry-packed, weighed, saturated with CO_2 gas and then with deionized water to ensure complete water saturation, and re-weighed to determine void space. Porosity values of 38% and 39% were calculated for the clean and natural soil experiments, respectively, and these values agree well with those determined in Table 2-1. Corresponding pore volumes were determined to be 204 mLs for the clean sand experiment and 214 mLs for the natural soil experiment. Columns were oriented horizontally during experiments. An HPLC pump (Dionex, Waters Corp., Milford, MA) was used to deliver solutions through the columns at a rate of 1 mL/min.

Isopropyl alcohol (2,000 mg/L) in deionized water was used as a conservative tracer in both experiments. Effluent samples were monitored for isopropyl concentration using a Shimadzu GC-17a gas chromatograph equipped with a flame ionization detector, and calibration standards were run before and after each set of column samples. Permanganate oxidant and xanthan polymer solutions were prepared separately at higher concentrations, and combined in a 1:4 ratio to produce stock influent mixture solution of 1,600 mg/L xanthan and 2,000 mg/L $KMnO_4$ (as in batch experiments, see section 3.2). Permanganate concentrations in filtered stock and effluent samples were monitored using a Hach DV4000U spectrophotometer after the method of Crimi and Siegrist (2004). Effluent samples (2 mL) were collected and analyzed within the hour for viscosity using a TA Instruments AR rheometer

Unimin mesh size #70 quartz sand was used in both experiments. For the natural soil experiment, a 1:2 mixture of Unimin mesh size #70 sand and soil obtained from a Colorado School of Mines experimental site. The soil was cut with Unimin sand to lessen the high natural oxidant demand (NOD) of the soil. This soil has been previously characterized (see Tillotson, 2008) as a sandy loam soil with moderate organic content (0.6 to 1.4%). Before mixing, the soil was sieved to retain particles of similar size to the Unimin sand so that average porosity would not differ greatly from the clean sand test. A 24-hour NOD batch test yielded an approximate value of 7 mg permanganate/g soil mixture, using various soil:liquid ratios, according to the method of Haselow et al. (2003). This rough estimate is moderately high and might normally

preclude the use of permanganate oxidation; therefore, any effects of NOM oxidation on the polymer solution should be evident using this soil mixture. The Unimin sand did not display appreciable oxidant demand over the same time period.

Results and Discussion

The isopropyl alcohol tracer test in the clean sand experiment yields almost ideal results as shown in Figure 2-12. No shift toward later pore volumes is observed for the permanganate data as a result of reaction or retardation, indicating almost ideal transport of this oxidant when introduced in a viscous polymer mixture. In Figure 4-12, the effluent viscosity is also plotted as a ratio of effluent to stock solution viscosity. This "viscosity breakthrough" curve, defined as the ratio of effluent to influent viscosity per unit time, is delayed slightly compared to the tracer data, as a result of polymer retention mechanisms (discussed in section 4.1), but no viscosity loss is observed over the duration of the column experiment (~6 hours). Monitored influent stock viscosity values were also not observed to decrease over this timespan. These observations agree well with viscosity retention data obtained from batch experiments (section 3.2).

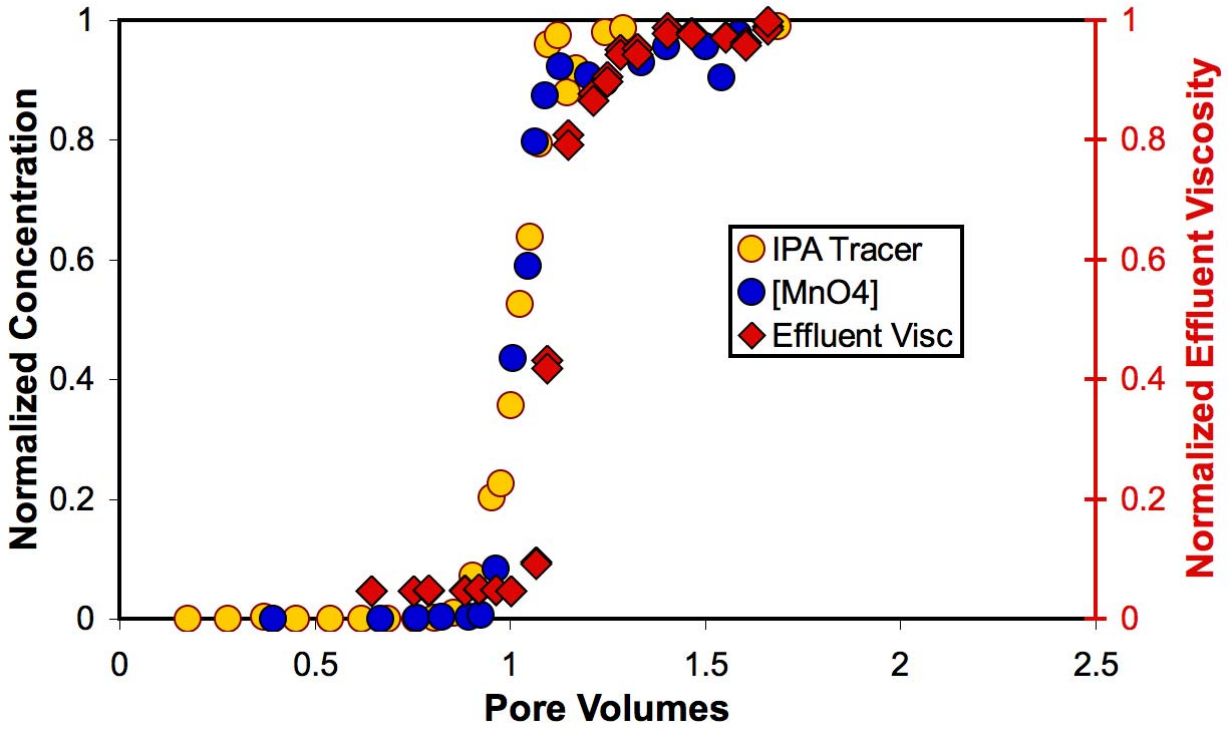

Figure 4-12: *Normalized effluent concentrations (shown in yellow and blue, left-hand y-axis) and normalized effluent viscosity (shown in red, right-hand y-axis) versus pore volumes, for the clean sand column experiment. Normalized effluent viscosity is calculated as effluent viscosity divided by influent stock viscosity (measured at one fixed shear rate). Note that the normalized effluent viscosity ratio is a non-zero value at early pore volume fractions, due to the non-zero influent stock viscosity value.*

The results of the natural soil column experiment are displayed in Figure 4-13. The isopropyl alcohol breakthrough curve is broader, with a less steep approach to $C/C_0 = 1$, than for the pure sand experiment. Unlike Figure 4-12, no permanganate data is shown for the natural soil

experiment. As indicated by the results of the natural oxidant demand batch testing, all of the introduced oxidant was completely consumed by the natural organic matter (NOM) present in the soil media. The oxidant consumption reaction was also confirmed by visible manganese dioxide solid precipitation in the column and the yellow color of the column effluent (created by suspended manganese dioxide solids).

The viscosity breakthrough in this experiment shows a distinctly different curve than in the clean sand experiment. At approximately 0.7 pore volumes, effluent viscosity values deviate from what would be expected from a non-reactive system (such as in Figure 4-12). Effluent viscosity continues to rise but remains lower than expected for ~1.5 pore volumes, at which point effluent viscosity has achieved 91% of the influent solution value. We interpret this deviation from the clean sand experiment curve not as degradation and polymer solution loss, but as the result of mechanical straining of the polymer solution through the deposited manganese dioxide particles. The effluent solution eventually reaches a normalized viscosity ratio of 1, but over a longer timespan than in a system lacking NOM/permanganate reaction.

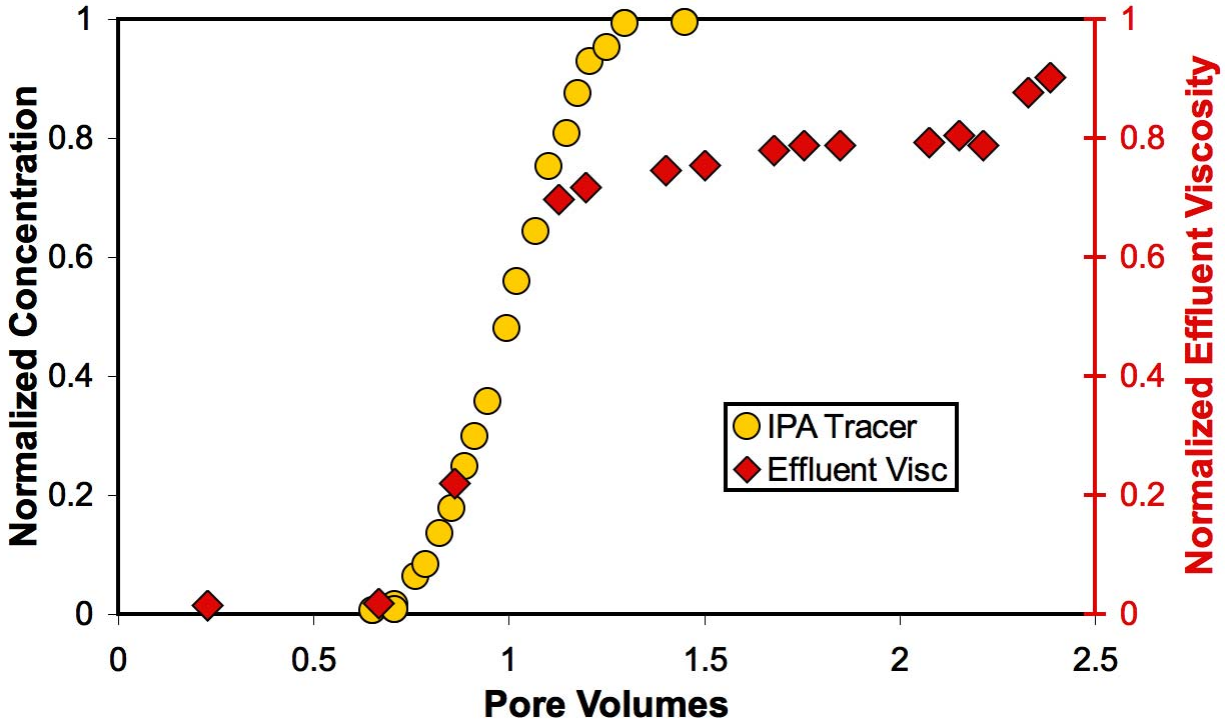

Figure 4-13: *Normalized effluent concentration (shown in yellow, left-hand y-axis) and normalized effluent viscosity (shown in red, right-hand y-axis) versus pore volumes, for the natural soil column experiment. Normalized effluent viscosity is calculated as effluent viscosity divided by influent stock viscosity (measured at one fixed shear rate). Although MnO_4^- was introduced into the column, it was completely consumed through reaction with natural organic matter and thus no MnO_4^- was measured in the column effluent.*

This natural soil column experiment demonstrates that permanganate reaction (in xanthan solution) with NOM does not result in the same effective viscosity loss that accompanies permanganate/PCE/xanthan reactions. While the formation of excessive manganese dioxide

precipitates may produce a mechanical straining effect that delays viscosity breakthrough, the xanthan polymer itself is resistant to degradation and ensuing viscosity loss. Thus, the presence of natural organic matter in a potential aquifer site need only cause concern for non-productive oxidant concern when considering polymer-enhanced chemical oxidation, just as it normally would for any aqueous oxidant application.

Chemical Oxidant Column Test Conclusions

- Permanganate oxidant in xanthan solution (2 g/L $KMnO_4$ in 1.6 g/L xanthan solution) is transported conservatively through a porous medium in the absence of natural oxidant demand (NOD) and oxidant reaction.
- In a demonstrably high NOD porous media, permanganate in xanthan solution is consumed but xanthan solution viscosity is not immediately decreased, in contrast to the viscosity loss noted during PCE oxidation by permanganate. Therefore if site conditions of generally low to moderate NOD (approximately 1-2 mg/kg or lower, Siegrist et al., 2010) are amenable to treatment by permanganate oxidant, mixtures of xanthan and permanganate should retain the increased solution viscosity necessary for increased aquifer sweep.

4.3 Sub-task C: Bioamendment Column Testing

Experiments at the 1-D scale (and accompanying batch characterization experiments) were conducted to understand the biological degradation of the xanthan polymer in field scenarios. This type of data is necessary for a more complete understanding of the microbially-mediated behavior and persistence of polymers in the subsurface. In the short-term, for instance, the propensity of soil microbes to feed on and grow near polymer injection sites may produce negative effects (such as permeability reductions due to biozone growth) or positive feedbacks (the formation of zones with redox conditions favorable for polishing biodegradation reactions). Data about the long-term interactions of microbes with injected polymers may also provide an idea of the length of time over which polymers may actively affect the flow field of an aquifer undergoing polymer-amended treatment. Column experiments in addition to batch-scale tests were utilized for this task in order to gain a more realistic dataset that incorporates the effects of fluid movement expected near injection sites.

Materials and Methods

Solutions of varying concentrations of xanthan polymer were prepared according to manufacturer's instructions in collected natural groundwater. The xanthan polymer solutions were equilibrated overnight to ensure 100 percent solvation. For all experiments, groundwater and soils were obtained from a monitoring well and 1-foot-deep sampling site located at an onsite wastewater field in Golden, Colorado, representing a microbially active subsurface community.

Necessary batch experiments were performed under both aerobic and anaerobic conditions. Ten mLs of a 1000 mg/L stock xanthan solution were added to 50 grams of soil (containing native microorganisms) in clear glass serum bottles. Soil and xanthan solutions intended for use in anaerobic batches were deoxygenated by isolation in an anaerobic chamber for 72 hours before microcosm assembly. Sterile batches composed of autoclaved soil and

xanthan solutions were used as baseline control experiments. Microcosms were sealed to prevent evaporative losses and/or additional microbial contamination, and were continuously agitated on a shaker table. A resazurin solution was used to verify that no oxygen contaminated the anaerobic batches over the course of the experiment. In total, approximately 10 mLs were removed from each batch over the course of the experiment, and this removal did not obviously interfere with degradation.

Column experiments, used to simulate subsurface flow, were constructed with both clean sand and field soils. Each column was constructed of polyvinyl chloride pipe, 62 cm long with a diameter of 8.7 cm. A 1000 mg/L xanthan solution was delivered aerobically by peristaltic pump at 2 mL/min into the bottom of the columns (up-column flow). The flow rate resulted in an average column residence time of approximately 12 hours. Static pressure head measurements were collected over 30 days at two locations, 5.5 cm above and below the top and bottom of each column.

To evaluate the extent of xanthan polymer degradation in both batch and column experiments, both solution viscosity reductions and reducing sugar concentrations were monitored as a function of time. Solution viscosities were measured using both a Brookfield bench-top viscometer and a TA Instruments AR-G2 rheometer. Sample measurements from batch and column experiments were taken at regular intervals for a period of several weeks. Because batch test analysis required the use of sacrificial samples from a finite volume, small sample size was preferred and thus the TA AR-G2 rheometer was preferable (sample size < 1 mL). The Brookfield viscometer, although more convenient for use, required a much larger sample volume (16 mLs) and was appropriate for column experiments only. Both instruments used a rotating spindle to measure solution viscosity over a variety of shear rates.

Reducing sugar concentrations (e.g., fructose or glucose) are derived from the cleavage of the long xanthan polymer molecule into smaller segments (usually accompanied by a decrease in solution viscosity). The pathway for the degradation of the xanthan polymer by Bacillus species strain GL1 into smaller sugars is shown in Figure 4-14 (Nankai et al., 1999). In this study, rather than monitoring individual compounds in the xanthan degradation pathway, the "bulk" presence of reducing sugars were monitored through a dinitrosalicylic acid (DNSA) assay. DNSA is an aromatic compound that reacts with reducing sugars to form an intermediate compound that is detectable by spectrophotometry according to the method of Miller (1959). DNSA reagent solution was purchased from Sigma-Aldrich (St. Louis, MO) and fresh reagent solutions were prepared weekly. A Hach DV4000U UV-Vis spectrophotometer was used to record 540 nm absorbance values proportional to sugars concentration.

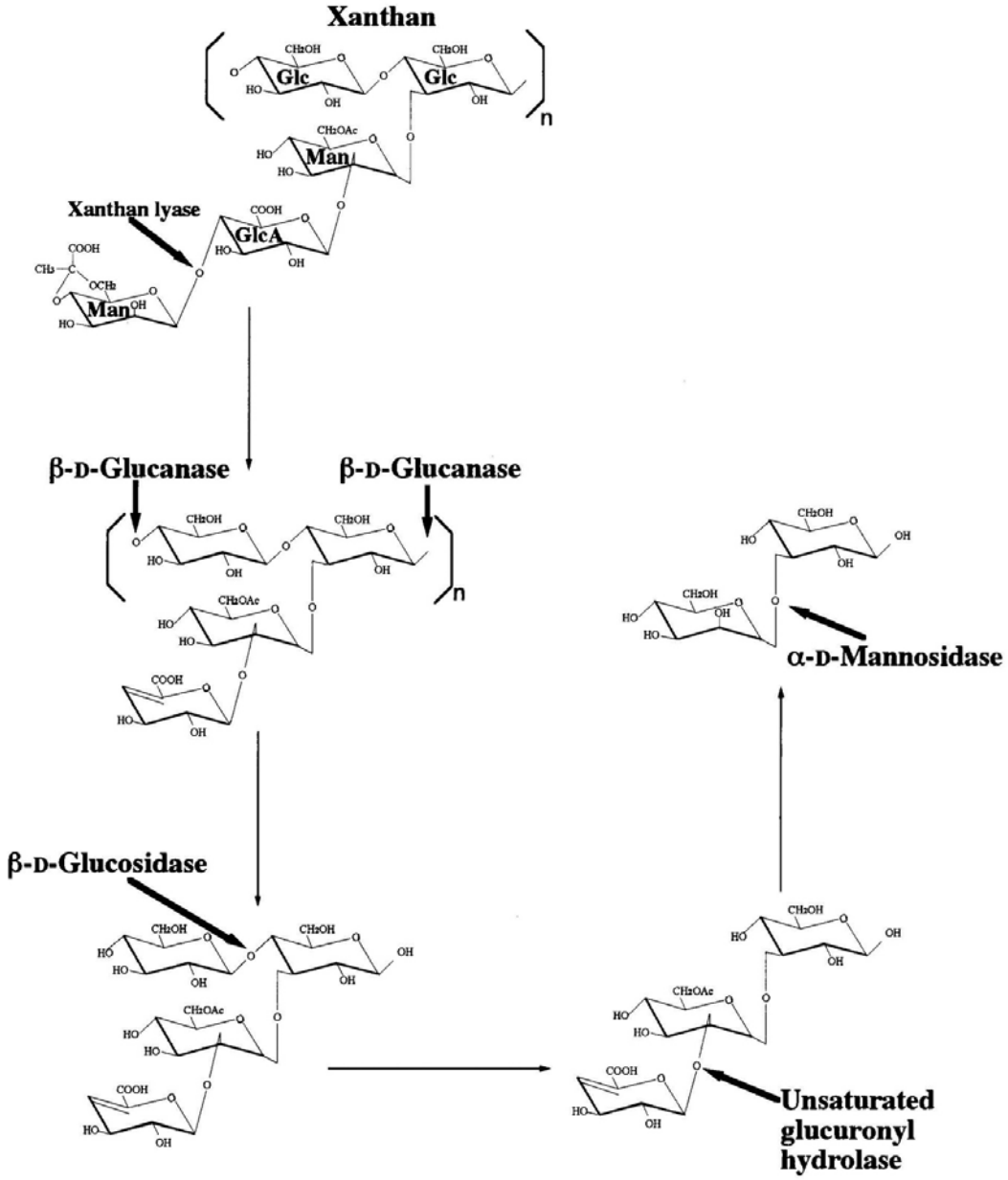

Figure 4-14: *Pathway for Bacillus sp. strain GL1 xanthan degradation (from Nankai et al., 1999).*

Results and Discussion

The results of batch experiments are shown in Figures 4-15 and 4-16. The plot shows the viscosity of the shear-thinning polymer solutions over a variety of shear rates. These curves represent the average of triplicate batch incubations under identical conditions. Standard deviations among the triplicates were too small to distinguish and were thus not plotted; therefore, we interpret all differences between curves as significant.

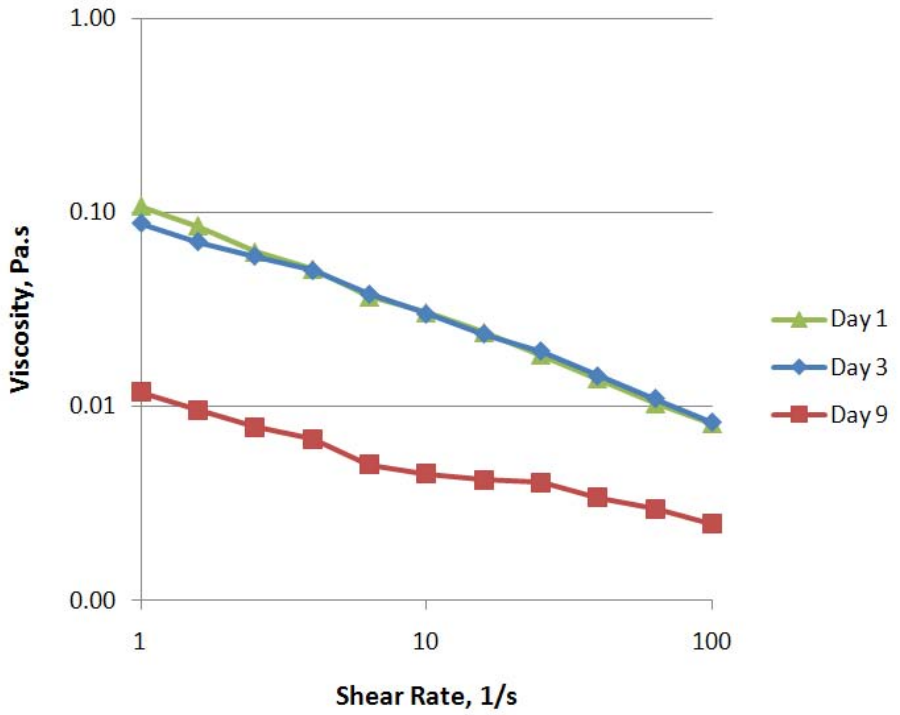

Figure 4-15: *Viscosity versus shear rate, for 1000 mg/L xanthan solutions in batch contact with native soil under anaerobic conditions. 1000 Pa·s = 1 cP.*

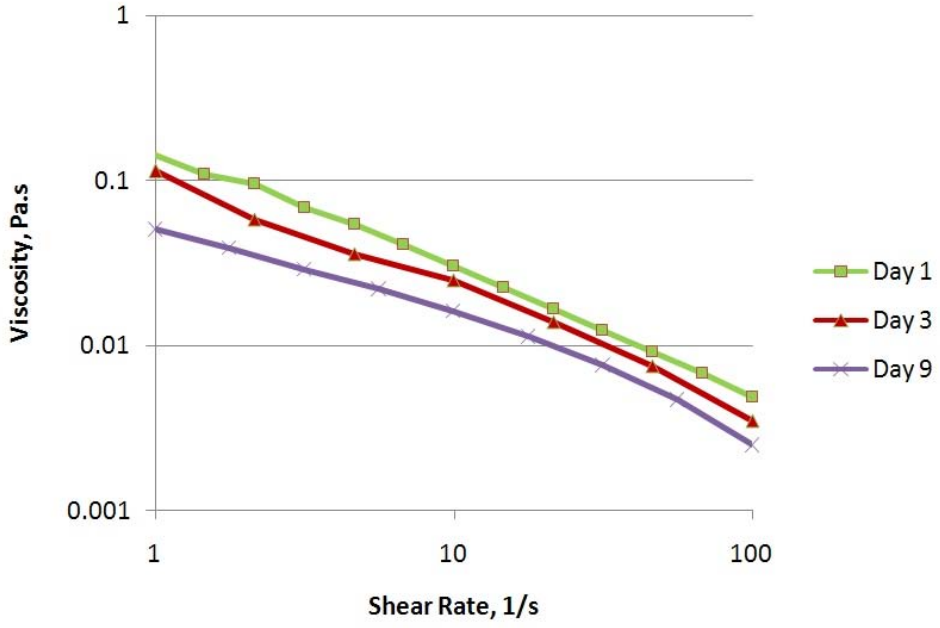

Figure 4-16: *Viscosity versus shear rate, from 1000 mg/L xanthan solutions in batch contact with native soil under aerobic conditions. 1000 Pa·s = 1 cP.*

These figures show that degradation, monitored by proxy using viscosity, occurs more rapidly under anaerobic conditions than aerobic condition. Under anaerobic conditions, a period occurs during which there is apparently little bacterial response. After this initial activation period, however, the polymer is rapidly degraded over the course of several days. Under aerobic conditions, degradation of the polymer appears steady and consistent albeit slower than under anaerobic conditions. At 9 days, solution viscosity had degraded to essentially that of water in the anaerobic batches, and all experiments were sacrificed at this point. As expected, the control batch showed no reduction in viscosity over the 9-day course of the experiment.

In addition to using batch tests to assess xanthan biodegradability, the potential for biofouling as a result of xanthan injection was also examined through a series of column tests using both a clean sand column and a natural soil column. These columns served to simulate hydrologic flow in the subsurface, and to compare the effects of soil-phase microbes versus microbes introduced through groundwater/xanthan additions. After four weeks, Figures 4-17 and 4-18 show increases in pressure of 15 to 20 cm, indicating a reduction in permeability along the column flowpath. While the static head pressure increased by approximately 10-20% over the 30 day study period, there was not a complete restriction of flow. Furthermore, while not directly tested in these experiments, we anticipate that the addition of permanganate to the xanthan polymer solutions would further inhibit the biological growth responsible for this clogging.

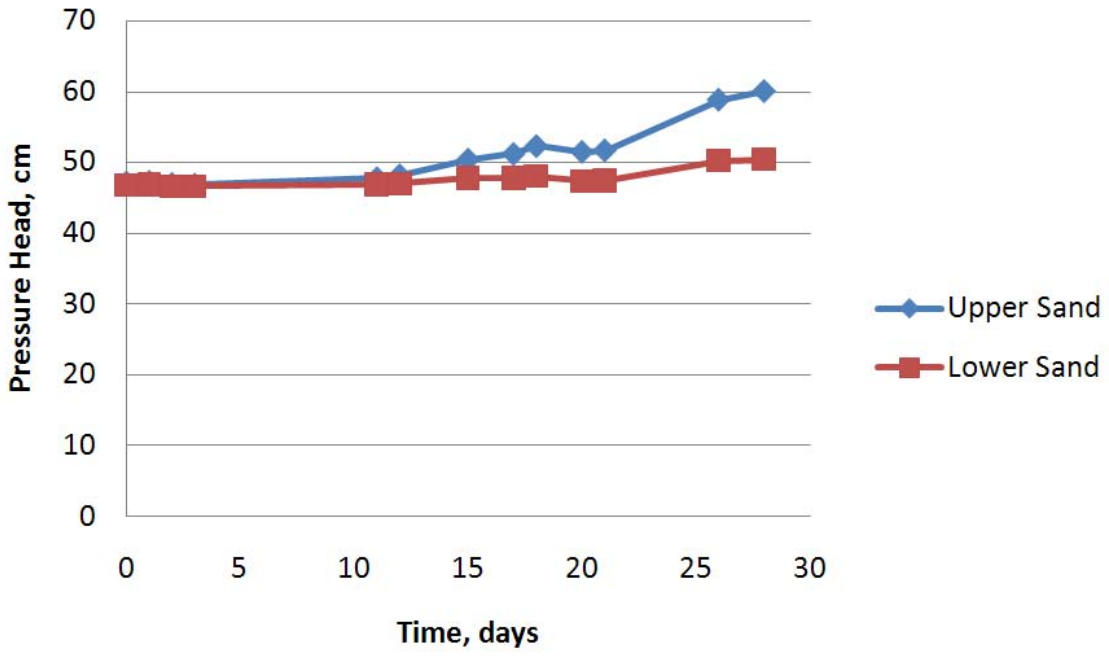

Figure 4-17: *Injection pressure versus time for 1000 mg/L xanthan solution applied to clean sand column. "Upper" refers to readings taken 5.5 cm above the column outlet, and "Lower" refers to readings taken 5.5 cm below the column inlet.*

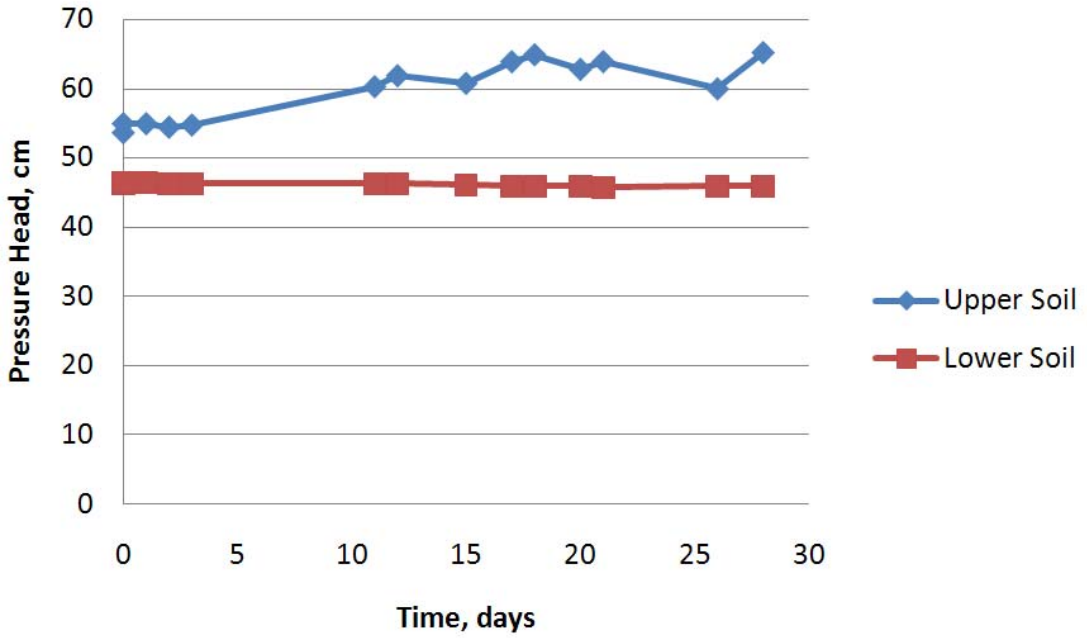

Figure 4-17: *Injection pressure versus time for 1000 mg/L xanthan solution applied to natural soil column. "Upper" refers to readings taken 5.5 cm above the column outlet, and "Lower" refers to readings taken 5.5 cm below the column inlet.*

In these column experiments, multiple ports along the length of the column were utilized for viscosity and reducing sugar concentration sampling. Analyses of these samples show that over the length of the column, the polymer viscosity (at a fixed shear rate of 24.5 sec^{-1}) decreases and the concentration of reducing sugars increases in the direction of flow (Figure 4-19). These changes reflect the breakdown of the xanthan polymer into smaller length segments, ultimately being degraded into single monomer sugar units. We speculate that these monomer sugar units then become available for consumption by common microorganisms, reflecting the partial to complete degradation of the polymer (as inferred by viscosity decreases).

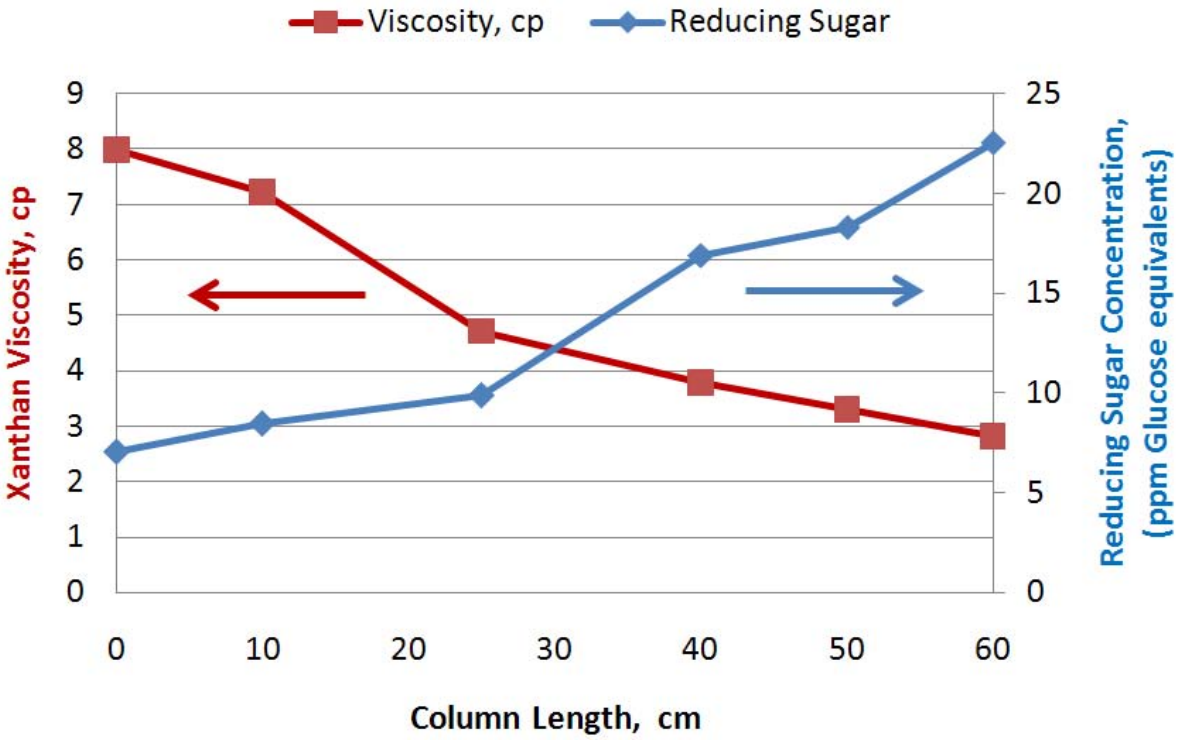

Figure 4-19: *Column effluent viscosity and reducing sugar concentration versus column length for natural soil column. Data obtained after 10 days of xanthan/groundwater flushing. Values corresponding to length = 0 cm represent stock influent values.*

Polymer/Bioamendment Column Test Conclusions

- Both batch and 1-D column experiments demonstrate degradation of the xanthan polymer by microorganisms present in soil and groundwater, with concurrent release of reducing sugars.
- Results from batch experiments indicate that xanthan is vulnerable to biodegradation under both aerobic and anaerobic conditions; however, xanthan degradation proceeded more rapidly under anaerobic conditions as a result of exposure to the native soil organisms present in our samples.
- The confirmation of the presence of simple reducing sugar compounds resulting from xanthan biodegradation leads us to infer that the use of xanthan polymers in the subsurface should not results in long-term deleterious effects on groundwater quality.
- Some bio-clogging resulted from polymer addition (based on pressure increases across the experimental apparatus), but this is not expected to significantly influence polymer delivery in field applications.

TASK 3: 2-D EXPERIMENTS & NUMERICAL MODELING

The objectives of this task are:

1. To explore injected fluid sweep efficiencies within two-dimensional (2-D) heterogeneous sand packs in the absence and presence of polymer.
2. To critically evaluate the utility of polymer addition to improve co-injected tracer (as a surrogate for a remediation amendment) sweep efficiencies in layer systems.
3. To evaluate the performance of a numerical simulator by comparison to experimental data, such that the simulator could be used to investigate numerous relevant heterogeneous systems (as in Task 5).

Numerical studies accompanied each experimental component of this task. The experimental work focused on providing experimental data with which to appropriately condition or "calibrate" the UTCHEM simulator, given the simulator input parameters determined during Subtask 2-1. These experimental data alone are also instructive. We elected to focus our 2-D experimental work on sweep efficiency improvements in layered sand packs, representing layered aquifer systems. Layered sediments are the primary type of heterogeneity in aquifer systems, particularly in mildly heterogeneous aquifers that appear to be homogeneous at larger scale. Such mild heterogeneities, however, have enough permeability contrast to cause strong preferential flow and bypassing, thereby greatly reducing the effectiveness of injected remediation fluids. Layer thickness, layer positioning (vertical order) and permeability contrast were the primary experimental variables.

The numerical research focused on evaluating the performance of the UTCHEM simulator for simulating experimental layered systems. The simulator is evaluated both by using model parameters determined primarily from batch and column experiments (Tasks 1-1 and 2-1) as well as using a more typical calibration procedure. Successful model performance would enable us to use simulator to conduct numerical experiments to build a dataset to better understand polymer effectiveness in a larger set of heterogeneous systems (Task 5).

Materials and Methods

The frame of the tank used for these experiments was constructed of 1½-inch square-tube aluminum and ½-inch aluminum sheet. The tank face could be removed for cleaning and repositioning of screened intervals. The back and side walls of the tank were constructed of ½-inch Delrin™ plastic sheet that was permanently bonded to the aluminum frame. Sampling ports were installed along the back of the tank in a 10 cm grid. Delrin ™ was used to construct well inserts at the left (inlet) and right (outlet) sides of the tank. These wells were completed by facing the inserts with rigid wire screen wrapped with stainless-steel mesh and packing the well volumes with pea gravel. The face of the tank was constructed of ½ inch clear acrylic plastic to support visual observation of transporting fluids within the tank. The tank face was temporarily sealed to the rest of the tank using a butyl sealant and clamps. The interior dimensions of the completed tank were 107 cm long, 51 cm tall and 5 cm wide. A cap was additionally constructed of ½-inch aluminum sheet and Delrin™ plastic to seal the top of the tank.

All tank experiments were packed with sand using a wet-packing procedure. Water was added to the tank to maintain a 2-3 inch water elevation above the sand at all times during

packing. Dry sands were slowly funneled into the tank at 1-inch intervals. At each interval, and ½-inch into the previous interval, the sand was physically stirred to dislodge air bubbles and promote complete water saturation within the pore space. After stirring, the sand pack was tamped at the surface to promote a consistent packing density during the procedure. Once the tank was packed, bentonite clay was used as an upper capillary barrier and the top of the tank was sealed.

All test solutions were prepared using a 400 mg/L solution of $CaCl_2$ (prepared in distilled water) to maintain a constant salinity. A red water-soluble dye (amaranth) was used as a conservative tracer in these experiments. Column experiments were performed to ensure the dye transported conservatively (i.e., without retention). Xanthan solutions were prepared similarly to that described in earlier tasks. For the majority of the tank experiments, the final xanthan polymer test solution was 500 mg/L polymer in 400 mg/L $CaCl_2$. However, in a few cases the xanthan concentration was elevated to 800 mg/L.

A variable-speed positive-displacement pump was used to drive fluids left-to-right through the sand tank. A pulse-dampener was constructed and installed between the pump outlet and the tank. Prior to entering the tank, fluids were routed through a manifold that diverted flow to five vertically-aligned valve positions installed on the inlet side of the tank. The purpose of this valving was to allow for better control over the vertical pressure distribution of fluids within the well during injection. Upon exiting the tank, fluids were collected at five additional valve positions along the tank outlet and directed to an effluent manifold. Fluids exiting the effluent manifold were then directed to a constant head device. Thus, the tank consisted of a constant-flow boundary at the inlet and a constant-head boundary at the outlet.

Procedurally, a single experiment consisted of:

1. purging all the tubing and the inlet well volume with the tracer solution;
2. noting the time and initiating flow into the sand pack;
3. documenting the position of the conservative dye front at regular time intervals (by physically tracing the dye front position on the tank, and by photo documentation) until the test solutions had fully swept the sand pack pore volume;
4. recording transient and steady state inlet pressure and flow rates;
5. removing all traces of the dye tracer by water-flooding with $CaCl_2$ solution;
6. purging all tubing and the inlet well volume with the polymer/dye tracer solution and repeating steps 1-5 for the polymer-amended dye solution.

Depending on flow rates and the specific heterogeneity structure of the sand pack, a single experiment required 5-9 days to complete.

Digital photographs documenting temporal dye front positions within the tanks were processed using the Groundwater Modeling System (GMS) software. Once uploaded into GMS, the images were cropped and a 0.5 cm grid was applied. GMS was then used to integrate the tank area swept by the dye tracer at each time step. Sweep-efficiency (*SE*) was then calculated as:

$$SE(\%) = \frac{Swept\ Area}{Total\ Area\ of\ the\ Tank} \times 100$$

Further, *SE* was evaluated at 10% of the injected dye concentration, or $C/C_{inj} = 0.1$. The selection of this concentration condition resulted from visual observations of the dye solution in sand packed in 40 mL vials. Below $C/C_{inj} = 0.1$ the dye could not be seen. Practically, for delivery of remediation fluids, the C/C_0 that would result in an enhanced sweep area differs depending on

the C_0 remediation fluid. For surfactants, the critical micelle concentration must be achieved, for oxidants, a net positive oxidant demand must be delivered, and for bioremediation, enough microbes must be delivered to effect growth, or nutrients delivered to enhance growth. In many polymer applications, we are attempting to deliver fluids to hydraulically inaccessible zones where concentrations are usually small. Thus, C/C_0 values of 0.1 are reasonable for defining the zone swept by remedial fluids.

Results and Discussions

The first series of 2-D tank experiments focused on investigating polymer sweep-efficiency improvement for layered heterogeneity structures. The focus of this work was to evaluate sweep-efficiency improvement potential as a function of:

1. Layer permeability contrast
2. Layer ordering and thickness.

Two-Layer – Equal Thicknesses of UNIMIN 30 and UNIMIN 70 Media

The first 2-layer tank experiment performed consisted of two layers of UNIMIN 30 and UNIMIN 70 sand of equal thickness. Hereafter, this tank will be designated tank 2L_50%UNI30_50%UNI70. As a tracer, an aqueous solution of aramanth dye (75 mg/L) was injected to the left side of the tank at a fixed rate of 17.6 cm^3/min (0.9 ft^3/day). The results of the initial tracer experiment (no polymer addition) are presented as Figure 5-1. As anticipated, the dye tracer front was observed to propagate more rapidly through the more permeable (top) sand layer (UNIMIN 30) than through the less permeable layer (UNIMIN 70). Tracer propagation was observed to occur independently within each layer, with little transverse fluid movement across layers. Tracer solution injection continued until the dye had completely swept the tank area, which took a total of 1.71 days.

Figure 5-1: *Photo results of amaranth dye tracer test (no polymer addition) within tank 2L_50%UNI30_50%UNI70. Top layer is the higher-permeability sand.*

After water-flooding to remove the dye, a 500 mg/L xanthan solution (in 400 mg/L $CaCl_2$ and 75 mg/L aramanth dye) was injected. The injection flow rate in this case was measured as 17.7 cm^3/min (0.9 ft^3/day). Figure 5-2 illustrates that the addition of polymer greatly improves the rate at which the tank was swept (compared to Figure 5-1). The increased viscosity of the polymer solution is shown to promote transverse fluid movement (or cross-flow) from the more

permeable UNIMIN 30 layer into the less permeable UNIMIN 70 layer, as a result of the mobility reduction (or reduced horizontal hydraulic conductivity) in the UNIMIN 30 layer. The rate of cross-flow into the UNIMIN 70 layer was determined to be the equivalent of 92 cm/day, based on the temporal positions of the dye front penetrating this layer. The total time to sweep the tank with polymer solution was 0.68 days (or 1.6 pore volumes), as opposed to the1.7 days (or 4 pore volumes) needed for the non-polymer case.

In addition to photo-documenting these experiments, the temporal positions of the dye fronts for both the tracer (i.e., no-polymer) and polymer experiments were physically traced on the front of the tank using a fine-tipped Sharpie™ pen. These positions were eventually darkened and photo-documented at test completion to assist in estimating swept areas over time. To estimate swept areas a 0.5 cm grid was super-imposed onto the digital photographs. Grid nodes that overlaid portions of the tank that were contacted by the dye were assigned a value of 1. Similarly, grid nodes that overlaid portions of the tank that were not impacted by the dye were assigned a value of zero. A simple counting program was then used to sum the impacted nodes at each time step and calculate sweep efficiencies as the ratio of swept area to total tank area. An example of this procedure is provided as Figures 5-3 and 5-4.

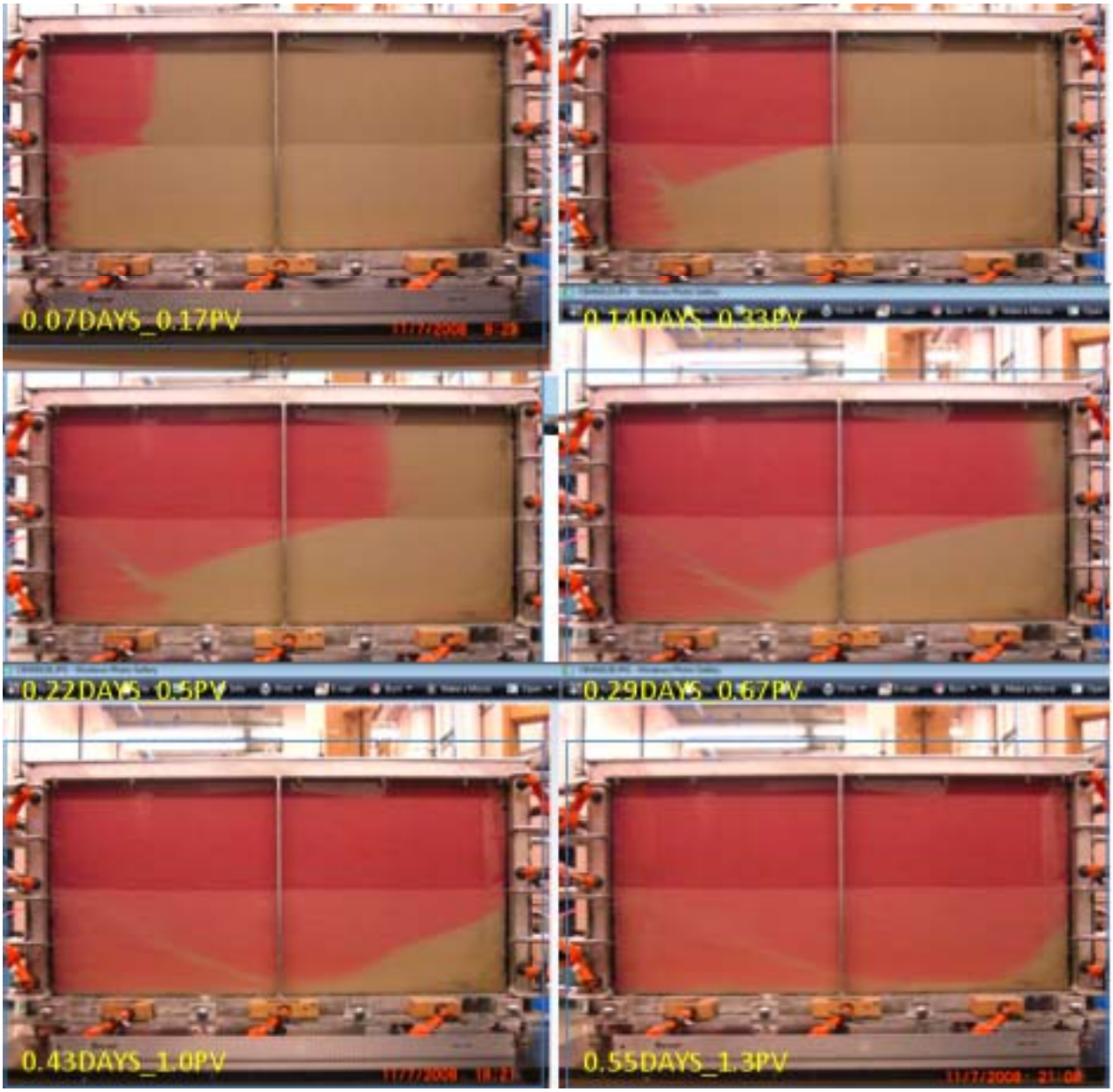

Figure 5-2: *Photo results of the polymer-amended tracer test within tank 2L_50%UNI30_50%UNI70.*

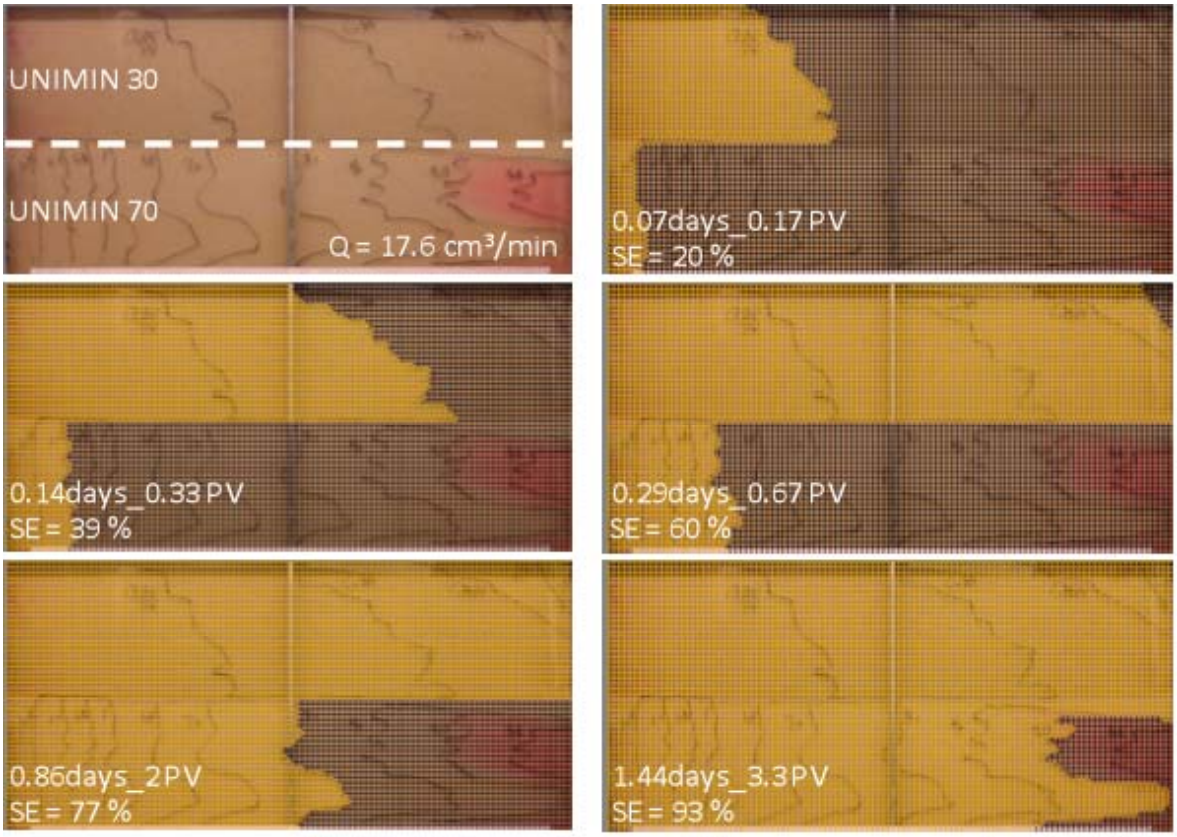

Figure 5-3: *Tracer propagation within 2L_50%UNI30_50%UNI70 tank.*

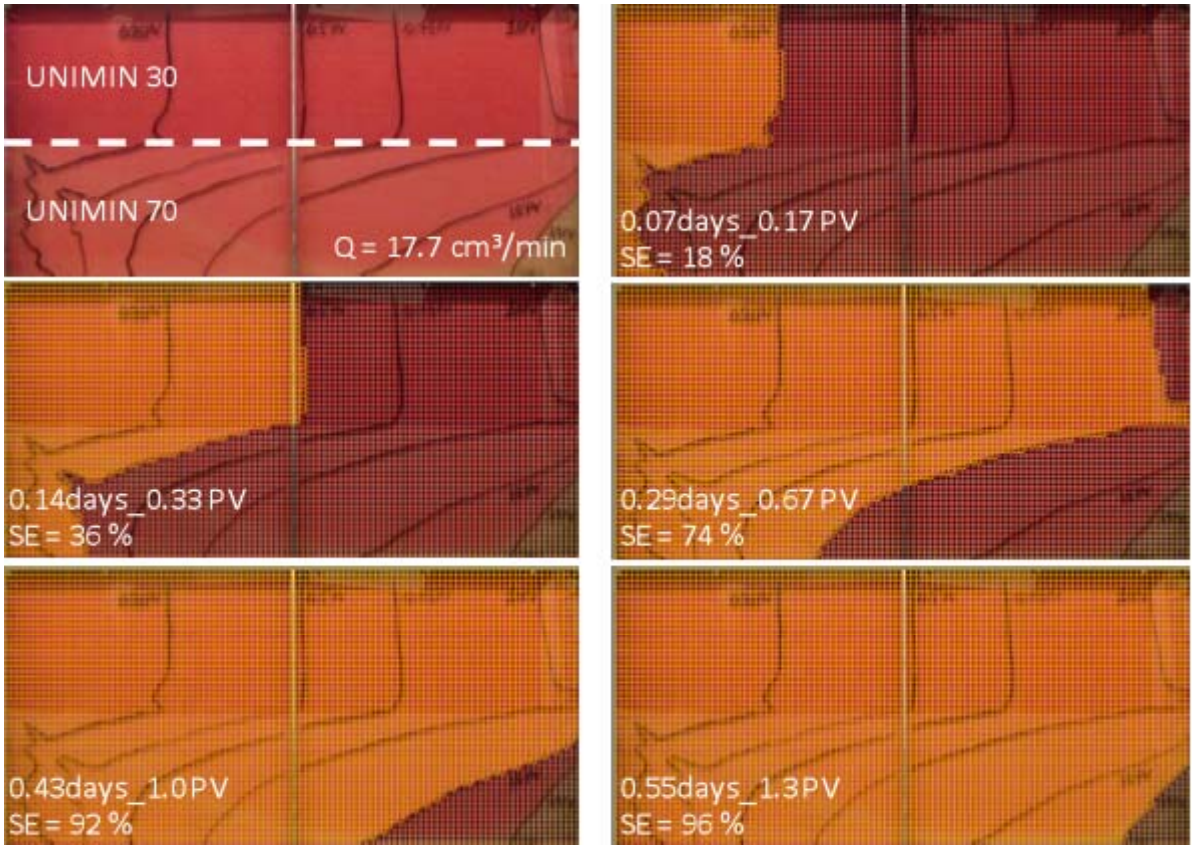

Figure 5-4: *Polymer propagation within 2L_50%UNI30_50%UNI70 tank.*

Calculated sweep efficiencies are plotted as a function of tank pore volumes in Figure 5-5. The most striking feature of these figures is the degree to which the addition of polymer improves the rate of sweep within this two-layered heterogeneity structure. For the polymer flood, 100% sweep efficiency was achieved in 1.6 pore volumes of injected fluid, as compared to the roughly 4 pore volumes required for the no-polymer case. For the tracer, the rate at which the tank is swept is shown to change at roughly 0.75 pore volumes, which corresponds to the arrival of the tracer at the effluent end of the tank within the UNIMIN 30 layer. Thereafter, the rate of sweep decreases to that corresponding to the rate of fluid advancement into the UNIMIN 70 layer. For the polymer-amended tracer, the rate of sweep appears to initially proceed optimally for this layer arrangement. That is, the addition of 500 mg/L xanthan is shown to enhance the efficiency of tracer sweep such that the rate of sweep proceeds as if the sand pack was homogeneous (as indicated by the dashed line in Figure 5-5). However, the rate of sweep was observed to decrease at roughly one pore volume, which corresponds with the arrival of the polymer-amended dye front at the tank effluent within the UNIMIN 30 sand layer. Beyond one pore volume the rate of sweep appears to mimic that observed for the no polymer case, suggesting that the driving force for cross-flow from the UNIMIN30 sand into the UNIMIN 70 sand had diminished after the UNIMIN30 layer had been wholly swept.

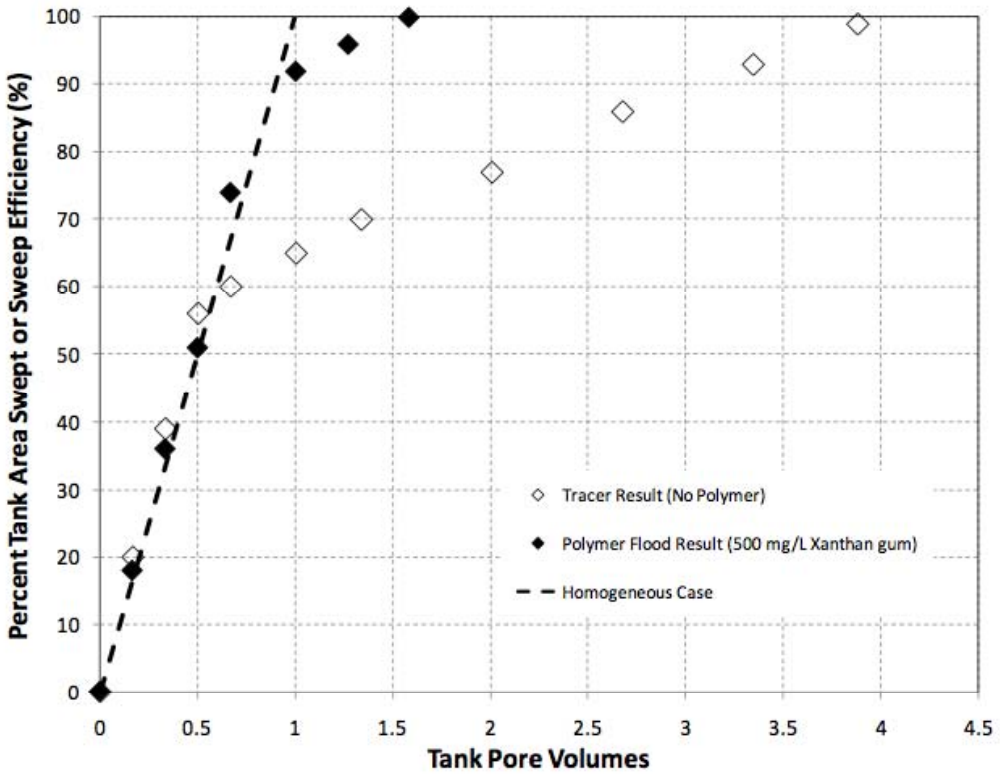

Figure 5-5: *Temporal sweep efficiency results for tank 2L_50%UNI30_50%UNI70.*

Two Layer – Varying Thicknesses of UNIMIN 30 and UNIMIN 70 Media

Two additional two-layer tanks were packed to investigate the effect of varied layer thickness on polymer sweep-efficiency improvement. The first of these tanks was packed such that the thickness of the upper UNIMIN 30 sand layer occupied 75% of the tank height, with the UNIMIN 70 sand occupying the remaining 25% (hereafter designated as tank 2L_75%UNI30_25%UNI70). The injection flow rate during the tracer experiment (no-polymer) was 19.7 cm^3/min (1 ft^3/day). The flow rate for the subsequent polymer experiment was 19.7 cm^3/min (1 ft^3/day). The results of these experiments for tank 2L_75%UNI30_25%UNI70 are presented in Figures 5-6 and 5-7.

The next tank in this series of experiments was packed with an upper UNIMIN 30 sand layer that occupied 25% of the tank height, with the UNIMIN 70 sand layer occupying the remaining 75% (hereafter designated as tank 2L_25%UNI30_75%UNI70). The injection flow rate during the tracer experiment (no-polymer) was 17.5 cm^3/min (0.89 ft^3/day). The flow rate for the subsequent polymer experiment was 19.2 cm^3/min (0.98 ft^3/day). The results of these experiments for tank 2L_25%UNI30_75%UNI70 are presented in Figures 5-8 through 5-11. A summary of the results for all two-layer tank experiments is presented in Table 5-1.

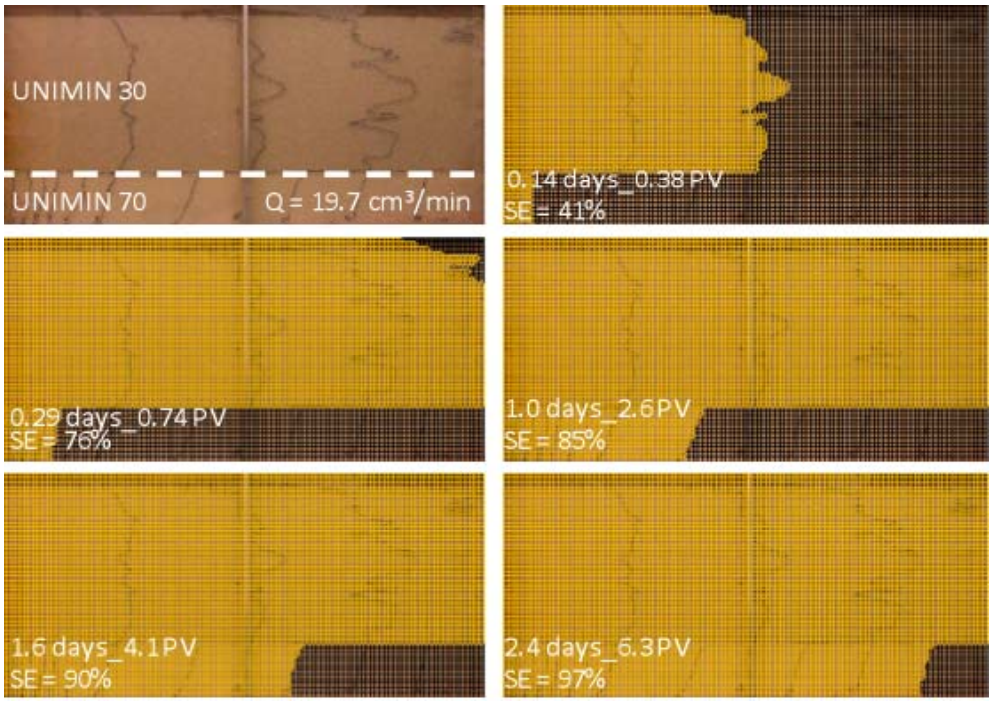

Figure 5-6: *Tracer propagation within 2L_75%UNI30_25%UNI670 tank.*

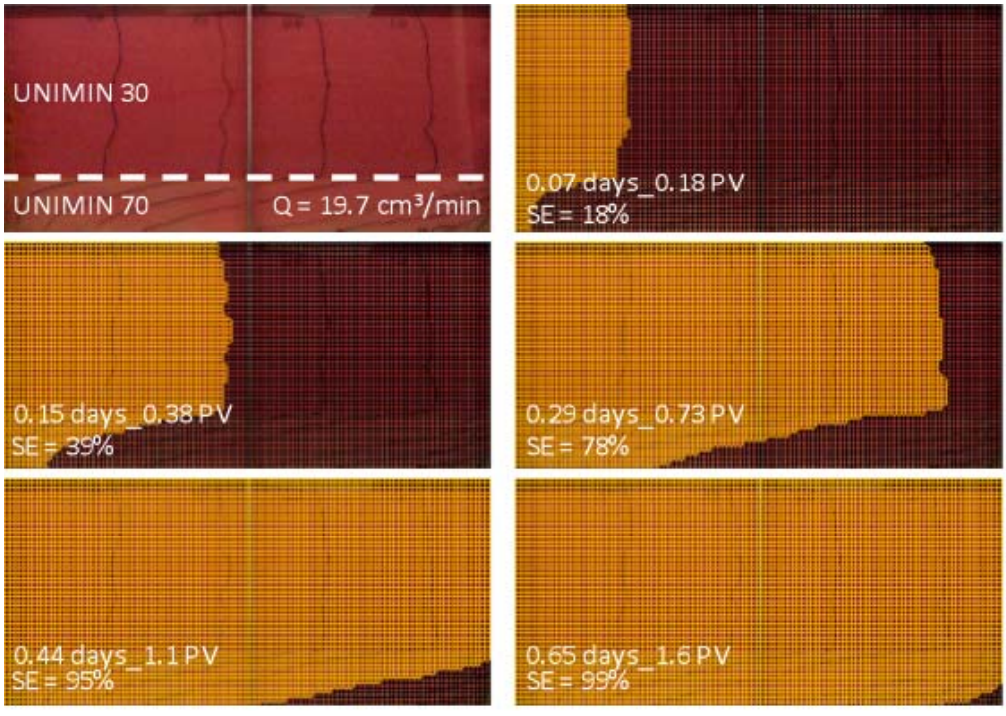

Figure 5-7: *Polymer propagation within 2L_75%UNI30_25%UNI70 tank.*

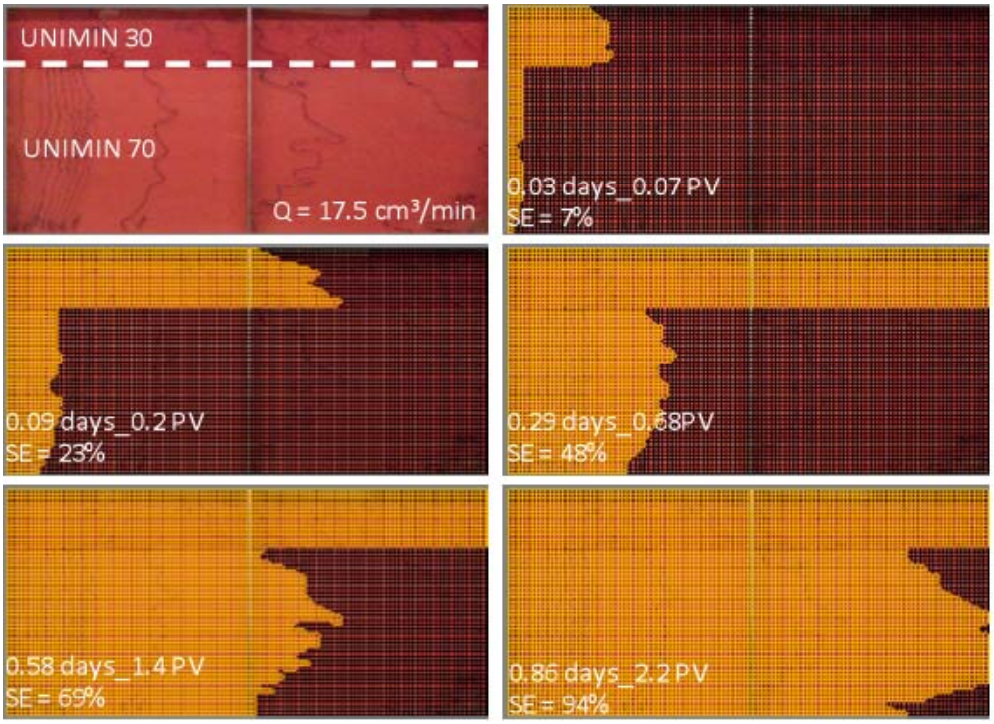

Figure 5-8: *Tracer propagation within 2L_25%UNI30_75%UNI70 tank.*

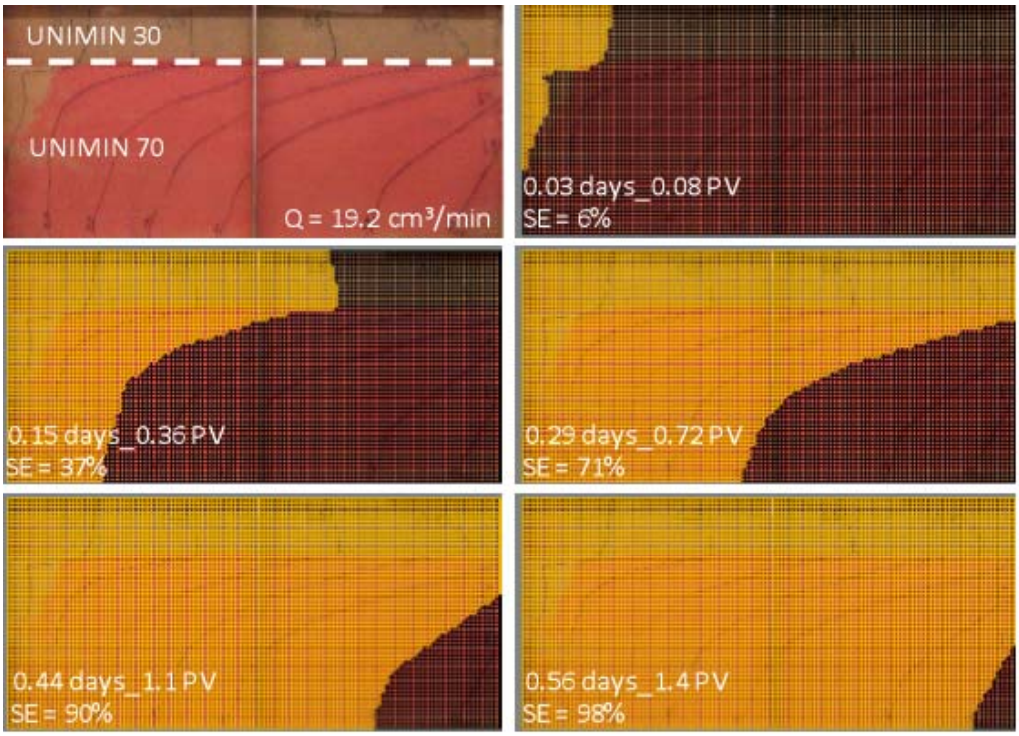

Figure 5-9: *Polymer propagation within 2L_25%UNI30_75%UNI70 tank.*

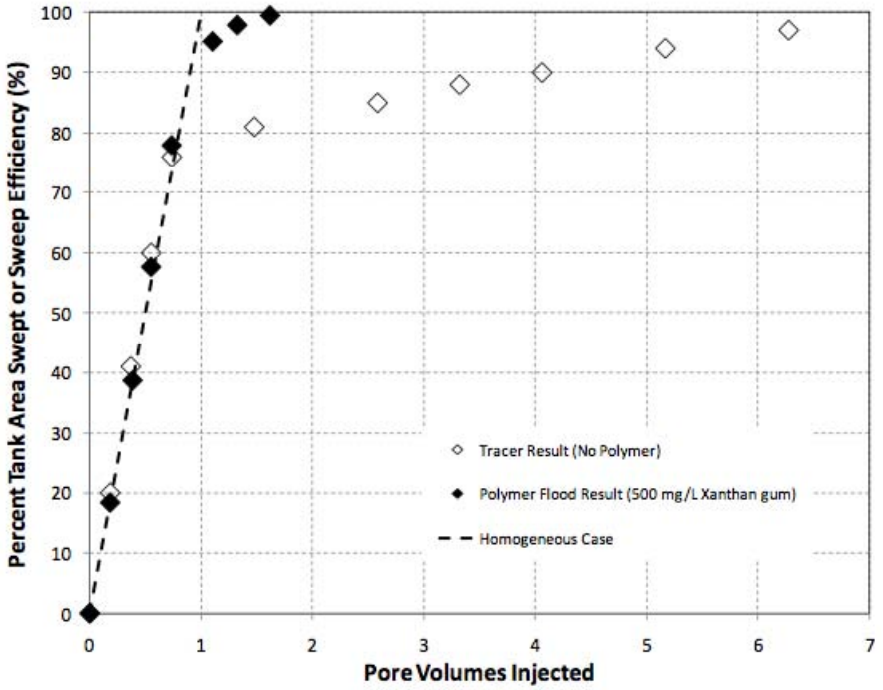

Figure 5-10: *Temporal sweep efficiency results for tank 2L_75%UNI30_25%UNI70.*

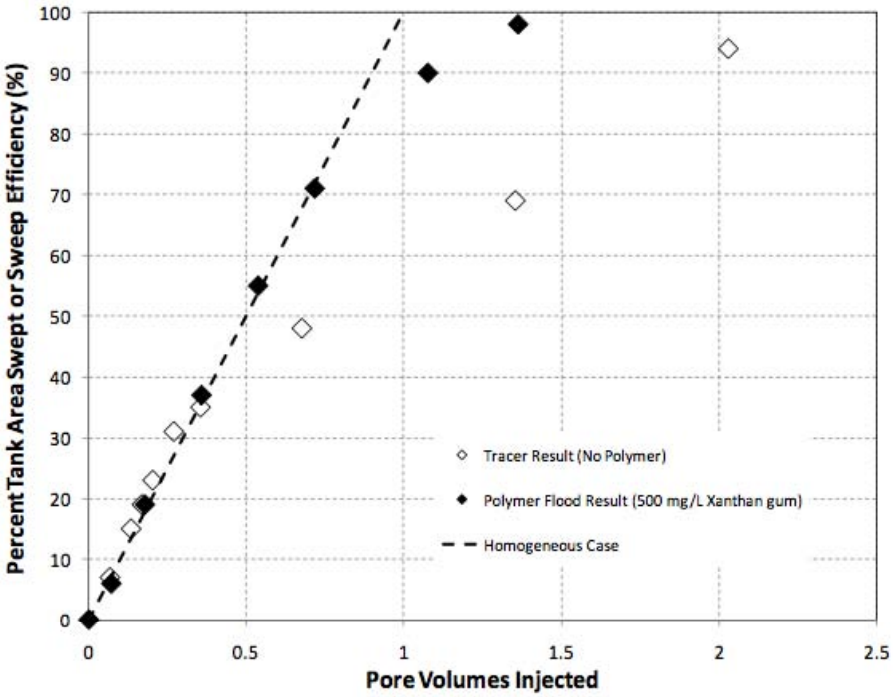

Figure 5-11: *Temporal sweep efficiency results for tank 2L_25%UNI30_75%UNI70.*

As was the case for the initial two-layer tank (i.e., 2L_50%UNI30_50%UNI70), the addition of polymer improved the sweep efficiency of these additional sand packs. For the 2L_75%UNI30_25%UNI70 tank the addition of 500 mg/L xanthan reduced the number of pore volumes required to completely sweep the tank from 7 (tracer) to 1.6 pore volumes (polymer), or better than a four-fold improvement. Likewise, the number of pore volumes required to completely sweep the 2L_25%UNI30_75%UNI70 tank was reduced from 2.2 to 1.54 pore volumes, or 1.5 times faster.

Table 5-1: *Summary of the sweep efficiency results for the two-layer experiments.*

	Tank A[a]	**Tank B[b]**	**Tank C[c]**
k (layer 1), darcy	82.5	82.5	82.5
k (layer 2), darcy	13.7	13.7	13.7
relative thickness (layer 1)	0.25	0.5	0.75
relative thickness (layer 2)	0.75	0.5	0.25
$k_{h,avg}$, darcy	30.9	48.1	65.3
flow capacity (layer 1), %	67	86	95
flow capacity (layer 2), %	33	14	5
Pore Volumes to 100% Sweep			
tracer (no polymer)	2.2	4.0	7.0
polymer (500 mg/L xanthan)	1.54	1.6	1.65
***SE*, %, at 1 Pore Volume**			
tracer (no polymer)	60	65	77
polymer (500 mg/L xanthan)	88	92	95

[a]*Tank A: 2L_25%UNI30_75%UNI70*
[b]*Tank B: 2L_50%UNI30_50%UNI70*
[c]*Tank C: 2L_75%UNI30_25%UNI70.*

As shown in Table 5-1, the effect of increasing the relative thickness of the more permeable layer (Layer 1) is an increase in the number of pore volumes required to completely sweep the tank. This effect appears to relate to the reduced capacity of Layer 2 to entertain flow within these 2-layer systems and is most pronounced for the tracer dataset. Flow capacities (*FC*) for each layer were calculated as:

$$FC = \sum_{i=1}^{n} \frac{k_n h_{r,n}}{k_{h,ave}}$$

with

$$k_{h,ave} = ave\ horizontal\ permeability = \sum_{i=1}^{n} (k_n h_{r,n})_i$$

where k_n is the permeability for a given layer, and $h_{r,n}$ is the thickness of a layer relative to the total thickness of the sand pack. The addition of 500 mg/L xanthan is shown to greatly reduce the effects of heterogeneity in these tank experiments by inducing cross-flow from Layer 1 into Layer 2. Thus, the addition of polymer enhances the effective flow capacity of the lower permeability layer (Layer 2) to improve the overall sweep-efficiency of the layered system. This enhanced flow capacity for Layer 2 is not accounted for in the FC calculation and is difficult to

quantify. As a result, attempts made to correlate *SE* to a metric describing heterogeneity in layered systems has been challenging. The task was further complicated because polymer solutions effectively diminish the effects of heterogeneity in these systems.

Model Performance Evaluation: UTCHEM Simulations of Two Layer 2-D Experiments

The results of the physical 2-D tank experiments were used to evaluate the performance of, or condition, the UTCHEM simulator. The principal objective of this modeling was to demonstrate that the model could reproduce the observed experimental data with regard to temporal sweep-efficiency, and therefore could reasonably be used to extend the analysis of to systems beyond the limits of the experimental data. A 3.5ft (107 cm, x-dimension) × 1.66 ft (51 cm, y-dimension) cell-centered grid was constructed to match the dimensions of the 2-D experimental tank. The 2-D grid was assigned a 0.167 ft thickness to allow the simulator to perform representative volume calculations. Grid node spacing was established on 0.021 ft (or 0.63 cm) centers to provide sufficient grid refinement for modeling fluid flow within this tank. All polymer-specific input parameters used were those determined from the 1-D column experiments as described for previous tasks.

Procedurally, the experimental results of conservative tracer sweep (i.e., no polymer case) were first used to condition the UTCHEM simulator to the experimental flow domain. Initial values for model-input parameters were taken from the bench-scale experiments described in Tasks 1 and 2. The simulator was conditioned by simulating tracer injections and systematically adjusting model permeabilities within either layer (as required) until simulated temporal sweep-efficiencies matched those observed within the experiments. In each case, UNIMIN 30 and UNIMIN 70 sand permeabilities were initially assigned values of 82.5 darcy and 13.7 darcy, respectively. In all cases, tank layer permeability adjustments did not exceed 10% of their measured 1-D values (Task 2, Table 4-1). Justification for modifying permeabilities in these simulations centers on the fact that the intrinsic media permeability measured from 1-D column experiments can differ from those within the 2-D tank due to differences in media packing procedures and resultant differences in particle packing and arrangement. As a secondary criterion, simulated pressure drops were compared to those determined experimentally. This procedure was repeated for each two-layer tank experiment.

Temporal tracer propagation profiles for each two-layer sand tank are compared to their corresponding simulated result in Figures 5-12 through 5-14. Likewise, experimental and simulated tracer sweep-efficiencies for each two-layer tank are presented as a function of injected pore volumes in Figure 5-15, for comparison. The UTCHEM simulator cannot reproduce the non-uniform tracer propagation fronts observed in Figures 5-12 through 5-14 that are likely due to smaller-scale heterogeneity within layers or fluid front instabilities. However, the agreement between experimental and simulated sweep-efficiencies observed in Figure 5-15 demonstrate that an appropriately assigned “effective” permeability for each layer can reproduce the bulk effect of tracer sweep-efficiency as a function of layer thickness. This is again demonstrated by the agreement between measured and simulated pressure drops for each two-layer tank as shown in Figure 5-16.

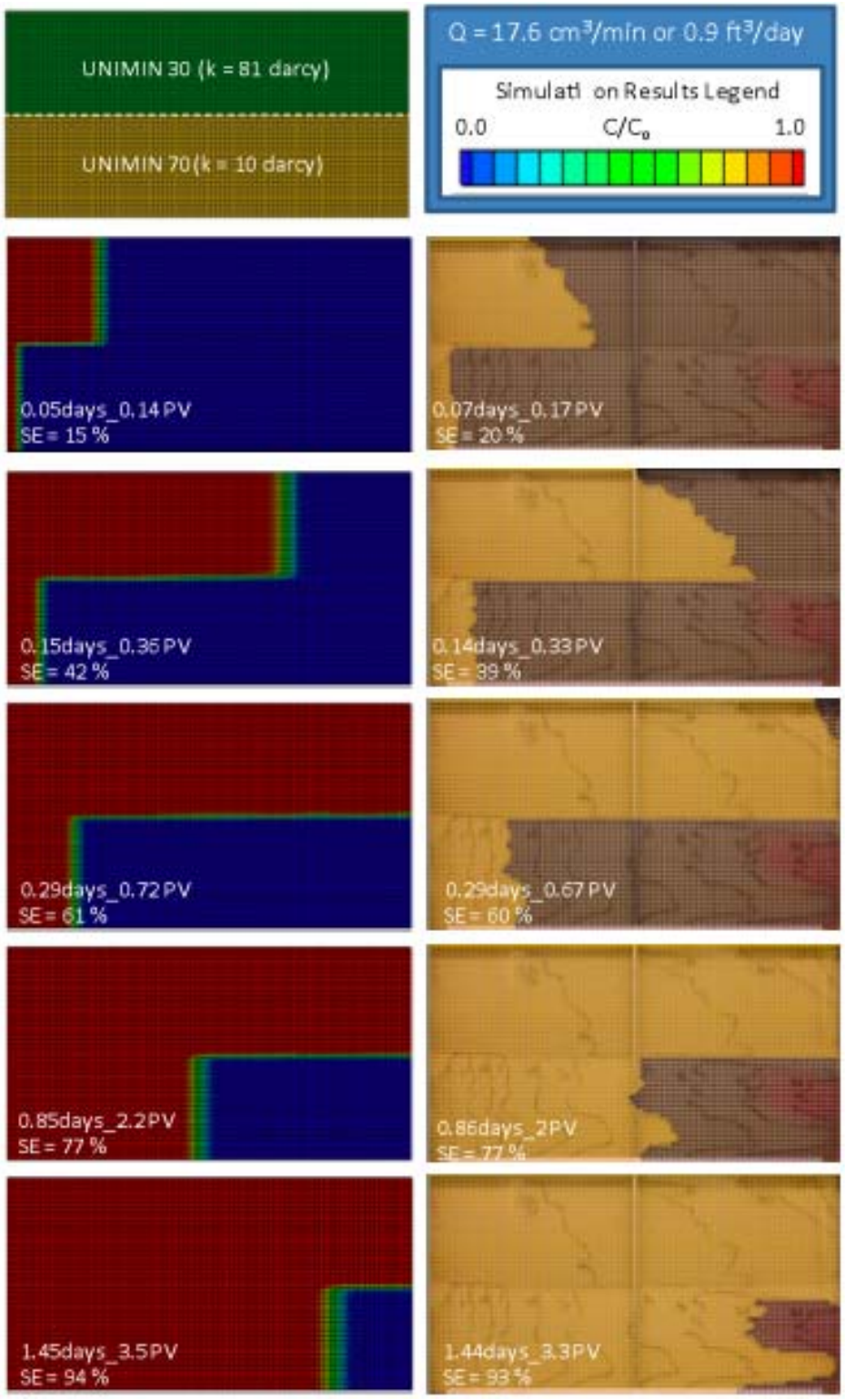

Figure 5-12: *Simulated tracer propagation within 2L_50%UNI30_50%UNI70 tank.*

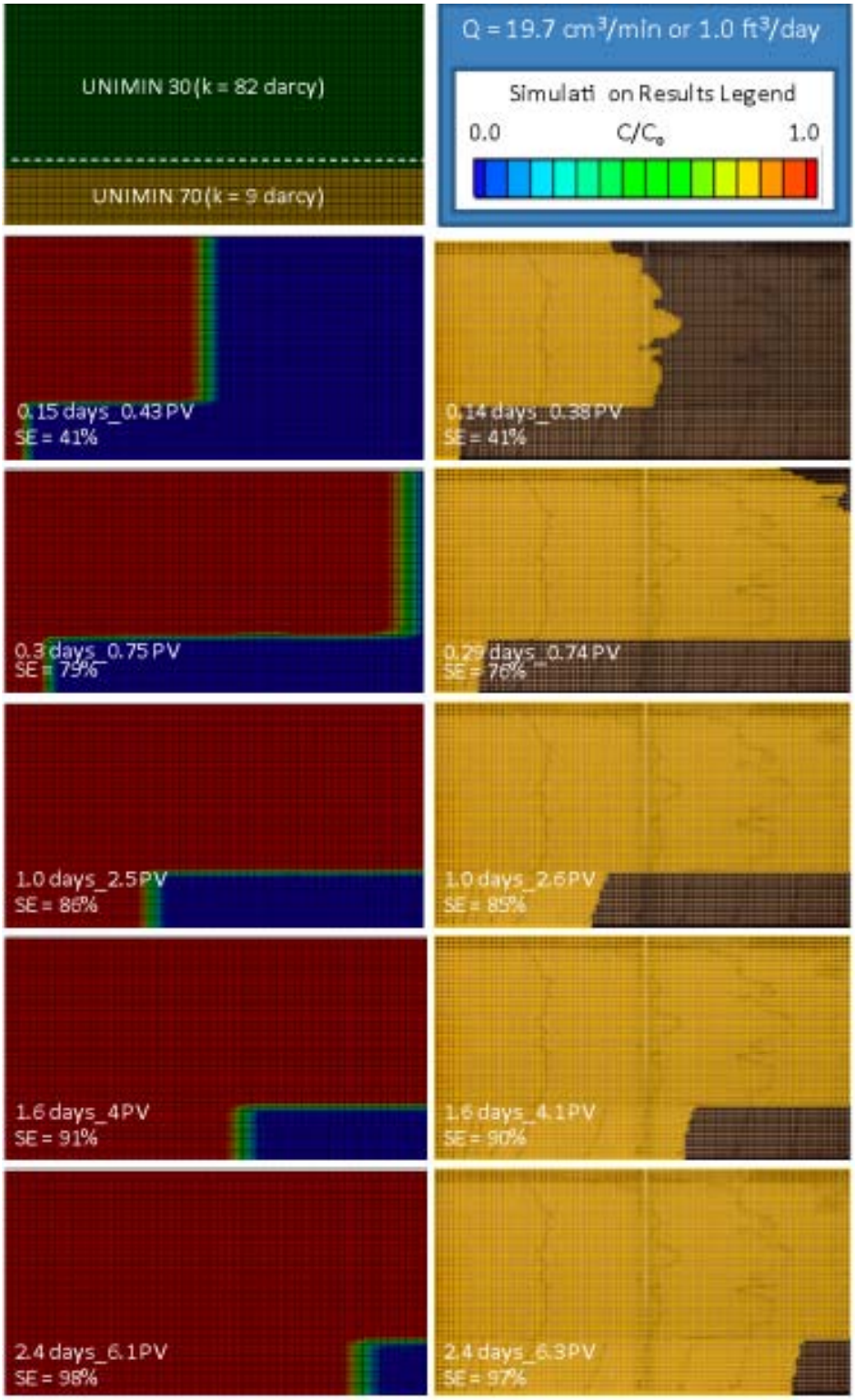

Figure 5-13: *Simulated tracer propagation within 2L_75%UNI30_25%UNI70 tank.*

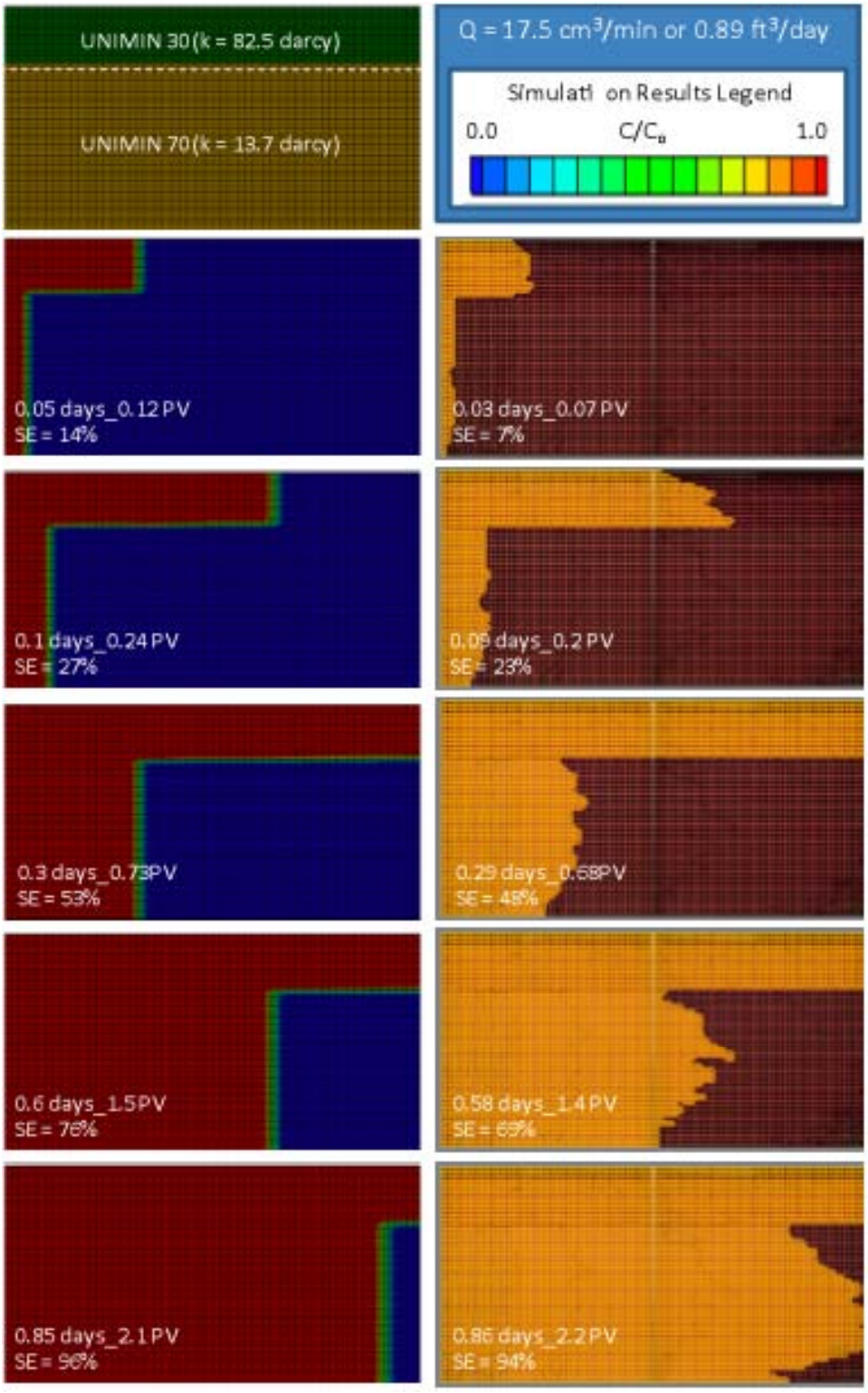

Figure 5-14: *Simulated tracer propagation within 2L_25%UNI30_75%UNI70 tank.*

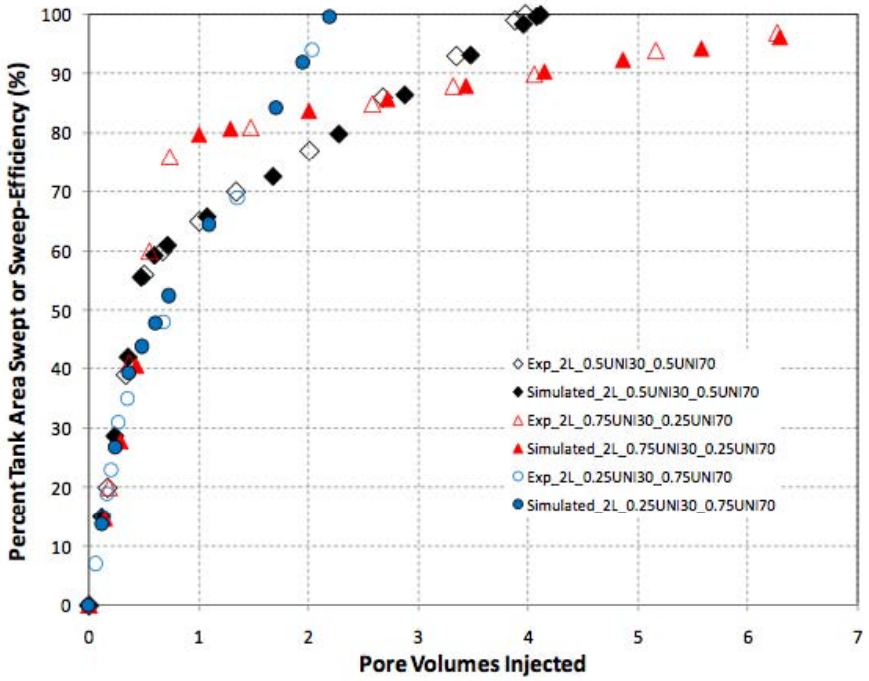

Figure 5-15: *Tracer sweep efficiency profiles for all two-layer experiments.*

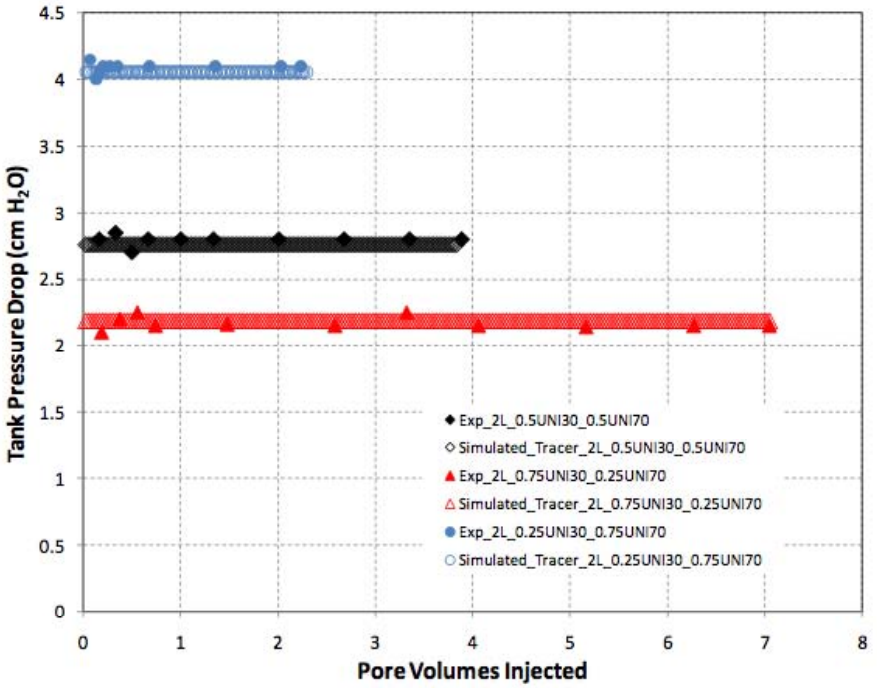

Figure 5-16: *Measured and simulated pressure drops for all two-layer tank experiments.*

After conditioning the UTCHEM simulator to the results of the tracer, simulations of tracer propagation within each tank layer arrangement were performed for 500 mg/L xanthan polymer solutions. The results of these simulations are presented in Figures 5-17 through 5-19; UTCHEM adequately simulates the rate and degree of polymer-induced crossflow observed experimentally for each two-layer sand pack. Calculated sweep-efficiencies for the polymer-amended tracer are presented as a function of injected pore volumes in Figure 5-20. The close agreement between experimental and simulated polymer-amended sweep-efficiencies indicates that the input parameters determined in Task 2 are appropriate to describe the physics of polymer flow and transport within these two-layer heterogeneous systems. Similarly, the agreement between experimental and simulated pressure drops, as shown in Figure 5-21, indicates that the simulator is reproducing the mobility reduction that results from the injection of a more viscous polymer solution.

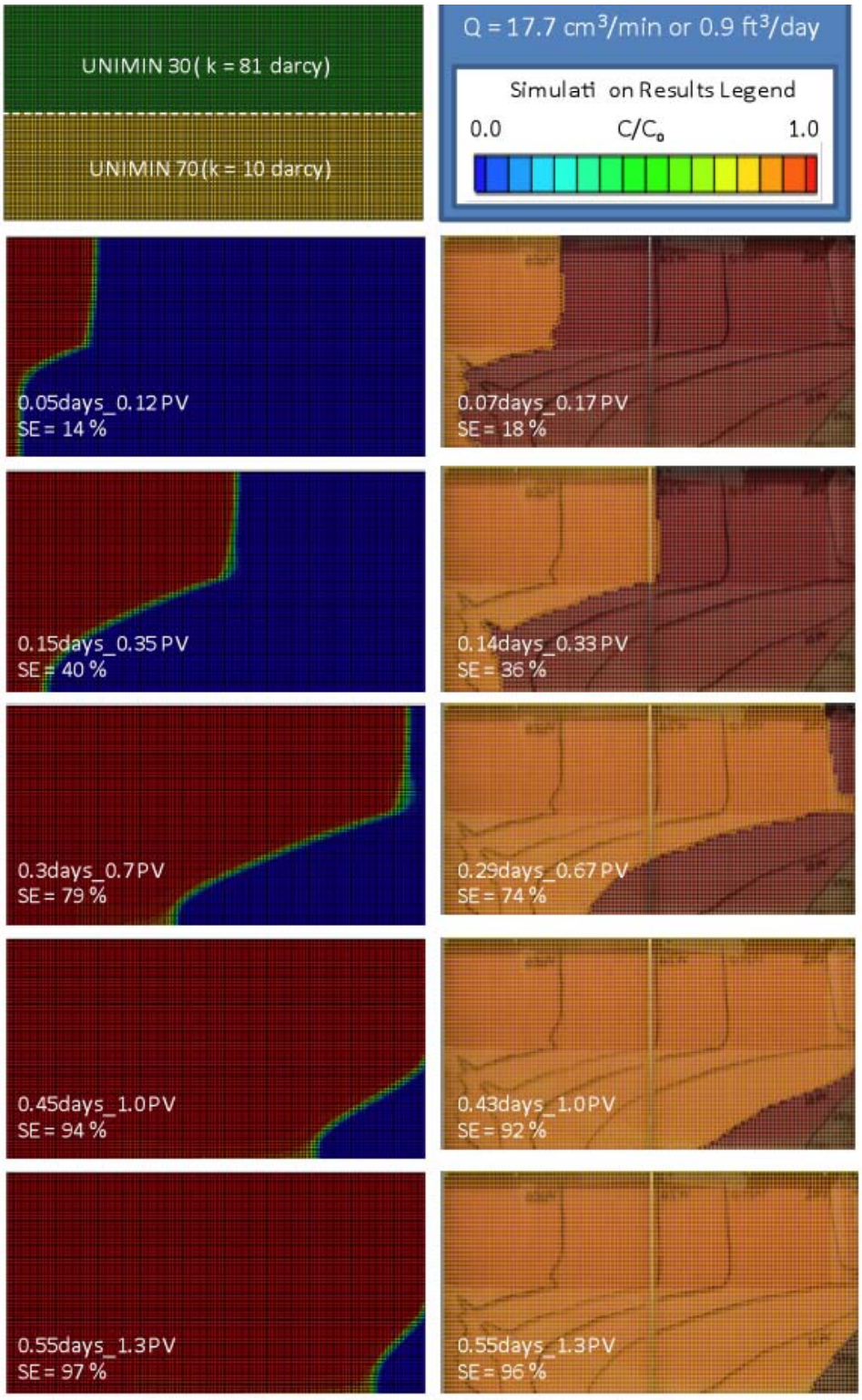

Figure 5-17: *Simulated tracer propagation polymer case) within 2L_50%UNI30_50%UNI70 tank.*

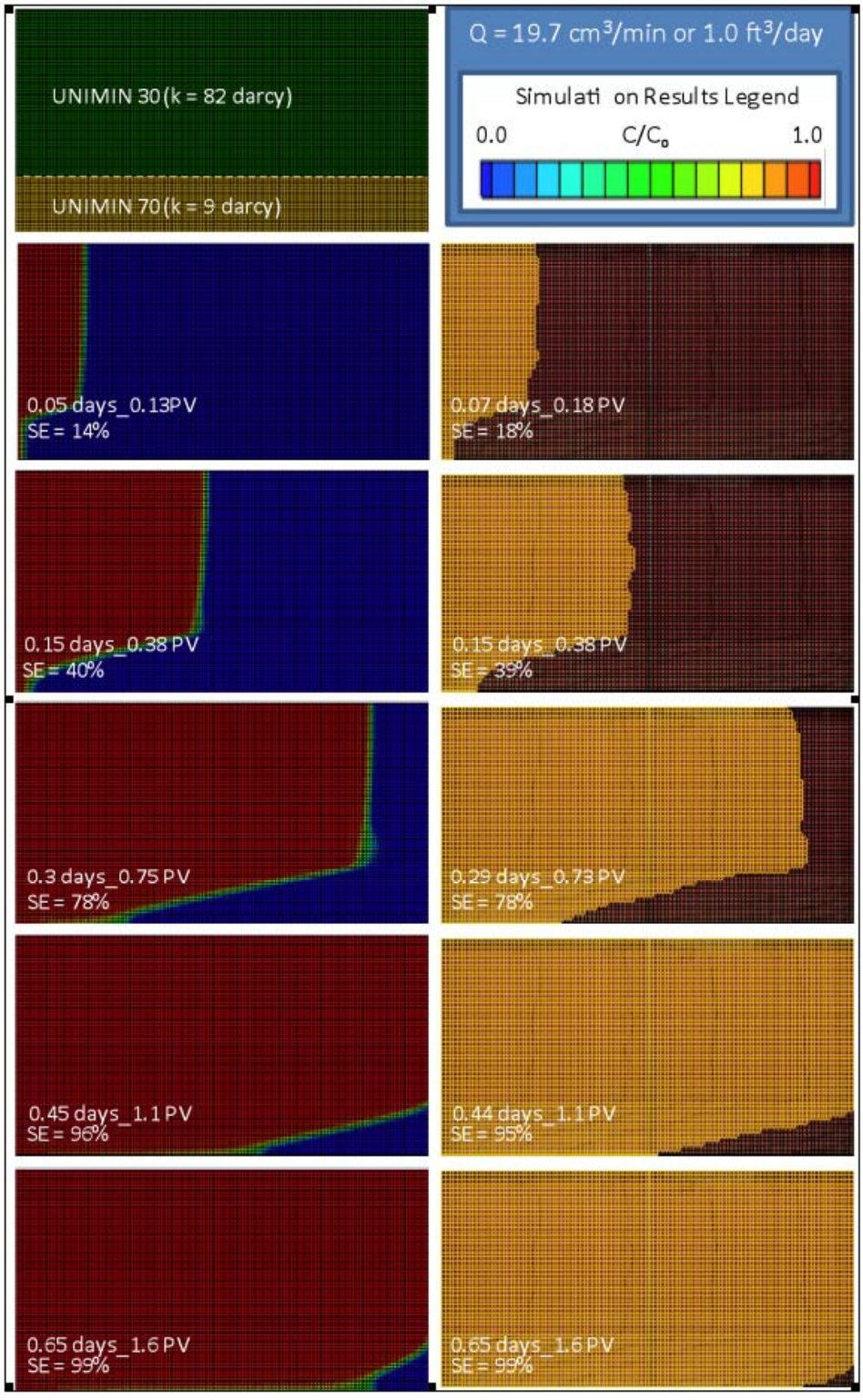

Figure 5-18: *Simulated tracer propagation (polymer case) within 2L_75%UNI30_25%UNI70 tank.*

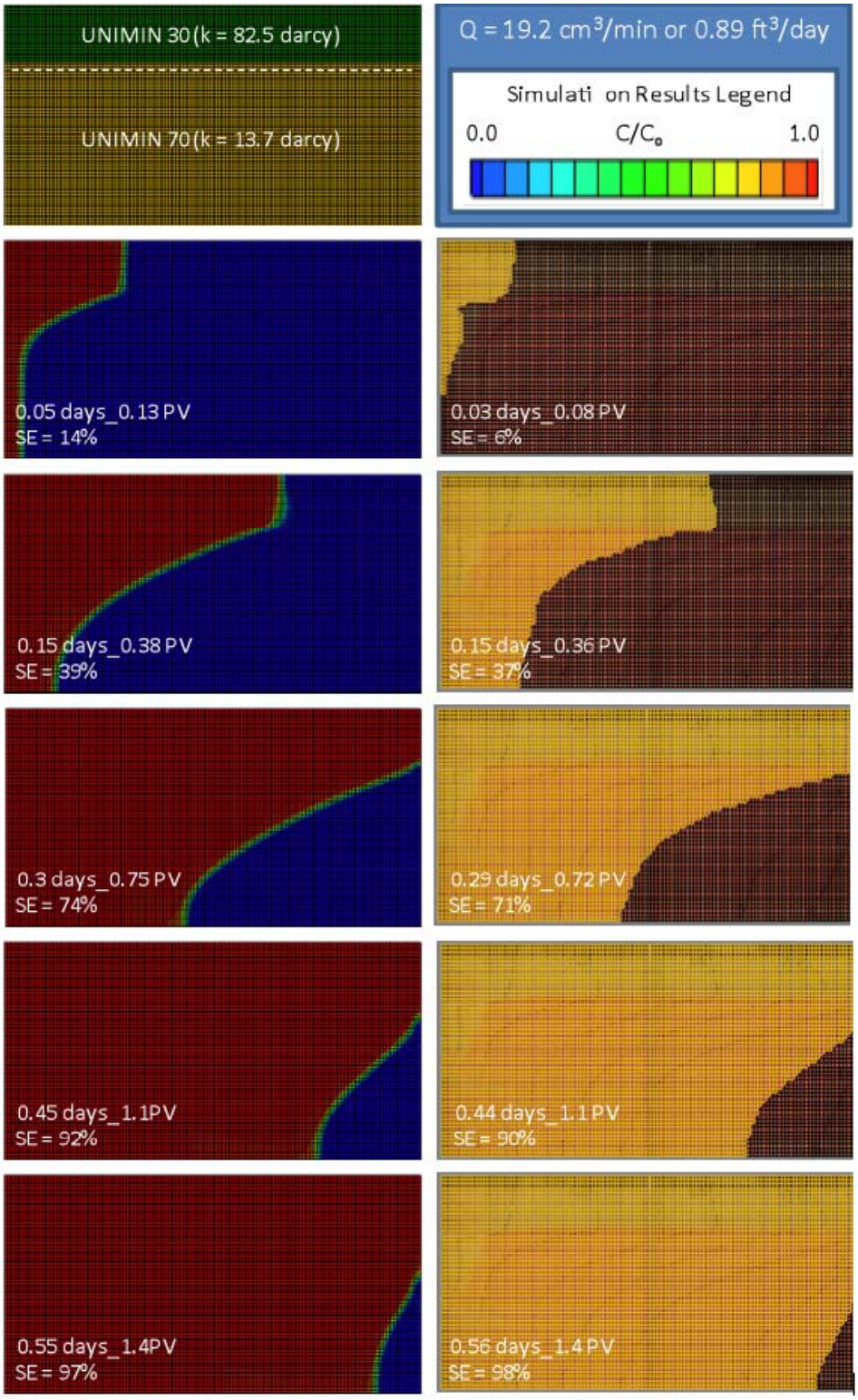

Figure 5-19: *Simulated tracer propagation (polymer case) within 2L_25%UNI30_75%UNI70 tank.*

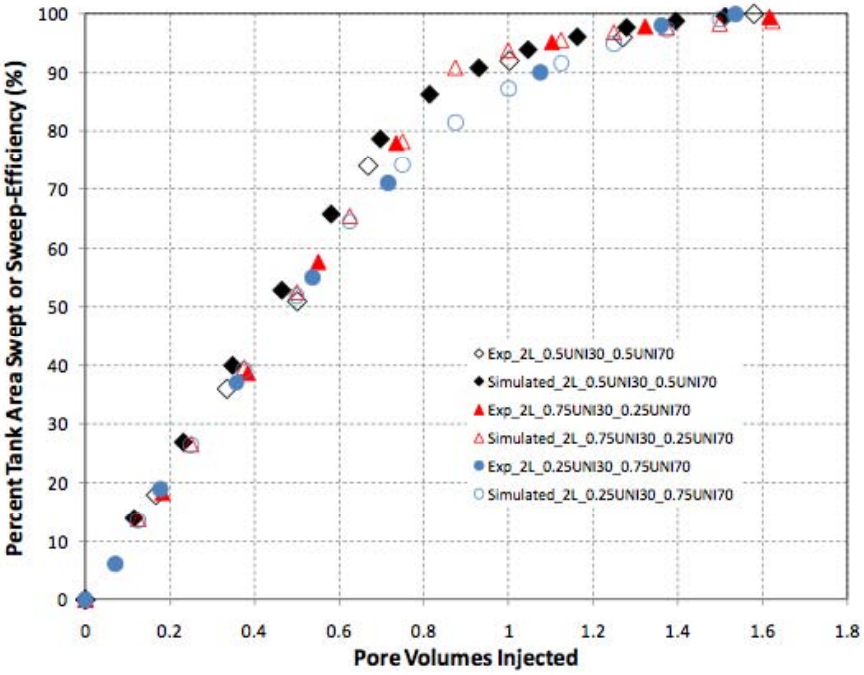

Figure 5-20: *Tracer sweep efficiencies profiles for all two-layer (polymer) tank experiments.*

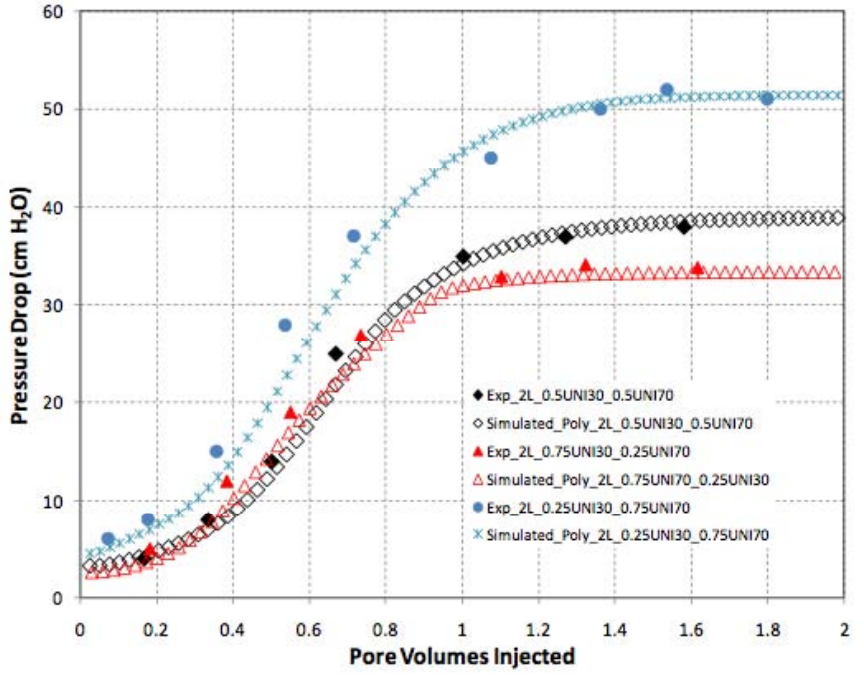

Figure 5-21: *Measured and simulated pressure drops for all two-layer (polymer) tank experiments.*

Three Layer Experimental Systems

Additional 2-D tank experiments were performed to investigate polymer-improved sweep efficiency three-layers systems. Two tank experiments were performed. The first tank experiment was constructed to mimic a fining-downward permeability sequence and consisted of three layers of UNIMIN 30, UNIMIN 70, and F110 Ottawa sands (a situation encountered for a field effort in North Carolina associated with a different project). The second three-layer tank experiment utilized each of the same sands (with identical layer thickness for each porous material), however, the order of the layers were modified such that the lowest permeability layer was located in between the other layers: UNIMIN 30, F110 Ottawa, UNIMIN 70. As was done for two-layer tank experiments, a conservative dye tracer experiment was performed prior to injecting a dyed polymer solution.

Three-Layer Tank – Fining-Downward Layered System

Temporal profiles of tracer and polymer (800 mg/L xanthan) propagation within the fining-downward layered system (hereafter designated experiment 3L_Fining_Down) are presented as Figures 5-22 and 5-23, respectively. Simulated tracer and polymer profiles are included for comparison. In the absence of polymer addition, the vertical distribution of tracer was observed to be highly dependent on the flow capacity of the individual layers and with little inter-layer mixing. Note that if the contamination results from a DNAPL spill, the differences in capillarity between these layers are not sufficient to prevent downward flow at any given layer, so the DNAPL would be distributed throughout all three layers. However, a remediation fluid injected and extracted via groundwater wells would exhibit preferential horizontal flow and bypassing of the lower permeability strata, which would limit contact between remediation agents and contaminants at the field-scale. As was the case for the two-layer tank experiments, the addition of xanthan is shown to greatly improve the efficiency of aqueous tracer sweep in the presence of this fining-downward heterogeneous system. The increased viscosity of the polymer solution reduced the mobility of the fluid in the most highly conductive layer (UNIMIN 30) and promotes the cross-flow of fluids into the next less conductive layer (middle, UNIMIN 70 layer), effectively enhancing the flow capacity of this middle layer. This effect proceeds sequentially, with the least conductive layer (bottom, F110 Ottawa sand layer) entertaining cross-flow from the UNIMIN 70 layer. The net result is a homogenization of the heterogeneous structure in regards to sweep-efficiency. This process is presented graphically in Figure 5-24. Measured and simulated pressure drops for this experiment are presented as Figure 5-25.

As shown in Figure 5-24, the tracer sweep-efficiency exhibits three slopes, the transition points that are associated with the number of pore volumes where the UNIMIN 30 and UNIMIN 70 layers were completely swept, respectively. In contrast, the rate of sweep with the addition of 800 mg/L xanthan is observed to proceed as if the tank were homogeneously packed until roughly 0.8 pore volumes, where after the rate of sweep decreases. This departure from the homogeneous line at 0.8 pore volumes coincides with the arrival of polymer-amended fluids at the tank effluent within the UNIMIN 30 layer. In this case, the addition of 800 mg/L xanthan reduced the number of pore volumes needed to completely sweep the tank from 4.8 to 2.5, or a reduction of 48%.

Note that the UTCHEM model does an excellent job simulating the 2D profile of the tracer and polymer fluids, as well as simulating the sweep efficiencies (Figure 5-24) and the pressure drops across the 2-D experimental apparatus.

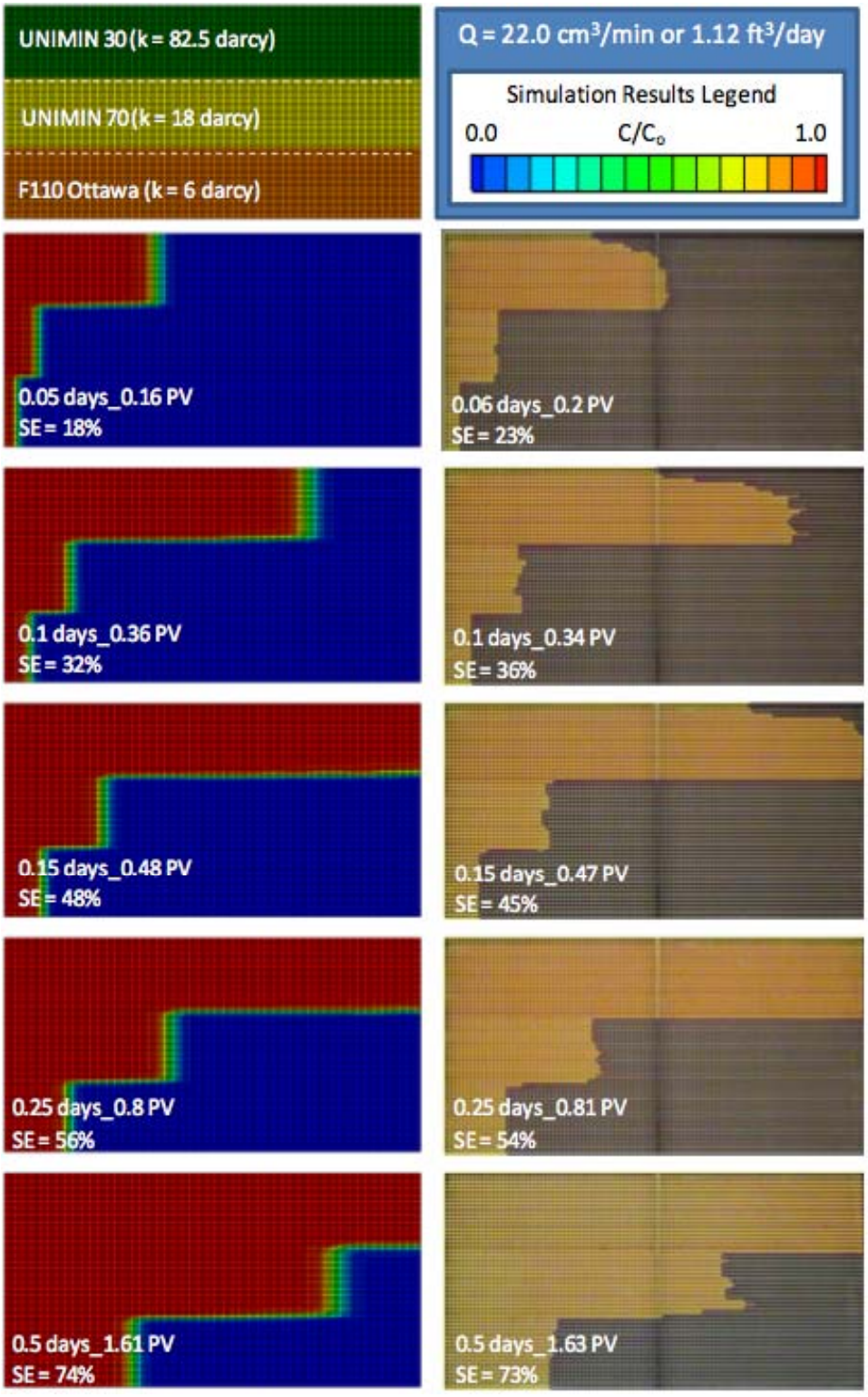

Figure 5-22: *Simulated tracer propagation within 3L_Fining_Down tank.*

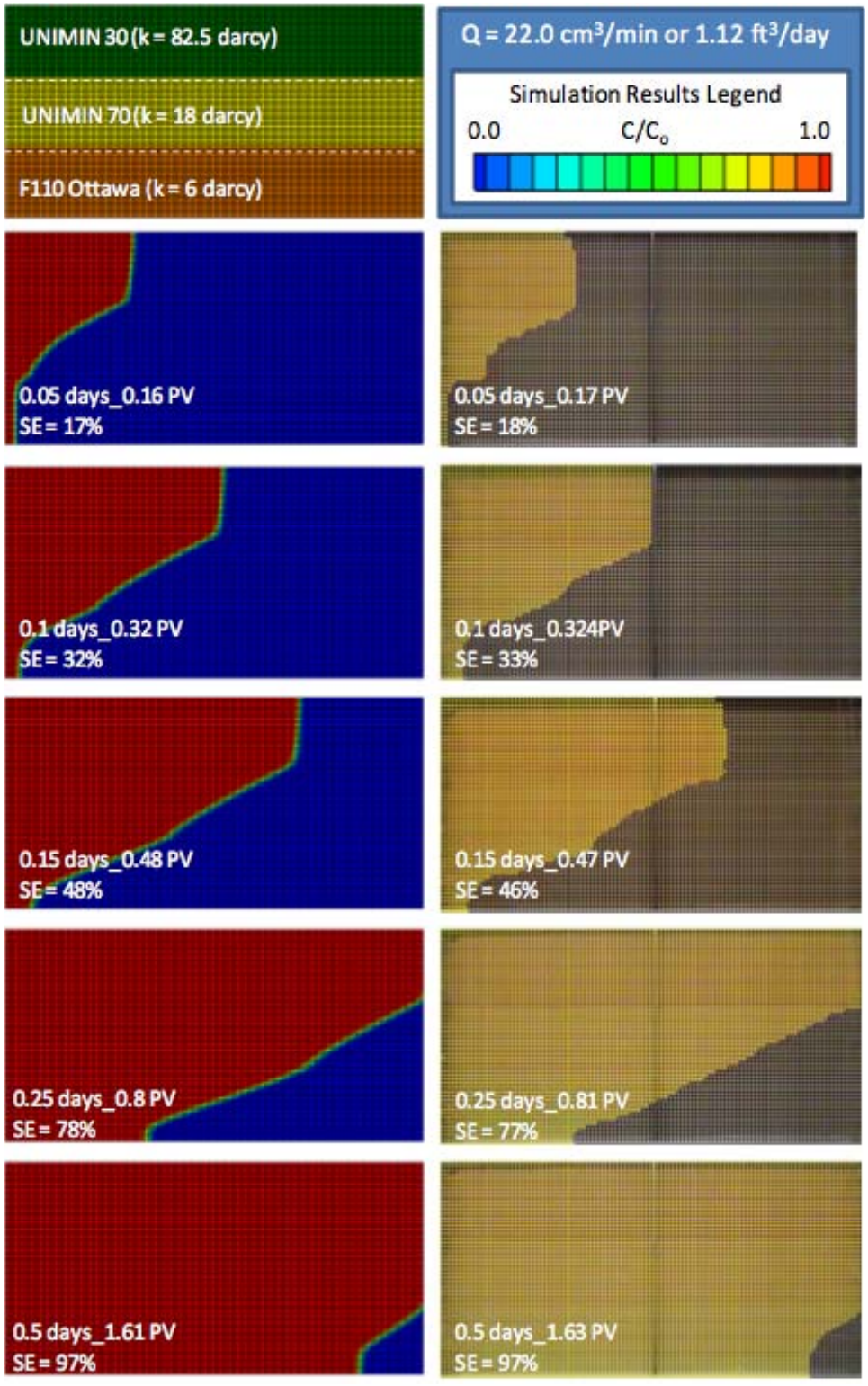

Figure 5-23: *Simulated tracer propagation (polymer case) within 3L_Fining_Down tank.*

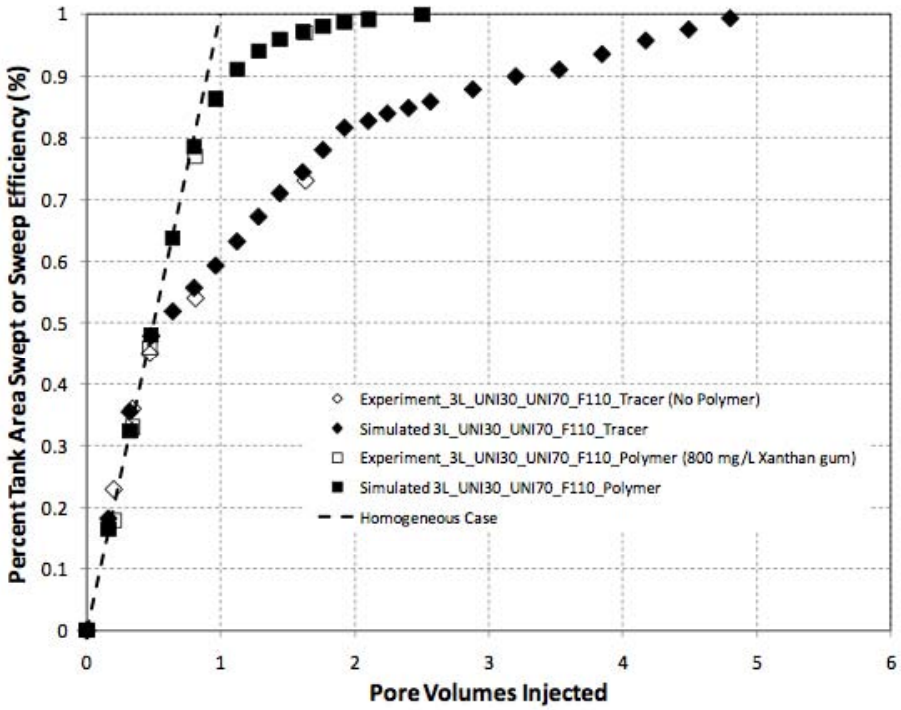

Figure 5-24: *Tracer sweep efficiency profiles for 3L_Fining_Down tank.*

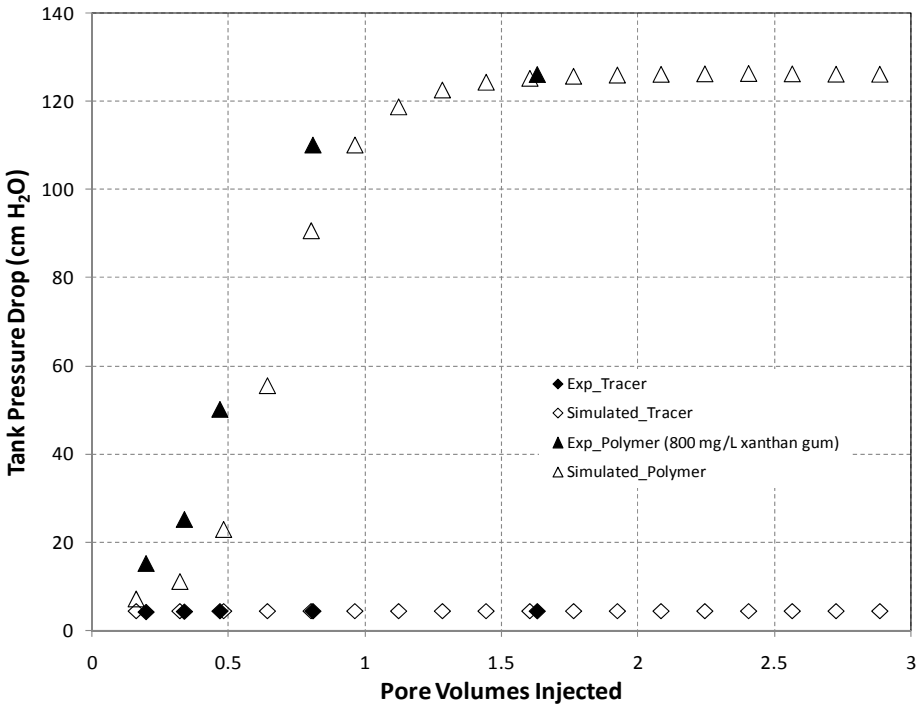

Figure 5-25: *Pressure drops for 3L_Fining_Down tank.*

Three-Layer System – Alternate Layer Ordering

To examine the effects of layer order on polymer-improved sweep efficiency a second three-layer tank was prepared wherein the lowest permeability layer (F110 Ottawa sand) was positioned as the middle layer, with the UNIMIN 30 and UNIMIN 70 sand layers comprising the upper and lower layers, respectively. Temporal profiles of tracer and polymer (500 mg/L xanthan, in this case) propagation within this alternate 3-layered system (hereafter designated 3L_Fine_Middle) are presented as Figures 5-26 and 5-27, respectively. Simulated tracer and polymer profiles are included for comparison. Here again the UTCHEM simulator was found to appropriately simulate tracer and polymer propagation in this heterogeneous flow system.

While tracer propagation in the absence of polymer-addition within this three-layer system is shown to proceed in order of layer flow capacity as expected (Figure 5-26), tracer propagation with the addition of 500 mg/L xanthan (Figure 5-27) exhibits some interesting results. In this case, cross-flow from the most conductive UNIMIN 30 layer into the least conductive F110 layer (here positioned as the middle layer) is observed to overwhelm the cross-flow contribution from the UNIMIN 70 layer (i.e., UNIMIN 70 cross-flow into the F110 layer is marginalized). However, flow into the all three layers is significantly improved compared to the solution with no polymer. This occurs despite the greater (i.e., 82.5:5 darcy) permeability contrast between the UNIMIN 30 and F110 media than for the UNIMIN 70 and F110 layers (14:5 darcy permeability contrast). In comparing polymer-amended tracer propagation in this three-layer arrangement (Figure 5-27) and that for the three-layer fining-downward packing (Figure 5-23) it is clear that the rate of cross-flow from the UNIMIN 30 layer and the middle layer is greater when the permeability contrast between the layers is less. This dependence of cross-flow on the permeability contrast between the UNIMIN 30 layer and that of the middle layer is also reflected in the sweep-efficiency profiles for these two three-layer cases (Figures 5-24 and 5-28), wherein the earlier departure from the homogeneous sweep line in Figure 5-28 indicates a more rapid completion of sweep within the UNIMIN 30 layer and less cross-flow into the F110 layer. These results suggest that polymer-improved sweep efficiency is not only dependent on the permeability contrast between layers but also on the positioning of layers relative to the most conductive layer in the system. For this three-layer arrangement, the addition of 500 mg/L xanthan reduced the number of pore volumes required to completely sweep the tank from 6.6 pore volumes (tracer, no polymer case) to 2.7 pore volumes, or a reduction of 59%. Measured and simulated pressure drops for this experiment are presented as Figure 5-29.

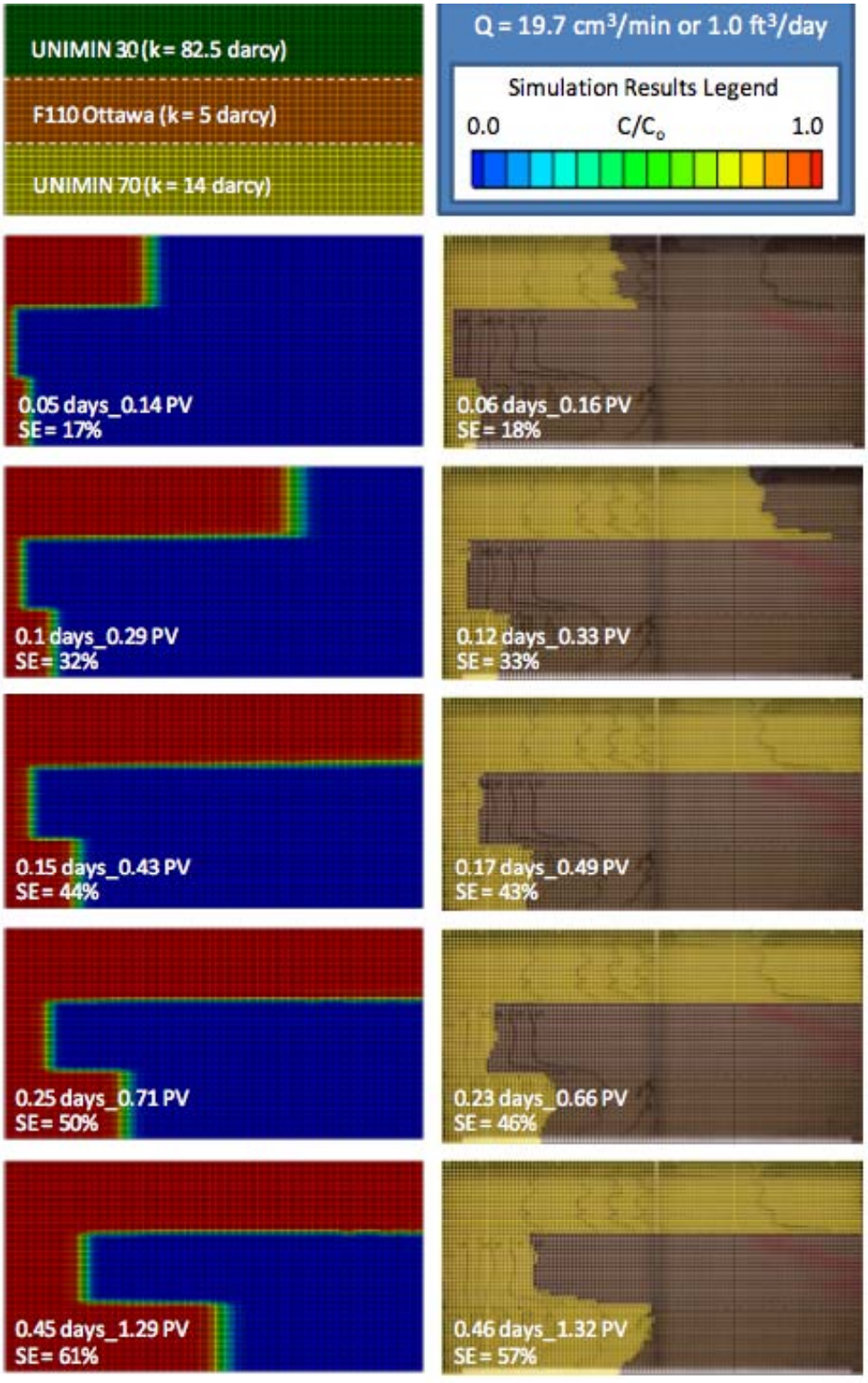

Figure 5-26: *Simulated tracer propagation within 3L_Fine_Middle tank.*

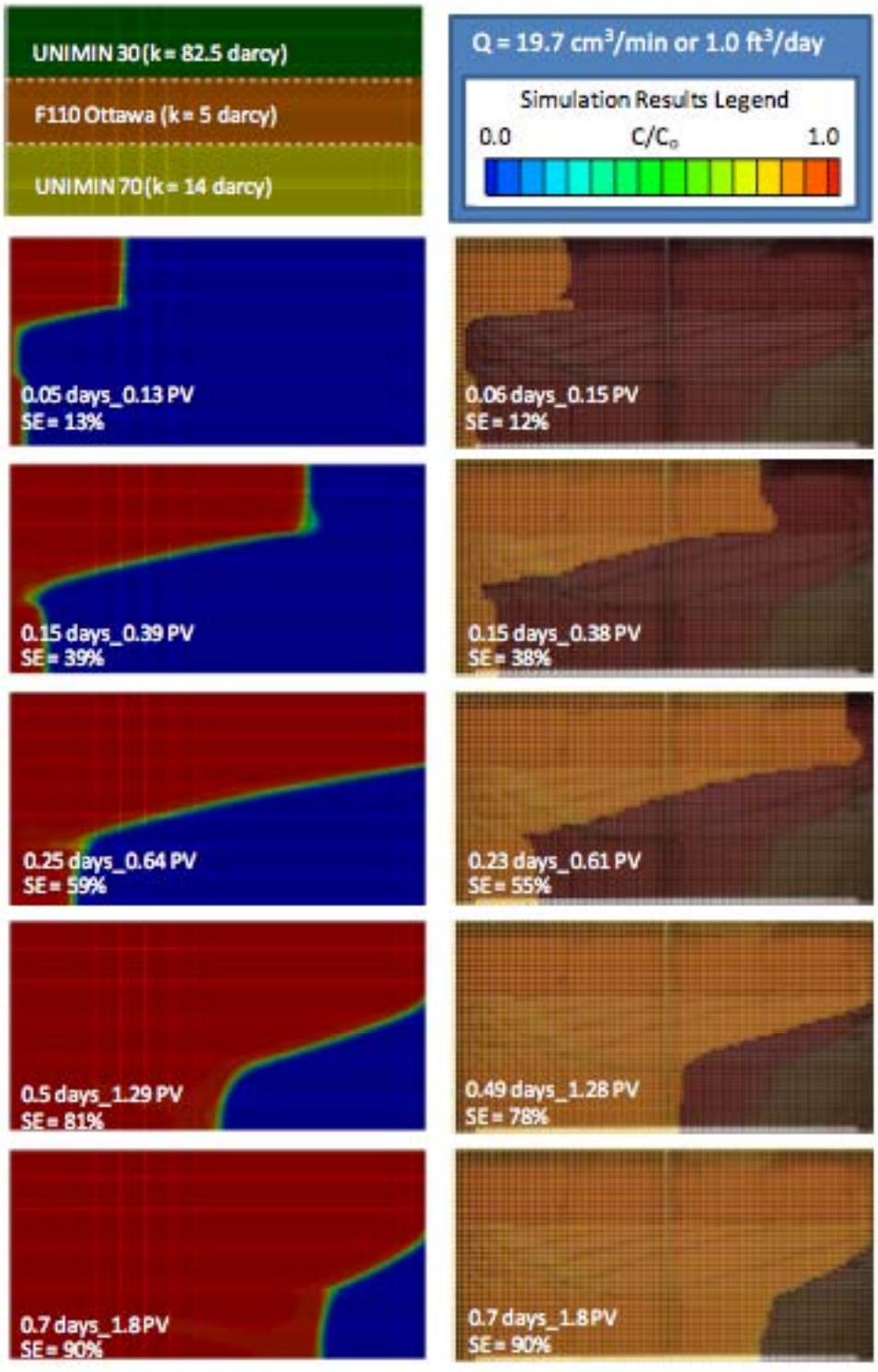

Figure 5-27: *Simulated tracer propagation (polymer case) within 3L_Fine_Middle tank.*

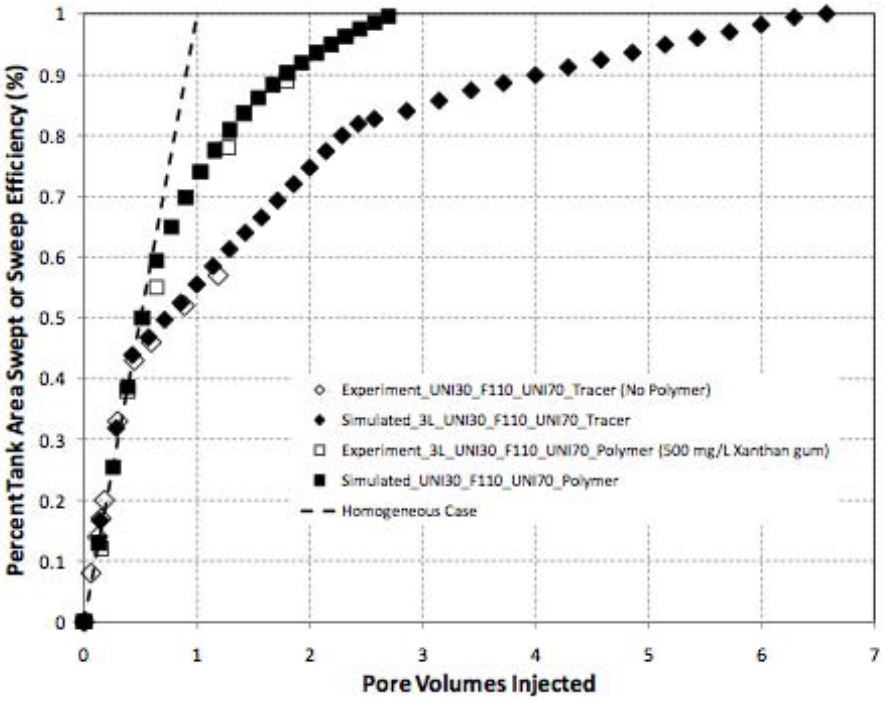

Figure 5-28: *Tracer sweep efficiency profiles for 3L_Fine_Middle tank.*

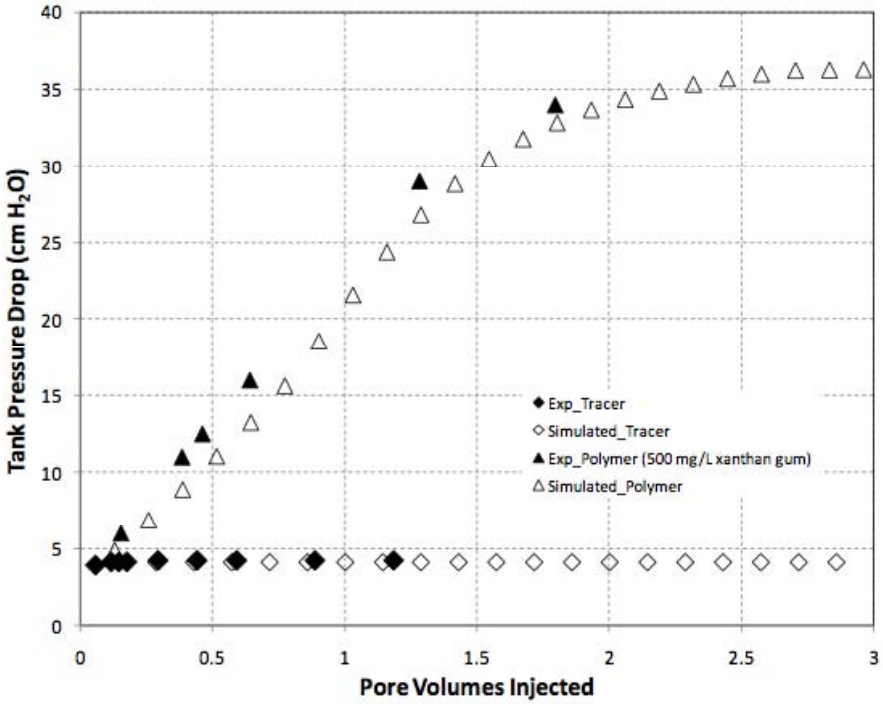

Figure 5-29: *Pressure drops for 3L_Fine_Middle tank.*

2-D Experimental Tank and Modeling Conclusions

- Polymers can greatly improve the sweep efficiencies in layered systems. These results demonstrated up to a four-fold improvement in the overall sweep efficiency with less than two pore volumes of injected fluid, and also showed a much greater improvement in the ability to sweep low permeability layers.
- Polymer-improved sweep efficiency is not only dependent on the permeability contrast between layers, but also on the positioning of layers relative to the most conductive layer in the system.
- The UTCHEM model was shown to perform very well with regard to simulating the shapes of the injected tracer and polymer solutions over time, the calculated sweep efficiencies, and the pressure drop over the flow domain.
- Most model input parameters for UTCHEM were obtained from bench-scale measurements with minor modifications to permeability, and yet were sufficient to simulate the larger-scale 2-D experiments. However, these 2-D experiments operate over a significantly smaller scale than a field site, and attempting to characterize the heterogeneity at the field scale could prevent an investigator from characterizing the site sufficiently to uniquely determine all UTCHEM input parameters This study suggests that the bench-scale studies are sufficient to parameterize the model for a larger-scale system, provided the larger system is appropriately characterized.
- By enabling sweep of lower-permeability zones by remediation fluid, use of polymers should minimize the impact of contaminant rebound caused by diffusion of contaminants from low-permeability zones into more permeable media that was initially cleaned by the remediation effort.

6. TASK 4: 2-D TANK EXPERIMENTS WITH OXIDANT

As a result of the positive results associated with the use of xanthan polymer and permanganate oxidant combinations in batch and 1-D experiments, larger-scale studies of polymer/oxidant applications were desired. The goal of this task was to test and refine delivery strategies for polymer-amended oxidant applications in the presence of NAPL-phase contaminant within a controlled heterogeneous setting. During these experimental investigations, analytical data was collected such that changes in oxidation effectiveness and efficiencies between individual strategies could be investigated and quantified. The outcomes from this study were expected to contribute towards a more cost-effective use of polymers and oxidants.

Materials and Methods

Solutions of xanthan polymers and permanganate oxidant were prepared as described previously (see Sections 3.2 and 4.2). For the co-injected mixture experiment, higher concentration stock solutions of 2 g/L xanthan and 10 g/L permanganate were prepared separately and mixed immediately prior to injection to achieve an influent solution concentrations of 1000 mg/L xanthan and 5000 mg/L $KMnO_4$ (31.6 mM MnO_4^-). For all other experiments, solutions were initially prepared at the desired concentrations of 1000 mg/L xanthan and 5000 mg/L permanganate. This ratio of polymer to oxidant was chosen as a result of the experiments presented in Figure 3-9, which indicated both significant viscosity retention coupled with low nonproductive oxidant demand at these concentrations. All solutions were constantly stirred with a magnetic stirplate during injection to ensure constant delivery concentrations of oxidant. An HPLC pump (Dionex, Waters Corp., Milford, MA) was used to deliver all influent solutions through the tanks at a constant one pore volume per day rate (0.8 mL/min). Filtered effluent permanganate concentrations were monitored spectrophotometrically as discussed in Section 3.2. Effluent viscosity was not monitored, but variations in fluid pressure, serving as a proxy for fluid viscosity, were monitored using manometers at several points in the tank (see Figure 6-1 for a diagram).

The test contaminant used in these experiments was tetrachloroethene, PCE, at ≥99.9% purity obtained from Sigma-Aldrich (St. Louis, MO). The equilibrium solubility of this compound was measured in water (155 ±20 mg/L) and found to be well within published limits. PCE solubility in xanthan polymer solutions (50 to 5000 mg/L xanthan) after 5 months of equilibration was measured at 148 ±26 mg/L. 1.2 mLs of pure-phase PCE was injected into the coarse-sand inner lens (as shown in Figure 6-1) via three ports in the back wall of the tank (for a total of 3.6 mLs; 36.2 mmoles PCE). In the first two tank experiments, PCE was dyed red with 300 mg/L Sudan IV dye, in order to track any possible movement of pure-phase NAPL (non-aqueous phase liquid). No bulk NAPL movement was visually detected and so the dye was omitted from the last two experiments.

This comparatively large PCE mass was utilized in order to provide excess PCE so that later-time dissolved-phase concentrations could be monitored and to allow for the possibility of manganese dioxide “rind” deposition (Tunnicliffe and Thomson, 2004) and observation of its effects on further contaminant oxidation. It is important to note that complete contaminant mass is neither expected nor desired in these experiments.

A solid-state ion-selective chloride probe (model ISM-146CLFT, Lazar, Los Angeles, CA) was used in these experiments to monitor both chloride tracer concentrations (conducted at relatively high chloride concentrations) and effluent chloride concentrations produced as a result of PCE oxidation by permanganate though the reaction:

$$3C_2Cl_4 + 4MnO_4^- + 4H_2O \rightarrow 6CO_2 + 12Cl^- + 4MnO_{2(s)} + 8H^+$$ (Hood et al., 2000)

The probe was calibrated with standards diluted from a gravimetrically prepared stock chloride solution before and after each phase of an experiment. The probe was plumbed into the tank via a custom-made PFTE flow-through cell with a dead-volume of 200 μL, attached at the tank effluent port. Chloride data was collected every two minutes using a model 610A digital pH/mV meter (Jenco Instruments, San Diego, CA) attached to a CR1000 datalogger (Campbell Scientific, Logan, UT).

A 2-mL total volume sample loop equipped with a three-way valve was installed on the effluent tubing side to provide a method for rapid collection of samples for PCE and permanganate analysis were collected. Filtered samples were analyzed for permanganate as described in Section 3.2. PCE samples were collected quickly using the sample loop valve and extracted in a 1:1 ratio with hexane. An aliquot of the hexane was transferred to a 200-μL glass reducing insert inside a GC vial. Samples were capped, refrigerated, and analyzed within two weeks of collection. An HP gas chromatograph equipped with an electron capture detector was used to quantify these low concentrations of PCE.

Porous media used in this series of experiments consisted of UNIMIN mesh 30 and UNIMIN mesh 70 clean quartz sands (used as received), and sieved pea gravel (portion retained on 1.70 mm mesh) used to construct inlet and outlet wells. The physical characteristics of the UNIMIN sands are tabulated in Table 4-1, and the permeability/hydraulic conductivity contrast between these two sands is less than half an order of magnitude. Because we could not initially estimate the increase in tank pressure that would arise from either manganese dioxide deposition or polymer solution viscosity, we chose to limit our experiments to the two highest conductivity media available. This contrast is close to the values reported by other authors utilizing polymer floods for experimental purposes (Martel et al., 1998; Robert et al., 2006; Zhong et al., 2008). Unfortunately, time did not permit the repeat of these experiments using a higher permeability contrast. Previous column experiments using permanganate oxidant and these sands (see Section 4-2) demonstrated that these sands possessed no significant natural oxidant demand (NOD). The gravel (porosity measured at 41%) was washed with deionized water, and then sequentially acid- and hydrogen peroxide-washed and water-washed again to decrease its NOD; visual observation of gravel after tank disassembly confirmed that this procedure was effective, as very little manganese dioxide oxidation deposition was noted in the gravel.

A previously designed nominally 2-D tank was utilized for these experiments (as depicted in Figure 6-1). The tank sides, back wall, and top were constructed of Delrin™ plastic (providing excellent resistance to pure-phase chlorinated solvents), while the front face was made of clear glass. The front face was clamped to the tank body for a water-tight and pressure-tight seal with 12 c-clamps and a circular Buna-N rubber gasket fitted into a groove within the tank body. After assembling the tank body, screened inserts were used to stabilize the gravel inlet and outlet wells (~0.5-inch thick). The tank was then wet-packed in the configuration shown in Figure 6-1, using shims to direct the two sands into the desired configuration and periodically tamping the layers to ensure tight packing. A thin layer of bentonite/fine sand was

laid over the top of the sands, and a 0.25-inch-thick Buna-N rubber gasket covered this layer. A Delrin top was then screwed through the gasket and into the tank body.

The packing arrangement used in these experiments was chosen to maximize the effects of potential flow bypassing in a tank with a limited flow length and thus it contains blunt boundaries between layers that are not representative of typical formation arrangements found in nature. Our goal in these experiments was to investigate the differences in oxidant delivery and treatment efficiency in the limited experimental setting available to us; we endeavored to mimic natural groundwater flow conditions by using low flow rates, but we could not and did not attempt to replicate natural aquifer stratigraphy. The NAPL zone was constructed using the coarser UNIMIN 30 sand, to act as a capillary trap for the emplaced PCE. The finer UNIMIN 70 sand was used in the barrier lens encasing the contaminated inner zone.

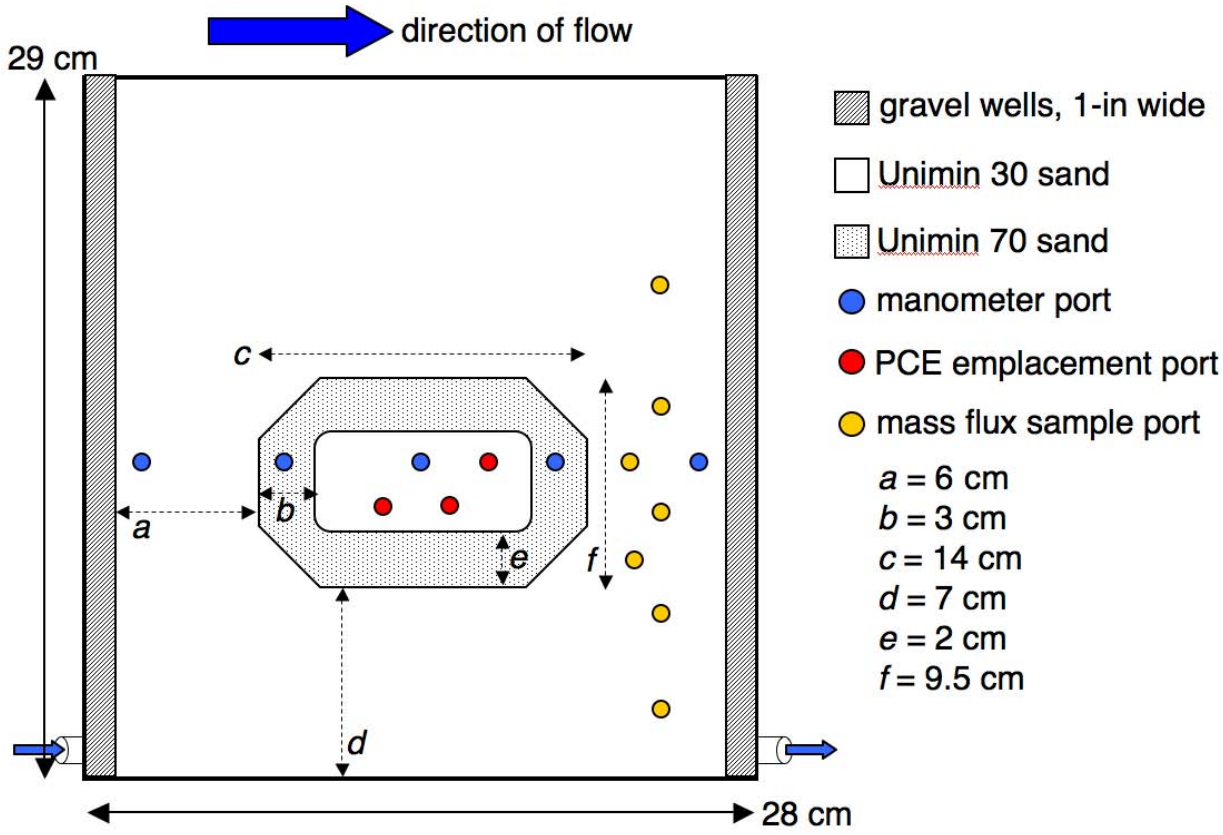

Figure 6-1: *Schematic diagram of 2-D tank and packing/sampling configuration (not to scale). Tank width is 3.5 cm and system pore volume is ~1150 mLs. Ports are arranged 2.5 cm apart, in staggered rows every 2.5 cm; only the ports utilized in the experiments are shown on this diagram.*

A typical experiment sequence consisted of at least 2 pore volumes of deionized water flushing and monitoring of pH; injection and monitoring of chloride tracer solution (discontinued in later experiments); injection of pure-phase PCE NAPL and at least five pore volumes of deionized water flushing and effluent monitoring; injection of the polymer/oxidant application (one of four variations); at least five additional deionized water pore flushes and effluent monitoring; port sampling of effluent concentrations; and injection and monitoring of chloride

tracer solution (discontinued in later experiments). Each experiment took approximately two weeks to complete, with sample analysis and data interpretation taking additional time.

Three different polymer-amended oxidant applications were contrasted to a conventional low (1 cP) viscosity oxidant treatment, for a total of four tank experiments (control, co-injection, unmixed, and bankflood) described here and represented in Figure 6-2. The control experiment consisted of delivering one pore volume (~1150 mLs) of aqueous permanganate oxidant solution, at a strength of 5 g/L, to the system at a flow rate of one pore volume per day (0.8 mL/min). This control experiment was expected to display flow-bypassing effects due to the low viscosity of the oxidant solution. In contrast, the first polymer-enhanced delivery strategy involved injecting one pore volume of pre-mixed permanganate oxidant at the same 5 g/L strength within a 1 g/L xanthan solution, at the same flow rate, to mitigate flow bypassing effects and contact more of the inner contaminated lens. This strategy could be viable at larger scales only if an in-line mixing apparatus were available to combine the reagents immediately prior to injection. The second polymer-enhanced strategy represented a situation where such mixing equipment would not be available, and involved separate injection of one pore volume of 5 g/L aqueous oxidant immediately followed by one pore volume of 1 g/L xanthan solution. The extent of fine-lens penetration was unknown for this unmixed application but was hypothesized to be less effective than the co-injected case. The final polymer-enhanced delivery strategy comprised three separate flooding injections: a lower concentration partial xanthan pre-flood (0.5 g/L, 0.75 pore volumes) to "condition" the subsurface (potentially spreading the NAPL and increasing available reactive surface area, as well as plugging pores within the more conductive formation), followed by one pore volume of aqueous 5 g/L oxidant, followed by a 1 g/L xanthan post-flood "push" injection. The pre-flood solution was expected to reduce the conductivity of the higher-permeability layer and increase the likelihood of oxidant flow through other (i.e., the finer-grained) regions; however, viscous fingering was also expected as a result of introducing a less viscous fluid into a more viscous resident fluid.

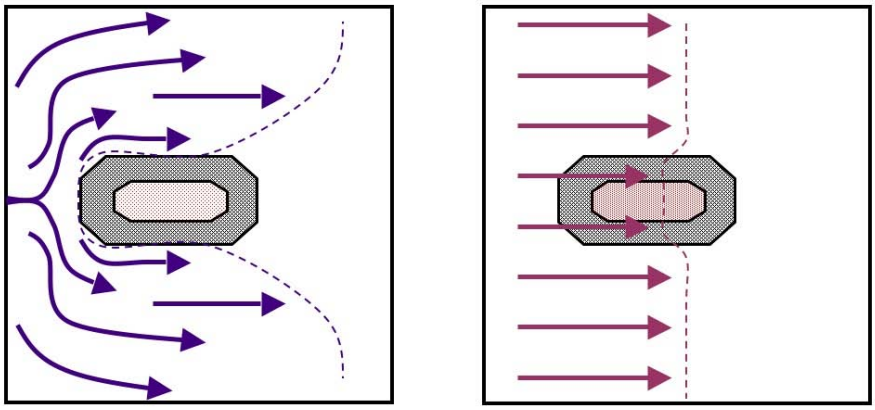

a. Control b. Co-injected Mix

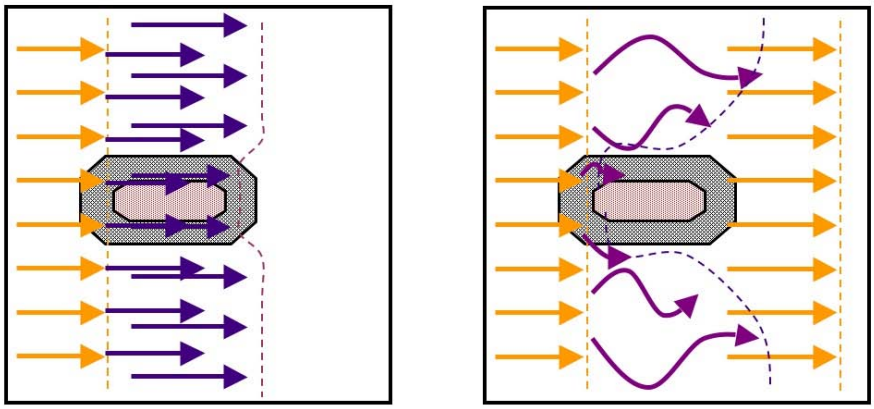

Figure 6-2: *Cartoon representation of experimental designs: a) one pore volume of conventional aqueous permanganate injection; b) one pore volume of pre-mixed xanthan/permanganate solution; c) one pore volume of conventional aqueous permanganate followed by one pore volume of xanthan solution; and d) partial pore volume of xanthan conditioning pre-flood, followed by one pore volume of conventional aqueous permanganate, followed by one pore volume of xanthan post-flood solution.*

Results and Discussion

Before commencing the series of experiments, we needed to ascertain if the two sands selected for this work would induce flow bypassing effects such that transport of a viscous solution would differ visibly from transport of an aqueous solution. To determine if our permeability contrast was great enough to encourage such effects, we observed a blue-dyed chloride tracer solution (see Figure 6-3). Although the fine-grained barrier lens was penetrated by the time one pore volume's worth of solution had been introduced to the tank, it was visually obvious that the majority of flow was occurring either above or below the fine-grained lens. This bypassing was also evident in the resulting chloride tracer breakthrough curves, which displayed double peaks interpreted as early (bypassed) fluid arrival and later (through-passed) fluid arrival. Unfortunately, chloride tracer data often produced mass recovery values far in excess or less than 100%, because the chloride probe had been selected to operate best at lower chloride values (equivalent to the concentrations produced during contaminant oxidation) instead of the higher values necessary for the tracer tests. These unreliable tracer mass recovery calculations coupled with the additional time necessary to ensure complete chloride tracer removal before PCE emplacement and subsequent oxidation led us to abandon the tracer tests for the remaining experiments.

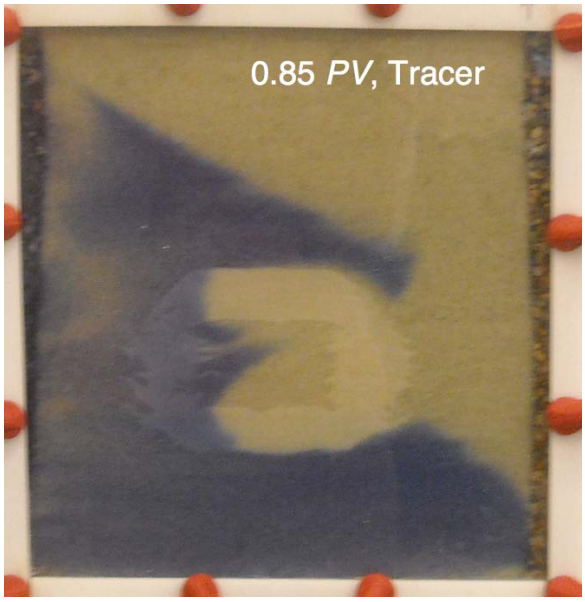

Figure 6-3: *Photograph of blue-dyed aqueous tracer solution traversing the dual-permeability packing arrangement after 0.85 PV of tracer injection. The inner lens has been penetrated, but the majority of flow occurs around the fine-grained barrier lens.*

The results of dissolved PCE, chloride ion (Cl-), permanganate ion (MnO4-), and pH values for tank effluent from each experiment are presented below in Figures 6-4, 6-6, 6-8, and 6-10. Accompanying each pore volume plot are photographs documenting the passage of the oxidant through the tank system at regular pore volume intervals (Figures 6-5, 6-7, 6-9, and 6-11). Time in these figures is represented as a dimensionless pore volume (*PV*), and $PV = 0$ is defined as the introduction of oxidant to the system. For example, in the "control" experiment, $PV = 0$ occurs as the aqueous oxidant is first introduced to the system, and for the "bankflood" experiment, the xanthan pre-flood begins at $PV = -0.75$, and oxidant introduction at $PV = 0$.

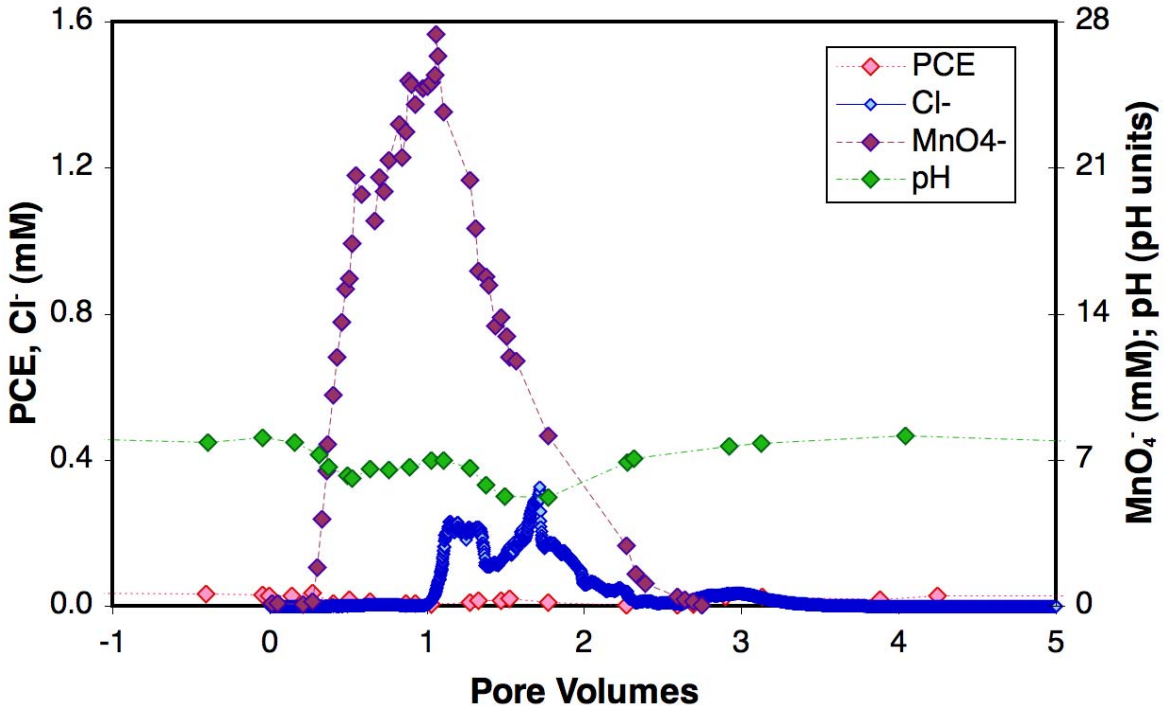

Figure 6-4: *Effluent PCE, chloride ion, permanganate ion concentrations and pH versus pore volume for "Control" tank – injection of one pore volume of aqueous permanganate oxidant.*

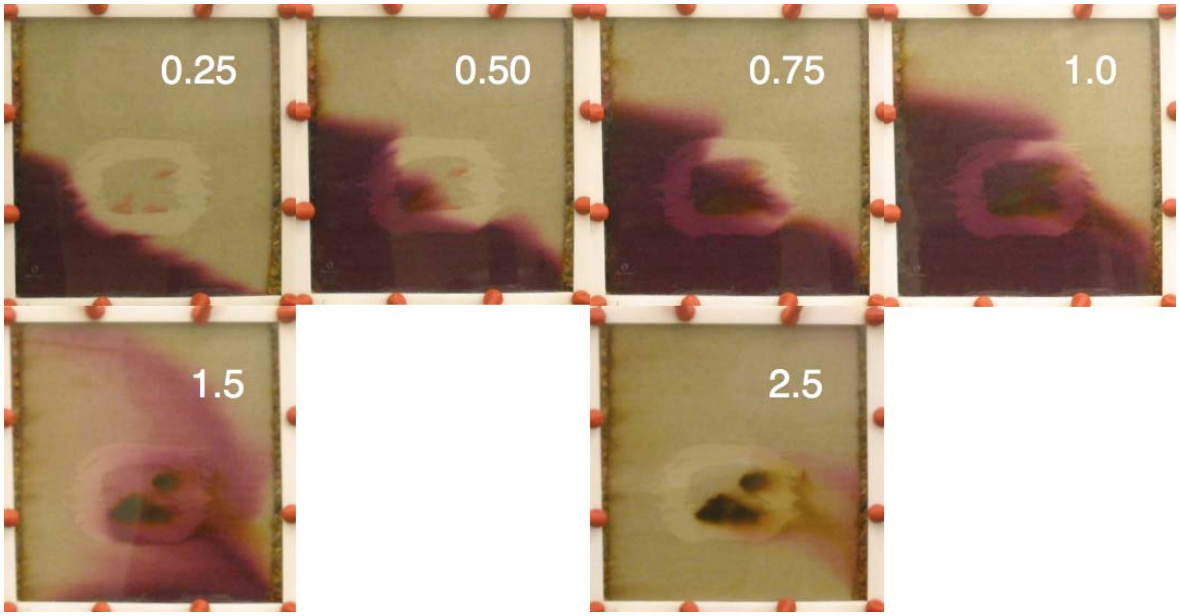

Figure 6-5: *Photographs of "Control" tank at pore volume intervals since introduction of oxidant solution.*

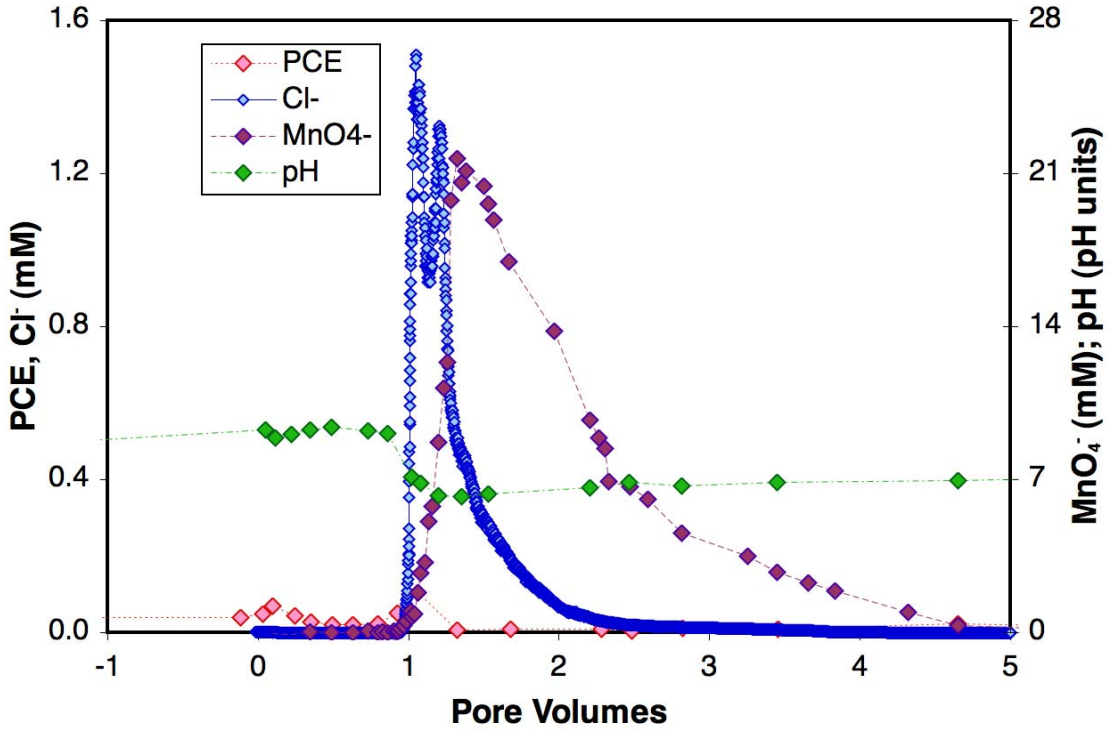

Figure 6-6: *Effluent PCE, chloride ion, permanganate ion concentrations and pH versus pore volume for "Co-injected" tank – injection of one pore volume of combined xanthan and permanganate solution.*

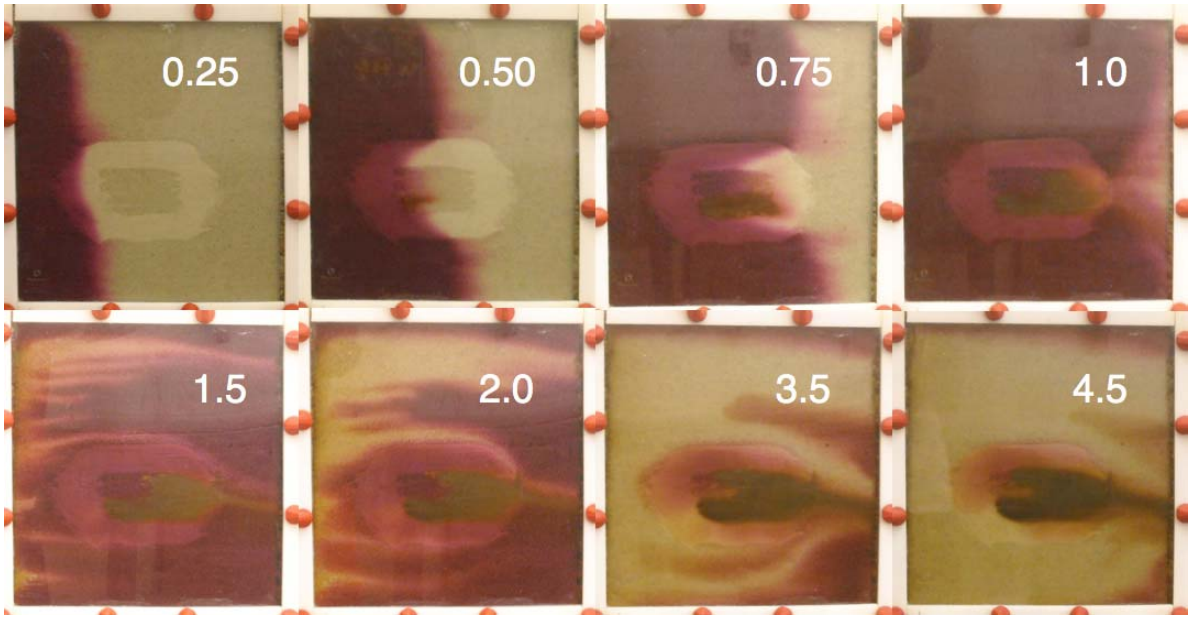

Figure 6-7: *Photographs of "Co-injected" tank at pore volume intervals since introduction of polymer/oxidant mixture.*

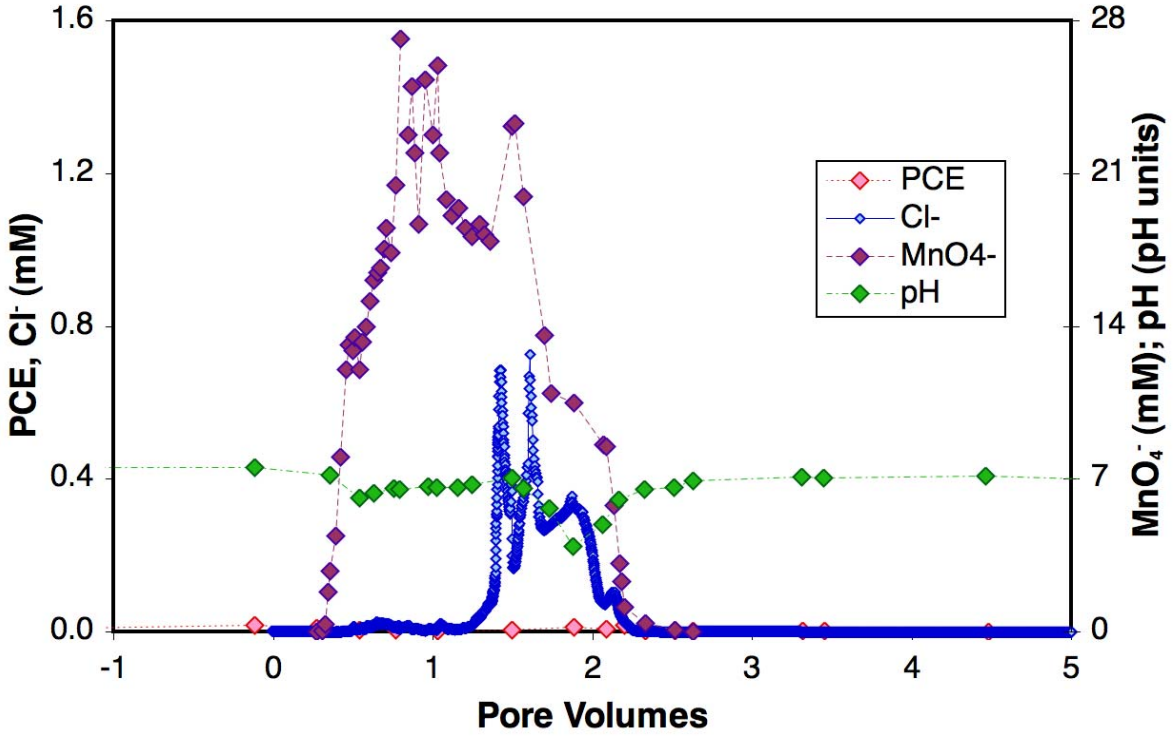

Figure 6-8: *Effluent PCE, chloride ion, permanganate ion concentrations and pH versus pore volume for "Unmixed" tank – injection of one pore volume of aqueous permanganate followed by one pore volume of xanthan solution.*

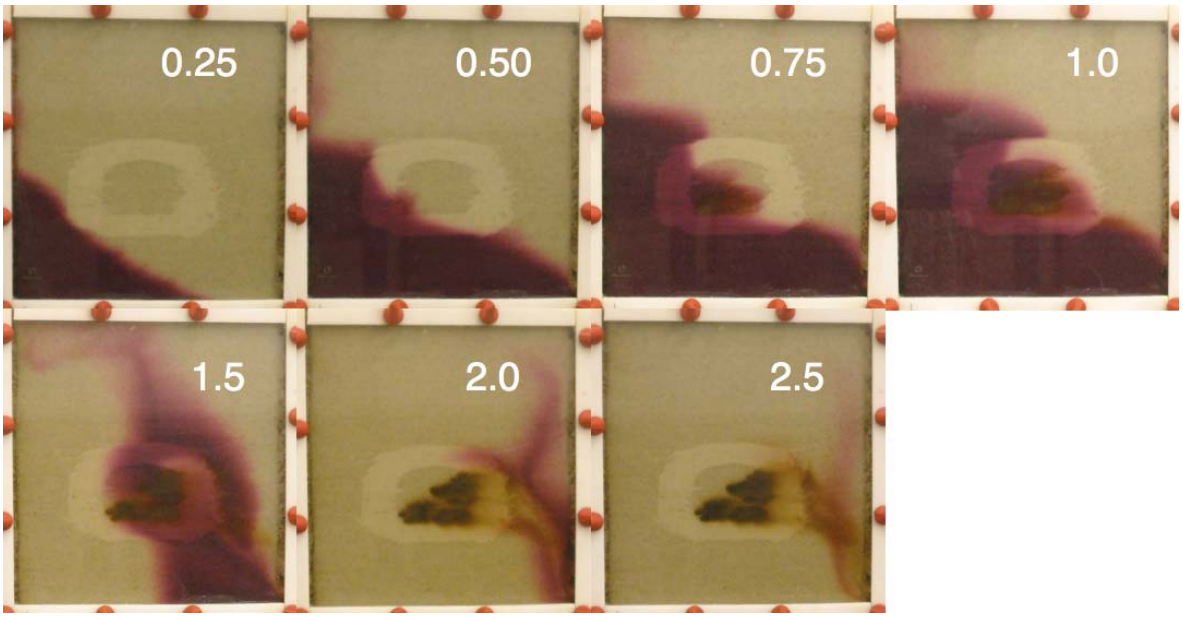

Figure 6-9: *Photographs of "Unmixed" tank at pore volume intervals since introduction of first injection of oxidant solution.*

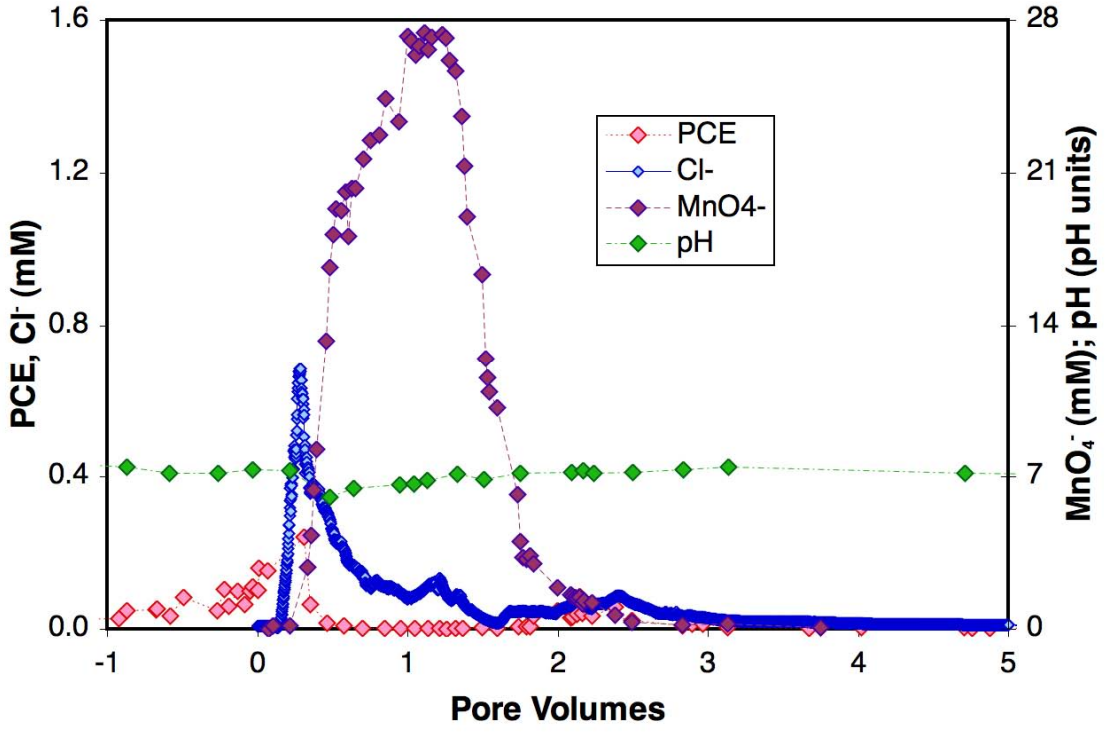

Figure 6-10: *Effluent PCE, chloride ion, permanganate ion concentrations and pH versus pore volume for "Bankflood" tank – injection of partial pore volume of xanthan, followed by one pore volume of aqueous permanganate, followed by one pore volume of xanthan solution.*

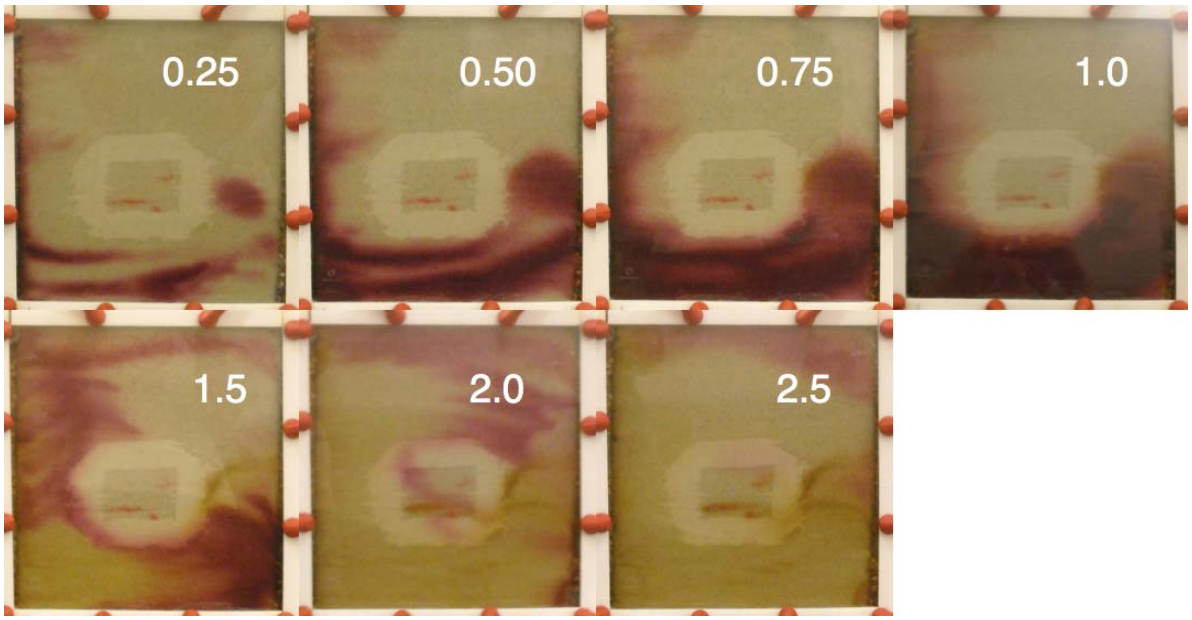

Figure 6-11: *Photographs of "Bankflood" tank at pore volume intervals since introduction of oxidant solution.*

The irregular shape of the chloride and permanganate breakthrough curves generally reflect the contributions of different flow regimes: early arriving bypassed fluid from below the contaminated lens creating an early peak, with later peaks caused by the arrival of fluid traveling over and through the contaminated region. This observation holds true especially for the results of the "Bankflood" experiments, as well as the "Control" and "Unmixed" tanks, but is least evident for the "Co-injected" experiment data, because the increased viscosity of the polymer/oxidant mixture diminished this bypassing effect. We also note slight increases in PCE effluent curve concentrations when xanthan polymer is passed through the system. It is not known how this effect would manifest itself in larger-scale scenarios (i.e., at a larger scale, larger amounts of mass may be present but dilution may also operate more strongly).

In the experiments where oxidant flow is unaffected by previous polymer application ("Control," Figures 6-4, 6-5; "Unmixed," Figures 6-8, 6-9), we see that the denser oxidant mixtures, injected through a port in the bottom level of the tank, flow mainly through the bottom half of the tank. In contrast, the xanthan/permanganate mixture flows much more evenly across the entire height of the tank (Figure 6-7). Extreme viscous fingering and flow bypassing effects can be noted in the "Bankflood" experiment (Figure 6-11). As a result of the more viscous resident fluid (the 0.5 g/L xanthan pre-flood), the aqueous permanganate is concentrated into a few flowpaths through the higher-permeability layer. As a result, these highly concentrated permanganate channels are capable of oxidizing all dissolved-phase PCE they may encounter, but it appears that relatively little NAPL-phase PCE is destroyed in this experiment. These data indicate that, unlike conventional applications of *in situ* permanganate oxidant, follow-on cycles of xanthan/permanganate mixtures may not be advisable unless the newly injected mixtures can maintain a favorable mobility ratio (i.e., more viscous fluids injected behind less viscous resident fluids).

The most striking difference among the four experiments can be noted by comparing the 1 *PV* photograph from each experiment. For the "Control," "Unmixed," and "Bankflood" cases, only 50% to 75% of the tank has been contacted at this time, even though one full pore volume has been injected. In the "Co-injection" experiment, nearly 100% of the tank has been contacted, illustrating the increased sweep efficiency of this delivery strategy over the other three. This increased sweep does result in the same amount of oxidant mass being spread over a larger area (or volume), as opposed to flow bypassing that tends to focus the oxidant into higher concentration flowpaths. Therefore, any dissolved-phase PCE present outside of the fine-grained lens or interior NAPL region is likely to be readily oxidized by the stronger plumes of oxidant present in the other three experiments. In a true aquifer system, though, contaminant is likely to be present in both NAPL and dissolved-phase, and in many different regions as a result of natural formation heterogeneity, and amendments with increased sweep capability will contact more contaminant, on average. In addition, the viscous injectate in the "Co-injection" experiment is much more persistent in the subsurface (see the 3.5 and 4.5 *PV* photographs in Figure 6-7), so targeted oxidant applications are more likely to penetrate finer-grained regions that may harbor contaminant, and diffuse into neighboring areas after delivery has been achieved.

Oxidant reaction with PCE contaminant generally results in decreases in effluent pH (as seen in Figures 6-4, 6-6, 6-8, and 6-10). In the "Control" and "Unmixed" tank, two pH decreases are observed, coincident first with the oxidation of dissolved-phase PCE down-gradient of the

fine-grained lens, which was oxidized by early arriving bypassed fluid. The second pH decrease, which occurs 1 to 1.5 pore volumes later, is greater (5.20 and 3.94 for control and unmixed results, respectively) and results from more intense oxidation occurring within the interior NAPL-filled lens as the aqueous permanganate eventually reaches that region. In the "Co-injected" experiment, however, only one moderate pH dip (6.26) is observed, occurring at a pore volume value of 1 and supporting the stable, plug-like flowfront illustrated in the experimental photos (Figure 6-7).

The amount of total destroyed PCE was calculated for each experiment from two sets of data. Integration of both the permanganate ion and the chloride ion breakthrough curves provided stoichiometric limits on the amount of destroyed contaminant. In theory, these two datasets should provide complementary results; the "true" amount of PCE destruction should be bracketed by a calculated maximum (as inferred from recovered/unreacted permanganate) and a calculated minimum value (derived from chloride detection). In practice, we found that these two calculated values differed by at least one order of magnitude. It is reassuring, however, to note that although the magnitude of PCE destruction values differs between MnO_4^--derived and Cl^--derived calculations, the trends among experiments are similar (see Table 6-1). PCE removal via dissolution was calculated for each experiment and was found to account for less than 1% of the total emplaced PCE mass.

Table 6-1: *PCE destruction/removal values for each tank experiment.*

Experiment	Cl-derived PCE destruction (mmoles)	MnO_4-derived PCE destruction (mmoles)
Co-injection	0.150	6.6
Bankflood	0.104	5.5
Unmixed	0.0718	4.3
Control	0.0577	3.4

Of the possible methods for deriving the mass of oxidized PCE, we place more confidence in the permanganate (MnO_4^-)-derived value, for two reasons. Although chloride data were logged more often than permanganate could be analyzed (every 2 minutes versus every 10-30 minutes), the chloride probe did experience some drift over the course of each experiment. No such "drifting" was detected in the spectrophotometer used to quantify permanganate measurements, as indicated by identical pre- and post-experiment calibration factors. Secondly, previous experiments with the same Unimin sand material (see Section 4.2) indicated that this media would pose little to no additional oxidant demand for the permanganate, at least over timescales of several hours. Therefore, additional media NOD is assumed to have consumed very little of the total applied oxidant. However, both sets of breakthrough data (chloride and permanganate) are useful for interpretation of the transport and reactive characteristics of each oxidant or polymer/oxidant treatment.

Changes in pressure head, as recorded across the span of the tank along a centerline running through the barrier lens and interior lens (see blue symbols in Figure 6-1), are presented in Figure 6-12. Prior to polymer or oxidant injection, head differences for all experiments were approximately zero over this same length. While overall head differences did not change for the control case, head differences were generally negative across the tank for the co-injected case and the majority of the bankflood case, and generally positive for the unmixed tank.

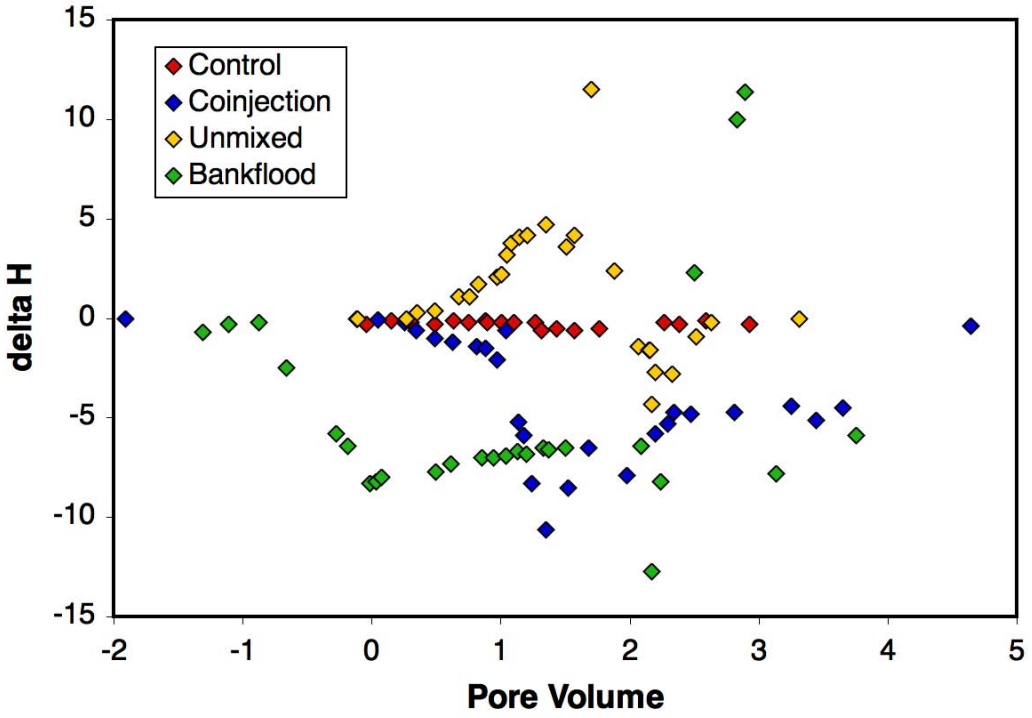

Figure 6-12: *Difference in head versus pore volume for the four experiments. Delta (Δ) head values were calculated as the difference in head between two manometers located 20 cm apart along a horizontal centerline spanning the fine-grained lens and inner NAPL region.*

After at least five pore volumes of deionized water flushes had been passed through each experiment following treatment application, samples taken from ports aligned along a vertical plane at the downstream edge of the tank (see gold symbols in Figure 6-13) were analyzed and used to compare residual PCE mass fluxes among the four different cases (Table 6-2). The mass flux values are highest for the control experiment results, but data from the co-injection case also show higher fluxes out of the contaminated region as compared to the other two experiments. It is recognized that this experimental lengthscale may not have been long enough to replicate natural groundwater dilution of contaminant fluxes that may occur downstream of *in situ* treated source zones.

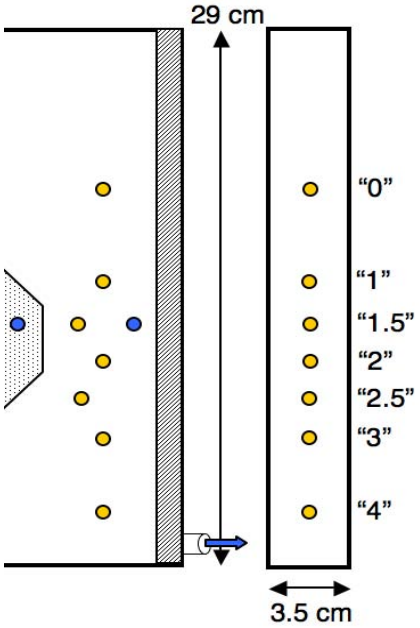

Figure 6-13: *Partial front view and effluent side view of tank, showing port labels and positions in gold.*

Table 6-2: *Post-oxidation PCE mass fluxes for each experiment.*

	average PCE concentration (mg/L) at tank ports, 5 *PV* after treatment cessation			
	Control	**Coinjection**	**Unmixed**	**Bankflood**
Effluent from port "0"	3.07	0.0621	0.117	0.0405
Effluent from port "1"	6.46	0.0722	0.195	0.104
Effluent from port "1.5"	n.m.[a]	138	1.49	n.m.
Effluent from port "2"	6.50	1.31	3.62	0.163
Effluent from port "2.5"	n.m.	0.0761	23.5	n.m.
Effluent from port "3"	69.3	0.214	8.26	55.0
Effluent from port "4"	34.4	0.226	25.6	0.134
Mass Flux[b] [mg·cm^{-2}·sec^{-1}]	0.163	0.0962	0.0308	0.0753

[a] *n.m. = not measured.*

[b] $\dot{m}(t) = v_{darcy}\left[\left(\frac{Area_i}{Area_{total}} \bullet C_i\right) + \ldots + \left(\frac{Area_n}{Area_{total}} \bullet C_n\right)\right]$, *where* v_{darcy} *= 0.00788 cm/min*

2-D Oxidant Tank Experiment Conclusions

- Viscous mixtures of xanthan polymer and permanganate oxidant flow more evenly through this experimental dual-permeability system, and the mixture penetrates more of the finer-grained layer than does a solution of aqueous low viscosity oxidant alone. As a result of this increased "sweep," more contaminant mass (~2-3 times) is destroyed per mass of oxidant.
- Discrete injections of oxidant followed by polymer (the "Unmixed" case) are less effective at penetrating finer-grained layers than mixed solutions, as a result of initial flow bypassing before the introduction of the later polymer flood.
- Polymer-amended chemical oxidant applications appear to produce lower mass flux values, as compared to those measured for the polymer-free conventional oxidant application.
- Permeability differences of less than one order of magnitude can severely impact the sweep capability of an aqueous, low (1 cP) viscosity fluid, indicating that increased viscosity polymer/oxidant solutions may improve treatment effectiveness over a wide variety of heterogeneous natural systems.

7. TASK 5: NUMERICAL SIMULATIONS

This task was originally designed to conduct 3D simulations, after successfully evaluating the performance of the model for 2D systems, so that we could provide insight on practical application. However, data from the two- and three-layer experiments were more insightful that we anticipated, suggesting that we could learn much about polymer applications in layered systems by conducting 2-D additional simulations. In addition, some larger-scale 2D and 3D simulations of our ESTCP field site were very problematic because of numerical problems. It was clear that adjusting for these issues would minimize the value of larger-scale simulations, and the time spent would likely result in completion of one successful run, giving us limited information about general application. Because layered systems are probably the most dominant aquifer systems, and because of these numerical difficulties, we chose to focus Task 5 on 2-D layered-strata simulations because we believed that we could achieve the highest impact from our research efforts. Thus, as part of this task, 256 numerical simulations were conducted.

After the performance of the UTCHEM simulator was demonstrated to be satisfactory based on the experimental 1-D and 2-D datasets, we used the model to investigate polymer-assisted sweep efficiency improvement in 2-D layered heterogeneous systems across a larger range of polymer concentrations and media permeability contrasts than could be practically performed experimentally.

The objectives of this Task are:

1. Investigate sweep efficiency improvement as a function of polymer concentration, layer structure, and permeability contrast for a tracer (to simulate a remediation amendment),

2. Evaluate the benefits and limitations of polymer-improved sweep efficiency for layered heterogeneous systems, and

3. Provide practical information on the potential to predict polymer-improved sweep efficiencies for layered heterogeneous systems

The numerical simulations and numerical-data analysis are presented below.

Methods, Results and Discussion

The first set of numerical simulations performed utilized the layered heterogeneity structures shown in Figure 7-1. Note that these layer structures are the same as those evaluated experimentally in Task 3. However, the experimental data provided many insights we had not anticipated (outlined in the conclusions of Task 3), and that warrant further investigation. These layer structures were selected to examine the effect of sweep-efficiency improvement relative to changes in the proportions (or layer thickness) compared to similar thicknesses but with different permeability arrangements.

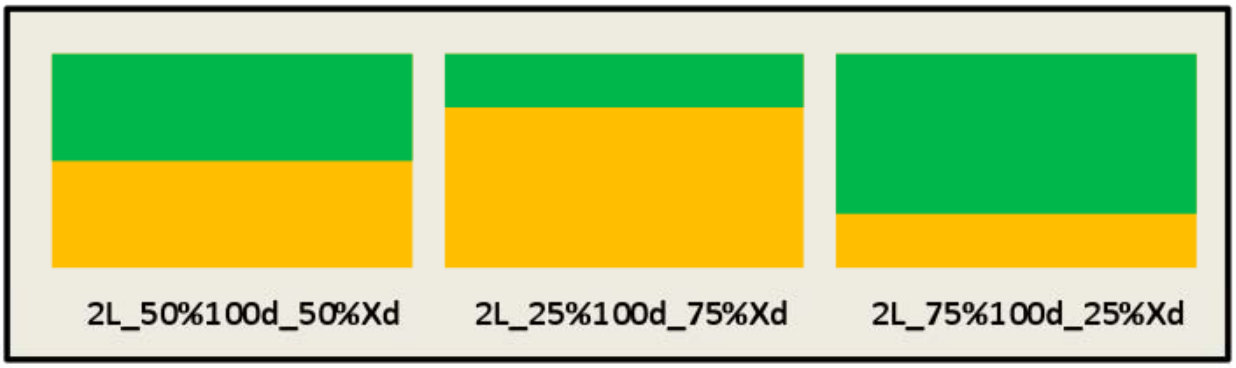

Figure 7-1. *Two-layer heterogeneity structures utilized to evaluate sweep efficiency improvement as a function of layer thickness. X refers to the lower layer permeability. Four different values of X were used for each of the three cases above (resulting in 12 simulations).*

The permeability of the upper layer in these simulations was fixed at 100 darcy in all simulated cases; the lower-layer permeability was varied between individual simulations to examine the additional effect of permeability contrast on sweep-efficiency improvement. Four different cases of lower permeability were chosen or each of the three cases shown in Figure 1. These 12 scenarios were each run with 8 different polymer concentrations (a highly variable factor in the subsurface during a field application), resulting in 96 numerical simulations. Finally, the concentration of xanthan gum polymer was varied within individual simulations. The injected volumetric flow rate was held constant at 1 ft^3/day (19.7 cm^3/min) for all simulations. All grid dimensions and boundary condition assumptions established during the model conditioning portion of this work (see Task 3) were maintained during this investigation. In all cases, tracer sweep efficiency calculations were performed for an endpoint tracer concentration of10% the injected concentration, or for $C_t/C_{t,inj} = 0.1$.

Tracer sweep efficiencies resulting from these simulations are presented as a function of injected pore volumes in Figures 7-2 through 7-4. As shown in Figures 7-2 through 7-4, the effect of increasing the concentration of xanthan gum within the injected solution is to decrease the number of injected pore volumes needed to achieve 100% sweep of the sand tank in all cases. However, this effect is shown to diminish as polymer concentrations exceed 500 mg/L.

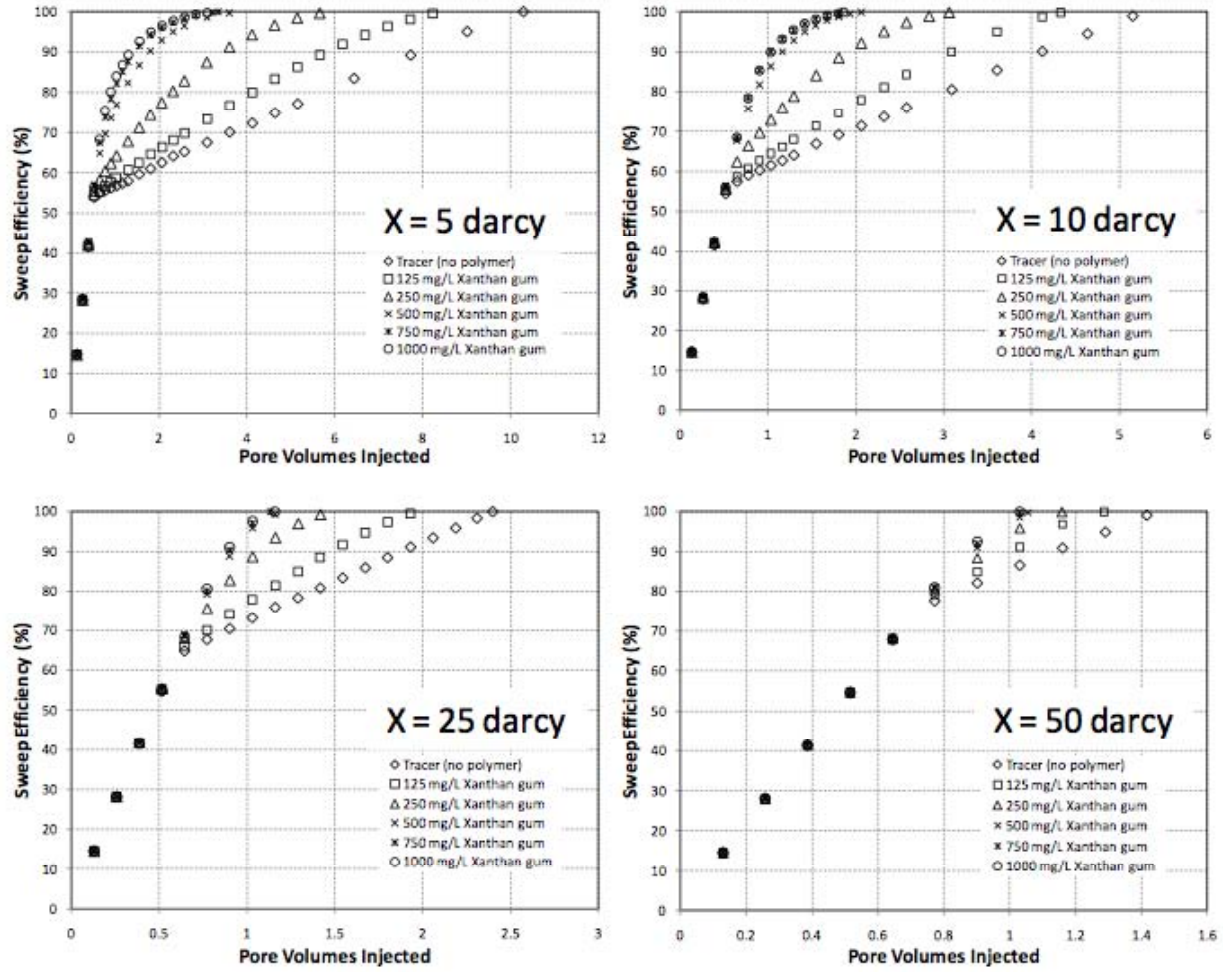

Figure 7-2. *Simulated tracer sweep efficiency profiles for the 2L_50%100darcy_50%Xdarcy layer arrangement as a function of polymer concentration and layer permeability contrast.*

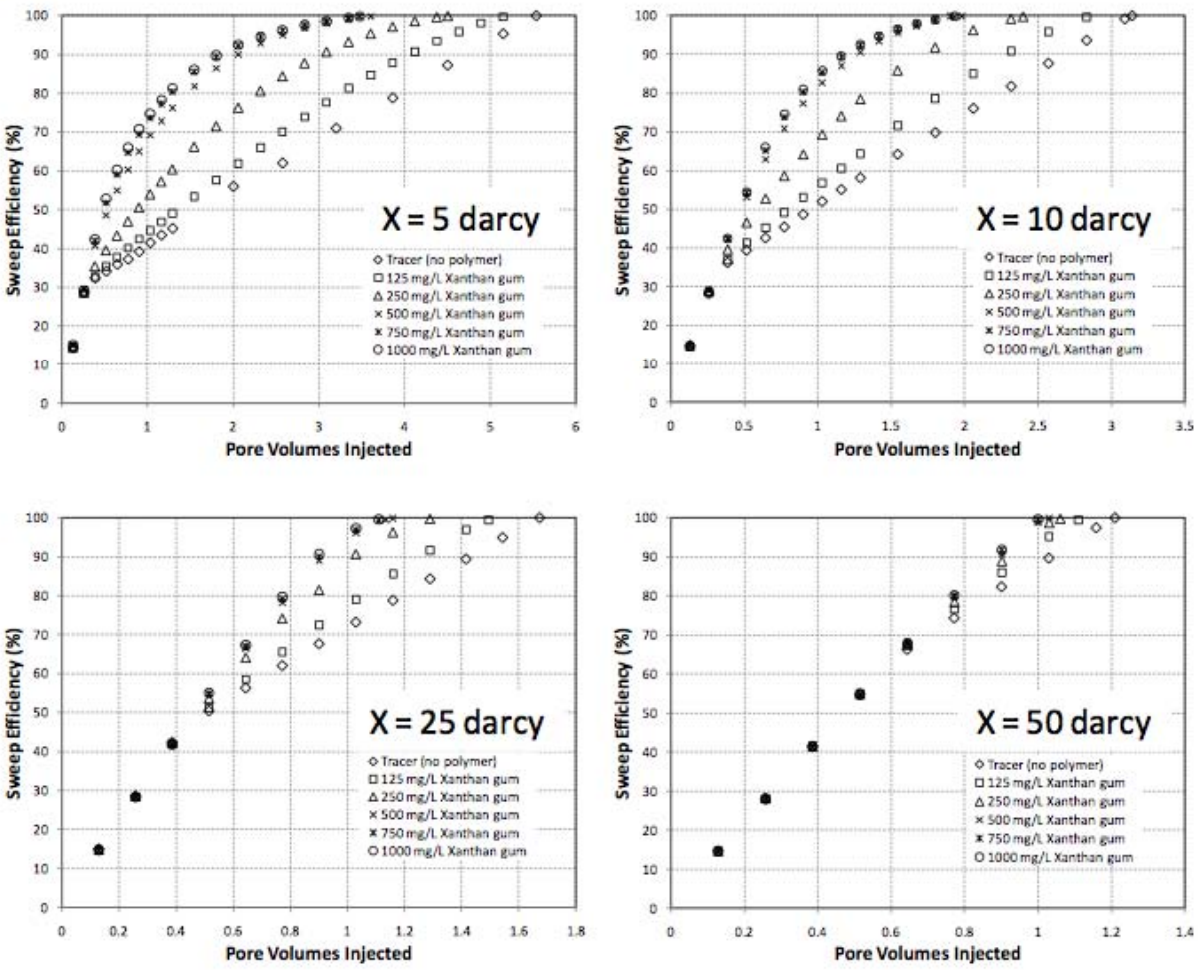

Figure 7-3. *Simulated tracer sweep efficiency profiles for the 2L_25%100darcy_75%Xdarcy layer arrangement as a function of polymer concentration and layer permeability contrast.*

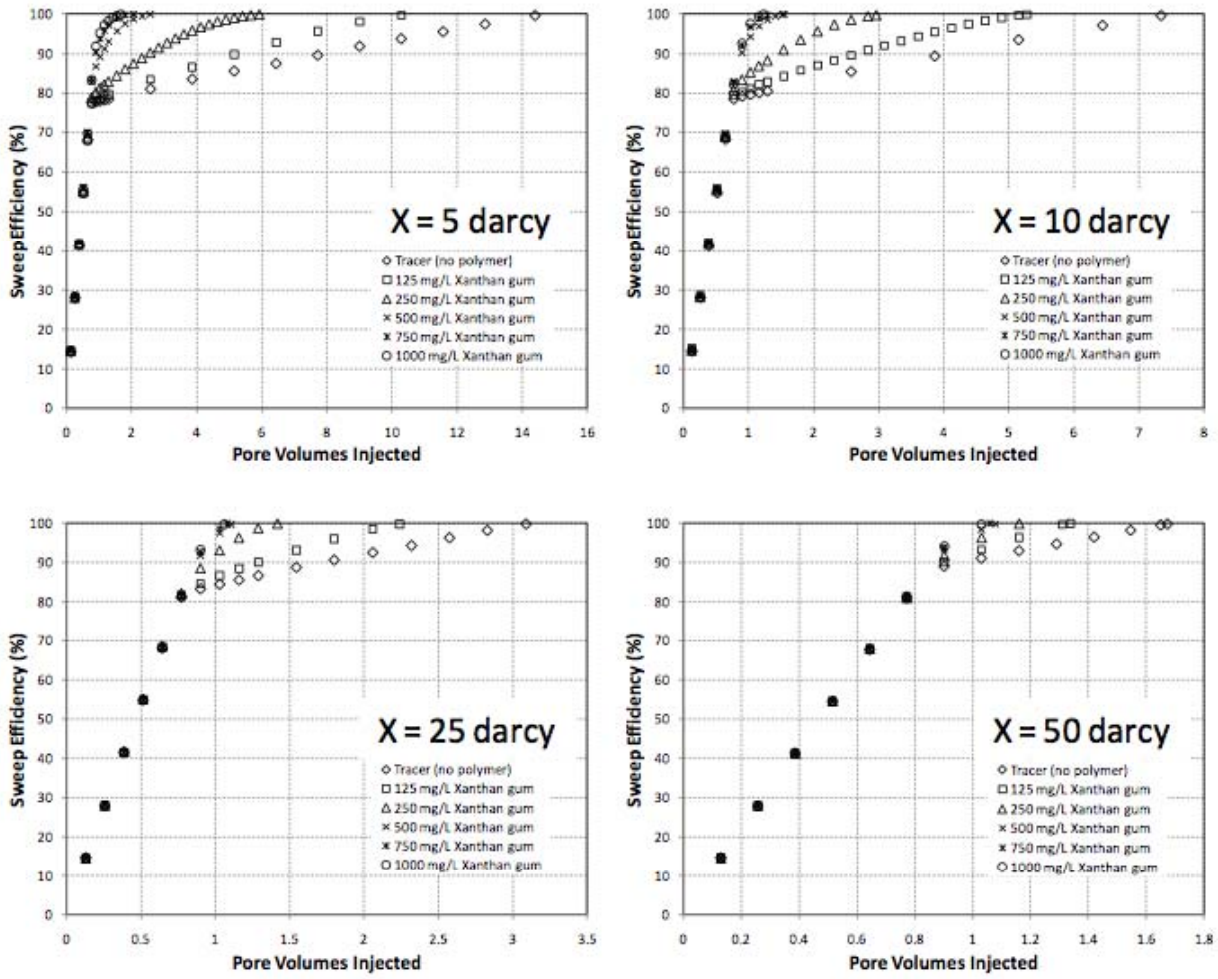

Figure 7-4. *Simulated tracer sweep efficiency profiles for the 2L_25%100darcy_75%Xdarcy layer arrangement as a function of polymer concentration and layer permeability contrast.*

This trend is more clearly represented in Figures 7-5, 7-6, and 7-7 wherein the number of pore volumes needed to achieve 100% sweep are presented as a direct function of polymer concentration. For each of these layered systems the effect of polymer concentration is marginal for concentrations less than 75 mg/L. As polymer concentration increases beyond 75 mg/L, the increasing injected fluid viscosity begins to reduce fluid mobility within the 100 darcy layer and promotes cross-flow into the lower permeability layer. This in turn improves tank sweep efficiencies and reduces the number of pore volumes needed to achieve 100% sweep. However, beyond a polymer concentration of 500 mg/L the effect of further increasing polymer concentration sweep improvement diminishes and the number of pore volumes needed to achieve 100% sweep approaches a nearly constant value. That is, a maximum level of sweep-efficiency improvement is attained within each of these layered systems.

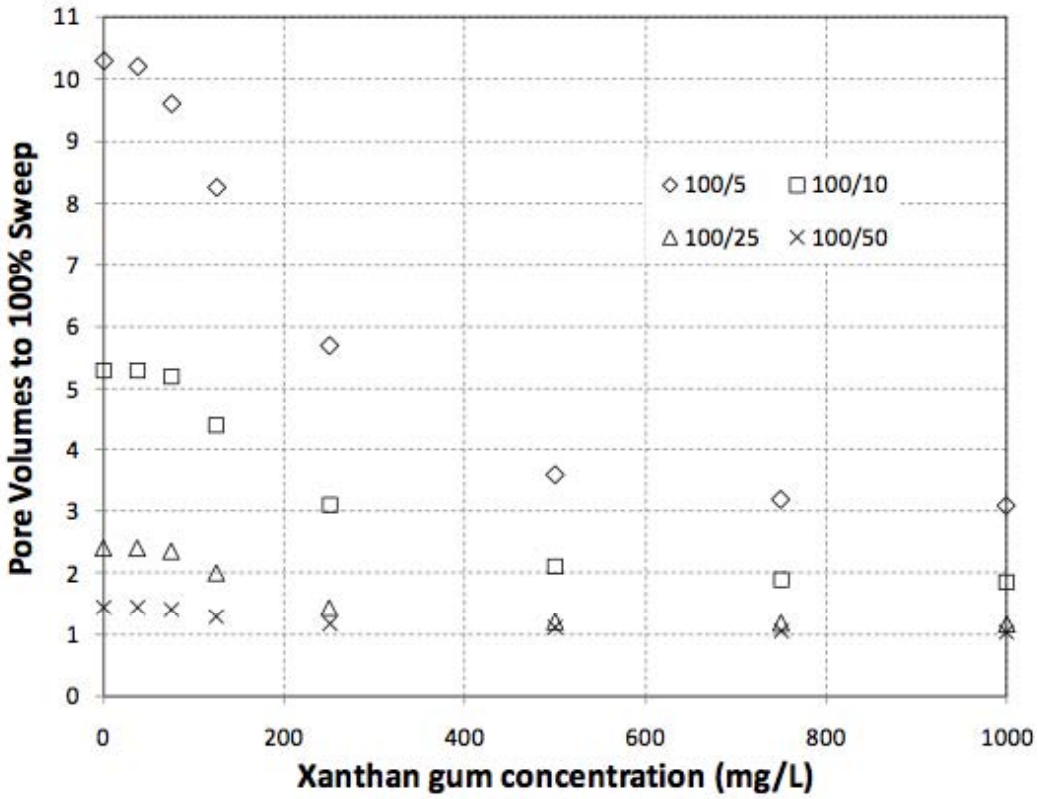

Figure 7-5. *The effect of polymer concentration on the number of pore volumes needed to achieve 100% sweep of the 2L_50%100darcy_50%Xdarcy layer arrangement to $C_t/C_{t,inj}$ = 0.1.*

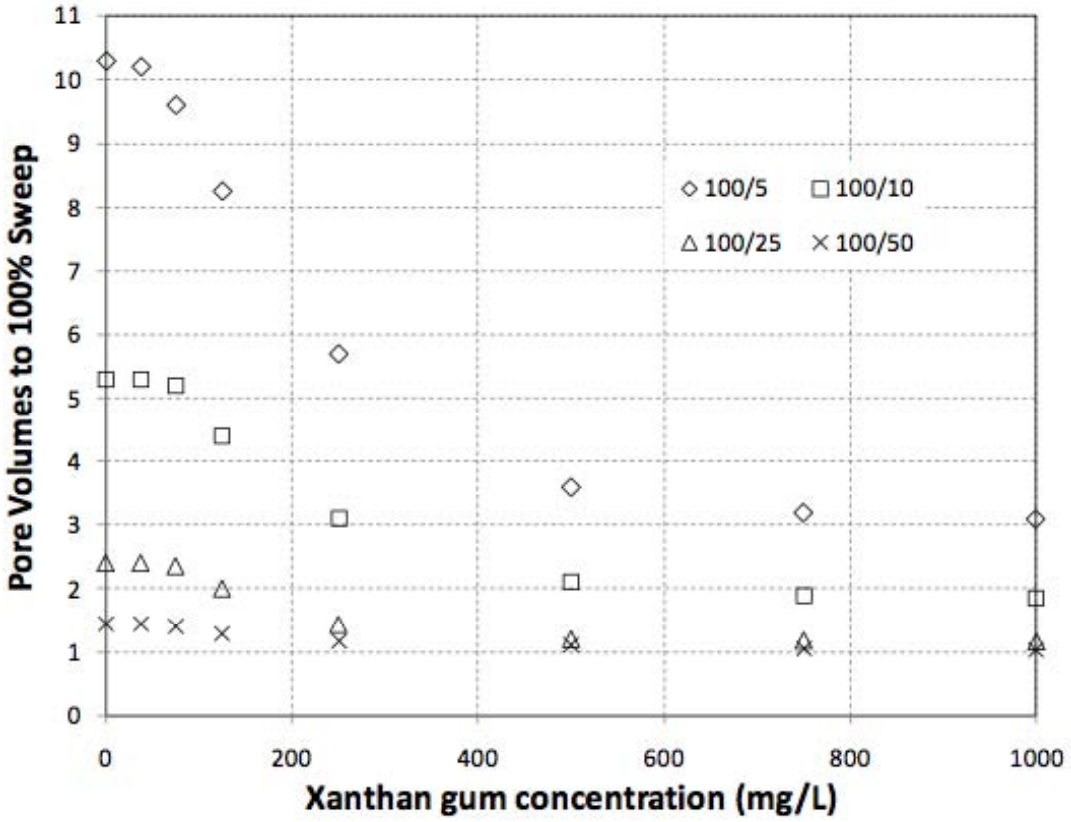

Figure 7-6. *The effect of polymer concentration on the number of pore volumes needed to achieve 100% sweep of the 2L_25%100darcy_75%Xdarcy layer arrangement to $C_t/C_{t,inj}$ = 0.1.*

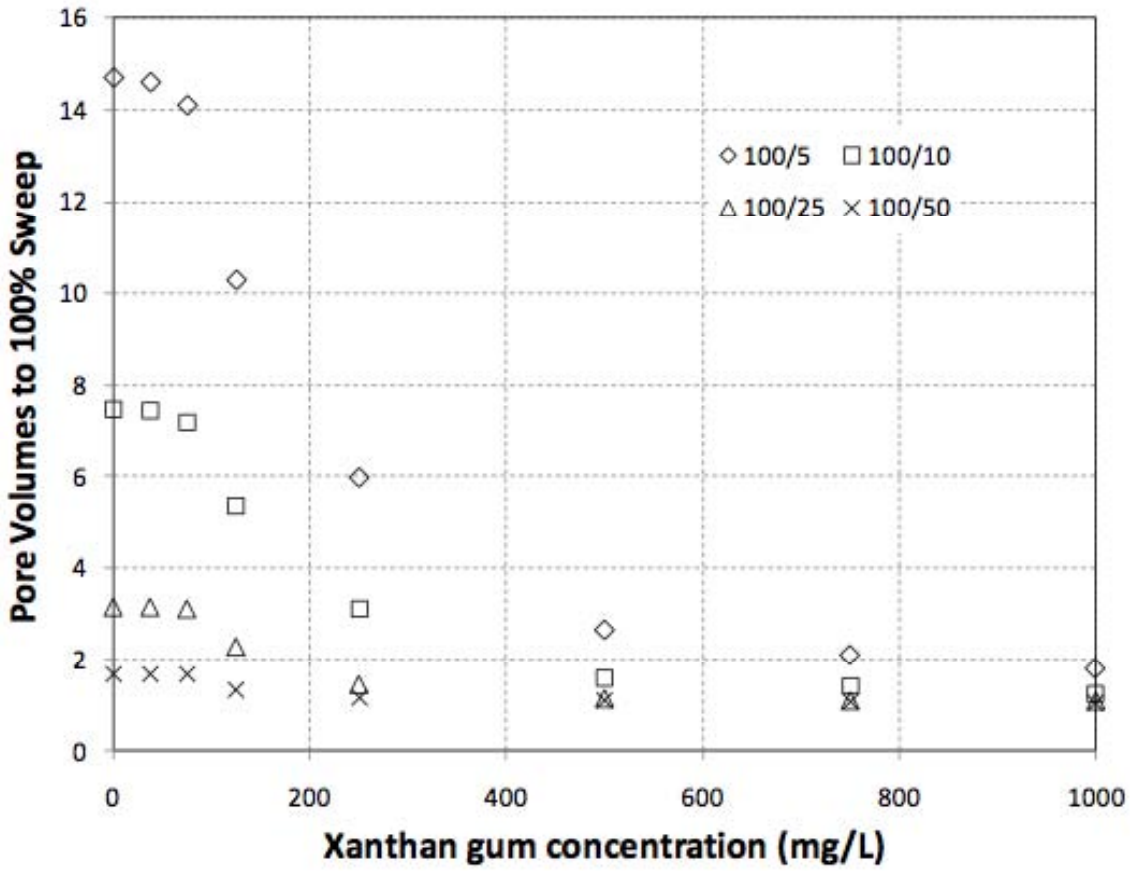

***Figure 7-7**. The effect of polymer concentration on the number of pore volumes needed to achieve 100% sweep of the 2L_75%100darcy_25%Xdarcy layer arrangement to $C_t/C_{t,inj}$ = 0.1.*

This region of diminished effectiveness is hereafter referred to as the maximum effectiveness limit (MEL) and is represented as the percent sweep efficiency improvement, relative to the tracer (i.e., no polymer) results, in Figures 7-8, 7-9, and 7-10. Note that the MEL varies not only as a function of the permeability contrast between layers, but also as a function of the relative thickness of layers. For a given permeability contrast, reducing the thickness of the lower permeability layer results in a decrease in the number of pore volumes needed to achieve 100% sweep. The opposite is true for the tracer result (no polymer addition) in that the number of pore volumes needed to achieve 100% sweep increases as the thickness of the lower permeability layer decreases. These trends are reflected in Figures 7-8, 7-9, and 7-10 in that the percent improvement in sweep efficiency increases as the thickness of the lower permeability layer decreases.

Additionally apparent in these figures is that achieving 100% sweep in 1 pore volume requires a permeability contrast of less than 4. As the permeability contrast increases, achieving 100% sweep in just 1 pore volume is not possible and the minimum number of pore volumes

needed to achieve 100% sweep increases. This phenomenon is related to the increased fluid mobility reduction within the lower permeability layer. For the conditions simulated (i.e., constant rate of injection, fixed polymer concentration, constant permeability assigned to the upper layer, shear-thinning polymer fluid), the polymer solution viscosity (or mobility) in the upper layer is only dependent on the pore flow velocity within the upper layer, which is in turn dependent on the thickness (or cross-sectional area) of that layer. As such, for any one of these 2-layer systems the mobility reduction, which is the driving force for cross-flow, is constant within the upper layer. As the polymer itself cross-flows into the lower permeability layer, fluid viscosities within the contacted portions of that layer increase which reduces pore fluid mobility and the rate of penetration of fluids into that layer. The rate of penetration into the lower layer is therefore dependent on the permeability of the lower layer.

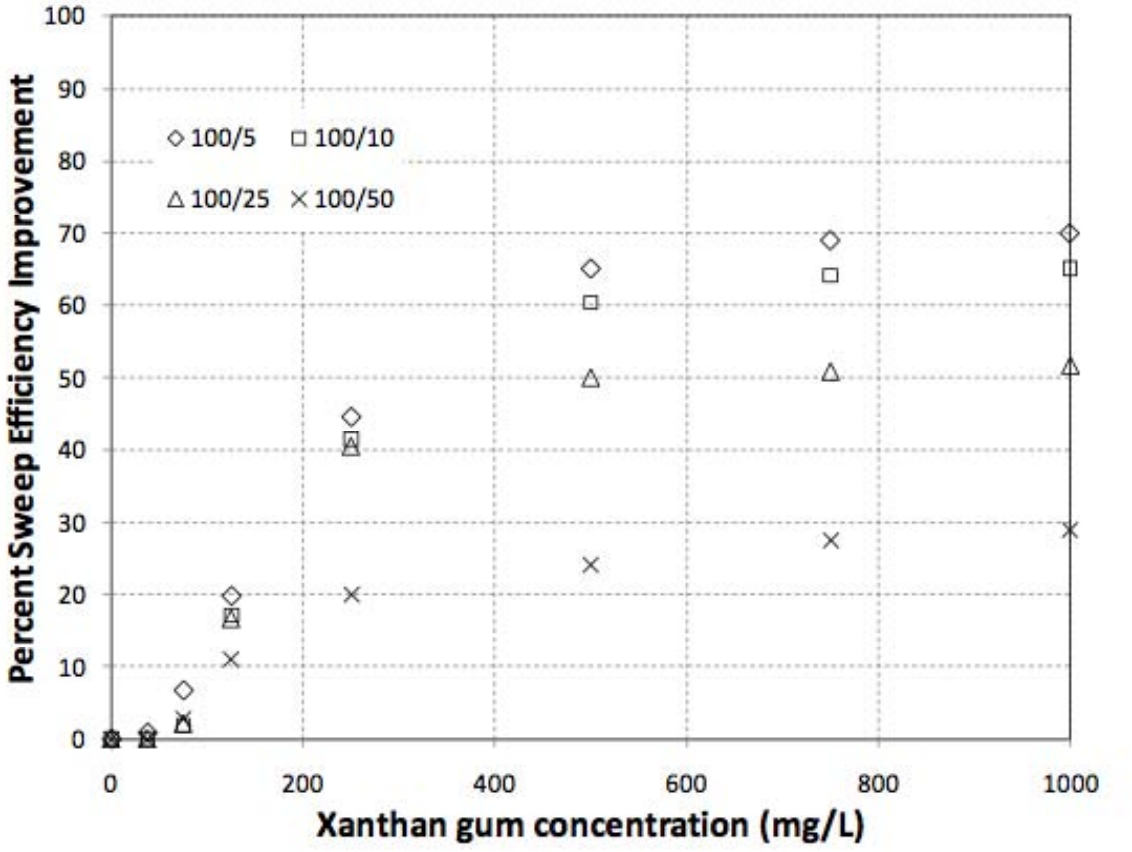

Figure 7-8. *Sweep efficiency improvement as a function of polymer concentration for the 2L_50%100darcy_50%Xdarcy layer arrangement.*

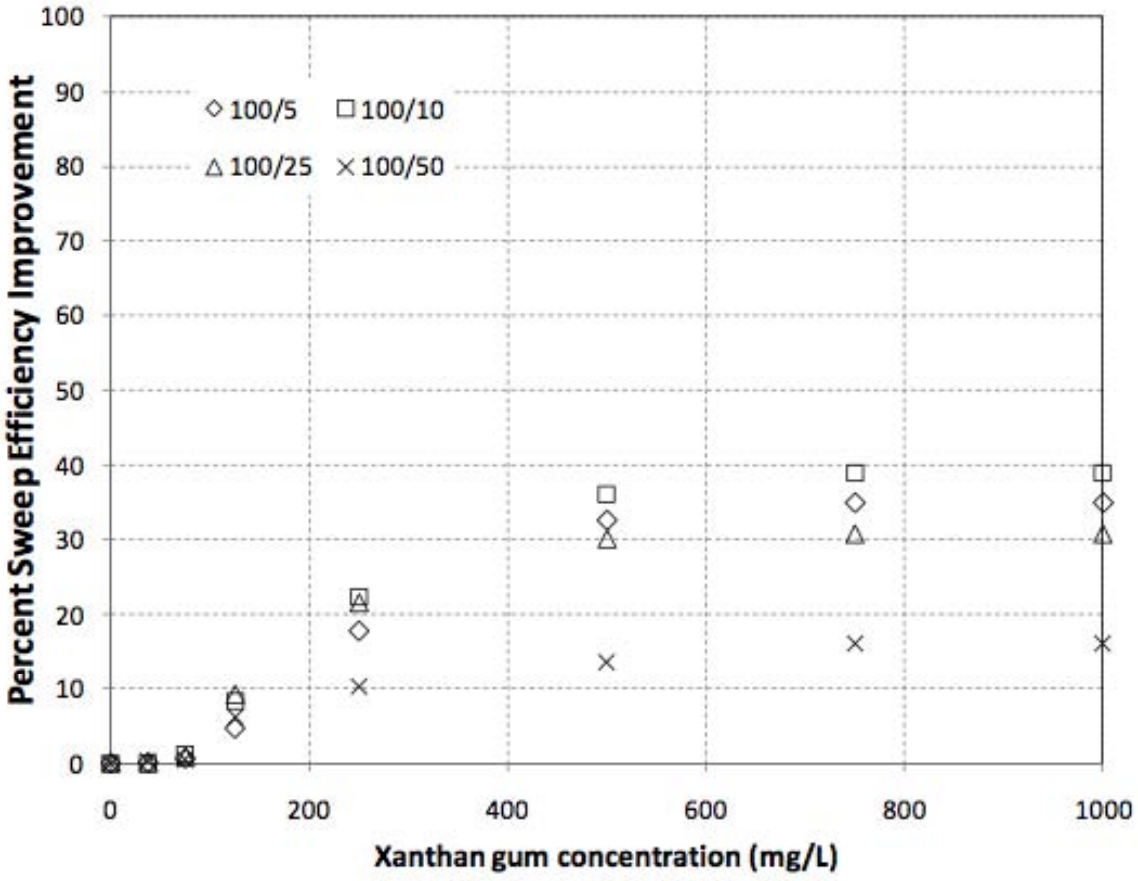

Figure 7-9. *Sweep efficiency improvement as a function of polymer concentration for the 2L_25%100darcy_75%Xdarcy layer arrangement.*

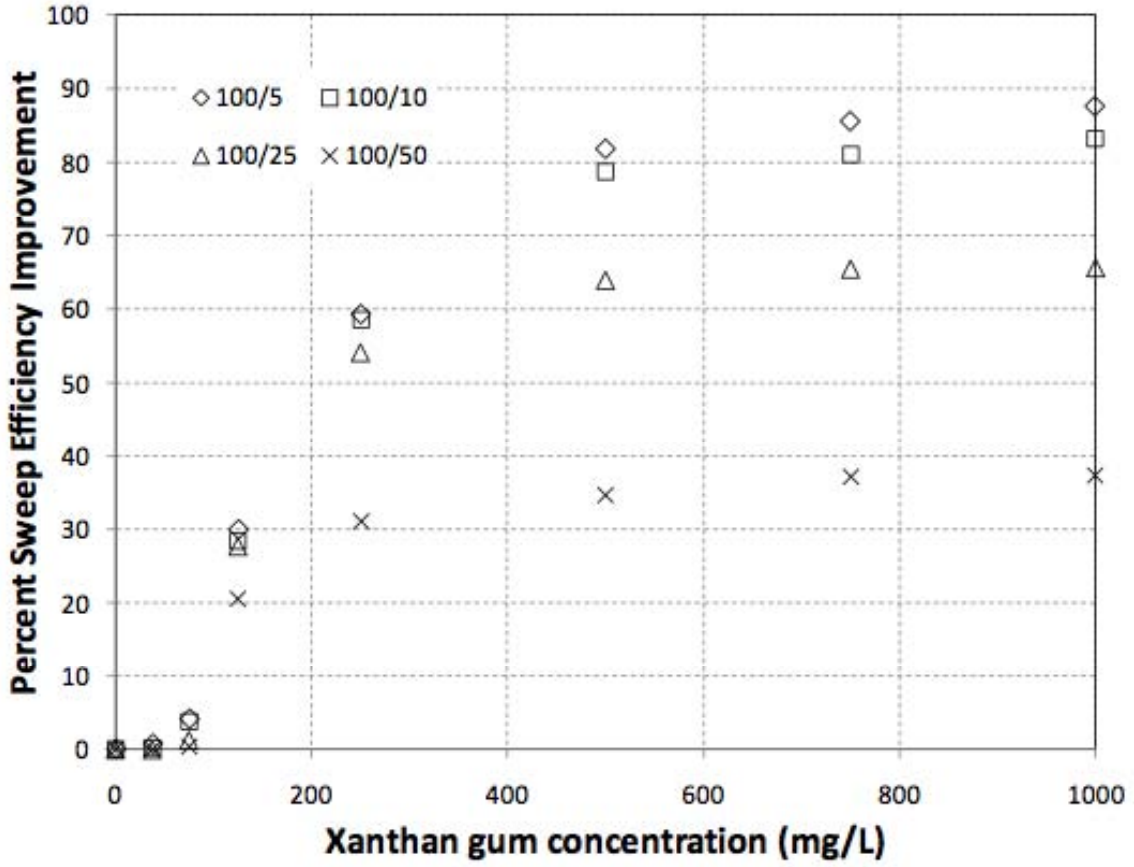

Figure 7-10. *Sweep efficiency improvement as a function of polymer concentration for the 2L_75%100darcy_25%Xdarcy layer arrangement.*

Sweep efficiency profiles for the 1000 mg/L polymer floods of each 2-layer tank arrangement are presented as Figure 7-11 to help elucidate these phenomena. Within each of these profiles, a dashed line has been plotted to represent a 1:1 sweep for a homogeneous sand pack. Note that, for homogeneous media, the tracer and polymer cases will achieve 100% sweep in one pore volume (by definition) for any permeability value of the homogenous media.

In each case, the tank is initially swept similarly to a homogeneous case. For a permeability contrast less than 4, the tank is swept in 1 pore volume. For permeability contrasts greater than 4, the rate of sweep (or rate of penetration into the lower permeability layer) decreases and departs from the homogeneous line at points indicative of the establishment of a steady state mobility reduction condition in the more permeable layer. Thereafter, the rate of cross-flow continues to diminish as more of the lower layer pore volume is contacted by polymer solution and the mobility within this contacted volume is reduced. For a given permeability contrast, the point of departure from the homogeneous line occurs at higher sweep efficiencies as the relative thickness of the lower permeability layer decreases. This is the result of an increased flow capacity of the upper layer resulting in a lower steady-state mobility reduction, as well as the fact that there is less volume associated with the lower layer as it gets thinner.

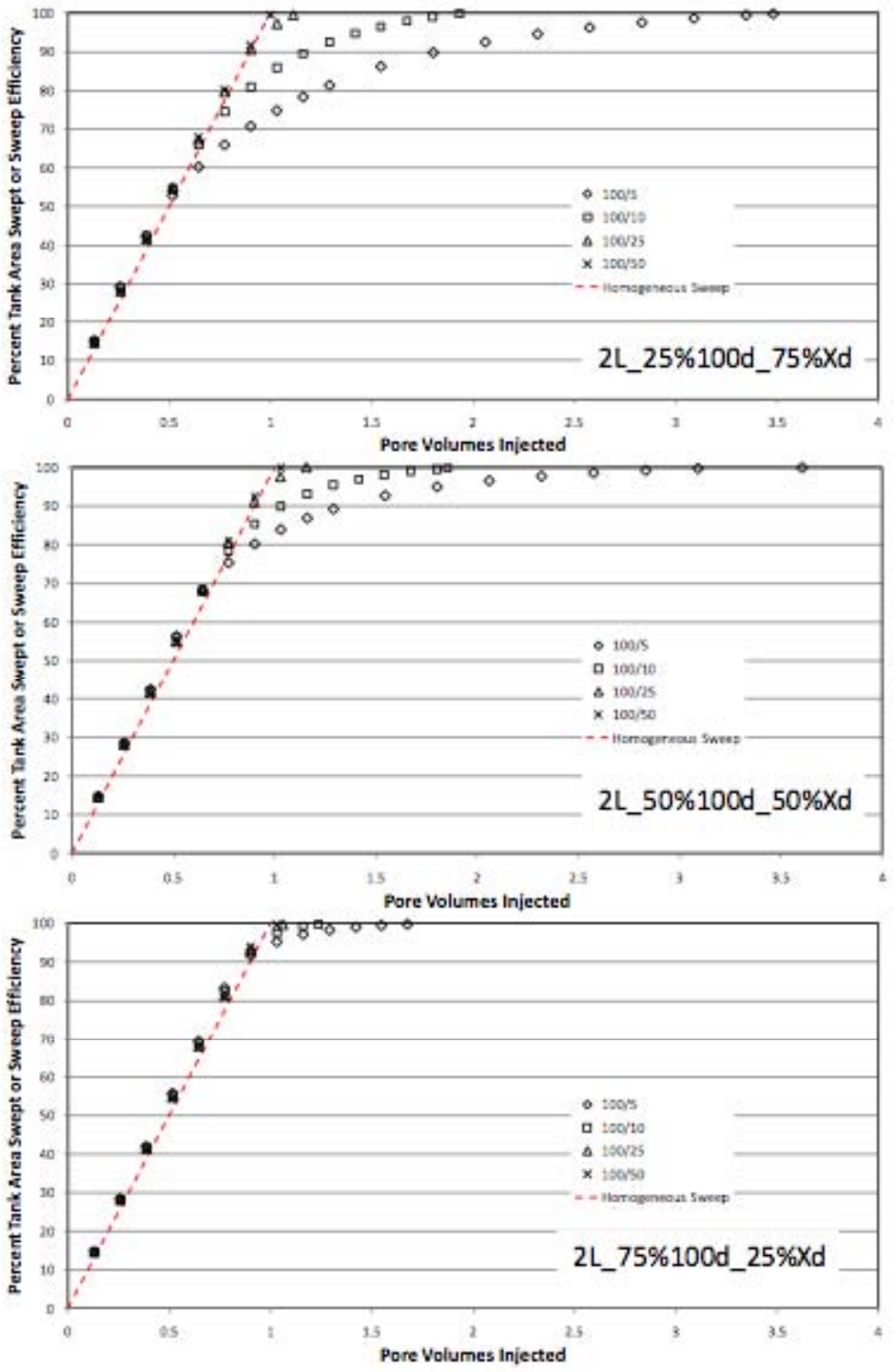

Figure 7-11. *Sweep efficiency as a function of pore volumes injected for the cases shown in Figure 7-1. The X refers to for different cases with varying bottom-layer permeability (see legend). The dashed red line represents a homogeneous case (any permeability)*

A second group of 2-D simulations was designed to evaluate sweep efficiency improvements for 2-D layered systems that possess the same proportion of two different permeability categories, but where the number of layers is sequentially increased from 2 to 8. The systems evaluated in this work are presented in Figure 7-12. . The simulations consisted of 2-layer strata, 3-layer strata (two cases), 4-layer strata and 8-layer strata, where layers are repositioned 4 different ways within each case. We also used 8 different polymer concentrations for each case. This resulted in 160 additional numerical simulations.

We started with the two-layer system termed 2L_50%100d_50%X (where 2L denotes a two-layer system, and X is permeability of the bottom layer) described earlier in this task. As was the case for the previous analysis, the green layers in Figure 7-12 were assigned a constant permeability of 100 darcy. The permeability of the orange layers was varied for individual simulations in the same manner as the previous analysis. The concentration of xanthan gum polymer was varied within individual simulations. The injected volumetric flow rate was held constant at 1 ft^3/day (19.7 cm^3/min) for all simulations. All grid dimensions and boundary condition assumptions were maintained during this analysis with the exception of 8L_Scenerio5, in which the number of simulation grid nodes was increased by a factor of 2. In all cases, tracer sweep efficiency calculations were performed for an endpoint tracer concentration of10% the injected concentration, or for $C_t/C_{t,inj} = 0.1$.

The number of pore volumes needed to achieve 100% sweep for these layer arrangements are presented as a function of polymer concentration in Figure 7-13 for each multi-layer scenario listed in Figure 7-12. Percent sweep efficiency improvements, relative to the tracer result (i.e., no polymer addition), are also presented as a function of concentration in Figure 7-14. For polymer concentration in excess of 125 mg/L, the effect of increased layering is shown to decrease the number of pore volumes needed to achieve 100% sweep. For example, in comparing 100:5 permeability contrast results between the 2-layer and 3-layer systems the minimum number of pore volumes needed to achieve 100% sweep is reduced by 51%. This occurs for the 1000 mg/L polymer concentration. As the concentration of polymer decreases, the percent reduction decreases.

Another interesting result is that the positioning of the 100 darcy layer in the 3-layer systems shows no variance on sweep efficiency improvements. That is, regardless of the distribution of the 100 darcy unit (i.e., positioned in the middle of the tank or distributed on either side of the lower permeability unit) the effect of polymer concentration on the number of pore volumes required to completely sweep the tank are the same. Similarly, keeping the proportions of media the same and increasing the number of layers from 3 to 4 provide the same efficiencies. Increasing the number of layers to 8, shows a less dramatic improvement in sweep efficiencies than was observed when the number of layers were increased from 2 to 4. This suggests that most aquifers (which can have many layers not discernible even from well borings) may achieve sweep efficiencies at least as favorable as those predicted by these 2-D experiments and simulations.

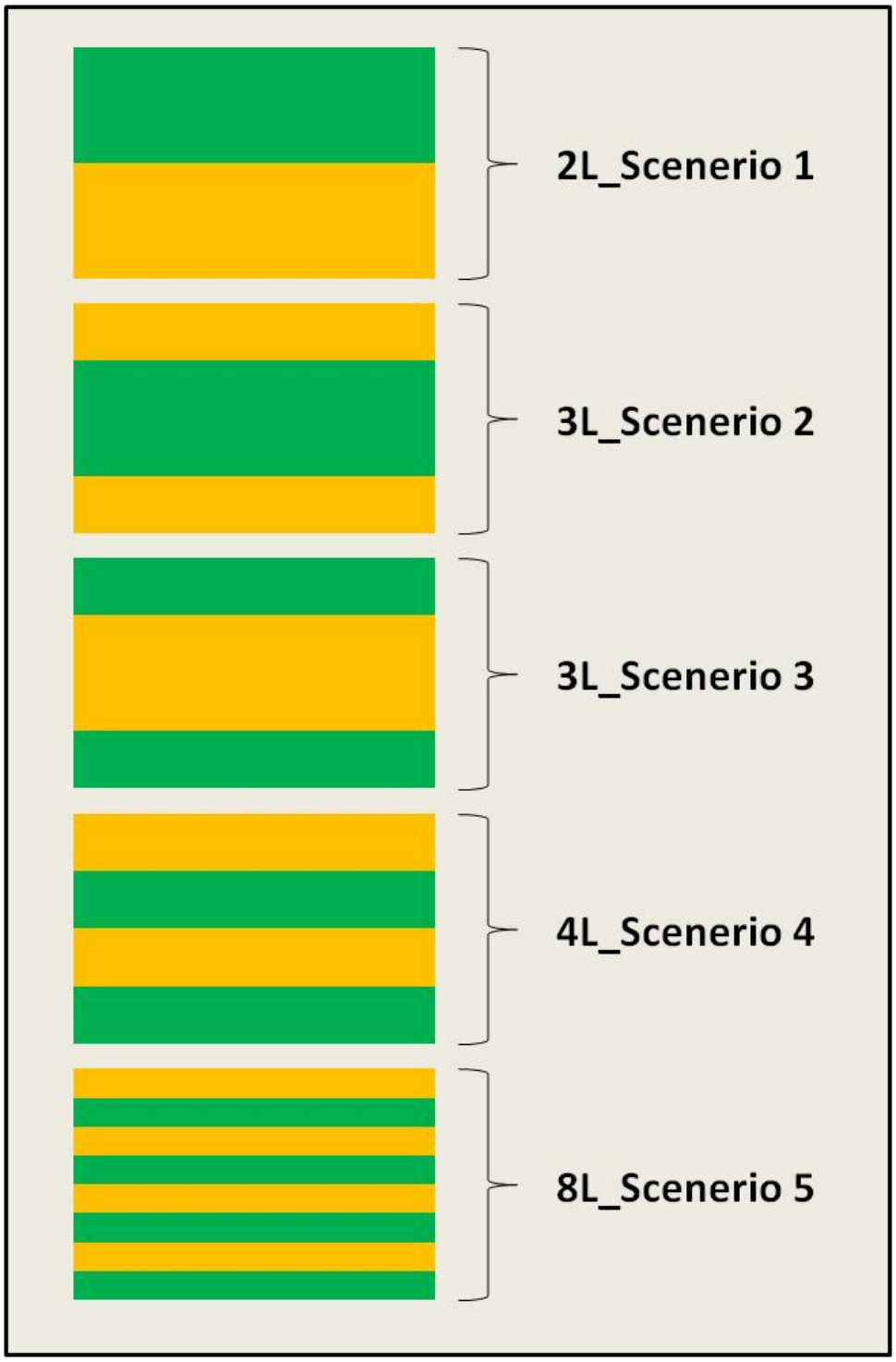

Figure 7-12. *Two-layer heterogeneity structures utilized to evaluate sweep efficiency improvement as a function of constant media proportions and increased layering. "2L" refers to a two-layer system; "8L" refers to an 8-layer system, etc.*

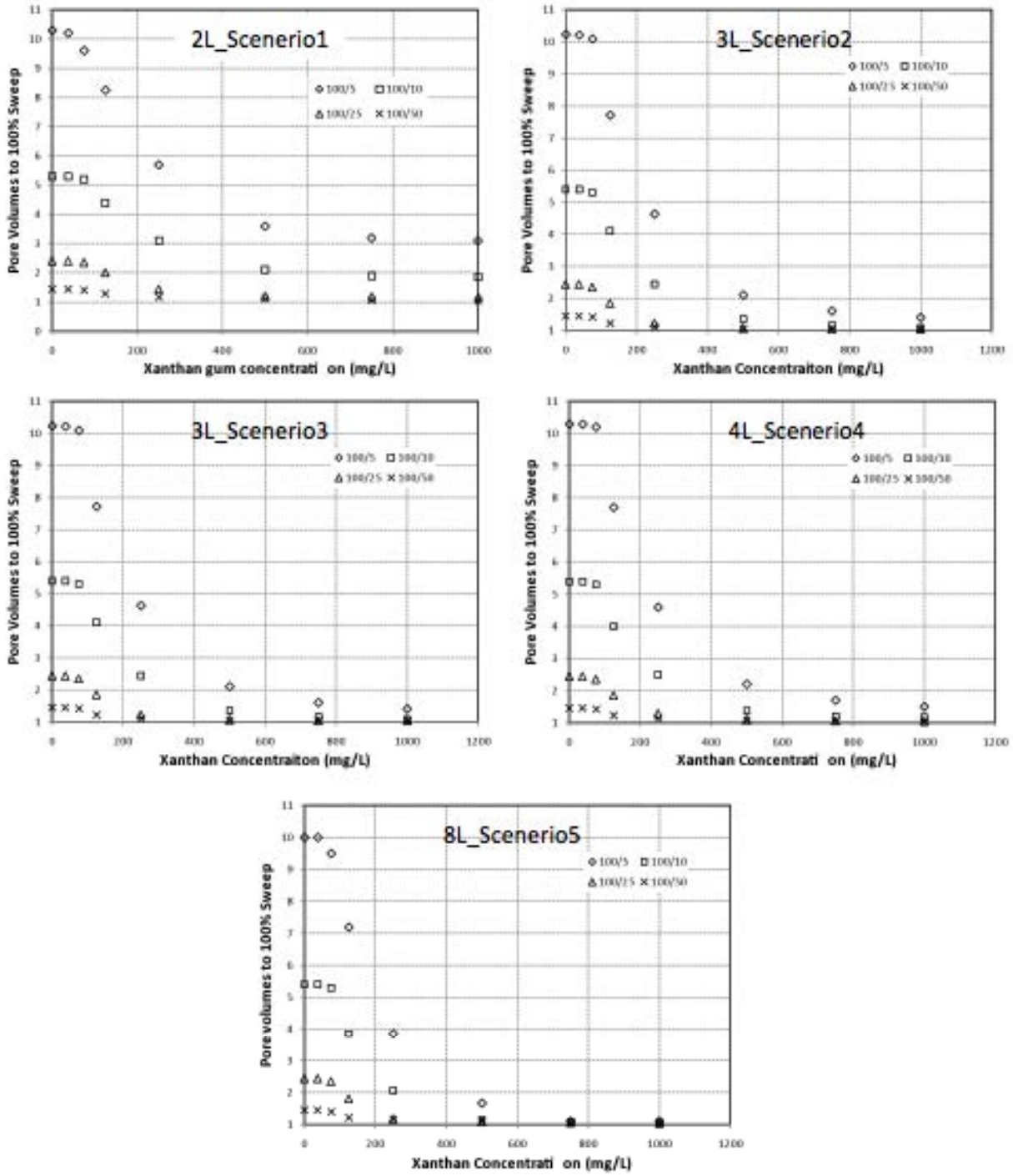

Figure 7-13: *The effect of polymer concentration on the number of pore volumes needed to achieve 100% sweep for each multi-layer scenario listed in Figure 7-12.*

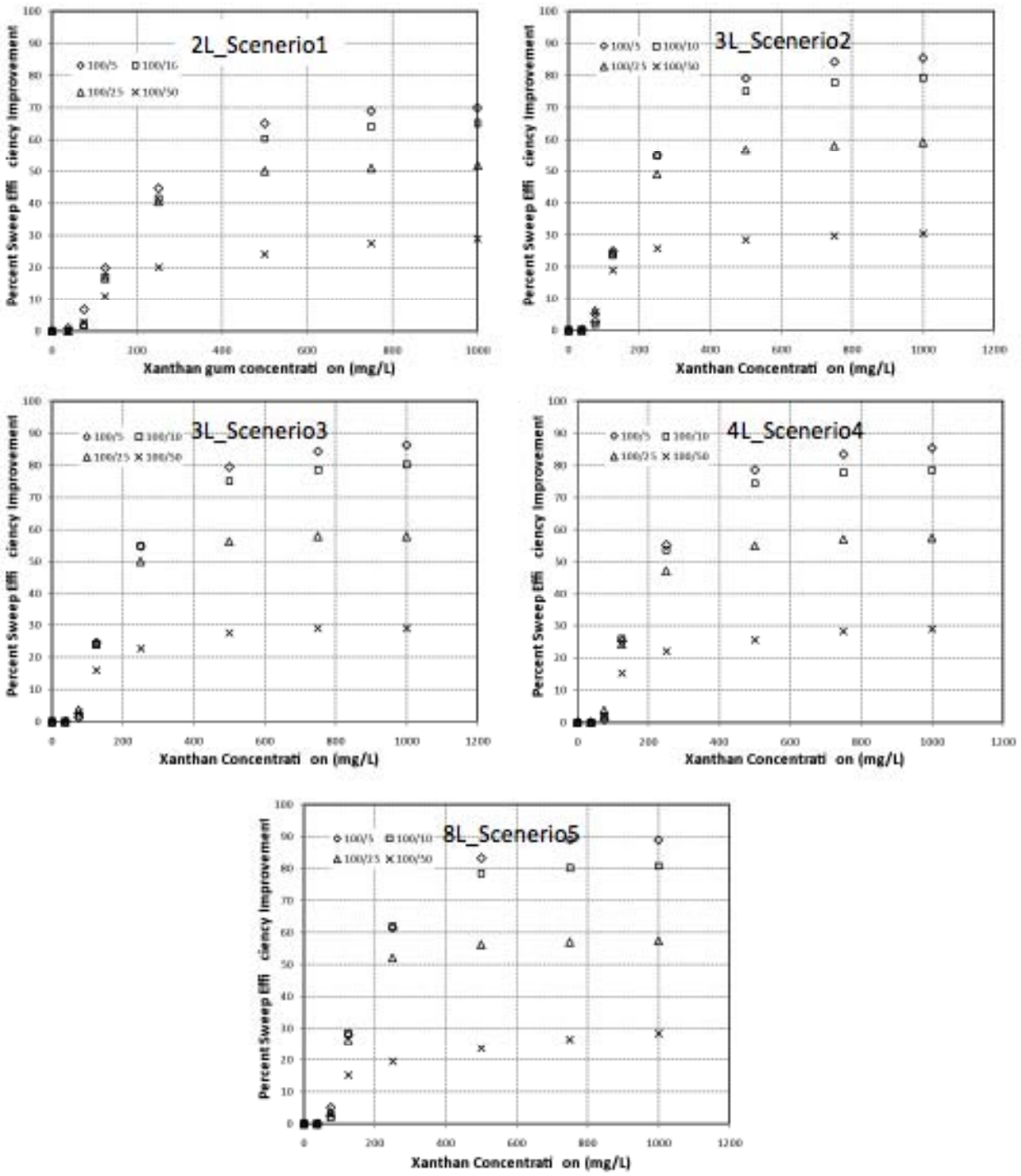

Figure 7-14: *Sweep efficiency improvement as a function of polymer concentration for all multi-layer systems listed in Figure 7-12.*

The minimum number of pore volumes needed to achieve 100% sweep is presented as of the number of layers for all permeability contrasts in Figure 7-15. For the permeability contrast greater than 4, the minimum number of pore volumes needed to completely sweep the tank (or maximum sweep efficiency) decreases as the number of layers increase. As the number of layers increase beyond 8, all permeability contrast conditions begin to approach homogeneous sweep. This work also suggests that aquifers with significant heterogeneity may be swept very effectively. However, this hypothesis requires additional research with experiments or simulations.

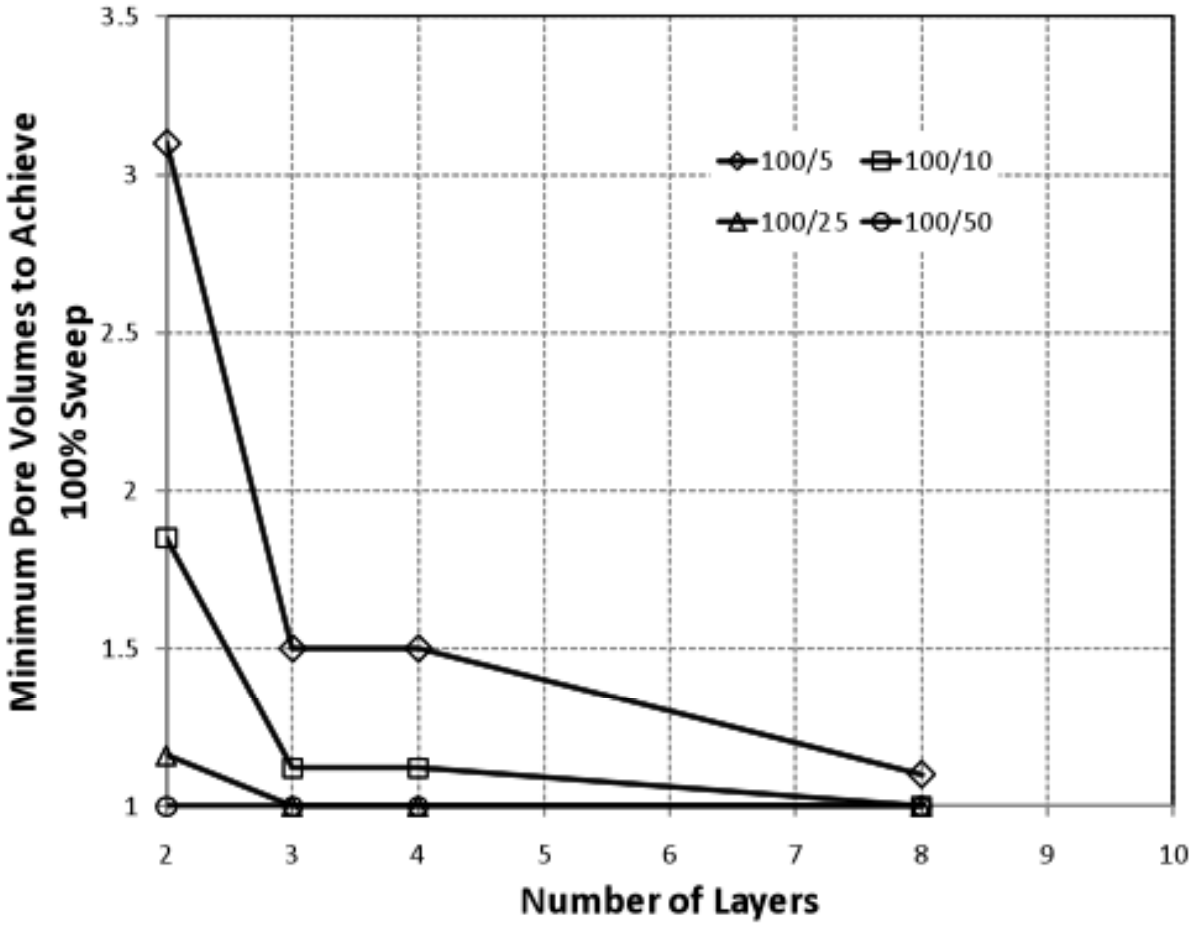

Figure 7-15: *Minimum number of pore volumes required to achieve 100% as a function of increasing the number of layers in the simulation.*

Task 5 Conclusions

The following conclusions for these layered-strata numerical simulations are provided below:

- Increasing the polymer concentration decreases the number of injected pore volumes needed to achieve 100% sweep of the sand tank in all cases.
- The sweep efficiency improvement diminishes as polymer concentrations exceed 500 mg/L.
- For a given permeability contrast, reducing the thickness of the lower permeability layer results in a decrease in the number of pore volumes needed to achieve 100% sweep. The opposite is true for a tracer (no polymer addition); the flushed pore volumes needed to achieve 100% sweep increases as the thickness of the lower permeability layer decreases.
- For two layer systems, polymer-enhanced solutions can achieve a 100% sweep in 1 pore volume if the permeability contrast is less than 4.
- The rate of cross-flow into a low-permeability layer (which improves sweep of this layer) continues to diminish as more of the lower layer pore volume is contacted by polymer solution.
- The effect of increasing the number of layers in a system, while maintaining constant media proportions reduces the number of pore volumes needed to achieve 100% sweep efficiency. The effect is most pronounced for permeability contrasts greater than 10. This suggests that most aquifers (which can have many layers not discernible even from well borings) may achieve sweep efficiencies more favorable than predicted by these 2-D experiments and simulations.

8. CONCLUDING SUMMARY

The over-arching goal of the project was to demonstrate the efficacy of using polymer solutions to improve the subsurface sweep efficiency of remediation-amendment fluids, particularly in heterogeneous media representative of aquifer systems. We have focused primarily on layered systems because this is the common condition for sedimentary aquifers. Achieving this goal involved investigating the compatibility between polymers and selected remediation agents (certain chemical oxidants and bioremediation agents). Our approach utilized numerical simulations and laboratory experiments conducted at the batch, column, and two-dimensional (2-D) intermediate scales (tank experiments).

This project included five primary tasks:

Task 1: Batch tests to evaluate polymer sorption characteristics and transport, the compatibility and transport of polymer/oxidant mixtures, and the compatibility and transport of oxidants and selected bioamendments;

Task 2: Column tests to evaluate polymer sorption characteristics and transport, the compatibility and transport of polymer/oxidant mixtures, and the compatibility and transport of oxidants and selected bioamendments;

Task 3: Two-dimensional (2-D) tank experiments to evaluate polymer flushing under heterogeneous conditions;

Task 4: To-dimensional (2-D) tank experiments to further investigate polymer/oxidant delivery and effectiveness; and

Task 5: Numerical simulations to evaluate polymer-flood application.

A brief overview of the project conclusions are provided in this paragraph, followed by the bulleted conclusions required by the reporting format. Our investigations revealed that the xanthan polymer may be compatible with both permanganate and persulfate oxidants, but the xanthan-permanganate pair is most promising for future use. Both polymers are compatible with bioaugmentation remediation of a chlorinated solvent contaminant, but neither polymer was demonstrated to be an effective electron donor to achieve complete dechlorination. The confirmation of the presence of simple reducing sugar compounds resulting from xanthan biodegradation leads us to infer that the use of xanthan polymers in the subsurface should not results in long-term deleterious effects on groundwater quality. Polymer injections will result in some clogging near the injection zone, but this is not expected to significantly influence field application. Batch and column tests were helpful in constructing numerical models in up-scaled systems (2-D tanks). The UTCHEM model was able to successfully simulate 2-D experimental data for layered heterogeneous systems. Experimental data from intermediate-scale 2-D systems, and from hundreds of numerical simulations, suggest that polymer floods are very effective at improving sweep efficiency in layered systems, and that performance improves in

systems with more layers. Additional 2-D experiments confirmed that a polymer-oxidant flood improved the mass removal compared to an oxidant-only flood, and reduced post-remediation mass flux. However, the polymer-delivery method used was important to achieve improvements. Overall, we believe that polymer flooding shows significant promise for improving chemical oxidation and bioattenuation in heterogeneous media to hydraulically inaccessible zones. A current ESTCP field effort to confirm the effectiveness of polymer-oxidant delivery is underway.

We are working on publications of these results in the near future (see Appendix B).

Bulleted conclusions from each Task are provided below.

Polymer Sorption Test

- Batch test results were inconclusive.
- The necessary parameters for UTCHEM model input can be alternatively derived from polymer transport column studies.

Polymer/Oxidant Compatibility Test Conclusions

- HPAM polymer does not retain any significant portion of its initial viscosity during 72-hour exposure tests with either permanganate or persulfate oxidant, and is thus chemically incompatible with these oxidants and unsuitable for further polymer-enhanced experimentation.
- Xanthan polymer, at "high" concentrations (1600 mg/L) retains a very small (<10%) percentage of its initial viscosity after 72 hours of exposure to activated persulfate oxidant, corresponding to a viscosity of 2-3 cP at an average shear rate of 10 sec-1. This viscosity is only a few times greater than that of water (1 cP) but may be great enough to permit increased crossflow in formations with a low degree of heterogeneity. Further investigation would be required to determine if this viscosity level and degree of remaining shear-thinning behavior would permit enhanced aquifer sweep, or if other polymers may prove more resistant to and more compatible with persulfate exposure.
- Xanthan polymer retains a large percentage of its initial viscosity after 72 hours of exposure to permanganate oxidant, with accompanying low to moderate levels of non-productive oxidant demand. Thus, this polymer/oxidant combination is deemed chemically compatible and is selected for further larger-scale experimentation for polymer-enhanced chemical oxidation.
- Unbuffered xanthan solutions experience near-complete loss of viscosity during oxidation of PCE contaminant by $KMnO_4$ in batch experiments. Buffering of the solutions to prevent pH decrease during contaminant oxidation can minimize this viscosity loss.

Polymer/Bioamendment Compatibility Test Conclusions

- Neither xanthan nor HPAM polymer impedes the dechlorinating ability of KB-1 microorganism to convert PCE into ethene, as long as methanol is supplied to the system as an electron donor, and in situations with initial methanol additions, microbial

dechlorination in polymer solutions often outperforms the corresponding nutrient medium control experiments.

- No complete PCE-ethene biotransformation is observed in polymer-containing experiments lacking methanol; instead, partial degradation often results in undesirable accumulations of more toxic daughter-products (DCE, or VC). Thus, xanthan and HPAM do not serve as adequate electron donors in the experimental matrices monitored here.
- In two experiments out of three complete sets, polymer solution viscosity decreases were not observed to accompany either complete or partial PCE dechlorination; this observation supports the inference that neither KB-1 nor NBB microbes can break down polymer molecules into smaller utilizable compounds for use as electron donors. The near-complete loss of viscosity in all xanthan-containing experiments during the second testing round is attributed to contamination by additional unknown microbes during microcosm assembly stage.
- Moderate (one-half an order of magnitude or more) decreases in solution pH were observed for all polymer solutions in contact with microbes over the duration of these experiments (multiple months).
- The viscosity decreases noted in xanthan and HPAM base tests (polymer, KB-1, PCE/methanol feed) were of such small magnitude, and were produced over such a relatively long timescale compared to the duration of a typical bioamendment injection, that they are unlikely to impact polymer-related flow effects or sweep efficiencies. These results, though, were obtained from idealized batch experiments involving intentionally controlled and limited microbial communities, and are thus not indicative of the timescales over which injected polymer viscosities would be retained at a more microbially diverse, natural subsurface site.

Polymer Transport Parameter Column Test Conclusions

- Many processes related to polymer retention (e.g., sorption, mechanical plugging, etc.) are interrelated and not easily mechanistically separated. We were able to identify and quantify the dominant processes regarding polymer retention and relate these processes to UTCHEM model input parameters. The parameters associated with these processes for the different soils (used in our later experiments) are also utilized as input parameters for the 2-D simulations of tank experiments in Task 3. We continue to analyze the data for journal manuscript preparation.

Chemical Oxidant Column Test Conclusions

- Permanganate oxidant in xanthan solution (2 g/L $KMnO_4$ in 1.6 g/L xanthan solution) is transported conservatively through a porous medium in the absence of natural oxidant demand (NOD) and oxidant reaction.
- In a demonstrably high-NOD porous media, permanganate in xanthan solution is consumed but xanthan solution viscosity is not immediately decreased, in contrast to the viscosity loss noted during PCE oxidation by permanganate. Therefore if site conditions of generally low to moderate NOD (approximately 1-2 mg/kg or lower, Siegrist et al., 2010) are

amenable to treatment by permanganate oxidant, mixtures of xanthan and permanganate should retain the increased solution viscosity necessary for increased aquifer sweep.

Polymer/Bioamendment Column Test Conclusions

- Both batch and 1-D column experiments demonstrate degradation of the xanthan polymer by microorganisms present in soil and groundwater, with concurrent release of reducing sugars.
- Results from batch experiments indicate that xanthan is vulnerable to biodegradation under both aerobic and anaerobic conditions; however, xanthan degradation proceeded more rapidly under anaerobic conditions as a result of exposure to the native soil organisms present in our samples.
- The confirmation of the presence of simple reducing sugar compounds resulting from xanthan biodegradation leads us to infer that the use of xanthan polymers in the subsurface should not results in long-term deleterious effects on groundwater quality.
- Some bio-clogging resulted from polymer addition (based on pressure increases across the experimental apparatus), but this is not expected to significantly influence polymer delivery in field applications.

2-D Experimental Tank and Modeling Conclusions

- Polymers can greatly improve the sweep efficiencies in layered systems. These results demonstrated up to a four-fold improvement in the overall sweep efficiency with less than two pore volumes of injected fluid, and also showed a much greater improvement in the ability to sweep low permeability layers.
- Polymer-improved sweep efficiency is not only dependent on the permeability contrast between layers, but also on the positioning of layers relative to the most conductive layer in the system.
- The UTCHEM model was shown to perform very well with regard to simulating the shapes of the injected tracer and polymer solutions over time, the calculated sweep efficiencies, and the pressure drop over the flow domain.
- Most model input parameters for UTCHEM were obtained from bench-scale measurements with minor modifications to permeability, and yet were sufficient to simulate the larger-scale 2-D experiments. However, these 2-D experiments operate over a significantly smaller scale than a field site, and attempting to characterize the heterogeneity at the field scale could prevent an investigator from characterizing the site sufficiently to uniquely determine all UTCHEM input parameters This study suggests that the bench-scale studies are sufficient to parameterize the model for a larger-scale system, provided the larger system is appropriately characterized.
- By enabling sweep of lower-permeability zones by remediation fluid, use of polymers should minimize the impact of contaminant rebound caused by diffusion of contaminants from low-permeability zones into more permeable media that was initially cleaned by the remediation effort.

2-D Oxidant Tank Experiment Conclusions

- Viscous mixtures of xanthan polymer and permanganate oxidant flow more evenly through this experimental dual-permeability system, and the mixture penetrates more of the finer-grained layer than does a solution of aqueous low viscosity oxidant alone. As a result of this increased "sweep," more contaminant mass (~2-3 times more) is destroyed per mass of oxidant.
- Discrete injections of oxidant followed by polymer (the "unmixed" case) are less effective at penetrating finer-grained layers than mixed solutions, as a result of initial flow bypassing before the introduction of the later polymer flood.
- Polymer-amended chemical oxidant applications appear to produce lower mass flux values, as compared to those measured for the polymer-free conventional oxidant application.
- Permeability differences of less than one order of magnitude can severely impact the sweep capability of an aqueous, low (1 cP) viscosity fluid, indicating that increased viscosity polymer/oxidant solutions may improve treatment effectiveness over a wide variety of heterogeneous natural systems.

Numerical Simulations Conclusions

- Increasing the polymer concentration decreases the number of injected pore volumes needed to achieve 100% sweep of the sand tank in all cases.
- The sweep efficiency improvement diminishes as polymer concentrations exceed 500 mg/L.
- For a given permeability contrast, reducing the thickness of the lower-permeability layer results in a decrease in the number of pore volumes needed to achieve 100% sweep. The opposite is true for a tracer (no polymer addition); the flushed pore volumes needed to achieve 100% sweep increases as the thickness of the lower-permeability layer decreases.
- For two-layer systems, polymer-enhanced solutions can achieve a 100% sweep in one pore volume if the permeability contrast is less than 4.
- The rate of cross-flow, which improves sweep, into a low-permeability layer continues to diminish as more of the lower layer pore volume is contacted by polymer solution.
- The effect of increasing the number of layers in a system, while maintaining constant media proportions, reduces the number of pore volumes needed to achieve 100% sweep efficiency. The effect is most pronounced for permeability contrasts greater than 10. This suggests that most aquifers (which can have many layers not discernible even from well borings) may achieve sweep efficiencies more favorable than predicted in these 2-D experiments and simulations.

9. REFERENCES

Abdel-Hamid, M.I., K.S. Khairou, and R.M. Hassan, 2003, Kinetics and mechanism of permanganate oxidation of pectin polysaccharide in acid perchlorate media. *Eur, Polymer. Jour.*, 39, 381-387.

Ahmed, G.A>, K.S. Khairou, and R.M. Hassan, 2003. Kinetics and mechanism of oxidation of chitosan polysaccharide by permanganate ion in aqueous perchlorate solutions. *Jour. Chem. Res.-S*, 4, 182-183.

Ahmed, G.A., A. Fawzy, and R.M. Hassan, 2007. Spectrophotometric evidence for the formation of short-lived hypomanganate(V) and manganate(V1) transient species during the oxidation of K-carrageenan by alkaline permanganate. *Carb. Res.*, 342, 1382-1386.

Bradley, P.M., 2003. History and ecology of chloroethene biodegradation: a review. *Bioremed. Jour*., 7, 81-109.

Chauveteau, G. and J. Lecourtier, 1986. Propagation of polymer slugs through adsorbent porous media. *Proceedings of the National Meeting of the ACS* entitled: Polymers in Enhanced Oil Recovery and the Recovery of Other Natural Resources, September 7-12, 1986, In: Water Soluble Polymers for Petroleum Recovery, Plenum Press, New York.

Chursin, V.I., 2007. Features of oxidative degradation of hydroxyethyl cellulose. *Russian Jour. Appl. Chem.*, 80, 654-659.

CP Kelco, 2004. Kelzan®/Keltrol® Xanthan gum book. 8th Edition, CP Kelco Company, Atlanta, GA.

CPGE, 2000a. UTCHEM 9.0: A three-dimensional chemical flood simulator. volume I: user's guide. Prepared by the Reservoir Engineering Research Program, Center for Petroleum and Geosystems Engineering, The University of Texas at Austin, Austin, TX.

CPGE, 2000b. UTCHEM 9.0: A three-dimensional chemical flood simulator. Volume II: technical documentation. Prepared by the Reservoir Engineering Research Program, Center for Petroleum and Geosystems Engineering, The University of Texas at Austin, Austin, TX.

Crimi, M. and R. Siegrist, 2004. Impact of reaction conditions on MnO_2 genesis during permanganate reaction. *Jour. Env. Eng.*, 130, 562-572.

Dontsova, K. M. and J. M. Bigham, 2005. Anionic polysaccharide sorption by clay minerals. *Soil Sci. Soc. Am. J.*, 69, 1026-1035.

Dubois, M., K.A. Gilles, J.K. Hamilton, P.A. Rebers, and F. Smith, 1956. Colorimetric method for determination of sugars and related substances. *Anal. Chem*., 28, 350.

Duhamel, M., S.D. Wehr, L. Yu, H. Rizvi, D. Seepersad, S. Dworatzek, E.E. Cox, and E.A. Edwards, 2002. Comparison of anaerobic dechlorinating enrichment cultures maintained on tetrachloroethene, trichloroethene, cis-dichloroethene and vinyl chloride. *Water Res.*, 36, 4193-4202.

Edwards, E.A. and D. Grbic-Galic 1994. Anaerobic biodegradation of toluene and *o*-xylene by a methanogenic consortium. *Appl. Env. Microbiol.*, 60, 313-3322.

El-Khatib, 2002. Spectrophotometric detection of methyl cellulose-manganate(VI) intermediate complex in the oxidation of methyl cellulose by alkaline permanganate. *Carb. Poly.*, 47, 377-385.

Flory, P.J. *Principles of polymer chemistry*. Cornell University Press: Ithaca, NY, 1953.

Gossett, J.M., 1987. Measurement of Henry's Law constants for C_1 and C_2 chlorinated hydrocarbons. *Env. Sci. Technol*., 21, 202-208.

Haselow, J.S., R.L,. Siegrist, M. Crimi, and T. Jarosch, 20033. Estimating the total oxidant demand for in situ chemical oxidation design. *Remed*., 13, 5-16.

Hassan, R.M., 1993. Alginate polyelectrolyte ionotropic gels. XIV: kinetics and mechanism of formation of intermediate complex during oxidation of alginate polysaccharide by alkaline permanganate with spectrophotometric evidence of manganate(VI) transient species. *Jour. Poly. Sci.(A),* 31, 51-59.

Hirasaki, G.J., and G.A. Pope, 1974. Analysis of factors influencing mobility and adsorption in the flow of polymer solutions through porous media. *SPE Jour.*, 14, 337-346.

Hood, E.D., N.R. Thomson, D. Grossi, and G.J. Farquhar, 2000. Experimental determination of the kinetic rate law for the oxidation of perchloroethylene by potassium permanganate. *Chem,* 40, 1383-1388.

Huang, K., G.E. Hoag, P. Chheda, B.A> Woody, and G.M. Dobbs, 2001. Oxidation of chlorinated ethenes by potassium permanganate: a kinetics study. *Jour. Haz. Mater.*, B87, 155-169.

Huang, K., Z. Zhao, G.E. Hoag, A. Dahmini, and P.A. Block. 2005. Degradation of volatile organic compounds with thermally activated persulfate oxidation. *Chem*., 61, 551-560.

Jackson, R.E., Dwarakanath, V., Meinardus, H. W., and Young, C. M., 2003. Mobility control: how injected surfactants and biostimulants may be forced into low-permeability units. *Remediation*, 13(3), 59-66.

Kishk, Y.F.M., and H.M.A. Al-Sayed, 2007. Free-radical scavenging and antioxidative activities of some polysaccharides in emulsions. *LWT,* 40, 270-277.

Krembs, F.J., 2008. Critical analysis of the field scale application of in situ chemical oxidation for the remediation of groundwater. M.S. thesis, Environmental Science & Engineering Division, Colorado School of Mines, Golden, CO.

Lake, L.W. 1989. *Enhanced oil recovery*, Prentice Hall, Englewood Cliffs, NJ.

Letey, J. 1994. Adsorption and desorption of polymers on soil. *Soil Sci*., 158, 244-248.

Liang, C.J., C.J. Bruell, M.C. Marley, and K.L. Sperry, 2004. Persulfate oxidation for in situ remediation of TCE. I. activated by ferrous iron with and without a persulfate-thiosulfate redox couple. *Chem*., 55, 1213-1223.

Lu, J.H., J. Wu and J. Letey. 2002. Effects of soil and water properties on anionic polyacrylamide sorption. *Soil Sci. Soc. Am. J.*, 66, 578-584.

Ma, J., G. Li, and N.J.D. Graham, 1994. Efficiency and mechanism of acrylamide removal by permanganate oxidation. *Jour. Water Supp. Res. And Technol.*, 43, 287-295.

Malik, M. and J. Letey. 1991. Adsorption of polyacrylamide and polysaccharide polymers on soil materials. *Soil Sci. Soc. Am. J.*, 55, 380-383.

Martel, K.E., R. Martel, R. Lefebvre, and P.J. Gelinas, 1998. Laboratory study of polymer solutions used for mobility control during in situ NAPL recovery. *Ground Water Monit. Remed.*, 18, 103-113.

Maymo-Gatell, X., V. Tandoi, J.M. Gossett, and S.H. Zinder, 1995. Characterization of an H_2-utilizing culture that reductively dechlorinates tetrachloroethene to vinyl chloride and ethene in the absence of methanogenesis and acetogenesis. *Appl. Env. Microbiol.*, 61, 3928-3933.

Meter, D.M., and R.B. Bird, 1964. Tube flow of non-Newtonian polymer solutions. Part 1. laminar flow and rheological models. *Am. Inst. Chem. Eng Jour.*, 10, 878-882.

Morelli, R., S. Russo-Volpe, N. Bruno, and R. LoScalzo, 2003. Fenton-dependent damage to carbohydrates: free radical scavenging activity of some simple sugars. *Jour. Agric, Food Chem.*, 51, 7418-7425.

Nadler, A. and J. Letey, 1989. Adsorption isotherms of polyanions on soils using tritium labeled compounds. *Soil Sci. Soc. Am. J.*, 53, 1375-1378.

Nankai, H., W. Hashimoto, H. Miki, S. Kawai, and K. Murata, 1999. Microbial system for polysaccharide depolymerization: enzymatic route for xanthan depolymerization by *Bacillus* sp. Strain GL1. *Appl. Env. Micro*., 65, 2520-2526.

Paraskevopoulou, D., D. Boskou, and A. Paraskevopoulou, 2007. Oxidative stability of olive oil-lemon juice salad dressing stabilized with polysaccharides. *Food Chem.*, 101, 1197-1204.

Poulson, S.R., and H. Naraoka, 2002. Carbon isotope fractionation during permanganate oxidation of chlorinated ethylenes (cDCE, TCE, PCE). *Env. Sci. Technol.*, 36:3270-3274.

Prabhakaran, P.V., S. Venkatachalam and K.N. Ninan, 1999. Permanganate ion supported over crosslinked polyvinylamine as an oxidizing agent for alcohols. *Eur. Poly. Jour.*, 35:1743-1746.

Robert, T., R. Martel, S.H. Conrad, R. Lefebvre, and U. Gabriel, 2006. Visualization of TCE recovery using surfactant-polymer solutions in a two-dimensional heterogeneous sand model. *Jour. Contam Hydrol.*, 86, 3-31.

Ross, C., L.C. Murdoch, D.L. Freedman, and R.L. Siegrist, 2005. Characteristics of potassium permanganate encapsulated in polymer. *Jour. Env. Eng.*, 131, 1203-1211.

Tillotson, B.E., 2009. The longer term removal of organic matter and nutrients from within the vadose zone of onsite wastewater treatment systems as affected by key system design parameters. M.S. Thesis, Environmental Science and Engineering Division, Colorado School of Mines, Golden, CO.

Sahl, J.W., J. Munakata-Marr, M. L. Crimi, and R.L. Siegriest, 2007. Coupling permanganate oxidation with microbial dechlorination of tetrachloroethene. *Water Environ. Res.*, 78, 5-12.

Seright, R.S. and Martin, F.D., 1991 "Fluid diversion and sweep improvement with chemical gels in oil recovery processes," second annual report (DOE/BC/14447-10), Contract No. DE-FG22-89BC14447, U.S. DOE.

Sharp, J.H., 1973. Total organic carbon in seawater – comparison of measurements using persulfate oxidation and high temperature combustion. *Marine Chem.*, 1, 211-229.

Siegrist, R.L., M. Crimi, and T.J. Simpkin, eds., 2010. *In Situ Chemical Oxidation for Groundwater Remediation*. Springer: New York, NY.

Smith, M.M., J.A.K. Silva, J. Munakata-Marr, and J.E. McCray, 2008. Compatibility of polymers and chemical oxidants for enhanced groundwater remediation. *Env. Sci. Technol.*, 42, 9296-9301.

Sorbie, K. S., 1991. *Polymer-improved oil recovery*. CRC Press, Boca Raton, FL.

Sorbie, K.S. and Y. Huang, 1991. Rheological and transport effects in the flow of low-concentration xanthan solution through porous media. *Jour. Coll. and Interf. Sci.*, 143(1), 74.

Spiteller, M., and C. Saiz-Jimenez, 1990. A two step degradative procedure for structural studies of aquatic humic acids. *Org. Geochem.*, 15, 449-455.

Stewart, R., 1964. *Oxidation mechanisms*. W.A. Benjamin, Inc.: New York, NY.

Sworn, G., 2000. Xanthan gum, in *Handbook of hydrocolloids*. Phillips, G.O., Williams, P.A., eds., CRC Press: Boca Raton, FL, 2000.

Tunnicliffe, B.S., and N.R. Thomson, 2004. Mass removal of chlorinated ethenes from rough-walled fractures using permanganate. *Jour. Contam. Hydrol.,* 75, 91-114.

Waldemer, R.L., and P.G. Tratnyek, 2006 Kinetics of contaminant degradation by permanganate. *Env. Sci. Technol*., 40, 1055-1061.

Wehmeier, K.R., and A.D. Mooradian, 1994. Autoxidative and antioxidative potential of simple carbohydrates. *Free Rad., Biol. Med.,* 17, 83-86.

Yan, Y.E., and F.W. Schwartz, 1999. Oxidative degradation and kinetics of chlorinated ethylenes by potassium permanganate. *Jour. Contam. Hydrol.,* 37, 343-365.

Yang, Y., and P.L. McCarty, 1998. Competition for hydrogen within a chlorinated solvent dehalogenating anaerobic mixed culture. *Env. Sci. Technol.*, 32, 3591-3597.

Zaitoun, A. and N. Kohler, 1987. The role of adsorption in polymer propagation through reservoir rocks. *Proceedings of the SPE International Symposium on Oilfield Chemistry*, San Antonio, Texas, 4 – 6 February, 1987.

Zhai, X., I. Hua, P.S.C. Rao, and L.S. Lee, 2006. Cosolvent-enhanced chemical oxidation of perchloroethylene by potassium permanganate. *Jour. Contam. Hydrol.,* 82, 61-74.

Zhong, L., M. Oostrum, T.W. Wiestsma, and M.A. Covert, 2008. Enhanced remedial amendment delivery through fluid viscosity modifications: experiments and numerical simulations. *Jour. Contam. Hydrol.,* 101, 29-41.

APPENDIX A: SUPPORTING DATA

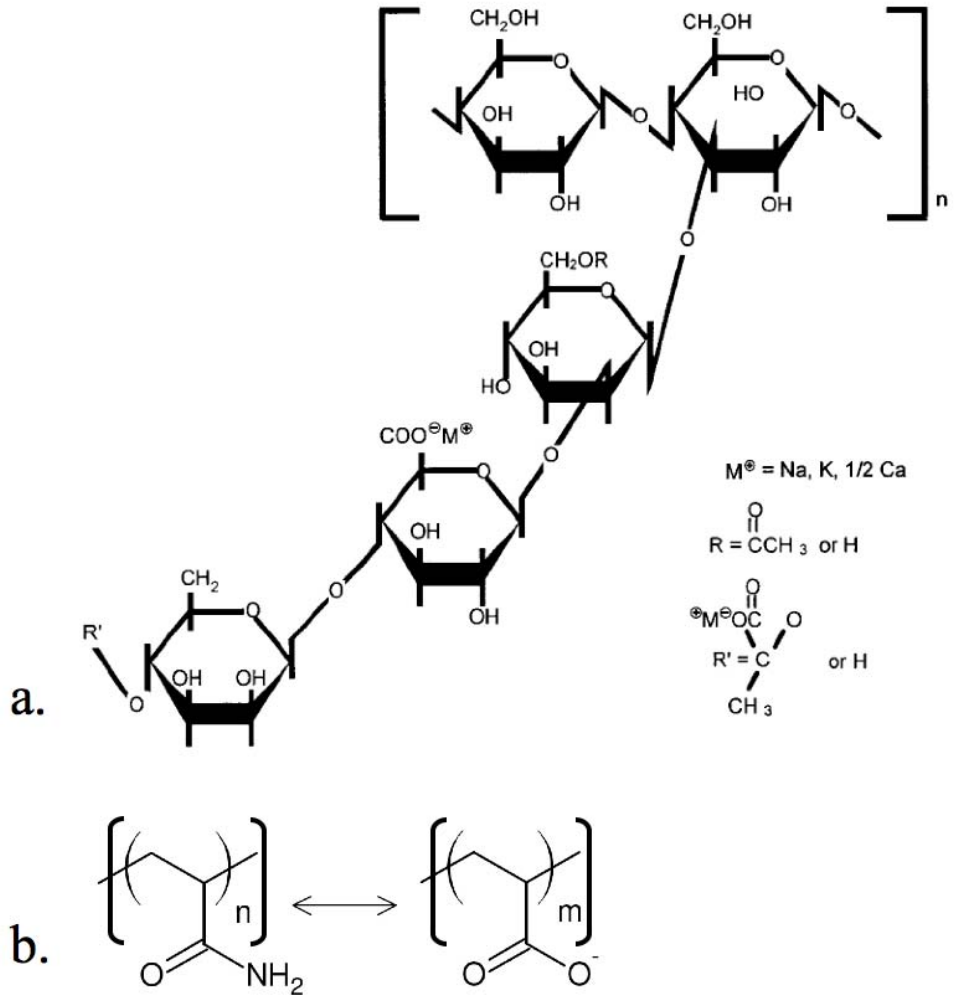

Figure A-1: *Molecular structures of a) xanthan polymer, from Sworn, 2000, and b) hydrolyzed polyacrylamide (HPAM).*

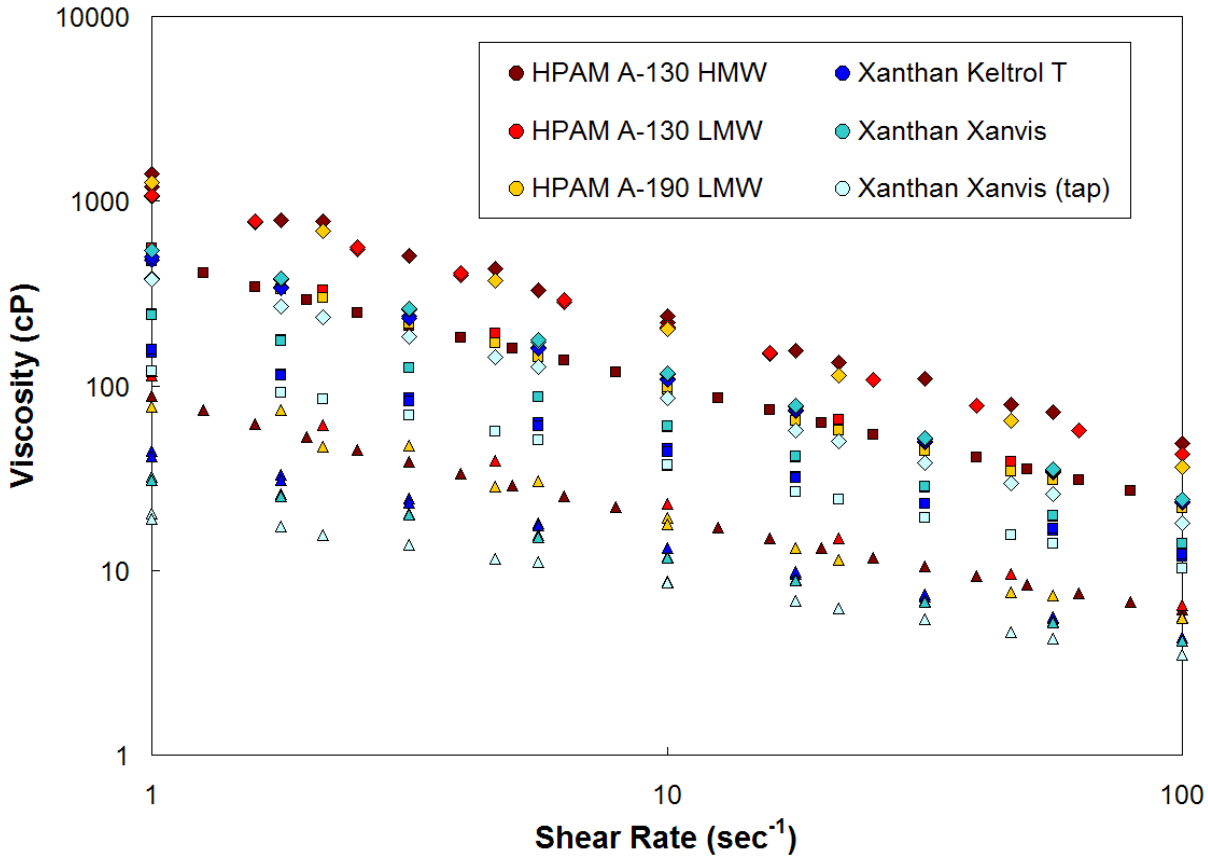

Figure A-2: *Measured viscosity (in centipoises) versus shear rate (in sec^{-1}) for the types and concentrations of polymers used in Sub-task 1B polymer/oxidant compatibility batch testing. Color indicates the particular type of polymer, while shape indicates polymer concentration (diamonds 1600 mg/L; squares 800 mg/L; triangles 160 mg/L). Note the log scales of both axes. Modified from Smith et al., 2008.*

Table A-1: *Viscosity data for 160 mg/L and 800 mg/L xanthan polymer controls, and viscosity retention percents for xanthan/$KMnO_4$ test batches (with 2 g/L $KMnO_4$) and xanthan/salt controls (with K^+ ions in solution), after 72 hours of batch exposure.*

Shear Rate (sec^{-1})	160 mg/L xanthan control viscosity (cP)	"test," with 2 g/L $KMnO_4$ retention (%)	"salt," with equiv [K_+] retention (%)	Shear Rate (sec^{-1})	800 mg/L xanthan control viscosity (cP)	"test," with 2 g/L $KMnO_4$ retention (%)	"salt," with equiv [K^+] retention (%)
1	20.24	14.8	19.0	1	243.5	19.5	33.7
1.778	17.31	17.8	22.1	1.778	176.6	23.3	37.1
3.162	13.8	21.8	27.2	3.162	125.3	27.6	40.2
5.623	11.05	25.8	31.1	5.623	87.18	31.9	43.5
10	8.707	31.3	36.8	10	59.79	36.4	46.5
17.78	6.857	37.5	42.4	17.78	40.82	40.5	49.5
31.62	5.422	43.7	48.3	31.62	28.06	44.4	52.2
56.23	4.295	50.5	54.5	56.23	19.53	47.9	54.8
100	3.474	57.1	60.4	100	13.89	51.0	57.3
100	3.480	56.9	60.2	100	13.94	50.8	57.3
46.42	4.606	48.3	52.2	56.23	19.68	47.6	54.8
21.54	6.261	39.9	43.9	31.62	28.34	44.1	52.1
10	8.625	31.7	36.6	17.78	41.24	40.3	49.4
4.642	11.56	26.3	29.8	10	60.12	36.2	46.8
2.154	15.51	20.0	25.2	5.623	87.37	32.2	43.9
1	19.08	18.0	20.9	3.162	124.9	28.0	41.2
				1.778	175.5	24.3	38.3
				1	241.1	20.6	35.6

Table A-2: *Composition of Nutrient Medium (Sahl et al., 2006; from Edwards and Grbic-Galic, 1994)*

Constituents (Volume Added per Liter)	Chemical Ingredient	Concentration (g/L)
Phosphate Buffer Solution (10 mL)	KH_2PO_4	27.2
	K_2HPO_4	34.8
Salt Solution (10 mL)	NH_4Cl	53.5
	$CaCl_2 \cdot 6H_2O$	7.0
	$FeCl_2 \cdot 4H_2O$	2.0
Trace Mineral Solution (2 mL)	H_3BO_3	0.3
	$ZnCl_2$	0.1
	NiCl2·6H2O	0.75
	$MnCl_2 \cdot 4H_2O$	1.0
	$Na_2MoO_4 \cdot 2H_2O$	0.1
	$CuCl_2 \cdot 2H_2O$	0.1
	$CoCl_2 \cdot 6H_2O$	1.5
	Na_2SeO_3	0.02
	$Al_2(SO_4)_3 \cdot 16H_2O$	0.1
	H_2SO_4	1 mL
Magnesium Sulfate Solution (2 mL)	$MgSO_4 \cdot 7H_2O$	62.5
Redox Indicator Solution (1 mL)	resazurin	1
Saturated Bicarbonate Solution (10 mL)	$NaHCO_3$	200
Vitamin Stock Solution (10 mL)	biotin	0.02
	folic acid	0.02
	pyridoxine hydrochloride	0.1
	riboflavin	0.05
	thiamine	0.05
	nicotinic acid	0.05
	pantothenic acid	0.05
	p-amino-benzoic acid	0.05
	cyanocobalamin	0.05
	thioctic acid	0.05
	mercaptoethanesulfonic acid	1
Amorphous Ferrous Sulfide Solution (10 mL)	$(NH4)_2Fe(SO_4)_2 \cdot 6H_2O$	39.2
	$Na_2S \cdot 9H_2O$	24.0

APPENDIX B: LIST OF PUBLICATIONS

Articles in peer-reviewed journals

Smith, M.M., J.A.K. Silva, J. Munakata-Marr, and J.E. McCray, 2008. Compatibility of polymers and chemical oxidants for enhanced groundwater remediation. *Environmental Science and Technology*, 42, 9296-9301.

Articles in preparation

Davenport, S.M., J. Munakata-Marr, M.M. Smith, J.A.K. Silva, and J.E. McCray. Bioclogging during enhanced polymer delivery for groundwater remediation. In preparation for Journal of Environmental Engineering.

Silva, J.A.K., M.M. Smith, J. Munakata-Marr, and J.E. McCray. Polymer transport and retention mechanisms in aquifer sediments. In preparation for Journal of Contaminant Hydrology.

Silva, J.A.K., M.M. Smith, J. Munakata-Marr, and J.E. McCray. Polymer-enhanced fluid delivery in layered heterogeneous media: experimental investigations. In preparation for Journal of Contaminant Hydrology.

Silva, J.A.K., and J.E. McCray. Designing polymer-enhanced fluid delivery in layered heterogeneous media. In preparation for Journal of Contaminant Hydrology.

Smith, M.M., J.A.K. Silva, J. Munakata-Marr, and J.E. McCray. Enhanced anaerobic biodegradation of chlorinated ethenes as a result of viscous polymer flooding. In preparation for Environmental Science and Technology.

Smith, M.M., J.A.K. Silva, J. Munakata-Marr, and J.E. McCray. Effectiveness of contaminant destruction using polymer-enhanced chemical oxidation delivery strategies versus conventional injections. In preparation for Journal of Contaminant Hydrology.

Conference or symposium abstracts

Davenport, S.M., J.E. McCray, J. Munakata-Marr, and J.A.K. Silva. Biodegradation of the xanthan polymer: use as a subsurface amendment. Poster presentation, SERDP/ESTCP Partners in Environmental Technology Technical Symposium. Washington, D.C., December 1-3, 2009.

Davenport, S.M., J.E. McCray, J. Munakata-Marr, and J.A.K. Silva. Investigation of xanthan degradation and potential for bioclogging. Poster presentation, National Ground Water Association Ground Water Summit. Tucson, AZ, April 19-23, 2009.

Silva, J.A.K., M.M. Smith, and J.E. McCray. The addition of water-soluble polymers to enhanced the delivery of in situ remediation agents in heterogeneous strata. Poster presentation, SERDP/ESTCP Partners in Environmental Technology Technical Symposium. Washington, D.C., December 2-4, 2008.

Silva, J.A.K., M.M. Smith, and J.E. McCray. Water-soluble polymers to enhanced the sweep-efficiency of in situ remediation agents. Poster presentation, SERDP/ESTCP Partners in Environmental Technology Technical Symposium. Washington, D.C., December 4-6, 2007.

Silva, J.A.K., M.M. Smith, and J.E. McCray. Water-soluble polymers to enhance sweep efficiencies of in situ remedation amendments. Oral presentaation, National Ground Water Association Ground Water Summit. Albuquerque, NM, April 29-May3, 2007.

Smith, M.M., J.A.K. Silva, J. Munakata-Marr, and J.E. McCray. Results of polymer-enhanced groundwater remediation experiments: xanthan coupled with potassium permanganate and reductive dechlorinators. Poster presentation, SERDP/ESTCP Partners in Environmental Technology Technical Symposium. Washington, D.C., December 1-3, 2009

Smith, M.M., J.A.K. Silva, J. Munakata-Marr, and J.E. McCray. Working smarter, not harder: using viscous polymer solutions to achieve increased contaminant destruction in heterogeneous aquifers. Oral presentation, Geological Society of America Annual Meeting. Portland, OR, October 18-21, 2009.

Smith, M.M., J.A.K. Silva, J. Munakata-Marr, and J.E. McCray. The use of polymer solutions for enhanced PCE biodegradation in heterogeneous aquifer settings. Oral presentation, Tenth International Bioremediation Symposium. Baltimore, MD, May 5-8, 2009.

Smith, M.M., J.A.K. Silva, J. Munakata-Marr, and J.E. McCray. Polymer-enhanced remediation techniques for more effective treatment of heterogeneous aquifers. Oral presentation, National Ground Water Association Ground Water Summit. Tucson, AZ, April 19-23, 2009.

Smith, M.M., J.A.K. Silva, J. Munakata-Marr, and J.E. McCray. Overcoming heterogeneity effects through polymer-enhanced groundwater remediation techniques: coupling polymer floods with chemical oxidants and bio-agents. Oral presentation, American Geophysical Union. San Francisco, CA, December 15-19, 2008.

Smith, M.M., J.A.K. Silva, J. Munakata-Marr, and J.E. McCray. Coupling polymer floods with biodegradation and chemical oxidation treatments – techniques to achieve more effective groundwater remediation in heterogeneous aquifers. Poster presentation, SERDP/ESTCP Partners in Environmental Technology Technical Symposium. Washington, D.C., December 2-4, 2008.

Smith, M.M., J.A.K. Silva, J. Munakata-Marr, and J.E. McCray. Polymer-enhanced delivery of chemical oxidants and bioamendments to DNAPL zones. Oral presentation, Remediation of Chlorinated and Recalcitrant Compounds Sixth International Conference. Monterey, CA, May 19-22, 2008.

Silva, J.A.K., M.M. Smith, J. Munakata-Marr, and J.E. McCray. Coupled polymer floods and bio-chemical remediation techniques for enhanced groundwater treatment. Oral presentation, American Society of Civil Engineers Groundwater Symposium. Honolulu, HI, May 13-16, 2008.

Smith, M.M., J.A.K. Silva, J. Munakata-Marr, and J.E. McCray. Using polymer floods to overcome heterogeneity effects during bioremediation and chemical oxidation ground water

treatments. Oral presentation, National Ground Water Association Ground Water Summit. Memphis, TN, March 30-April 3, 2008.

Smith, M.M., J.A.K. Silva, J. Munakata-Marr, and J.E. McCray. Coupled techniques for more efficient groundwater remediation: polymer floods and oxidation treatment. Poster presentation, SERDP/ESTCP Partners in Environmental Technology Technical Symposium. Washington, D.C., December 4-6, 2007.

Smith, M.M., J.A.K. Silva, J. Munakata-Marr, and J.E. McCray. Polymer-enhanced chemical oxidation: compatibility and effectiveness for ground water remediation of chlorinated contaminants. Oral presentation, Geological Society of American Annual Meeting. Denver, CO, October 28-31, 2007.

Smith, M.M., J.A.K. Silva, J. Munakata-Marr, and J.E. McCray. Polymer-oxidant compatibility for use as a combined groundwater remediation treatment. Oral presentaation, National Ground Water Association Ground Water Summit. Albuquerque, NM, April 29-May3, 2007.